LEABHARLANN CHOLÁISTE NA TRÍONÓIDE, BAILE ÁTHA CLIATH | TRINITY COLLEGE LIBRARY DUBLIN
Ollscoil Átha Cliath | The University of Dublin

Terms and Conditions of Use of Digitised Theses from Trinity College Library Dublin

Copyright statement

All material supplied by Trinity College Library is protected by copyright (under the Copyright and Related Rights Act, 2000 as amended) and other relevant Intellectual Property Rights. By accessing and using a Digitised Thesis from Trinity College Library you acknowledge that all Intellectual Property Rights in any Works supplied are the sole and exclusive property of the copyright and/or other IPR holder. Specific copyright holders may not be explicitly identified. Use of materials from other sources within a thesis should not be construed as a claim over them.

A non-exclusive, non-transferable licence is hereby granted to those using or reproducing, in whole or in part, the material for valid purposes, providing the copyright owners are acknowledged using the normal conventions. Where specific permission to use material is required, this is identified and such permission must be sought from the copyright holder or agency cited.

Liability statement

By using a Digitised Thesis, I accept that Trinity College Dublin bears no legal responsibility for the accuracy, legality or comprehensiveness of materials contained within the thesis, and that Trinity College Dublin accepts no liability for indirect, consequential, or incidental, damages or losses arising from use of the thesis for whatever reason. Information located in a thesis may be subject to specific use constraints, details of which may not be explicitly described. It is the responsibility of potential and actual users to be aware of such constraints and to abide by them. By making use of material from a digitised thesis, you accept these copyright and disclaimer provisions. Where it is brought to the attention of Trinity College Library that there may be a breach of copyright or other restraint, it is the policy to withdraw or take down access to a thesis while the issue is being resolved.

Access Agreement

By using a Digitised Thesis from Trinity College Library you are bound by the following Terms & Conditions. Please read them carefully.

I have read and I understand the following statement: All material supplied via a Digitised Thesis from Trinity College Library is protected by copyright and other intellectual property rights, and duplication or sale of all or part of any of a thesis is not permitted, except that material may be duplicated by you for your research use or for educational purposes in electronic or print form providing the copyright owners are acknowledged using the normal conventions. You must obtain permission for any other use. Electronic or print copies may not be offered, whether for sale or otherwise to anyone. This copy has been supplied on the understanding that it is copyright material and that no quotation from the thesis may be published without proper acknowledgement.

An investigation of the role of caspase-9-interacting proteins in the molecular control of apoptosis

Colin Adrain

Thesis submitted to Trinity College Dublin
for the degree of Doctor of Philosophy

TRINITY COLLEGE
0 8 JUN 2001
LIBRARY DUBLIN

Molecular Cell Biology Laboratory,
Department of Genetics,
University of Dublin,
Trinity College,
Dublin 2

November 2000

TRINITY COLLEGE
06 JUN 2001
LIBRARY DUBLIN
Thesis
6186

DECLARATION

I certify that this thesis, submitted to Trinity College Dublin for the degree of Doctor of Philosophy, has not been submitted as an exercise for a degree at this or any other university. I certify that the work presented here is entirely my own, except where otherwise acknowledged. This thesis may be made available for consultation within the university library and may be copied or lent to other libraries upon request.

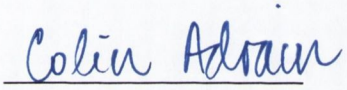

Colin Adrain

November, 2000

To my parents

ACKNOWLEDGEMENTS

I would sincerely like to thank Dr Helen Egan, Dr Liz Slee, Dr Mary Harte and Liam Carlin for permission to use some of the data in the thesis. This applies in particular to the DRADD project.

I am especially indebted to my supervisor, Professor Seamus Martin. Over the past three years I have benefited enormously from your upbeat and enthusiastic supervisory skills. Thanks also for your friendship and your willingness to help resolve even the smallest problems.

I would like to thank Seamus, Liam and Daniela for their company on numerous coffee breaks, an essential part of the investigative process. Thanks to all of the members of the lab, past and present for making the long working hours an enjoyable experience.

Thanks also to my friends in Maynooth for their loyalty in spite of my virtual disappearance over the past few months.

Finally, thanks Emma and my parents. I couldn't have managed without your care and support over the past few months.

I am grateful for the financial support of the Dept. of Education for Northern Ireland (DENI), Enterprise Ireland and the Daniel O'Connell fellowship I enjoyed during two years of study in NUI Maynooth.

TABLE OF CONTENTS

	Page
SUMMARY	I
ABBREVIATIONS	III
PUBLICATIONS	V
CHAPTER I: INTRODUCTION	
1.1. MODES OF CELL DEATH	2
1.2. ROLES OF APOPTOSIS	3
1.2.1. Apoptosis as a counterbalance to mitosis	3
1.2.2. The immune system	4
1.2.3. Differentiation	4
1.2.4 Development	5
1.3. APOPTOSIS AND HUMAN DISEASE	5
1.3.1. Cancer	6
1.3.2. Immune disorders	7
1.3.3. Cardiovascular disease	9
1.3.4. Neurodegeneration	9
1.3.5. Viruses	10
1.4. PROGRAMMED CELL DEATH IN *C.elegans*	10
1.4.1. Nematode death genes	10
1.4.2. Nematode cell death proteins	13
1.5. MAMMALIAN RELATIVES OF *C.elegans* DEATH GENES	14
1.5.1 Human ICE and CED-3	14
1.5.2. Human Bcl-2: and *C.elegans* CED-9	16

1.6. CASPASES **16**

1.6.1 Caspase structure and activation 16

1.6.2. Criteria for subdividing the caspases 18

1.6.3. Non-redundant role of caspases 19

1.6.4. Functional consequences of caspase activation 21

1.6.4.1. Phagocytosis 22

1.6.4.2. Nucleases 23

1.7 REGULATION OF CASPASE ACTIVITY **23**

1.7.1 Caspase inhibitory proteins 23

1.7.1.2. Caspase pseudosubstrates 24

1.7.1.3. The IAPs 24

1.7.2 The induced proximity model 25

1.7.2. Caspase Activating pathways 27

1.7.2.1. Death receptors 27

1.7.2.2. Granzyme-B 27

1.7.2.3. Nuclear stimuli 28

1.8. MITOCHONDRIAL CONTROL OF APOPTOSIS **29**

1.8.1. Cytochrome *c* 31

1.8.2. Integration of death signals via mitochondria: the Bcl-2 family 33

1.8.3. Apaf-1 36

1.8.4. Apaf-1 and Caspase-9 37

1.8.5. Apaf-1 and caspase-9: murine knockout studies 37

1.9. AIMS OF THIS THESIS **40**

1.9.1. Molecular dissection of Apaf-1 function 40

1.9.2. Screening for Apaf-1-interacting proteins 40

1.9.3. Characterization of DRADD, 41

a Caspase-9-interacting protein 41

1.9.4. Screening for DRADD-interacting proteins 41

CHAPTER II: MATERIALS AND METHODS

2.1. MATERIALS **43**

2.1.1 Chemicals and general reagents 43

2.1.2. Enzymes 43

2.1.3. Antibodies 43

2.2. PURIFICATION AND MANIPULATION OF NUCLEIC ACIDS **43**

2.2.1. Bacterial strains used for plasmid isolation purposes 43

2.2.2. Preparation of chemically competent cells 43

2.2.3. Transformation of competent DH5α 43

2.2.4. Plasmid DNA isolation procedures 44

2.2.4.1. Minipreparation procedure 44

2.2.4.2. Midiprep procedure 45

2.2.4.3. Phenol/chloroform extraction procedure. 46

2.2.4.4. Qiagen procedure. 46

2.2.5. Agarose gel electrophoresis 47

2.2.6. Quantitation of nucleic acids 47

2.2.7. Genecleaning 48

2.2.7.1. Genecleaning nucleic acids from suspension 48

2.2.7.2. Genecleaning nucleic acids from agarose gel 48

2.2.8. Restriction digestion 48

2.2.9. Ligations 48

2.3. PCR **49**

2.4. AUTOMATED DNA SEQUENCING **50**

2.5. PLASMIDS **51**

2.6. PROTEIN PRODUCTION AND ANALYSIS **51**

2.6.1. *In vitro* transcription and translation (ITT) 51

2.6.2. Induction of GST-fused proteins in bacteria 52

2.6.3. SDS-PAGE 53

2.6.4. Immunoblotting 53

2.6.5. Coomassie staining. 54

2.6.6. Enhanced fluorography. 54

2.6.7. GST pulldown *in vitro* capture assay 54

2.6.8. Immunoprecipitation 55

2.7. THE YEAST TWO-HYBRID SYSTEM **56**

2.7.1. Yeast strains 57

2.7.2. Media for maintenance of yeast strains 57

2.7.3. Routine yeast culture and inocula for transformation 58

2.7.4. Inoculation of liquid yeast cultures (Starter cultures) 58

2.7.5.1. Midi yeast transformation protocol 58
(Untransformed yeast strains)

2.7.5.2. Midi yeast transformation protocol 60
(Sequential transformations)

2.7.6. Two hybrid protein-protein interaction assays 60

2.7.6.1. *HIS3* nutritional selection assay 60

2.7.6.2. *LacZ* colony lift assay. 61

2.7.6.3. *LacZ* liquid assay 61

2.7.7. Preparation of Yeast protein lysates for immunoblotting 62

2.7.8. Two hybrid library screening 62

2.7.8.1.Preparation of library plasmid 62

2.7.8.2. Library scale screening 62
2.7.8.3. Plasmid rescue and insert amplification from yeast library clones 63

2.8. MAMMALIAN CELL CULTURE 64
2.8.1. Routine cell culture conditions 64
2.8.2. Cell cryopreservation and thawing 64
2.8.3. Transient Transfection 65
2.8.3.1. Calcium phosphate precipitation method 65
2.8.3.2. Liposome-mediated transient transfection. 65
2.8.4. Subcellular localization analysis 67
2.8.5. Jurkat cell-free extract 67
2.8.6. Trypan blue exclusion and Hoechst cell viability assays. 67

CHAPTER III: MOLECULAR DISSECTION OF APAF-1 FUNCTION

3.1. INTRODUCTION 69

3.2. CHAPTER AIMS 71

3.3. RESULTS 73
3.3.1. Design and generation of Apaf-1 two-hybrid deletion mutants 73
3.3.2. Detection of Apaf-1 self-association by two-hybrid analysis 74
3.3.3. Generation of GST-Apaf-1 fusions and ^{35}S-labeled *in vitro* translated (ITT) Apaf-1 mutants for *in vitro* pulldown analysis 75
3.3.4. Detection of Apaf-1 self-association by GST pulldown analysis 76
3.3.5. The WDR inhibits Apaf-1 self-association 76

3.3.6. Cytochrome *c*/dATP overcome the inhibitory effect of the WDR 77
3.3.7. Caspase-9 recruitment of Apaf-1 is negatively regulated by the WDR 77
3.3.8. Deletion of the WDR renders Apaf-1 constitutively pro-apoptotic 78
3.3.9 *In vitro* modulation of caspase-9 activity 79
3.3.9.1 Attempts to recapitulate caspase-9 activation *in vitro* 79
3.3.9.2. Attempts to repress caspase-9 activation *in vitro* 80
3.4. Two-hybrid Screening for Apaf-1 interactors 80

3.5. DISCUSSION **87**
3.5.1. Summary 87
3.5.2. Apaf-1 functions via an induced proximity mechanism 87
3.5.3. Apaf-1 oligomerization requires the CED-4-homologous domain 88
3.5.4. The WDR plays a dual role in regulating Apaf-1 activity 88
3.5.5. The WDR represses the pro-apoptotic activity of Apaf-1 89
3.5.6. Screening for Apaf-1-interacting proteins 90
3.5.7. Modulation of Apaf-1 oligomerization represents an important therapeutic target 91

CHAPTER IV: MOLECULAR CHARACTERIZATION OF DRADD, A NOVEL CASPASE-9-INTERACTING MOLECULE

4.1. INTRODUCTION AND AIMS **93**

4.2. RESULTS **93**
4.2.1 Identification of DRADD 93

4.2.2 p84 binds specifically to caspase-9^{CARD} 95
4.2.3. Domain structure of p84 95
4.2.4. Identification of DRADD homologues 96
4.2.5. A CARD-like region within DRADD 96
is responsible for caspase-9 binding
4.2.6. Detection of DRADD/caspase-9 association 98
by a GST *in vitro* capture assay
4.2.7. DRADD and caspase-9 interact in mammalian cells 98
4.2.8. Detection of DRADD oligomerization 100
4.2.9. DRADD interacts with pRb in yeast 100
4.2.10. DRADD interacts with pRb in mammalian cells 101
4.2.11. DRADD is a nuclear protein 102
4.2.12. Forced DRADD expression induces apoptosis 103
4.2.13. DRADD-associated cell death is caspase-9-dependent 105
4.2.14. DRADD dominant negative studies 105
4.2.14.1. DRADD-DN does not potentiate 106
death receptor-associated apoptosis
4.2.14.2. DRADD-DN does not potentiate 108
death adaptor-associated apoptosis
4.2.14.3. DRADD-DN does not potentiate 108
genotoxic stress-associated apoptosis
4.2.15. Generation of a stable GFP-DRADD 110
dominant negative cell line
4.2.16. DRADD does not translocate
from the nucleus upon induction of the death program 111
4.2.17. Detection of stimulus-specific DRADD cleavage 113
4.2.18. Ectopic expression of pRb induces apoptosis 114
4.2.19. pRb and DRADD collaborate to induce apoptosis 115
4.2.20. Generation of DRADD antisera 115

4.3. DISCUSSION **118**

4.3.1. Summary 118

4.3.2. DRADD does not potentiate death receptor-associated apoptosis 118

4.3.4. DRADD interacts with cell cycle regulator, pRb 118

4.3.5. DRADD is a nuclear protein 120

4.3.6. Does DRADD participate in a caspase-activating pathway within the nucleus? 121

4.3.7. DRADD remains within the nucleus in dying cells 122

4.3.8. DRADD undergoes proteolytic cleavage during Bax-mediated apoptosis 123

4.3.9. Concluding remarks 125

CHAPTER V: CLONING OF DRADD-INTERACTING MOLECULES BY YEAST-TWO HYBRID SCREENING

5.1. INTRODUCTION **128**

5.2. RESULTS **129**

5.2.1. Design and generation of DRADD two-hybrid bait proteins 130

5.2.2. Toxicity tesing of the DB-DRADD^{FL} bait plasmid 130

5.2.3. Library screening with DB-DRADD^{FL} 130

5.2.4. Preliminary outcome of the DB-DRADD^{FL} screen 131

5.2.5. Alu-1 digestion of DB-DRADD^{FL}-interacting library clones 132

5.2.6. DNA sequence analysis of clones 133

5.2.7. The identity of the DRADD^{FL}-interacting library clones 133

5.2.8. Analysis of the DRAMP amino acid sequence 134

5.2.9. Identification of DRAMP homologues 135

5.2.10. Preliminary analysis of the DRADD/DRAMP interaction 135

5.2.11. The minimal DRADD interaction motif of DRAMP 136

5.2.12. DRAMP binds to the DRADD N-terminus 137

5.2.13. Verifying the molecular weight of DRAMP protein 137

5.3. Preliminary analysis of a further DRADD^{FL}-interacting library clone 138

5.4. DISCUSSION **140**

5.4.1. Summary 140

5.4.2. The DRADD/DRAMP interaction 141

5.4.3. Sequence analysis of DRAMP 141

5.4.4. What is the role of DRAMP? 142

5.4.5. Is DRAMP a motor protein? 142

5.4.6. What is the subcellular localization of DRAMP? 143

5.4.7. DRAMP and LC-8: parallels? 145

5.4.8. Conclusion 145

CHAPTER VI: General Discussion

6.1. Summary 148

6.2. Concluding comments: Chapter III 150

6.3. Concluding remarks: Chapter IV 152

6.4. Concluding remarks: Chapter V 155

APPENDIX

REFERENCES

LIST OF FIGURES AND TABLES

CHAPTER I

Figure 1 Schematic diagram illustrating the hallmark phenotypical changes that a cell undergoes during apoptosis

Figure 2 The ordering of *C.elegans* death genes

Figure 3 Schematic diagram illustrating the structure of a typical procaspase

Figure 4 Activation of caspase-3 during apoptosis

Figure 5 Phylogenetic tree illustrating the relationship amongst members of the human caspase family

Figure 6 Death receptor-mediated activation of caspases

Figure 7 Diagram illustrating how DNA damaging stimuli achieve stabilization of p53 via a kinase cascade

Figure 8 Diagram illustrating the principle that cytochrome *c* release is an important integration point for diverse upstream stimuli

Figure 9 Schematic diagram illustrating the modular structure of Apaf-1

CHAPTER II

Figure 10 Schematic diagram illustrating the principle of the two hybrid protein-protein interaction assay

CHAPTER III

Figure 11 The modular structure of Apaf-1

Figure 12 Generation and expression of Apaf-1 two-hybrid deletion mutants

Figure 13 Yeast Two-hybrid protein-protein interaction assay illustrating Apaf-1 dimerization

Figure 14 Purification of recombinant GST-Apaf-1 fusion proteins

Figure 15 Design and production of radiolabeled Apaf-1 deletion mutant proteins

Figure 16 Detection of Apaf-1 self-association using GST-pulldowns

Figure 17 The WDR region of Apaf-1 inhibits self-association in *in vitro* GST pulldown assays

Figure 18 Detection of caspase-9^{CARD} recruitment of radiolabeled Apaf-1 by the GST pulldown *in vitro* capture assay

Figure 19 Evaluation of apoptosis associated with forced Apaf-1 expression

Figure 20 Attempts to modulate caspase-9 activation using recombinant Apaf-1

Figure 21 Attempt to repress in vitro activation of caspase-9 using recombinant Apaf-1

Figure 22 Selection of an Apaf-1 Gal-4 DB mutant suitable for screening purposes

CHAPTER IV

Figure 23 Illustration of the caspase-9^{CARD} bait used for two-hybrid library screening

Figure 24 Flow diagram illustrating the stages involved in the identification of DRADD as a caspase-9 interacting protein

Figure 25 *HIS3* yeast Two-Hybrid protein-protein interaction assay illustrating the selectivity of DRADD binding for caspase-9^{CARD}

Figure 26 Identification of DRADD

Figure 27 Identification of DRADD homologues

Figure 28 Deletional analysis of DRADD/caspase-9 interaction in yeast

Figure 30 DRADD interacts with the retinoblastoma protein, pRb

Figure 29 DRADD interacts with caspase-9 *in vitro* and in mammalian cells

Figure 31 DRADD sublocalizes to the nucleus

Figure 32 Evaluation of apoptosis associated with DRADD overexpression

Figure 33 Investigation of DRADD function using a dominant negative-based approach

Figure 34 Evaluation of apoptosis associated with transient overexpression of death receptors or their intracellular death domain-containing moieties

Figure 35 DRADD DN fails to block genotoxic stress-associated apoptosis

Figure 36 Determining the electroporation conditions required for the generation of stable Jurkat DRADD-overexpressing cells

Figure 37 DRADD does not undergo redistribution from the nucleus in dying cells

Figure 38 Cleavage of DRADD specific to Bax-induced apoptosis

Figure 39 pRb augments DRADD-associated apoptosis

Figure 40 Production of DRADD antisera

CHAPTER V

Figure 41 Selection of the DB-DRADD bait protein for 2-hybrid screening

Figure 42 Flow chart illustrating the stages involved in the identification of DRAMP as a DRADD- interacting protein using Two-Hybrid library screening

Figure 43 LacZ two-hybrid colony lift assay of putative DRADD-interacting clones

Figure 44 Designation of library clones into groups on the basis of Alu-1 digestion patterns

Figure 46 Identification of non-human DRAMP homologues

Figure 45 Characterization of the DRAMP amino acid sequence

Figure 47 Two-hybrid *LacZ* colony lift assay illustrating interaction between DRAMP library clones and DRADD in yeast

Figure 48 The minimal DRADD-interacting motif of DRAMP coincidentally encodes a weak CARD-like motif

Figure 49 Assessment of the DRAMP binding motif within DRADD using the *LacZ* liquid protein-protein interaction assay

Figure 50 Autorad illustrating the molecular weight of *in vitro* transcribed and translated (ITT) DRAMP protein

Figure 51 Two-hybrid LacZ colony lift assay illustrating interaction between library clones #37 and #40 in yeast

Figure 52 The identity of the protein encoded by clone #40

Figure 53 Alignment of DRAMP with human proteins containing Walker's A and B nucleotide binding consensus sequences

CHAPTER VI

Figure 54 Schematic diagram illustrating assembly of the Apaf-1 apoptosome

Figure 55 Schematic diagram illustrating a hypothetical "Nuclear Apoptosome" complex composed of DRADD and Caspase-9, regulated by the Retinoblastoma protein, pRb

Figure 56 Models illustrating the hypothetical role of DRAMP as a regulator of the pro-apoptotic activity of DRADD

TABLES

CHAPTER I

Table-1 Table illustrating some of the wide range of stimuli that can induce apoptosis

Table 2 Table indicating the subdivision of caspases based on their tetrapeptide substrate specificity

Table 3 Summary of the phenotype of mice nullizygous for the indicated caspases

CHAPTER III

Table 4 Summary of all the two-hybrid Apaf-1/Apaf-1 combinations tested in the *HIS3* and *LacZ* b-galactosidase assays

Table 5 Summary of the suitability of the Two-Hybrid

Apaf-1 DB mutants for screening purposes

Table 6 Table illustrating a comparison in the average transformation efficiency of yeast strains Y190, Y190 DB and Y190 DB-Apaf-1CED-4 when transformed with library plasmid

Table 7 Table illustrating the relationship between yeast transformation efficiency and the scale of library screening undertaken

Table 8 Table illustrating a comparison between the library transformation efficiency of Y190 pGBT-8 empty vector and Y190 pGBT-8 Apaf-1 CED-4 strains

Table 9 Table illustrating clones obtained from the Apaf-1 Yeast-Two–hybrid Screen identified by DNA sequencing followed by BLAST database searching

Table 10 Table illustrating clones obtained from the Apaf-1 Yeast-Two–hybrid screen identified by DNA sequencing and BLAST database searching

CHAPTER IV

Table 11 Detection of DRADD self-association in yeast

Table 12 The position of putative NLSs within DRADD

Table 13 Table illustrating the electroporation parameters tested in order to optimize the electroporation efficiency of Jurkat cells

CHAPTER V

Table 14 Table illustrating that the DB-DRADD$^{387-657}$ mutant auto-activates the *HIS3* and *LacZ* reporter genes when co-expressed with the unfused Gal-4 AD

Table-15 Table summarizing the individual groups of that shared common Alu-1 restriction digest banding patterns

Table 16 Table illustrating the identity of single copy clones, as revealed by DNA sequencing and database interrogation

Table 17 Table illustrating the identity of single copy clones, as revealed by DNA sequencing and subsequent database interrogation

Table 18 Table illustrating clones obtained from the DRADD two-hybrid screen of which two copies were identified following DNA sequencing and subsequent database interrogation

Table 19 Table summarizing the mode of identification of all 22 of the DRAMP clones

Table 20 Table illustrating the N-terminal amino acid position of DRAMP clones

Table 21 Summary of the identity of Alu-1-grouped clones, as revealed by database interrogation

APPENDIX

Table 22 Table indicating plasmids that were generated by the author for work undertaken in Chapter III

Table 23 Table indicating plasmids that were generated by the author for work undertaken in Chapters IV and V

Table 24 Table indicating the oligonucleotide primers that were used to generate some of the plasmids used for work undertaken in the thesis

Table 25 Table identifying the origin of some of the plasmids used for work undertaken in this thesis

SUMMARY

Apoptosis is an important homeostatic mechanism that multicellular organisms utilize to delete cells during development and on an ongoing basis in the adult. At the molecular level, this requires the activation of a family of proteolytic enzymes called caspases. Caspases are constitutively present in healthy cells as inactive zymogens (procaspases). In cells stimulated to die, caspases become activated via proteolytic cleavage, mediated by other active caspases. Evidence suggests that because inactive caspases possess a basal level of proteolytic activity, enforced aggregation can stimulate their activation. Through the proteolysis of strategic cellular substrates, active caspases mediate the biochemical and phenotypical changes required during apoptosis.

Several human diseases, including cancer, autoimmunity and neurodegeneration can arise from either insufficient or excessive caspase activation. In this regard, human caspase-9 constitutes an attractive therapeutical target. *CASP-9*-nullizygous mice exhibit severe brain and craniofacial abnormalities due to a failure to delete neuroepithelial progenitor cells during embryogenesis. Although it has not yet been demonstrated, this molecule may thus play a role in modulating neuronal cell death in the adult. Significantly, *CASP-9*-null cells are resistant to a range of chemotherapeutically relevant pro-apoptotic stimuli. Thus, it is desirable to elucidate how caspase-9 activation is regulated. To further the understanding of factors that regulate caspase-9 activation, this thesis focuses on the molecular characterization of two caspase-9-interacting molecules, Apaf-1 and DRADD.

CHAPTER III

Apaf-1 (Apoptotic Protease Activating Factor-1) has recently been identified as an important regulator of caspase-9 activation in response to stimuli that integrate at the point of provoking cytochrome *c* release from mitochondria. Cytosolic cytochrome *c* stimulates Apaf-1 to activate caspase-9 via an as yet unknown mechanism. We employed a variety of protein-protein interaction assays to investigate the mode of Apaf-1 action. Using the yeast two-hybrid system and *in*

vitro capture assays, we observed that Apaf-1 can form oligomers. We propose that Apaf-1 oligomerization may mediate caspase-9 activation. Deletional analysis revealed that the CED-4-homologous and adjacent linker regions mediate Apaf-1 self association. Critically, we report that Apaf-1 oligomerization and caspase-9 recruitment is repressed by the C-terminal WD-40 repeat (WDR) region of the molecule. We observed that *in vitro*, cytochrome *c* overcomes the inhibitory effects of the WDR, promoting Apaf-1 oligomerization. Deletion of the WDR resulted in a constitutively active Apaf-1 that provoked considerably greater cytoxicity than the wild type molecule in transient overexpression studies. From our findings, we propose that cytochrome *c* overcomes the inhibitory effect of the WDR, promoting Apaf-1 oligomerization, caspase-9 recruitment and activation.

CHAPTER IV describes the characterization of DRADD (Death-inducing Rb-Associated Death Domain protein), a novel caspase-9-binding, death domain adaptor molecule. Using protein-protein interaction assays, we demonstrate that a CARD-like region within DRADD is responsible for caspase-9-binding. In transient expression assays, CARD-containing DRADD deletion mutants provoke caspase-9-dependent apoptosis. In contrast to the cytosolic distribution of other death domain molecules, DRADD is sharply localized within the nuclear compartment. In co-immunoprecipitation assays, DRADD interacts with the key cell cycle regulator, Rb. Moreover, when co-expressed, DRADD and Rb collaborate to provoke apoptosis. We propose that cell cycle deregulation or nuclear damage may engage a DRADD/caspase-9-dependent apoptotic pathway within the nucleus.

CHAPTER V concerns a yeast two-hybrid library screen that was performed to obtain DRADD-binding partners. This approach yielded multiple copies of a molecule we called DRAMP (DRADD-associated myosin-like protein). DRAMP possesses a coiled-coil motif, a putative nuclear localization signal and associates with the N-terminus of DRADD. Future studies will evaluate how DRAMP regulates the pro-apoptotic activity of DRADD.

ABBREVIATIONS

3-AT:	3-aminotriazole
ACINUS:	apoptotic chromatin condenser in the nucleus
AD:	Gal-4 activation domain
AICD:	activation-induced cell death
AIF:	apoptosis-inducing factor
ALPS:	acute lymphoproliferative syndrome
Apaf-1:	apoptotic protease activating factor-1
Bcl-2:	B-cell lymphoma-2
BH:	Bcl-2 homology region
BIR:	baculovirus IAP repeats
BLAST:	basic local alignment search tool
CAD:	caspase activated Dnase
CARD:	caspase recruitment domain
CASPASE:	cysteinyl aspartate-specific proteinases
CED:	cell death defective
CFE:	cell free extract
cFLIP	FLICE-like inhibitory protein
CFU:	colony forming units
CHK:	checkpoint kinase
CrmA:	cytokine response modifier
CTL:	cytotoxic lymphocyte
DB:	Gal-4 DNA binding domain
DcR3:	decoy receptor-3
DD:	death domain
DED:	death effector domain
DISC:	death-inducing signaling complex
DMSO:	dimethyl sulphoxide
DN:	dominant negative
DR:	death receptor
DRADD:	death-inducing Rb-associated death domain protein
DRAMP:	DRADD-associated myosin-like protein
DTT:	dithiothreitol
EDTA:	ethylinediaminetetraacetic acid
EGFP:	enhanced green fluorescent protein
ER:	endoplasmic reticulum
FADD:	Fas associated protein with death domain
FasL:	Fas ligand
FCS:	foetal calf serum
FITC:	fluorescein isothiocyanate
FL:	full length
GFP:	green fluorescent protein
GST:	glutathione-S-transferase
HA:	haemagglutin
HEK:	human embryonic kidney
HEPES:	N-[2-hydroxyethyl]piperazine -N′-[2-ethanesulphonic acid]
HPIP:	haematopoietic PBX-interacting protein
IAP:	inhibitor of apoptosis protein

ABBREVIATIONS

ICAD:	inhibitor of caspase activated Dnase
ICE:	interleukin-1β converting enzyme
ICELAP-6:	ICE-like apoptotic protease-6
Ig:	immunoglobulin
IL-3:	interleukin-3
IPTG:	isopropylthio-β-D-galactoside
ITT:	*in vitro* transcription and translation
kDa:	kilodaltons
kbp:	kilobase pairs
LA/TE:	lithium acetate/TE buffer
MDM-2:	murine double minute-2
NCBI:	national center for biotechnology information
NGF:	nerve growth factor
NLS:	nuclear localization signal
ONPG	o-nitrophenyl β-D-galactopyranoside
ORF:	open reading frame
PAGE:	polyacrylamide gel electrophoresis
PARP:	poly(ADP-ribose) polymerase
PBS:	phosphate buffered saline
PCD:	programmed cell death
PCR:	polymerase chain reaction
PIDD:	p53-inducible death domain
PIPES:	Piperazine-N-N′-bis[2-ethanesulphonic acid]
PML:	promyelocytic leukaemia protein
PMSF:	phenylmethylsulphonylfluoride
PS:	phosphatidylserine
RAIDD:	RIP-associated Ich-1/CED homologous protein with a DD
Rb:	retinoblastoma protein
RIP:	receptor-interacting protein
SD:	synthetic dropout medium
SDS:	sodium dodecyl sulphate
SERPIN:	serine protease inhibitor
SMAC:	second mitochondrial activator of caspases
SV40:	simian virus-40
TNF:	tumour necrosis factor
TRAIL:	TNF-related apoptosis-inducing ligand
UAS:	upstream activating sequence
UV:	ultraviolet irradiation
WDR:	WD-40 repeat region
X-Gal:	5-bromo-4-chloro-3-indolyl-β-D-galactoside
X-IAP:	X-linked inhibitor of apoptosis protein
Z-VAD.fmk:	benzyloxycarbonyl-Val-Ala-Asp-(OMe) fluoromethylketone

PUBLICATIONS

Adrain C, Slee EA, Harte MT, Martin SJ (1999). Regulation of apoptotic protease activating factor-1 oligomerization and Apoptosis by the WD-40 repeat region. *J Biol Chem.* **274**, 20855-60.

Slee EA, Adrain C, Martin SJ (1999). Serial killers: ordering caspase activation events in apoptosis. *Cell Death Differ.* **6**, 1067-74.

Slee EA, Adrain C, Martin SJ (2001). Executioner caspases-3, -6 and -7 perform distinct, non-redundant, roles during the demolition phase of apoptosis. *J Biol Chem.* **276** 7320-7326.

Adrain C, Harte MT, Egan, H, Carlin WJ, Slee EA, Martin SJ (2001). DRADD, a nuclear-localized death domain protein, interacts with caspase-9 and Rb to promote apoptosis. Submitted.

Adrain C and Martin SJ (2001). The mitochondrial apoptosome: a killer unleashed by the cytochrome seas. *Trends Biochem Sci.* In press.

Adrain C and Martin SJ (2001). Search for *Drosophila* caspases bears fruit: STRICA enters the fray. *Cell Death Differ.* **8**, 319-323.

CHAPTER I
Introduction

1.1. MODES OF CELL DEATH

Apoptosis is a phrase first used in 1972 by Kerr, Wyllie and Currie to describe a controlled form of cell death that is widespread during normal physiological function, during development, as well as within the context of various pathological states (Kerr *et al.*, 1972). Apoptosis is characterized by a series of hallmark phenotypical changes (See Figure 1), including shrinkage of the cell body and nuclear condensation (Kerr *et al.*, 1972). This culminates in the formation of small, membrane-bounded sacs composed of cytosol and nuclear fragments, achieved through a process of membrane blebbing. The products of this process, apoptotic bodies, become engulfed by macrophages, thus completing this cell-specific ablation mechanism (Kerr *et al.*, 1972). As a result, no traces of the dead cell remain.

The authors of this landmark study established the distinction between the physiological cell-autonomous suicide program of apoptosis and necrotic cell death (Kerr *et al.*, 1972). Necrosis is passive, characterized by rapid cellular swelling, cell rupture and loss of plasma membrane integrity. A key difference between the two processes is that necrosis provokes an inflammatory response, whereas apoptotic cells retain their plasma membrane integrity and therefore do not. For this crucial reason, necrosis involves the unscheduled death of multiple cells in the same locality. In contrast, a single apoptotic cell harnesses an innate death program, leaving neighbouring cells completely unaffected.

As it transpired, it is not the case that specific stimuli provoke one or other of these radically different modes of cell death. Rather, the severity of the insult governs how a cell will die. Less severe stimuli allow apoptosis to occur, whereas more noxious doses of the same agent otherwise force the cell unwillingly into necrosis (Lennon *et al.*, 1991).

As will be discussed later, in spite of the fact that diverse stimuli can provoke apoptosis, these become channeled into relatively few core components of a suicide machine. A summary of some of these diverse apoptosis-inducing agents can be found in Table 1.

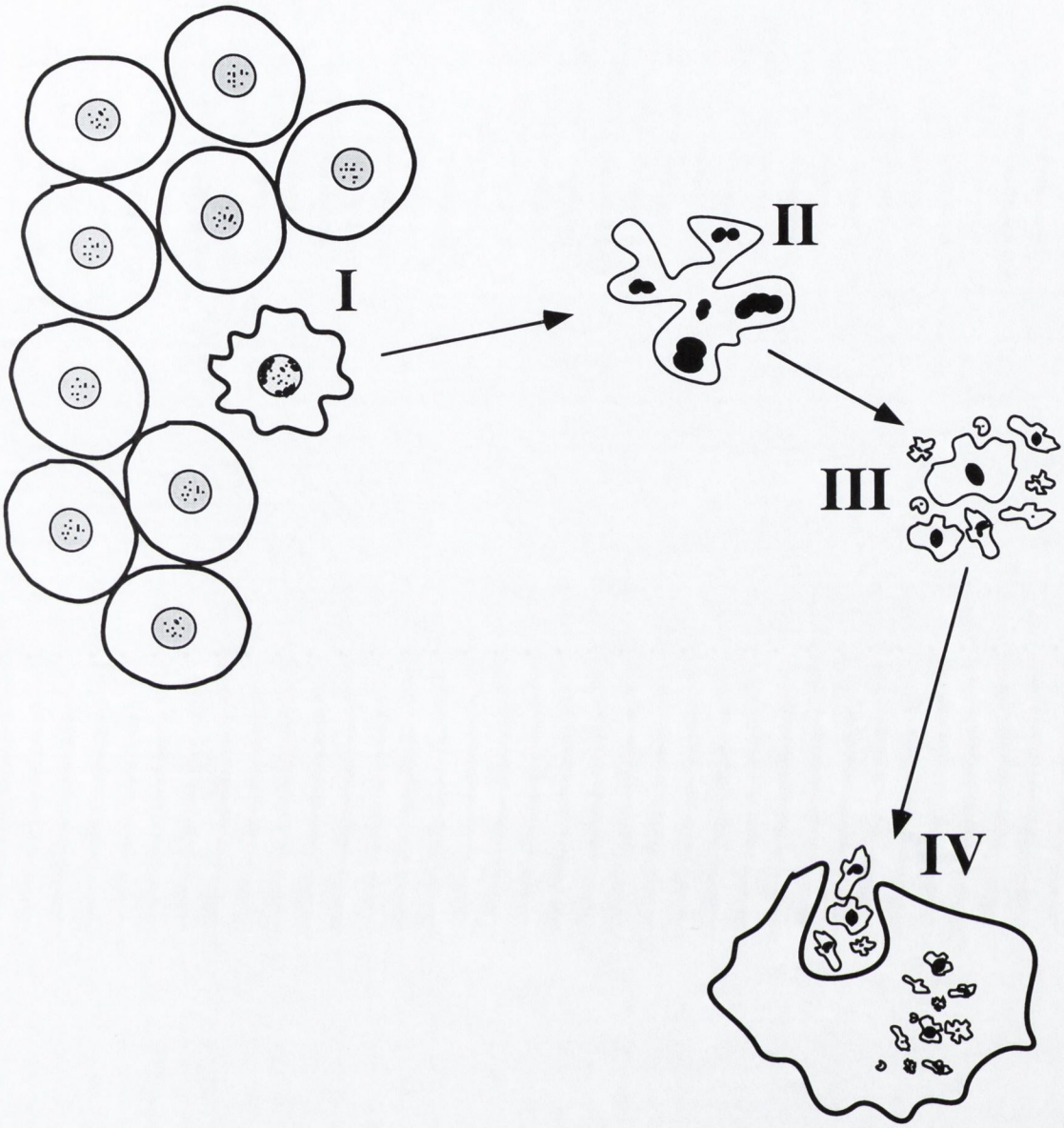

Figure 1

Schematic diagram illustrating the hallmark phenotypical changes that a cell undergoes during apoptosis.

Within the tissue, the cell destined to die shrinks away from other neighbouring healthy cells, undergoing margination of chromatin to the periphery of the nucleus (**I**). During the next stage (**II**), the cell undergoes severe condensation/shrinkage, typified by blebbing—the appearance of membrane-bound inclusions. In addition, the nucleus undergoes fragmentation into discrete, condensed entities. The membrane blebbing then culminates in fragmentation of the cell into numerous, discrete membrane-enclosed fragments containing cytoplasm, nucleus and organelles, called apoptotic bodies (**III**). These are then engulfed through phagocytosis, thus removing any traces of the dead cell from the surrounding environment (**IV**).

Table 1

Table illustrating some of the wide range of stimuli that can induce apoptosis

Proapoptotic stimulus			
General Cellular Stresses	Genotoxic Stresses	Cytokines/ Receptors	Other
Heat Shock	UV irradiation	Cytokine withdrawal	Microtubule depolymerization
Ethanol	Chemotherapeutic drugs	T-Cell receptor stimulation	Inhibition of proteasome function
Hypoxia	γ-Irradiation	Death Ligand (FasL, TNFa, TRAIL etc)	Kinase inhibition
Excessive Light		Anti death receptor agonistic antibodies	Kinase overexpression
H_2O_2			Mitotic catastrophe
			Inhibition of protein synthesis
			RGD peptides
			Glucocorticoids
			Calcium ionophores

Kerr and colleagues proposed that most cell deaths were accomplished through apoptosis, not necrosis as was previously believed. They also highlighted that apoptosis was not simply restricted to a specific disease state or pathology, somewhat divorced from normal physiological conditions (Kerr *et al.*, 1972). These observations established programmed cell death as an ongoing physiological process as critically important as mitosis.

Subsequent evidence confirmed the premise that programmed cell death events occur throughout every stage of the life cycle. For instance, apoptosis occurs widely during embryogenesis, in development of the juvenile and throughout adulthood (Jacobson *et al.*, 1997). Indeed, by way of example, every single minute, millions of cell deaths occur in the adult human. Clearly, given this seemingly uneconomical ongoing large-scale loss of cells, one would expect that this must be fulfilling an important biological imperative. This is indeed the case. The paragraphs that follow highlight the numerous scenarios that rely on apoptosis in order to stress the biological necessity for a regulated cell death programme.

1.2. ROLES OF APOPTOSIS

1.2.1. Apoptosis as a counterbalance to mitosis

An obvious rationale for apoptosis is to provide a counterbalance to the opposing cellular process of mitosis. Clearly, while adult multicellular organisms maintain a constant size and cell number, many cell types are continually dividing. Apoptosis therefore represents a homeostatic safety valve essential for the maintenance of a stringently defined cell number (Jacobson *et al.*, 1997). This form of homeostasis also enables organisms to shed aged, worn, superfluous or transformed cells, that constitute a risk to the organism as a whole. For example, the human digestive tract and skin surfaces are sites of ongoing cell death. Via apoptosis, worn or damaged cells are shed from tissue, in order to be replaced by properly functioning healthy cells: the products of cell division.

By deleting transformed cells, apoptosis helps to maintain of the integrity of the genome, a prerequisite for multicellularity. Cells subjected to DNA damage die for the collective good of the entire organism. This is an essential anti-neoplastic mechanism. Typical of this is the loss of epidermal cells following sunburn. Interestingly, similar to the ability of different levels of the same stimulus to engage apoptotic or necrotic responses, apoptosis is the most severe of the two possible cellular outcomes to DNA damage. If the DNA damage incurred is suitably trivial, a block on mitosis is triggered. In more severe cases, the cell enters apoptosis, rather than risk deregulated cell cycle progression and ultimately, tumourigenesis.

1.2.2. The immune system

In numerous scenarios, apoptosis is used to reduce a large cohort of cells to a subpopulation of cells bearing a specific characteristic. This is typified by the fine-tuning of the immune system. For instance, the vast majority of cells that enter the thymus (some 95%) die during positive and negative selection (Nagata, 1997). Apoptosis enables the selection of cells capable of responding to antigen, that do not exhibit self-reactivity. A combination of mitosis and apoptosis enables our bodies to produce superfluous cells on a just-in-case basis. This allows a rapid immune response to fight infection, and eliminates cells which constitute a risk to proper immune function.

1.2.3. Differentiation

A phenomenon similar to apoptosis plays a key role in the terminal differentiation of several cell types. For example, the surface of human skin is composed of dead keratinocytes. Thus these cells play their intended cellular role as corpses (Jacobson *et al.*, 1997; Weil *et al.*, 1999). Intriguingly, expression of the death-inhibitory gene, Bcl-2, interferes with the terminal differentiation of these cells, suggesting that they must die in order to realize their intended differentiated role (Nataraj *et al.*, 1994). Certain cell types selectively harness some of the components of the suicide machinery without succumbing to death *per se*. For example, during erythropoiesis, erythroblasts undergo an enucleation process typified by nuclear condensation and DNA fragmentation (De Maria *et al.*, 1999). In addition, there is evidence to suggest that lens

epithelial cells undergo a differentiation process that shares some of the hallmarks of apoptosis, including the appearance of pyknotic nuclei, fragmented DNA and even cleavage of certain protein substrates commonly encountered in apoptotic cells (Ishizaki *et al.*, 1998).

1.2.4 Development

During development, organ morphogenesis relies heavily upon programmed cell death to delete masses of cells not required in the mature tissue. This is akin to sculpture, whereby an amorphous block of material is selectively chiseled into a defined shape, the surplus material being deleted. This mechanism is typified by the developing mammalian limb bud, where formation of the digits is achieved by the selective death of superfluous cells within the interdigital regions (Jacobson *et al.*, 1997). In a similar example, the sculpting of the nervous system is achieved through the selective death of some 50% of total neurons produced. This selective culling is mediated through the secretion of a nerve growth factor (NGF) by target cells that require innervation (Barde, 1989). Thus, in the case of neurons, superfluous cells are eliminated by something akin to neglect, since they require a survival factor in order to evade programmed death.

Apoptosis is a convenient means of ridding the body of obsolete structures, typified by the degeneration of the tadpole tail upon development into a frog. In this scenario, increases in the levels of thyroid hormone provoke programmed death within the obsolete tail. Similarly, during human embryogenesis, structures that are non-essential in one or other gender, such as the müllerian duct in the case of male mammals, are thought to die by apoptosis (Jacobson *et al.*, 1997).

1.3 APOPTOSIS AND HUMAN DISEASE

The evidence above attests to the importance of apoptosis as a key developmental, anti-neoplastic and homeostatic mechanism, essential to the functioning of multicellular organisms. That factors either promote or repress cell death suggests that this process involves a defined molecular program that can be invoked, as required on a cell-specific basis. Given the ubiquitous roles

of apoptosis, it is unsurprising that many diseases are the result of abberant regulation of this process. The examples below illustrate some of this range of diseases.

1.3.1. Cancer

To reiterate, apoptosis is a counterbalance to mitosis. Clearly, cancer can arise either as a result of an increased rate of proliferation, or a reduced level of cell death. An aggressively transformed cell possessing both of these characteristics has a selective advantage over a cell possessing only one of these possible tumorigenic determinants.

There is ample epidemiological evidence of transformed cells harbouring defects in the mitosis side of the equation, as evidenced by how frequently the tumour suppressor genes p53 and pRb are mutated in human neoplasias (Weinberg, 1995; Caspari, 2000). p53 is an important transcriptional modulator of apoptosis, via expression of death agonist molecules such as Bax and Noxa (Miyashita *et al.*, 1995; Oda *et al.*, 2000). In addition, it is also an important cell cycle regulator. It is therefore easy to see how this dual regulator of both sides of the homeostatic equation is mutated in half of all human cancers (Caspari, 2000).

There is also evidence that some human malignancies arise from defects in the death machinery. However, the frequency of mutation of these molecules in cancers is substantially rarer than that of their cell cycle regulatory counterparts (Martin and Green, 1995a). One reason for this paradox is that the death machinery may also be required for cell cycle progression (Martin and Green, 1995a). Thus, the loss of some of the components of the suicide machine may be mutually exclusive with enhanced cellular proliferation (Martin and Green, 1995a Martin and Green, 1995b). In support of this, many life-threatening tumours inducibly undergo apoptosis during chemo- and radiotherapy, suggesting that most of the components of the death machine are intact even in aggressively transformed cells. Moreover, cells transformed by deregulated expression of the transcriptional regulator c-Myc are actually

sensitised to apoptosis, again suggesting that the death machinery and cell cycle machinery are mechanistically interwoven (Evan *et al.*, 1992).

One of the best examples of a cell death regulator falling foul of mutation is the phenomenon of heightened levels of the Bcl-2 death antagonist in human follicular B-cell lymphomas (Bakhsi *et al.*, 1985). Bcl-2 was identified within the context of a chromosomal abnormality involving a translocation breakpoint between chromosomes 14 and 18 in these leukaemic cells (Tsujimoto *et al.*, 1985). It was initially hypothesized that Bcl-2 promoted oncogenesis through a pro-proliferative effect. However, it subsequently transpired that the cytoprotective effect of Bcl-2 in this malignancy related to its ability to repress cell death (Hockenbery *et al.*, 1993). The juxtaposition of the IgH promoter and enhancer elements upstream of the Bcl-2 coding sequence results in massively heightened levels of the protein in B cell lymphomas (Tsujimoto *et al.*, 1985). This exemplifies how a disruption in the relative levels of pro- and anti-apoptotic molecules can alter a cell's sensitivity to death stimuli. A decreased susceptibility to death may then allow the acquisition of further proliferative advantages. This principle has been aptly demonstrated by studies that show a cooperative effect of deregulated c-Myc expression alongside increased Bcl-2 levels in transformed cells (Vaux *et al.*, 1988; Bissonnette *et al.*, 1992).

1.3.2. Immune disorders

Apoptosis plays a key role in regulating one of the key effector components of the immune system: T lymphocytes (Nagata, 1997). One of the most important functions of cytotoxic T-lymphocytes (CTLs) lies in their ability to induce apoptosis in certain target cells displaying non-self peptides. For example, cells that are abnormal due to being infected or transformed, are CTL targets (Abbas, 1996). T cells thus represent a means of immune surveillance, whereby cells that in some way stand out as aberrant, get detected and deleted before further harm can manifest.

In order to explain how mutations in the cell death machinery can impair normal immune function, it is first necessary to deal briefly with the biology

of one of the most important cell death effector mechanisms of the immune system: the Fas (CD95R/CD95L) system (Abbas, 1996; Nagata, 1997). This is one of several systems that ultimately engage cell death via a mechanism of limited proteolysis of strategic cellular protein substrates. In the case of the Fas/CD95 system, binding of an extracellular ligand (known as FasL) to a transmembrane death receptor (FasR) provides a means of engaging a family of cell death proteases called the caspases (Nagata, 1997). These molecules will be discussed in detail later.

Mutations targeting both FasR and FasL result in a variety of similar lymphoproliferative diseases collectively called ALPS (Autoimmune Lymphoproliferative Syndrome) (Cohen and Eisenberg, 1991; Nagata and Suda, 1995; Abbas, 1996). These conditions are typified by a failure in activation-induced death (AICD) of T-cells that arise by clonal expansion. This results in lymphadenopathy and splenomegaly as a result of an accumulation of superfluous T lymphocytes in these lymphoid organs. Interestingly, in addition to mutations targeting the Fas death receptor or Fas ligand, mutations in caspase-10, one of the key family of proteases that modulate the proteolytic changes essential for apoptosis, have been detected in a similar disorder of lymphocyte homeostasis: ALPS type II (Wang *et al.*, 1999).

A further example of how a mutation within the cell death machinery gives rise to neoplasia lies in the phenomonon of immune escape. A limited number of tissues within the body—notably, the eye and testes—enjoy immune privilege (Nagata, 1997). These cells are protected from the negative effects of inflammatory cells and cytotoxic T-lymphocytes through expression of FasL. A similar strategy is adopted in a variety of human tumours (Medema *et al.*, 1999). These tumours may either secrete FasL inappropriately, or harbour defects in other components of the Fas/CD95 pathway. For instance, certain malignant melanomas have been found to express Fas ligand, thus protecting themselves by inducing apoptosis in Fas-sensitive CTLs (Hahne *et al.*, 1996). In addition, upregulation of an endogenous inhibitor of the Fas pathway, cFLIP, has been proposed to contribute to the immune escape of certain tumours (Medema *et al.*, 1999). In a final example, upregulation of a

soluble decoy receptor (DcR3), sequesters FasL away from receptors on the tumour cell, thus facilitating immune escape (Pitti *et al.*, 1998).

The examples above illustrate scenarios where the disease arises from a failure to engage the cell death machinery as would normally be required. In the examples that follow, defects in the regulation of cell death that give rise to unscheduled apoptosis, are operative.

1.3.3. Cardiovascular disease

Inappropriate apoptosis is thought to mediate some of the neuronal loss associated with diseases of the cardiovascular system, such as strokes and coronary heart disease, whereby a temporary blockade of oxygenated blood flow leads to cell death in the brain (Cheng *et al.*, 1998). These disorders initially trigger widespread necrotic cell death in the immediate locality of the blockade, as a result of oxygen and glucose deficiency. However, recent evidence suggests that the subsequent wave of cell death during ischemia may be apoptotic, provoked by less severe hypoxia away from the immediate epicentre of the occlusion. A peptide-based apoptosis inhibitor, Z-VAD-fmk, can attenuate cell death associated with reperfusion injury, suggesting that apoptosis plays a role in the pathology of cardiovascular disease (Cheng *et al.*, 1998).

1.3.4. Neurodegeneration

An increasing body of evidence suggests that apoptosis may play a role in neurodegenerative disorders, such as Alzheimer's disease and Huntington's disease (Yuan and Yankner, 2000). In both cases, it is hypothesized that the accumulation of insoluble protein aggregates provoke neuronal loss. Interestingly, a dominant negative version of one of the caspase family of proteases, caspase-1, has been demonstrated to block progression of the disease in a transgenic mouse model of huntington's disease (Ona *et al.*, 1999). Moreover, there is evidence that caspases play a role in the cleavage of amyloid precursor protein (APP) into the cytotoxic Amyloid-β (Aβ) moiety thought to be responsible for neuronal loss associated with Alzheimer's disease (Gervais *et al.*, 1999). In another example, inappropriate photoreceptor

cell death is thought to contribute to the early onset of blindness in individuals suffering from retinitis pigmentosa (Humphries *et al.*, 1992).

1.3.5. Viruses

Many viruses hijack the death machinery in order either to promote death, or extend the life of the infected cells (Meinl *et al.*, 1998). In many cases, this involves expression of viral relatives of mammalian genes, including homologues of the Bcl-2 family and the caspase inhibitors, crmA and p35 (Clem *et al.*, 1991; Ray *et al.*, 1992; Meinl *et al.*, 1998). The cellular counterparts of these viral proteins will be discussed later.

All of these examples highlight the importance of apoptosis as a principle or secondary determinant in many human diseases. By extension, it is highly desirable that the molecules that regulate cell death be identified and their roles dissected. Resultingly, apoptosis has been the subject of intense research efforts, largely within the past decade. As will be discussed below, our understanding of the molecular basis of this process has been strongly influenced by information gleaned from the study of a simplified model organism: the nematode.

1.4. PROGRAMMED CELL DEATH IN *C.elegans*

1.4.1. Nematode death genes

The first evidence that programmed cell death was under molecular control came from studies of genetic mutants isolated from the nematode, *C.elegans* (Metzstein *et al.*, 1998). This model was successful in revealing a genetic connection underpinning developmentally-regulated cell deaths, largely because the fate of defined individual worm cells can be monitored throughout embryogenesis and development using simple visual microscopy. The use of a pool of worm genetic mutants not only identified candidate death genes, but actually enabled the ordering of these cell death gene products into a single signaling pathway (Hengartner, 1997; Metzstein *et al.*, 1998). Critically, the discovery that many worm cell death proteins resemble their human counterparts, stimulated an explosive effort to unravel the complexities of human cell death. Thus, the basic paradigm established through the study of

worm cell deaths has proved a useful framework from which mammalian cell death can be studied.

In the worm, from a total of 1090 cells generated during hermaphrodite somatic development, 131 are programmed to die (Sulston and Horvitz, 1977; Ellis and Horvitz, 1986; Hengartner, 1997). Intriguingly, monitoring the fate of these cells, the majority of which become deleted during embryogenesis, revealed that specific dying cells were invariant amongst individual worms. Moreover, the death of these cells always occurred at specific times and places during development, strongly suggesting that the process was underpinned by a molecular program (Ellis and Horvitz, 1986; Hengartner, 1997). Of more than 100 candidate mutations isolated that affect PCD or the subsequent engulfment phase, more than a dozen worm cell death genes have been identified (Ellis and Horvitz, 1986; Hengartner, 1997). Collectively, these are named the *ced* genes (cell death abnormal). These genes can be subclassified on the basis of their involvement in: the decision to die, execution of the death program, the engulfment of the doomed cell, or the degradation of the dying phagocytosed corpse (Hengartner, 1997). Those that regulate the execution of the death program will be discussed below.

Three nematode genes, *ced-3* and *ced-4* and *egl-1,* were identified as being essential components for the execution of virtually all worm cell deaths (Ellis and Horvitz, 1986; Yuan and Horvitz, 1990; Hengartner *et al.,* 1992). Initial clues that a cell-autonomous death program existed came from genetic mosaic studies (Yuan and Horvitz, 1990). These revealed a direct correlation between the loss of function of the *ced* genes and the failure of cells harboring the mutations to die (Yuan and Horvitz, 1990).

Intriguingly, loss of one, or combinations of several of the three genes, resulted in identical phenotypes, namely, a failure to ablate the majority of somatic cells normally programmed to die (Hengartner, 1997; Metzstein *et al.,* 1998). This suggested that these molecules cooperated in a common pathway (Hengartner, 1997; Metzstein *et al.,* 1998). Further analysis of worm mutants defective in one or other these genes revealed that *ced*-3 and *ced-4* formed part

of a common suicide pathway. It was thought that *ced-4* exerted its function upsteam of *ced-3*, since overexpression of the *ced-4* gene in worms lacking *ced-3* failed to invoke the death program, whereas overexpressed *ced-3* weakly promoted death in the absence of *ced-4* (Shaham and Horvitz, 1996). Several lines of evidence suggested that the *egl-1* gene (egg laying defective) also played a role within the *ced-3/ced-4* genetic framework (Lavoie *et al.*, 1998). First, the *ced-4* gene was identified within the context of a loss-of-function allele that nullified the cell death promoting characteristics of the *egl-1* gain of function mutant, placing *egl-1* upstream of *ced-4* (Shaham and Horvitz, 1996). Additionally, ectoptic expression of *egl-1* results in unscheduled cell loss, requiring wild type *ced-3* and *ced-4* alleles, demonstrating that these molecules participate in a common death pathway (Conradt and Horvitz, 1998).

A fourth essential regulator of worm programmed cell deaths was also identified: *ced-9* (Hengartner *et al.*, 1992). Interestingly, whereas *ced-3*, *ced-4* and *egl-1* appeared to cooperate to promote apoptosis, overexpression of *ced-9* or ectopic expression of the *ced-9*(n1950) gain of function mutant prevented developmentally scheduled deaths (Hengartner *et al.*, 1992). This resulted in a phenotype essentially identical to worms harbouring loss of function mutations in *ced-3* or *ced-4* (Hengartner *et al.*, 1992). Further proof that *ced-9* suppressed cell death was revealed by the discovery of a *ced-9* loss of function mutant that spontaneously promoted the death of cells normally scheduled to survive (Hengartner *et al.*, 1992). Interestingly, mutations in *ced-3* and *ced-4* were able to counteract the cell loss associated with the *ced-9* mutant, implying that *ced-3*, *ced-4* and *ced-9* operated within the same pathway to regulate worm programmed cell deaths, with *ced-9* lying upstream of *ced-4* and *ced-3* (Hengartner *et al.*, 1992). Moreover, whereas loss of *egl-1* function prevented somatic cell death, as did loss of *ced-3/ced-4* function, the concomitant loss of *ced-9* plus *egl-1* function did not rescue the lethality associated with the loss of *ced-9*. This placed *egl-1* upstream of *ced-9* (Conradt and Horvitz, 1998).

1.4.2. Nematode cell death proteins

On the basis of the genetic analyses described above, a prototypical framework for death was established. However, since this model was assembled from genetic information, exactly how the gene products participated in a common pathway was unknown. Intriguingly, subsequent observations, most of which were published within a single year, revealed that this death pathway was mediated through a series of protein-protein interactions.

These data revealed that CED-4 protein could bind to CED-3, in agreement with the observation that CED-4 expression could activate CED-3 (Irmler *et al.*, 1997; Chinnaiyan *et al.*, 1997a; Seshagiri *et al.*, 1997a; Seshagiri *et al.*, 1997b). In addition, another study reported the physical interaction between CED-9 and CED-4, suggesting that this was the likely means by which the the death promoting properties of CED-4 were repressed (Spector *et al.*, 1997).

Critically, it transpired that CED-3, CED-4 and CED-9 could interact simultaneously and under these conditions, CED-3 failed to be activated (Chinnaiyan *et al.*, 1997b; Wu *et al.*, 1997a). This trimolecular complex perfectly fitted the predictions of the gene hierarchy obtained from the previous genetic studies, summarized in Figure 2. The position of the death promoting EGL-1 protein within this pathway was subsequently confirmed: EGL-1 binds to CED-9 and in doing so displaces the CED-9/CED-4 interaction, thus freeing up the CED-3 activating activity of CED-4 (del Peso *et al.*, 1998; del Peso *et al.*, 2000). Moreover, the binding of EGL-1 to CED-9 induces a relocalization of CED-4 from mitochondrial membranes to the cytosol (del Peso *et al.*, 1998). Since a previous report suggested that co-expression of CED-9 changed the localization of CED-4 to a punctate, mitochondrial-like distribution, this suggested that EGL-1 freed CED-4 of its CED-9 mitochondrial tether, thereby explaining its role upstream of CED-9 in the pathway (Wu *et al.*, 1997b; del Peso *et al.*, 1998). Finally, a study by Yang and colleagues (Yang *et al.*, 1998a) completed the picture with the observation that CED-4 appeared to form oligomers and in doing so, activate CED-3. The significance of this mechanism will be dealt with more extensively later.

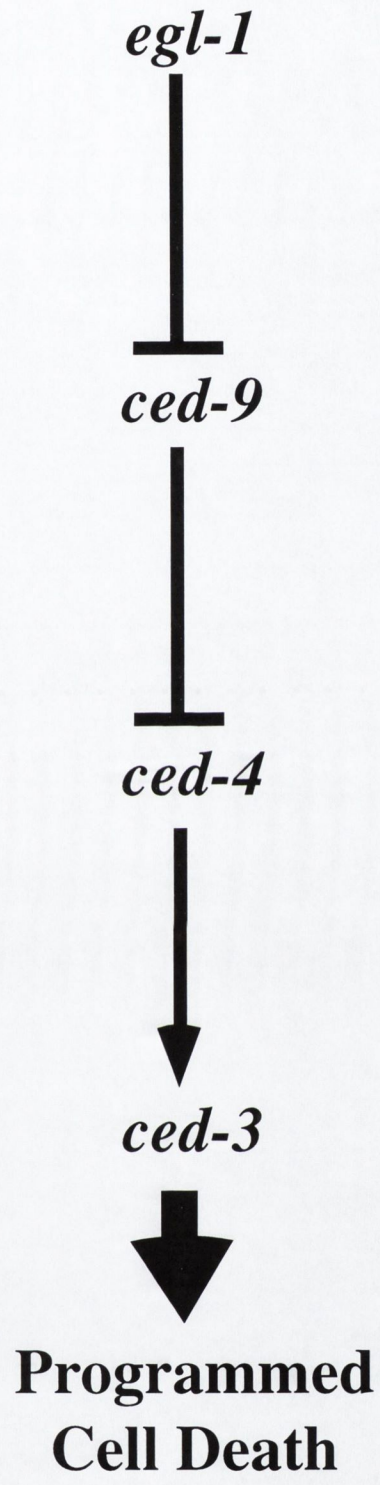

Figure 2

The ordering of *C.elegans* death genes

Diagram illustrating the relative hierarchy in the nematode cell death pathway of the indicated cell death genes, as judged by analysis of genetic mutants. The ability of ***ced-4*** to promote cell death is dependent on ***ced-3***. In turn, the pro-apoptotic effect of ***ced-4*** is nullified by ***ced-9***. The death inhibitory effect of ***ced-9*** upon ***ced-4*** is neutralized by the most proximal component of this pathway—***egl-1***.

The studies described above provided the first evidence that cells direct their own demise, by engaging a defined molecular death program, mediated by a series of protein-protein interactions. The striking discovery that mammalian cell deaths are orchestrated through a similar mechanism, is detailed in the paragraphs that follow.

1.5. MAMMALIAN RELATIVES OF *C.elegans* DEATH GENES

1.5.1 Human ICE and CED-3

The first clue that unlocked the identity of the mammalian executioner came with the discovery that CED-3 had an evolutionarily conserved relative: a human protein called ICE (Yuan and Horvitz, 1993). In 1993, Junying Yuan and Robert Horvitz reported that the CED-3 amino acid sequence resembled that of a cysteine proteinase termed ICE (interleukin-1β converting enzyme). Intriguingly, one year prior to this, ICE had been identified as a protease that mediated the maturation of the cytokine interleukin-1-β specifically through proteolytic cleavage (Thornberry *et al.*, 1992). CED-3 and ICE shared some 29% identity throughout their entire length (Yuan and Horvitz, 1993). Interestingly, a region of significantly higher identity between the two molecules (some 43%) included a completely conserved pentapeptide motif (Yuan and Horvitz, 1993). Since the central cysteine residue (cysteine-285) within this shared QACRG motif was necessary for the proteolytic activity of ICE, this discovery strongly suggested that CED-3 functioned as an ICE-like proteinase (Thornberry *et al.*, 1992; Yuan and Horvitz, 1993). In addition a similar molecule called Nedd-2, identified by Kumar and colleagues within the context of a message upregulated in the developing murine embryonic brain, also shared 27% identity with CED-3 (Kumar and Noda, 1992; Yuan and Horvitz, 1993).

The implications associated with this observation were manifold. Firstly, it appeared that some worm cell death proteins were well conserved in mammals. This increased the value of the framework laid down in the original nematode genetic analyses. Moreover, the discovery that ICE was a cysteinyl protease with an unusual specificity for aspartate residues suggested a molecular mechanism for cell death. This was possibly via cysteinyl protease-

mediated cleavage of as yet undefined cellular substrates (Thornberry *et al.*, 1992; Yuan and Horvitz, 1993). Thus, the concept of apoptosis as a molecular process that culminates in proteolysis, was established.

There were further rich gleanings as a result of this discovery. In characterizing ICE as an IL-1β processing enzyme, Thornberry and colleagues reported that ICE became activated as a result of proteolytic cleavage of a precursor molecule (Thornberry *et al.*, 1992). Interestingly, active ICE could induce the maturation of immature ICE precursor molecules (Thornberry *et al.*, 1992). The aspartate acid residues thought to mediate the maturation of ICE were also conserved in CED-3 (Yuan and Horvitz, 1993). Moreover, in addition Yuan and colleagues reported that six of the eight *ced-3* missense mutations identified in cell death defective worms altered amino acid residues that were identical in wild type CED-3 and ICE proteins (Yuan and Horvitz, 1993). This strongly suggested a shared mechanistic death activity amongst mammals and worms: proteolysis.

The hypothesis that an ICE-like activity may mediate mammalian cell death was further tested (Miura *et al.*, 1993). Intriguingly, overexpression of murine ICE or worm CED-3 induced hallmark apoptotic changes in fibroblasts, suggesting that a cysteine-aspartate proteinase activity was indeed responsible for apoptosis (Miura *et al.*, 1993). As will be detailed in the passages that follow, CED-3, ICE and Nedd-2 constitute the founding members of a family of enzymes called the caspases (Alnemri *et al.*, 1996). Subsequent studies demonstrated that ICE (caspase-1) played a role in cytokine processing rather than in apoptosis *per se*. Nonetheless, these observations were pivotal in initiating a search to find those caspase-1 relatives, that play a key role in apoptosis. Before introducing these caspases, a further landmark discovery will be discussed.

1.5.2. Human Bcl-2: and *C.elegans* CED-9

Further work from the nematologists strengthened the connections between apoptosis in humans and worms. A year following the discovery of the CED-3/ICE connection, it was reported that the CED-9 amino acid sequence resembled human Bcl-2 (Hengartner and Horvitz, 1994). Thus, applying the nematode paradigm, it was hypothesized that Bcl-2 blocked caspase activation by binding to and inhibiting human CED-4 homologues. It is currently unclear whether this particular mechanism is conserved in humans. However, this discovery identified Bcl-2 as an upstream inhibitor of the caspases, albeit probably indirectly in the case of mammalian apoptosis. Thus, the collective evidence suggested that mammalian apoptosis was regulated primarily by promoting or inhibiting caspase activation.

1.6. CASPASES

The discovery that proteolysis constituted the core apoptotic mechanism provoked a frantic research effort to identify CED-3/ICE homologues. As it transpires, there are multiple CED-3 relatives, currently 14 mammalian caspases, of which 12 members have been identified in humans (Slee *et al.*, 1999a; Nicholson, 1999). According to the nomenclature established by a working group in the field, human CED-3-related enzymes are termed caspases (cysteinyl aspartate specific proteases), so-called since they are cysteine proteases possessing an unusual substrate specificity for aspartate amino acid residues (Alnemri *et al.*, 1996). Evidence suggests that caspases are omnipresent in healthy cells as inactive precursor pro-enyzmes. Thus, in many cases, cell death can proceed without the requirement to synthesize components the death machinery (Weil *et al.*, 1996). This explained the observation that inhibitors of transcription and protein synthesis not only fail to block apoptosis, but actually accelerate it (Martin *et al.*, 1990). As will be detailed later, some cell deaths involve *de novo* gene expression and are thus an exception to this general rule.

1.6.1 Caspase structure and activation

Structurally, inactive caspases (procaspases) consist of a large subunit, typically 17-21 kDa in size, flanked by a prodomain at the N-terminus of the molecule

of varying size (3-24kDa) and at the C-terminus by a small subunit of some 10-13 kDa, depending on the individual caspase (Nicholson, 1999) (See Figure 3). The junction between each of these modules is flanked by a tetrapeptide motif, that includes an aspartate residue. This suggests that caspases may be activated by an autoactivation mechanism. It also suggests that a trickle of active caspase can provoke a cascade involving the transactivation of multiple caspase species. This has indeed been verified by experimental evidence and will be discussed in greater detail later and in the general discussion (Chapter VI).

Caspases become converted into their active forms via a two step process (Martin *et al.*, 1996a). As is demonstrated in Figure 4, the first step in caspase-3 activation involves active caspase-mediated cleavage between the large and small subunits of the molecule, generating p12 and p24 moieties (Martin *et al.*, 1996a). This may also be achieved by a non-caspase protease called granzyme B (Martin *et al.*, 1996a). In a secondary step, caspase-3 then proteolytically removes its own prodomain, further truncating the p24 product into the p17 large subunit (Martin *et.al.*, 1996a).

Interestingly, the X-ray cystallographic structures of long prodomain caspase-1 (ICE) and short prodomain caspase-3 revealed that an active caspase molecule is composed of a tetramer consisting of a two large:small subunit heterodimers (p20:p10, caspase-1; p17:p12, caspase-3) (Walker *et al.*, 1994; Mittl *et al.*, 1997). This also revealed that both caspase subunits contribute the residues (S1-S4) required for substrate binding (Walker *et al.*, 1994; Mittl *et al.*, 1997; Nicholson, 1999). The S4 cleft, a major determinant of substrate specificity, resides within the small subunit (Walker *et al.*, 1994; Mittl *et al.*, 1997; Nicholson, 1999). In addition, all caspases possess several conserved hallmark amino acids essential for enzymatic activity (Nicholson, 1999). Most notable of these is the invariant QACXG motif contained within the large subunit, of which the cysteine residue is critical for catalysis (Nicholson, 1999). In addition, a conserved histidine residue that acts in proximity to the active site cysteine, is also thought to play an important catalytic role (Walker *et al.*, 1994).

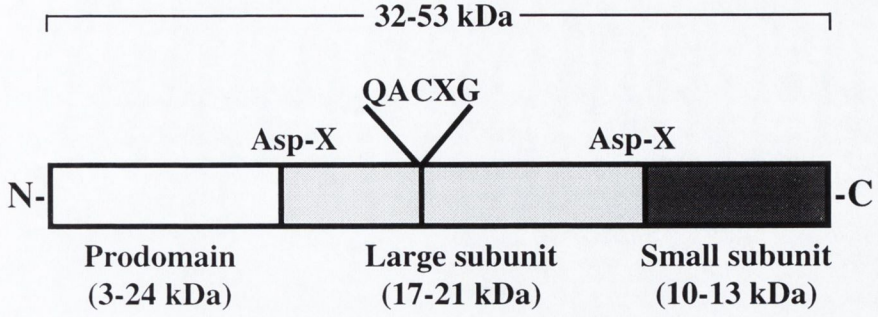

Figure 3

Schematic diagram illustrating the structure of a typical procaspase.

The prodomain, large and small subunits are indicated. The range of sizes in kDa that these respective subunits comprise in different caspase members is shown. Indicated within the large subunit is the conserved active site motif possessing the central cysteine residue. X denotes any amino acid. Also indicated flanking the large subunit is a conserved aspartate residue required for proteolytic cleavage-mediated maturation of the enzyme. Cleavage occurs between the Asp residue at the P1 position and the adjacent residue indicated by "X". The diagram is adapted from Nicholson, 2000.

Table 2

Table indicating the subdivision of caspases based on their tetrapeptide substrate specificity, as reported by Thornberry *et al.*, 1997.

Group	P4	P3	P2	P1	Caspases
I	Hydrophobic	Glu	X	Asp	-1, -4, -5, -13
II	Asp	Glu	X	Asp	-2, -3, -7
III	Aliphatic	Glu	X	Asp	-6, -8, -9, -10

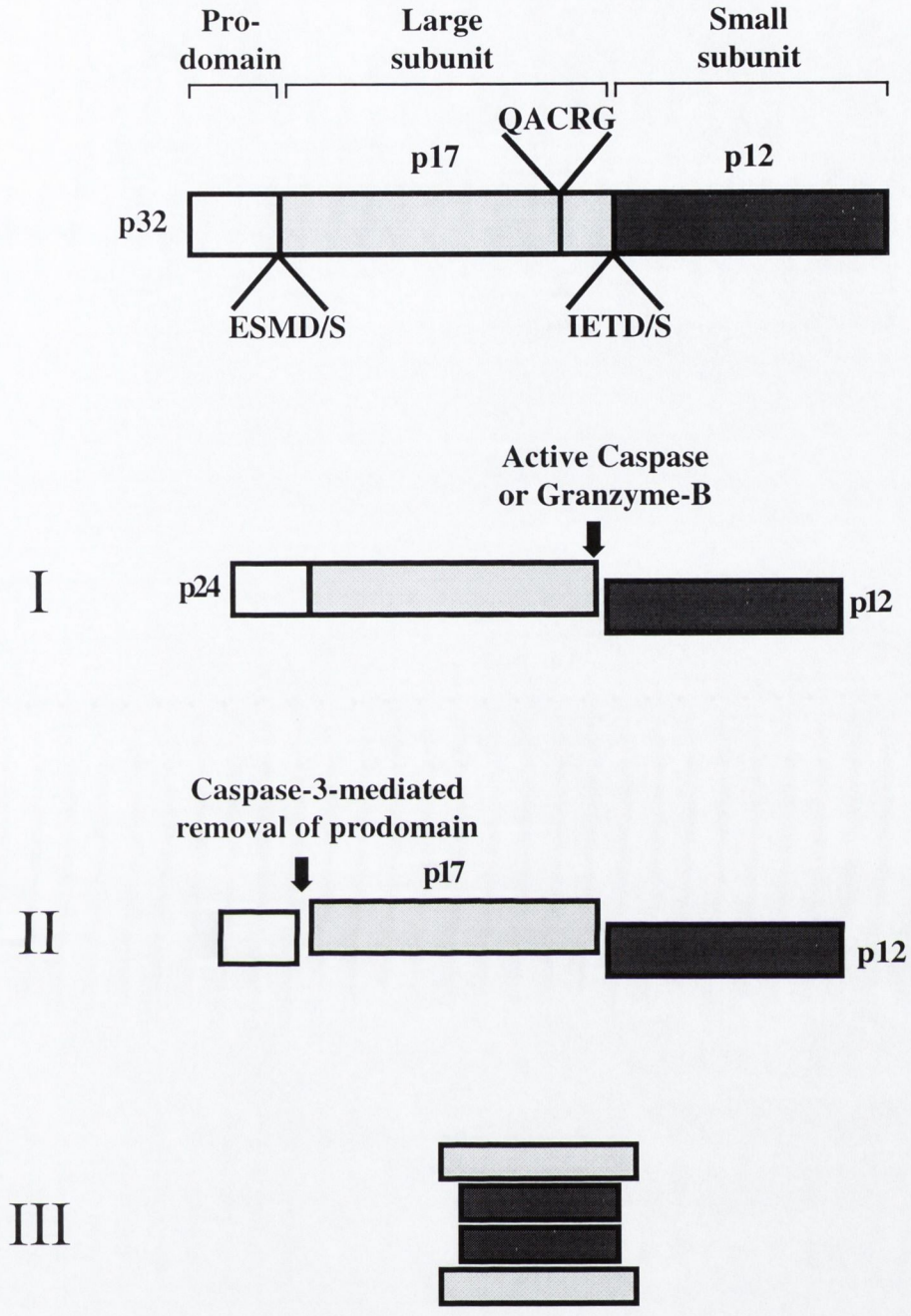

Figure 4

Activation of caspase-3 during apoptosis.

Schematic diagram illustrating the two-step mechanism involved in the maturation of caspase-3. Inactive procaspase-3 is a ~32 kDa molecule composed of large and small subunits and a N-terminal prodomain. Indicated are the active site QACRG motif within the large subunit and the tetrapeptide motifs flanking the large subunit that represent the sites of proteolytic processing. The cleavage site after the P1 aspartate residue is indicated by "/". Numbers refer to the molecular weight in kDa of the subunits or cleavage products.

Activation of the molecule is initiated by cleavage between the large and small subunits (**I**) by an active caspase species or by Granzyme-B. Active caspase-3 then facilitates removal of its own prodomain as indicated (**II**). Finally, the mature enzyme assumes a tetrameric structure, composed of a core of two small subunits flanked on the periphery by two large subunits (**III**).

1.6.2. Criteria for subdividing the caspases

Caspase family members can be subdivided according to a variety of criteria. However, it is important to note that none of these classifications completely mirrors their role in apoptosis. Based on structural criteria, in particular, the length of the N-terminal prodomain, caspases can be demarcated either into long or short prodomain species. There have been attempts to make functional inferences based on this criterion alone, namely that the long prodomain species tend to occupy apical signaling roles, while short prodomain caspases function as downstream executioners. This useful guideline is not unilaterally applicable. Nonetheless, evidence suggests that all of the long pro-domain caspases can be recruited by adaptor molecules that promote their activation during apoptosis. This interaction is mediated through a conserved motif within the prodomain called the CARD domain (caspase recruitment domain) (Hofmann *et al.*, 1997). CARDs and their structurally and functionally similar relative, the death effector domain (DED) are characterized by an abundance of leucines or similar aliphatic amino acids in addition to conserved acidic and basic amino acids within the prodomain (Hofmann *et al.*, 1997). Structurally, the CARD motif is composed of six α-helices (Hofmann *et al.*, 1997).

Another means of subdividing the caspases relies on their preferred substrate specificity—as identified by a combinatorial screening approach using tetrapeptides (Thornberry *et al.*, 1997). All caspases have a stringent tetrapeptide substrate profile (NH_3-P4-P3-P2-P1-COOH) that is characterized by an invariant requirement for an aspartate residue in the P1 position (Thornberry *et al.*, 1997). This is the site where proteolytic scission occurs in substrate proteins. In addition to this essential determinant, the combinatorial approach identified a preference for hydrophobic residues in the P4 position of so-called group I caspases (caspases-1, -4, -5 and -13); an aspartate preference for group II caspases (-2, -3, -7 and CED-3); finally, the preference for a P4 aliphatic residue in group III caspases (-6,-8,-9,-10; as well as aspase, Granzyme B) (Thornberry *et al.*, 1997). This information is summarized in Table-2. This does not easily explain the presence of short pro-domain caspase-6 amongst established initiator caspases, or explain the presence of CARD-bearing

caspase-2 amongst executioner caspases -3 and -7. Nonetheless, it is interesting to note that most of the caspases that bind to adaptor molecules (with the exception of caspase-6) fall into group III; the caspases that are thought to mediate key substrate proteolytic events, group II, and the caspases that are thought to have an involvement primarily in cytokine processing, rather than apoptosis, *per se*, group I (Thornberry *et al.*, 1997).

Another way of subdividing the members of the caspase family—generating a dendogram based on multiple alignment data—concurs roughly with the putative subdivisions laid down by combinatorial chemistry (Figure 5). In this analysis, caspases-4 and -5 form a subgroup within a broader ICE subfamily that includes caspase-1. These caspases collectively diverge from the CED-3 subfamily composed of the long and short-prodomain apoptotic caspases. Moreover, the short prodomain caspases thought to mediate key proteolytic events fall into one subfamily (caspases-3, -6 and -7). Finally, caspases-2 and -9 segregate together and caspases -8 and -10, possessing two death effector domains within the prodomain, fall into another distinct subfamily. In conclusion, as yet, no particular classification particularly well fits all of the evidence concerning the role of these proteases *in vivo*.

1.6.3. Non-redundant role of caspases

Since there are multiple human caspases that apparently share overlapping tetrapeptide substrate specificites, one critical question pertinent with respect to therapeutic targeting strategies is: do these molecules actually have overlapping or redundant roles in vivo?

The answers to this essential question are beginning to accumulate, derived largely from knockout (See Table-3) and immunodepletion-based studies (Zheng *et al.*, 1999; Slee *et al.*, 2001). One of the most compelling lessons from gene targeting experiments in caspase-null mice is that most of these molecules occupy non-redundant roles (Zheng *et al.*, 1999). In some cases, the knockout phenotype attributable to the loss of a single caspase is profound. For example, *CASP-9*$^{-/-}$ mice incur abnormal brain development and the phenotype is lethal before or around birth (Hakem *et al.*, 1998; Kuida *et al.*,

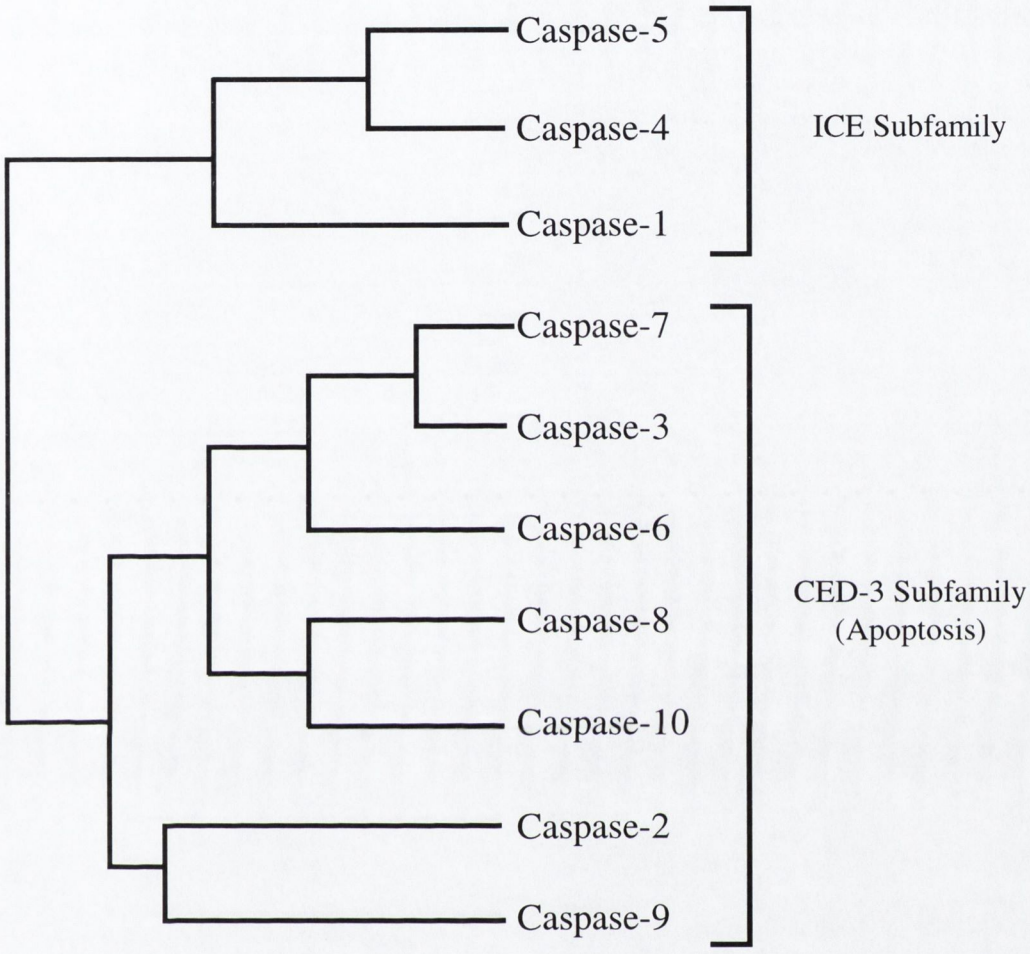

Figure 5

Phylogenetic tree illustrating the relationship between members of the human caspase family. Indicated are the ICE subfamily of cytokine processing enzymes and the caspases that are known to play a role specifically in apoptosis (CED-3 subfamily). The tree is adapted from Alnemri *et al.*, 1996.

Table 3

Summary of the phenotype of mice nullizygous for the indicated caspases.
N/D, not determined. Adapted from Zheng *et al.*, 2000.

Caspase	Developmental phenotype	Apoptotic phenotype	References
Caspase-1	Normal	Fas? (thymocytes)	Kuida *et al.*, 1995; Li *et al.*, 1995
Caspase-2	Normal	Germ cells	Bergeron *et al.*, 1998
Caspase-3	Perinatal lethal	Neuroepithelial progenitors; lack of or delayed morphological changes and DNA fragmentation	Kuida *et al.*, 1996; Woo *et al.*, 1998
Caspase-6	Normal (Unpublished)	N/D	
Caspase-7	Embryonic lethal (Unpublished)	N/D	
Caspase-8	Embryonic lethal	Death receptor (Fas, TNF, DR-3)-MEFs	Varfolomeev *et al.*, 1998
Caspase-9	Embryonic lethal	Neuroepithelial progenitors; mitochondrial defects (dexamethasone, staurosporine, etoposide, g-irradiation pathways impaired) -thymocytes	Kuida *et al.*, 1998; Hakem *et al.*, 1998
Caspase-11	Normal	Fas? (thymocytes)	Wang *et al.*, 1998

1998). *CASP-8*$^{-/-}$ mice also exhibit a severe phenotype including embryonic lethality, abnormal haematopoietic progenitor development and interestingly, abnormal development of heart muscle (Varfolomeev *et al.*, 1998). However, the organs and tissues affected in this instance differ substantially from that exhibited in the *CASP-9*-null counterparts. Thus, it appears that these individual caspases have non-overlapping, distinct roles. While both of these phenotypes are arguably severe, another perspective is that in spite of these defects, the mice actually undergo a surprising amount of development and differentiation, before lethality occurs.

In contrast, long prodomain *CASP-2*-null mice are essentially phenotypically normal, with the exception of a transient accumulation in the number of oocytes (Bergeron *et al.*, 1998). It is therefore difficult to make predictions about the role of a particular caspases as judged by simple structural or *in vitro* substrate criteria alone. This caveat is particularly well illustrated in caspase-3-null mice: obviously the so-called "initiator" caspases are intact in these animals—and thus one may generously assume, available to channel death stimuli as a functional alternative through "executioner" caspases-6 and -7. In fact, *CASP-3*$^{-/-}$ mice actually exhibit a phenotype reminiscent of the caspase-9 knockout, in terms of impaired brain development and perinatal lethality, suggesting that caspases -6 and -7 are incapable of substituting for the absence of caspase-3 (Kuida *et al.*, 1996; Woo *et al.*, 1998).

The non-redundancy of executioner caspases in terms of substrate proteolysis has recently been demonstrated (Slee *et al.*, 2001). Immunodepletion of caspase-3 from cell free extracts halts the proteolysis of the majority of substrates tested when the extracts are triggered to undergo apoptotic changes (Slee *et al.*, 2001). This again suggests that caspases-6 and -7 are not simply functionally-redundant quasi copies of caspase-3 (Slee *et al.*, 2001). Thus, in spite of the relative promiscuity of peptide inhibitors based on a DEXD substrate preference for these executioners, *in vivo* it appears that the choice of substrate is much more restrictive (Thornberry *et al.*, 1997; Slee *et al.*, 2001).

This could relate to steric contraints placed on the substrate cleavage site within the context of the full-length molecule, as opposed to a simple tetrapeptide, particularly the P4 site. Further reasons that may account for this non-redundancy may relate to temporal or spatial restrictions in caspase expression (Zheng *et al.*, 1999). In particular, it is interesting to note that in addition to maintaining a general presence within the cytoplasm, individual caspases may reside in other cellular compartments. For instance, there is evidence that caspases -2 and -9 may reside within the nuclear compartment (Colussi *et al.*, 1998; Ritter *et al.*, 2000). In addition, there is evidence to suggest that caspases-2,-9 and -3 may undergo release from mitochondria during the apoptotic program (Mancini *et al.*, 1998; Krajewski *et al.*, 1999; Zhivotovsky *et al.*, 1999). During apoptosis, caspase-3 may translocate to the nucleus, whereas caspase-7 is found in association with microsomes (Zhivotovsky *et al.*, 1999). Finally, caspase-12 may sublocalize to the ER, the locality where it may exert its pro-apoptotic effects, as suggested by knockout studies (Nakagawa *et al.*, 2000).

1.6.4. Functional consequences of caspase activation

In conclusion, since proteolysis forms an irreversible step on the path to cell death, caspases constitute an essential core of the suicide machinery. Indeed, as is aptly demonstrated by studies using both the pan-caspase inhibitor Z-VAD.fmk, as well as similar aspartate-based tetrapeptide drugs presumed to act more locally on specific caspases or caspase subfamilies, caspases are clearly indispensible for apoptosis (Nicholson *et al.*, 1995). Given the absolute requirement for these enzymes, what is the functional consequence of caspase-mediated proteolysis during apoptosis?

Caspase substrates can be conveniently subdivided into proteolytic events that active a death-promoting factor, those that disable a mechanism essential for survival, or those that promote the structural dismantlement of the cell (Nicholson, 1999). In terms of disabling a cellular mechanism, substrates include the DNA repair enzyme, PARP (poly(ADP-ribose) polymerase) and cell cycle regulatory molecules such as the PITSLRE kinases (Nicholson, 1999). During disassembly of cellular structures, caspase substrates such as nuclear lamins A and B and actin are cleaved by active caspases (Nicholson, 1999).

1.6.4.1. Phagocytosis

Arguably, one of the most critical caspase-mediated events involves the changes that a dying cell undergoes that enables it to be recognized and engulfed by phagocytes. This endpoint is important for two reasons. First, it provides a convenient means of ridding the surrounding tissue of apoptotic corpses required for organ morphogenesis. Additionally, it is imperative that the apoptotic cell is removed from the surrounding environment before the corpse undergoes a loss of plasma membrane integrity associated with secondary necrosis. Failure to do this would otherwise lead to an undesirable pro-inflammatory response within the locality.

One caspase-dependent mechanism that has been identified as important in facilitating the engulfment of dying cells involves the externalization of a phospholipid called phosphatidylserine (PS) (Fadok *et al.*, 1992; Martin *et al.*, 1996b). Interestingly in healthy cells, PS is confined to the inner leaflet of the plasma membrane. Induction of the death program in diverse cell types triggers a radical reorganization in the lipid membrane, leading to exposure of PS on the surface of dying cells (Fadok *et al.*, 1992; Martin *et al.*, 1996b). Moreover, studies using the PS-specific probe, Annexin V, demonstrate that PS exposure is actually an earlier event than the changes associated with the apoptotic nucleus (Martin *et al.*, 1995c).

The requirement for PS exposure to enable macrophage engulfment of apoptotic cells was demonstrated in a study by Fadok and colleagues (Fadok *et al.*, 1992). Macrophages isolated from the murine peritoneal cavity were unable to recognize apoptotic cells when co-incubated with PS liposomes (Fadok *et al.*, 1992). Intriguingly, further evidence for the requirement for PS externalization in engulfment came from another study that identified a human receptor capable of mediating PS-dependent phagocytosis (Fadok *et al.*, 2000). Phagocytic cells expressing the receptor were incapable of engulfing apoptotic cells when incubated with an antibody specific to the receptor (Fadok *et al.*, 2000). In addition, expression of the receptor enabled non-phagocytic Jurkat cells to engulf apoptotic cells (Fadok *et al.*, 2000). Interestingly, current

evidence suggests that lipid membrane reorganization and PS exposure may occur not only in the dying cell, but also in the engulfing cell (Marguet *et al.*, 1999). This notion was strengthened by the identification of the human homologue of the *C.elegans ced-7* engulfment gene, ABC1, that appears to promote engulfment of dead cells by promoting a redistribution of the lipid bilayer that induces PS externalization (Hamon *et al.*, 2000).

1.6.4.2. Nucleases

Caspases also switch on the molecules responsible for generating the apoptotic nucleus. In the case of DNA fragmentation, this is achieved by caspase-3-mediated cleavage of an inhibitor of the nuclease CAD (caspase activated deoxyribonuclease). Within the cytosol of healthy cells, the binding of the inhibitor, ICAD, muzzles CAD activity. However, cleavage of ICAD releases CAD, promoting its nuclear import. This facilitates internucleosomal DNA degradation (Sakahira *et al.*, 1998; Enari *et al.*, 1998). Similarly, the C-terminal caspase-3 cleavage product of Acinus (apoptotic chromatin condenser in the nucleus) undergoes nuclear import, wherein it promotes chromatin condensation (Sahara *et al.*, 1999).

1.7 REGULATION OF CASPASE ACTIVITY

1.7.1 Caspase inhibitory proteins

Since caspases bear the critical reponsibility as to whether a cell lives or dies, many molecules that can prevent cell death do so by inhibiting these enzymes. There are two main scenarios where it is desirable to limit or block caspase activity. First, in healthy cells, endogenous inhibitors of caspases or caspase activation dampen down any unscheduled, accidental caspase activation that may endanger an otherwise normally functioning cell. This sets the threshold of susceptibility of a given cell to prevailing stimuli. In another example, the genome of many viruses encode caspase inhibitors that act to suppress the suicide attempt of the host cell upon infection, thus maximizing the ability of the virus to replicate and productively infect further cells (Meinl *et al.*, 1998).

1.7.1.2. Caspase pseudosubstrates

One strategy adopted by viral caspase inhibitors amounts to playing the role of a decoy substrate, or pseudosubstrate for active caspases. The baculovirus p35 protein inhibits cell death by acting as a caspase substrate, achieved by possession of a tetrapeptide caspase cleavage site (Clem *et al.*, 1991; Xue and Horvitz, 1995). Interestingly, in addition to undergoing cleavage, this protein forms stoichiometric complexes with active caspases, thus blocking their activity (Bump *et al.*, 1995).

A further class of molecules, the serpins, suppress caspase activity in a similar manner, as caspase substrates and competitive inhibitors (Ray *et al.*, 1992; Enari *et al.*, 1995). The prototypical member of this family, the cowpox serpin CrmA, dampens down pro-inflammatory responses in infected cells by blocking the proIL-1β processing activity of caspase-1 (Ray *et al.*, 1992; Xue and Horvitz, 1995). When transfected into human cells, CrmA can also successfully inhibit the proximal protease in the Fas/TNFR pathway: caspase-8, thus suggesting that serpins can inhibit apoptosis as well as cytokine processing (Zhou *et al.*, 1997). Since mammalian serpins have been identified, it is likely that these molecules are present as endogenous inhibitors of caspase activity in non-infected cells (Young *et al.*, 2000).

1.7.1.3. The IAPs

A further class of inhibitory molecules, the IAPs (inhibitor of apoptosis proteins) also have a specificity for individual caspases. For instance, human IAPs cIAP-1 and -2 are effective inhibitors of caspases-3 and -7, whereas they are ineffective in blocking the activity of caspases -1, -6 and -8 (Roy *et al.*, 1997). How these molecules actually target caspases is currently unclear. However, evidence suggests that IAPs may prevent both caspase activation and activity. In the case of XIAP inhibition of caspase-9, this involves interaction between the molecules (Deveraux *et al.*, 1998). However, it remains to be seen if this involves the formation of a stable stoichiometric complex, since several *in vitro* studies that reported the inhibitory properties of these molecules have employed massively higher molar ratios of IAP: caspases (Roy *et al.*, 1997; Deveraux *et al.*, 1998). Interestingly, some IAPs actually possess CARDS,

although an inhibitory role specific to this domain has yet to be demonstrated. Moreover, a region known as the BIR (baculovirus IAP repeats), common to all IAPs has been demonstrated to be necessary and sufficient to modulate the inhibitory effects of these molecules, suggesting a non-essential role for the IAP CARD in caspase inhibition (Takahashi *et al.*, 1998). Moreover, the so-called executioner caspases lack the CARD interaction motif, yet are readily inhibited by these molecules. Interestingly, similarly to the p35 and crmA, XIAP is cleaved in apoptotic cells. However, since one of the BIR domains of this molecule from a region outside of the caspase cleavage site, is sufficient to block death, XIAP cleavage may not be the primary mechanism by which this molecule inhibits caspases (Takahashi *et al.*, 1998). Finally, another hypothesis suggests that these molecules may act as ubiquitin ligases, stimulating the proteasome-mediated removal of certain target proteins. While current data suggests that they may catalyze their own removal in this manner, it remains to be proven conclusively whether they also target caspases for degradation (Yang *et al.*, 2000).

1.7.2 The induced proximity model

How is caspase activation achieved? As has been discussed, the presence of aspartate residues in the regions flanking the caspase large subunit suggests that caspases may undergo self-activation and may process other dormant caspase molecules. A variety of evidence supports the "induced proximity" model of caspase activation (Salvesen and Dixit, 1999). This model hypothesizes that caspases in their inactive zymogen form possess a latent degree of catalytic activity sufficient to mediate autoactivation if multiple caspase molecules are brought into close enough proximity. The first evidence in support of the induced proximity model came from a study using transgenic murine thymocytes expressing a membrane-targeted FKBP-fusion (FK102 binding protein) of the cytoplasmic portion of the Fas receptor (Spencer *et al.*, 1996). Upon exposure to a drug that induced dimerization of the fusion protein, these cells underwent apoptosis. This notion of death receptor aggregation as a means of triggering the death program was supported by several other lines of evidence. First, the cognate ligands of the Fas and TNF receptors exist in a multimeric form, consistent with the notion of ligand-

induced receptor multimerization (Tanaka *et al.*, 1995; Suda *et al.*, 1993). Second, several of the antibodies generated against the Fas/Apo-1 receptor exhibited death agonistic properties and these were indeed multimeric in structure, either as a result of being of the IgM antibody subclass, or in the case of the anti-Apo-1 antibody, the IgG_3 species that is known to form aggregates (Yonehara *et al.*, 1989; Trauth *et al.*, 1989). Moreover, it was appreciated from a much wider cell biology field that the binding of a ligand to its cognate receptor frequently causes a phenomenon called 'capping', resulting in a localized cluster of multiple receptor: ligand aggregates.

While it was suspected that aggregation of death receptors induced by ligand binding constituted the death signal in a variety of cellular contexts, it was not appreciated how this mechanism was transduced into caspase activation. This perplexing question was answered in 1996/1997 by several groups, headed by Vishva Dixit, Marcus Peter and David Wallach (Muzio *et al.*, 1996; Bolden *et al.*, 1996; Medema *et al.*, 1997). Strikingly, the connection between the caspase component of the death machine and the Fas and TNFR-1 receptors was surprisingly intimate: achieved through a single mutual molecular intermediary, FADD. This bipartite death adaptor modulates the recruitment of caspase-8 into death receptor aggregates via through two homophilic interactions: firstly, between the death effector domains of FADD and caspase-8, and secondly, via the death domains of FADD and the Fas/CD95 or TNFR-1 receptors (Muzio *et al.*, 1996; Bolden *et al.*, 1996; Medema *et al.*, 1997).

Further studies using FKBP-caspase-8 fusions confirmed that induced aggregation of the proenzyme was indeed sufficient to induce its activation (Yang *et al.*, 1998b) This highlighted the simplicity of the caspase activation process. Moreover, this study revealed that whereas caspase-1 could be inducibly activated using the same system, short prodomain caspase-3 failed to become activated when forceably aggregated (Yang *et al.*, 1998b). These data are thus consistent with a model whereby the apical caspase activating signal is an aggregation based mechanism, whereas executioner caspases must undergo maturation as a result of proteolytic cleavage by an active caspase. While this is undoubtedly a useful working model, it is worth noting the tentative caveat

that peptides containing the RGD motif (known to inhibit cell/extracellular matrix contact) may induce the activation of caspase-3 directly, possibly by inducing a conformational change in the molecule (Buckley *et al.*, 1999). Finally, further evidence in favour of the induced proximity model came from the observation that worm CED-4 could aggregate—and thus activate—CED-3, suggesting that a common caspase activating mechanism was conserved between nematodes and mammals (Yang *et al.*, 1998a).

1.7.2. Caspase Activating pathways

While apoptosis can be induced by a broad range of stimuli (Table-1), surprisingly, current understanding suggests that there are probably four major cell death pathways upon which most of these diverse stimuli converge at the point of caspase activation.

1.7.2.1. Death receptors

Until recently, our understanding of the molecular specifics of cell death signaling was restricted to the biology of the death receptors of the TNF (tumour necrosis family) (Ashkenazi and Dixit, 1998). As has already been partially illustrated, the death receptors (Fas, TNFR-1, DR-3, DR-4, DR-5 and DR-6) provide a membrane-localized point at which caspases can be aggregated (Kitson *et al.*, 1996; Pan *et al.*, 1997a; Pan *et al.*, 1997b; Nagata, 1997; Walczak *et al.*, 1997; Pan *et al.*, 1998a). In this example of death signaling, extracellular ligands of the TNF family bind their cognate transmembrane death receptor, thus provoking the aggregation of a target initiator caspase such as caspase-8, via bipartite adaptor molecules such as FADD (specific to caspase-8) and RAIDD (specific to caspase-2) (Boldin *et al.*, 1996; Duan and Dixit, 1997). Death receptor-mediated caspase activation is illustrated in Figure 6.

1.7.2.2. Granzyme-B

A second mechanism utilized in cell deaths characterized by CTL-mediated killing, involves the serine protease Granzyme B, the only non-caspase protease that has a substrate preference for aspartate residues. In addition to issuing the kiss of death through the Fas death receptor system described previously, these cells can also provoke death by releasing cytotoxic granules

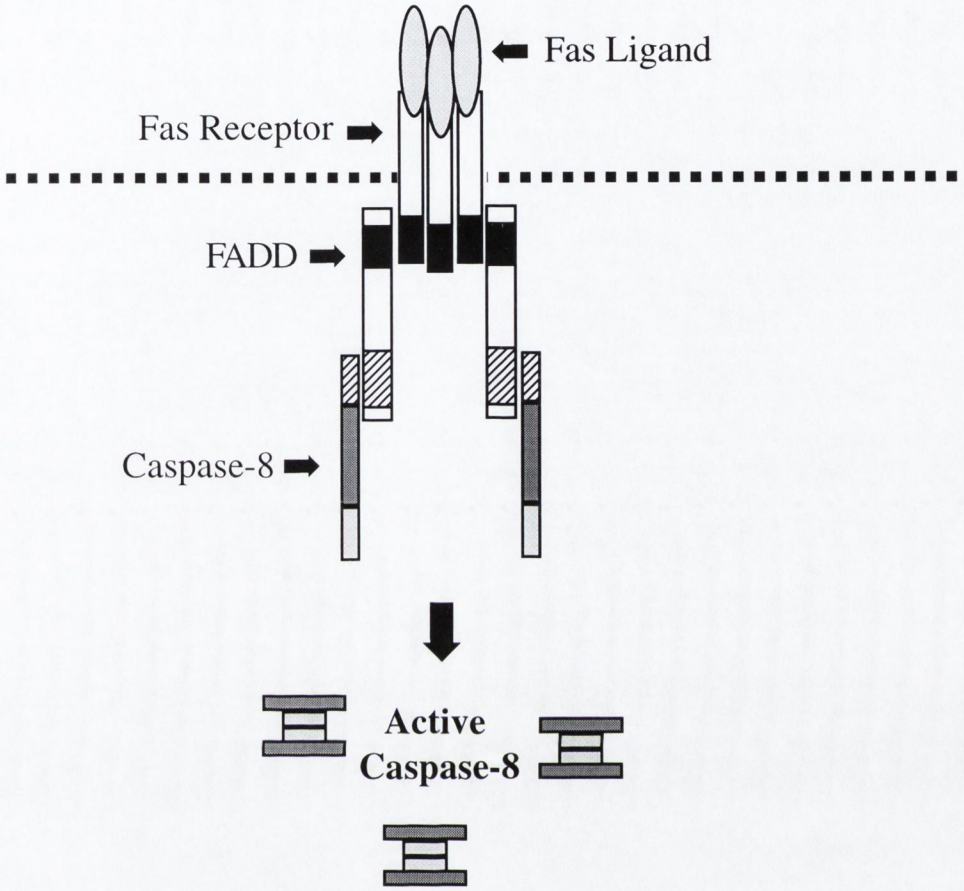

Figure 6

Death receptor-mediated activation of caspases.

Schematic diagram illustrating activation of caspase-8 via ligation of the Fas transmembrane death receptor. Binding of multimeric Fas Ligand (FasL) to the extracellular moiety of the Fas Receptor (FasR) induces aggregation of the intracellular, death domain-containing portions. This enables adaptor molecule FADD to recruit procaspase-8 into a membrane-localized aggregate, thus promoting the proximity-induced autocatalytic activation of the molecule and its subsequent assembly into the mature tetrameric structure.

harbouring Granzyme B. Upon entry into the target cell, assisted by CTL granule component perforin, Granzyme B kick-strarts the apoptotic machinery by activating caspase-3 (Martin *et al.*, 1996a). The necessity of this pathway in CTL-mediated killing is demonstrated by targeted deletion of Granzyme B in mice, since these animals incur impaired CTL-mediated target cell killing (Heusel *et al*, 1994; Shresta *et al.*, 1995).

1.7.2.3. Nuclear stimuli

A third mechanism lies in the ability of cells to commit suicide in response to nuclear damage. Evidence suggests that many DNA damage-related cell deaths are executed through a p53-mediated transcriptionally dependent system (Miyashita and Reed, 1995; Polyak *et al.*, 1997; Komatsu *et al.*, 2000 Oda *et al.*, 2000; Lin *et al.*, 2000). However, p53-dependent but transcriptionally independent cell deaths have also been reported (Caelles *et al.*,1994). While the proximal signaling events leading to p53-dependent apoptosis are not as yet fully clear, this involves an accumulation in p53 protein levels (Fritsche *et al.*, 1993). Normally, the cellular levels of p53 are stringently held in check via proteasome-mediated degradation of the molecule as a result of its association with the ubiquitin ligase, MDM-2 (Haupt *et al.*, 1997). Amino acid residue, serine 20, within the N-terminus of p53 is important in mediating this association (Unger *et al.*, 1999; Shieh *et al.*, 1999).

Downstream of DNA damage, a kinase cascade is reponsible for the stabilization of p53 (Caspari, 2000; Matsuoka *et al.*, 1998; Chehab *et al.*, 2000; Shieh *et al.*, 2000; Tibbetts *et al.*, 1999). This partially characterized pathway is summarized in Figure 7. In response to DNA damage, the kinases thusfar identified to be most proximal to the DNA damaging stimulus—ATM and ATR—phosphorylate downstream kinases, CHK-1 and CHK-2, respectively. In turn, either of these downstream kinases can phosphorylate p53 at serine-20 (Chebab *et al.*, 2000; Shieh *et al.*, 2000). This likely alters the ability of p53 to associate with MDM-2, promoting dissociation of p53/MDM-2 complexes, therefore preventing degradation of p53. Moreover, MDM-2 may be directly phosphorylated by ATM in response to ionizing radiation, thereby providing a

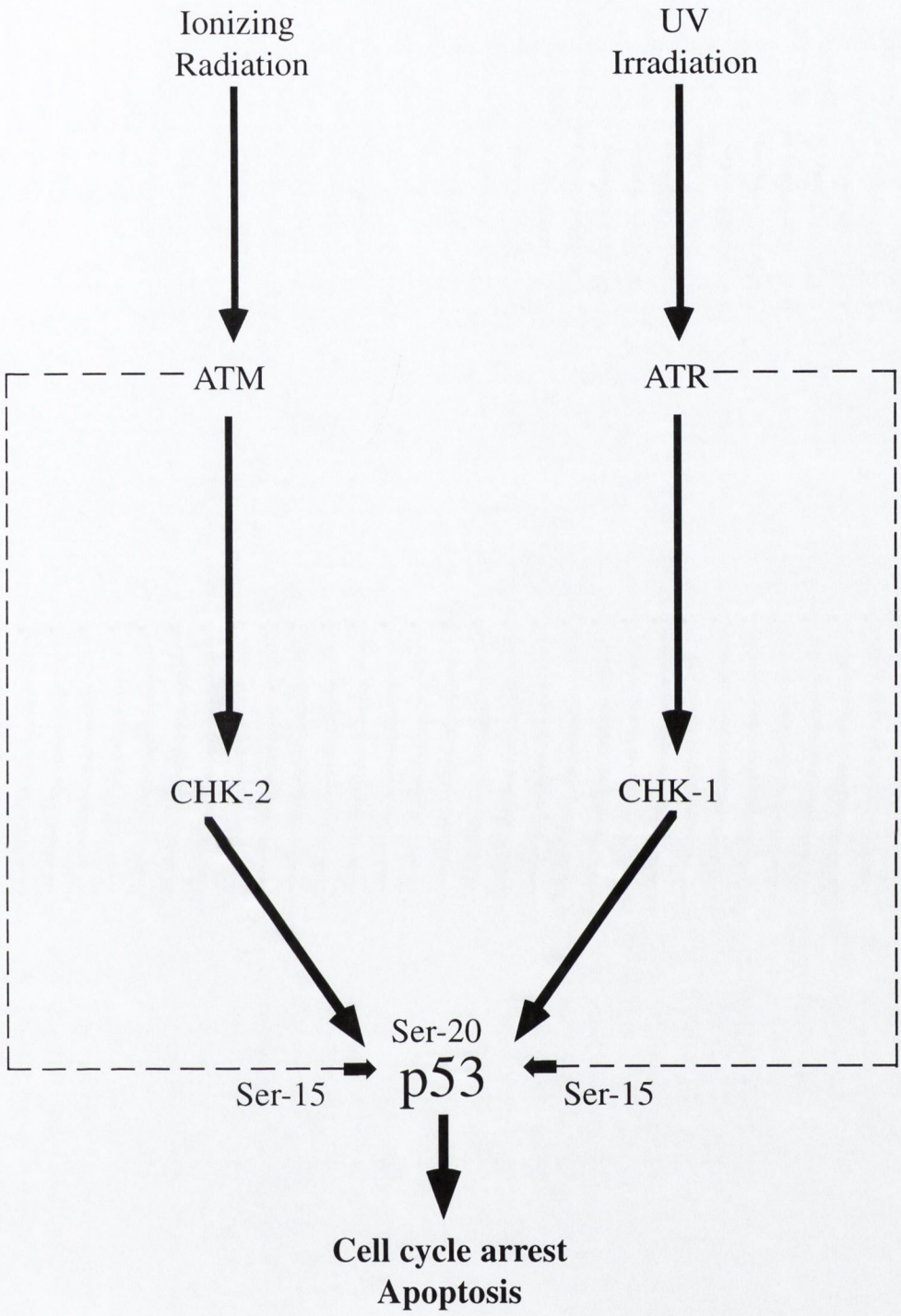

Figure 7

Diagram illustrating how DNA damaging stimuli achieve stabilization of p53 via a kinase cascade involving ATM/ATR and the human homologues of yeast checkpoint kinases, CHK-1/CHK-2. Phosphorylation of either CHK-1 or CHK-2 by upstream kinases ATM or ATR results in their activation and subsequent phosphorylation of p53 at residue serine-20. This results in dissociation of p53/MDM-2 complexes, increasing the cellular levels of p53, facilitating expression of cell cycle arrest or apoptosis genes. Also indicated is the pathway where upstream kinases ATM and ATR directly phosphorylate p53 on residue serine-15, thereby increasing the affinity of the molecule for transcriptional activator CBP, promoting p53-dependent gene expression.

further means of disrupting the binding of this molecule to p53. (Khosravi *et al.*, 1999).

In addition, it is known that ATM and ATR can actually phosphorylate p53 directly, at serine 15 within the N-terminal transcriptional activation domain of the molecule (Siliciano *et al.*, 1997; Tibbetts *et al.*, 1999). However, this modification is thought to mediate enhanced binding of p53 to the CBP transcriptional activator protein, rather than affecting the p53/MDM-2 association (Dumaz and Meek, 1999). Thus, DNA damage appears to have at least two distinct effects on p53: increasing the stabiliy and enhancing the transcriptional ability of the molecule, mediated directly and indirectly by ATM and ATR. In addition, evidence suggests that ATM acts to stabilize p53 in response to ionizing radiation (IR), whereas ATR may play a role in signal transduction resulting from UV irradiation (Lu and Lane, 1993; Siliciano *et al.*, 1997; Tibbetts *et al.*, 1999).

Interestingly, evidence suggests that the ability of p53 to upregulate genes involved in cell cycle arrest can be separated from its capacity as a transcriptional mediator of apoptosis (Haupt *et al.*, 1995). Thus, depending on the perceived severity of the cellular assault, stimuli that have established cell-cycle arresting properties seem to provoke expression of a different set of p53 target genes in dying as apposed to cell cycle-arresting cells (Zhao *et al.*, 2000).

1.8. MITOCHONDRIAL CONTROL OF APOPTOSIS

Intriguingly, the third major cell-autonomous suicide mechanism involves the cellular powerhouse: the mitochondrion. An accumulating body of evidence suggests that many cell deaths are regulated through the translocation of several important apoptogenic factors from the mitochondrial intermembrane space into the cytosol (Adrain and Martin, 2001; Green, 2000). These include cytochrome *c*; a nuclease called AIF; (apoptosis-inducing factor) and the IAP-neutralizing pro-apoptotic molecule, Smac/Diablo (Liu *et al.*, 1996; Susin *et al.*, 1999; Verhagen *et al.*, 2000; Du *et al.*, 2000). Surprising as it seems, in addition to its essential role as a key player in the production of ATP (the cell's principal energy currency), cytochrome *c* plays a role as an

intracellular death-inducing ligand (Mathews, 1985; Liu *et al.*, 1996; Zhivotovsky *et al.*, 1998; Slee *et al.*, 1999b). In terms of its caspase-activating abilities, cytosolic cytochrome *c* could be considered analogous to the extracellular ligands that mediate death receptor-dependent apoptosis.

How was this seemingly bizarre connection between the mitochondrial powerhouse and the death machinery realized? For some time it had been suspected that mitochondria may play some role during the apoptotic program. For instance, Guido Kroemer and colleagues observed that upon induction of the death program by various cytotoxic drugs, mitochondria in these cells appeared to lose their integrity (Zamzami *et al.*, 1996; Marzo *et al.*, 1998; Susin *et al.*, 1998). This was judged by a readout called permeability transition, whereby mitochondrial function becomes disrupted and the electron transport system becomes uncoupled.

One of the first suggestions that mitochondria may play a direct role apoptosis came from the use of a cell-free system derived from *Xenopus* egg extracts (Newmeyer *et al.*, 1994). Using this system, Donald Newmeyer and colleagues routinely performed nuclear assembly and import assays on eggs derived from female *Xenopus* frogs that had been stimulated to undergo oogenesis as a result of injection of Pregnant Mare Serum Gonadotrophin (Newmewyer *et al.*, 1994). Eggs routinely stripped from frogs 3-10 days following stimulation readily supported both the nuclear assembly and import phenomena studied by this group. Eggs obtained from similar frogs at a later timepoint, some 14-28 days post-stimulation, also initially exhibited normal readouts for nuclear assembly and import. However, 2-4 hours after initiation of the experiment using the older eggs, the extracts appeared to exhibit some of the hallmark features of apoptosis, including DNA condensation and fragmentation (Newmeyer *et al.*, 1994). Moreover, addition of Bcl-2 blocked these events, suggesting that this phenomenon involved apoptosis. Presumably, the eggs that were harvested later were primed to die, perhaps as part of a program designed to facilitate the resorption of eggs in female *Xenopus* frogs when mating failed to occur within a defined time following oogenesis. To characterize this feature of the extracts, Newmeyer and colleagues then refined

the extracts into cytosolic, light membrane and heavy membrane fractions (Newmeyer *et al.*, 1994). Extracts composed of cytosol only, or cytosol plus light membrane fractions now failed to support these apoptotic changes. However, extracts supplemented with the heavy membrane fraction became apoptotic. Since these extracts were particularly enriched with mitochondria—as judged by electron microscopy of the heavy membrane fraction—the suspicion thus fell on this organelle as a putative instigator of the death programme, at least in *Xenopus* cells.

1.8.1. Cytochrome *c*

In, 1996 suspicions concerning the possibility that mitochondria might regulate apoptosis were confirmed in an elegant study by Xiaodong Wang and colleagues (Liu *et al.*, 1996). Using a mammalian cell-free extract from healthy Hela cells, Wang and co-workers searched for a means of triggering induction of the death program *in vitro* by adding an apoptosis-inducing agent into the extracts. The utility of mammalian cell extracts as an *in vitro* tool for dissecting apoptotic signaling, including hallmark apoptotic changes such as caspase activation, substrate cleavage and nuclear fragmentation, had been previously demonstrated (Martin *et al.*, 1995d). However, these authors stimulated cells to die in advance of harvesting them for extracts (Martin *et al.*, 1995d). Using extracts made from healthy cells, Wang and colleagues discovered that addition of dATP actually forced otherwise non-apoptotic extracts to succumb to the death program. These extracts spontaneously underwent hallmark apoptotic changes, including enhanced activation of cell death protease caspase-3 and proteolysis of death susbtrate PARP (Liu *et al.*, 1996). Wang's group identified the components responsible for directing these dATP-associated apoptotic changes. Using a biochemical fractionation-based approach, the group discovered that this activity was derived from several distinct components, collectively called Apafs (Apafs, Apoptotic Protease Activating Factors) (Liu *et al.*, 1996). The first of the Apafs to be identified using the fractionation approach was Apaf-2. Surprisingly, this molecule turned out to have the same absorption spectra and amino acid sequence as cytochrome *c* (Liu *et al.*, 1996).

While this result initially seemed somewhat too bizarre to be genuine, several lines of evidence fom Wang and colleagues offered solid proof for an apoptotic signaling role for this molecule. First, they discovered that extracts made using a buffer supplemented with sorbitol, that was known to preserve mitochondrial integrity, failed to undergo apoptotic changes in a dATP-dependent manner. This suggesed that a mitochondrial escapee, likely cytochrome *c*, may be essential in inducing the apoptotic changes observed in these extracts (Liu *et al.*, 1996). Second, immunodepletion of cytochrome *c* eliminated the death-inducing ability of these extracts. Finally, Wang and colleagues reported that cells primed to die by treatment with the cytotoxic drug staurosporine underwent cytochrome *c* release from mitochondria at an early stage during induction of the death program. This suggested that this may indeed be an important upstream signaling event. Moreover, the significance of long-held observations about Bcl-2 could now be explained: the death-inhibitory properties of the molecule appeared to stem from its sublocalization to mitochondrial membranes (Hockenbery *et al.*, 1990; Krajewski *et al.*, 1993). Finally, the ability of Bcl-2 to block death in many death scenarios, was discovered to relate to its ability to block cytochrome *c* release (Kluck *et al.*, 1997; Yang *et al.*, 1997), suggesting that cytochrome *c* had an important death effector function.

As it transpires, once an individual mitochondrion is persuaded to part with its cytochrome *c*, the process of efflux into the cytosol is accomplished in a single, all-or-nothing step, lasting approximately 5 minutes (Goldstein *et al.*, 2000). Evidence suggests that mitochondria remain coupled during cytochrome *c* release, suggesting that the phenomenon of mitochondrial depolarization widely observed during a variety of cell deaths is a secondary, caspase-dependent event (Bossy-Wetzel *et al.*, 1998). Indeed, the pancaspase inhibitor Z-VAD-fmk is effective in blocking mitochondrial damage observed during cell death, whereas cytochrome *c* release is, in many cases, Z-VAD-fmk-insensitive (Bossy-Wetzel *et al.*, 1998). These data support the notion that cytochrome *c* release is a signaling event rather than a bystander event during apoptosis.

1.8.2. Integration of death signals via mitochondria: the Bcl-2 family

Current evidence suggests that mitochondria constitute an important integration point for numerous upstream stimuli that converge at the point of provoking cytochrome *c* release (Adrain and Martin, 2001; Green, 2000). Cytochrome *c* release from mitochondria is thought to be governed by an agonistic/antagonistic interplay between the death promoting and death inhibitory members of the Bcl-2 family (Kelekar and Thompson, 1998; Vander Heiden *et al.*, 1999). This is likely achieved through the formation of dimers or heterodimers of these molecules (Minn *et al.*, 1999; Yang *et al.*, 1995). Thus, the relative ratios of death agonists: antagonists of the Bcl-2 family constitutes the equation for cytochrome *c* release.

Dealing firstly with the survival promoting side of the equation, as has been discussed already, Bcl-2 regulates apoptosis by inhibiting cytochrome *c* release (Kluck *et al.*, 1997; Yang *et al.*, 1997). On the other side of the cytochrome *c* release equation lie the death agonist members of the family, including those that share a only a single Bcl-2-homology (BH) domain in common with other family members: the BH-3 only proteins (Kelekar and Thompson, 1998; Vander Heiden *et al.*, 1999). Whereas their closest relative, worm EGL-1 appears to act primarily to displace CED-9 from CED-9/CED-4, evidence suggests that in mammals, these molecules link diverse upstream signaling pathways into the commonality of cytochrome *c* release (del Peso *et al.*, 1998). The paragraphs that follow will illustrate examples of the range of stimuli that employ BH-3-only proteins as cytochrome *c* release-promoting factors.

One of the best characterized of these BH-3-only cytochrome *c* -releasing mechanisms is that of death agonist Bid (Wang *et al.*,1996; Li *et al.*, 1998; Luo *et al.*, 1998; Gross *et al.*, 1999). It had been appreciated for some time that Bcl-2 was capable of blocking cell death induced by Fas death receptor ligation in some cells, but ineffective in other cell types treated with the same stimulus (Scaffidi *et al.*, 1998). Possibly as a result of some deficiency in the receptor signaling components, or because of higher levels of dominant negative caspase-8-related inhibitor cFLIP, some cell types cannot activate enough caspase-8 to die (Scaffidi *et al.*, 1998; Medema *et al.*, 1999). In these cell types, a

Bid-dependent amplification loop is invoked (Li *et al.*, 1998; Luo *et al.*, 1998; Gross *et al.*, 1999). As a result of caspase-8 cleavage, the C-terminal portion of Bid (tBid), translocates into mitochondria where it provokes cytochrome *c* release (Li *et al.*, 1998; Luo *et al.*, 1998; Gross *et al.*, 1999). The essential role of this Bid-mediated amplification loop is demonstrated by Bid-null mice (Yin *et al.*, 1999). Whereas systemic injection of an α-Fas agonistic antibody normally provokes severe liver damage as a result of widespread hepatocyte death, Bid-null mice are protected from these lethal effects, likely because of the failure of these cells to engage the mitochondrial death pathway via cytochrome *c* release (Yin *et al.*, 1999).

A variety of other death pathways have been identified as integrating into the central mitochondrial executioner. For example, BH-3 protein Bad links growth factor deprivation to cytochrome *c* release (Datta *et al.*, 2000). The death agonistic properties of Bad are normally restrained through phosphorylation of one or more serine residues by kinase Akt, downstream of IL-3 receptor stimulation and PI3 kinase activation (Datta *et al.*, 1997; Datta *et al.*, 2000). When the IL-3 receptor is stimulated, Bad is tethered to the phosphoserine-binding protein 14-3-3 (Datta *et al.*, 2000). However, dephosphorylated Bad releases from this complex, ultimately engaging cytochrome *c* release.

Nuclear stimuli also access cytochrome *c* release via BH-3 intermediaries. For instance, p53-inducible BH-3-only death agonist, Noxa mediates death signaling in response to genotoxic stresses by engaging a cytochrome *c* release pathway (Oda *et al.*, 2000). In addition, the human BH-3-like homologue of yeast Rad9 protein can dimerize with Bcl-2/Bcl-x and induce BH-3-dependent apoptosis in response to DNA damage, presumably by provoking cytochrome *c* release (Komatsu *et al.*, 2000).

How do these seemingly disparate upstream molecules (summarized in Figure 8) that share in common only the BH-3 peptide, actually engage cytochrome *c* release? An accumulating number of hypotheses have emerged

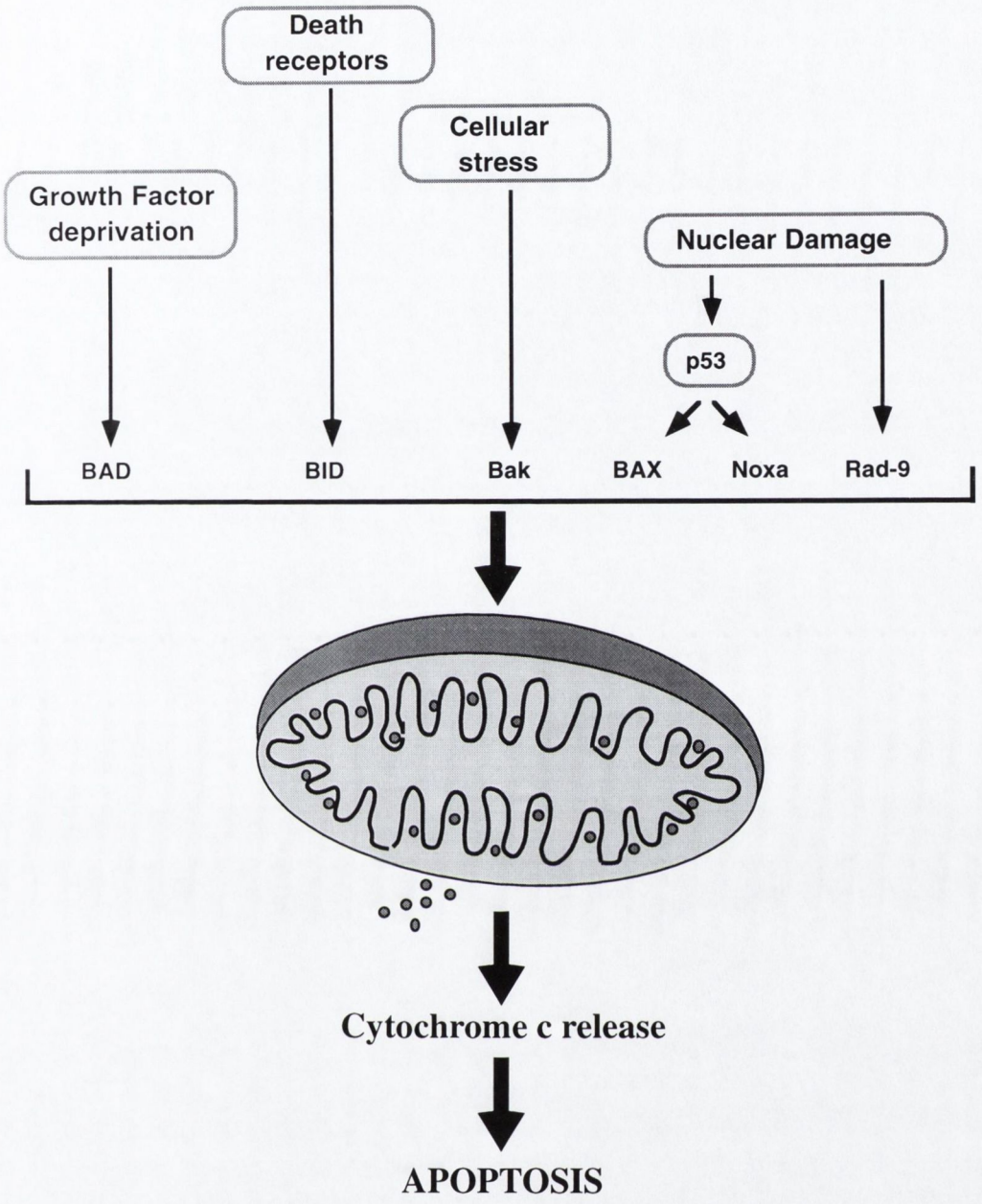

Figure 8

Diagram illustrating the principle that cytochrome *c* release is an important integration point for diverse upstream stimuli, including DNA damage, death receptor ligation and growth factor deprivation, achieved via death-promoting members of the Bcl-2 family, including the BH-3-only proteins.

to account for this phenomenon, some of which suggest that they must heterodimerize with other Bcl-2 relatives, as previously discussed.

Other studies suggest that tBid can directly integrate into lipid membranes and may possess ion channel forming abilities, suggesting that it can engage cytochrome *c* release in the absence of other Bcl-2 relatives (Schendel *et al.*, 1999; Kudla *et al.*, 2000). However, further studies suggest that tBid may provoke cytochrome *c* release by heterodimerizing not with death antagonists such as Bcl-2, but with the death-inducing molecule Bax, promoting oligomerization of this molecule and its insertion into the mitochondrial membrane (Eskes *et al.*, 2000). In turn, Bax which undergoes translocation from the cytoplasm to mitochondria in cells undergoing apoptosis, has been shown to be sufficient to induce cytochrome *c* release from mitochondria and even pure liposomes (Wolter *et al.*, 1997; Jürgensmeier *et al.*, 1998; Saito *et al.*, 2000). In addition, it has recently been suggested that tBid may provoke cytochrome *c* release by inducing oligomerization of Bcl-2-like death agonist Bak (Wei *et al.*, 2000). Finally, in response to growth factor withdrawal, dephosphorylated Bad may displace Bax from inhibitory complexes with Bcl-2 and Bcl-XL (Yang *et al.*, 1995; Datta *et al.*, 2000).

In addition to the variety of stimuli discussed above, it is possible that deregulated oncogenes may also sensitize cells to apoptosis by provoking cytochrome *c* release. For example, it has been demonstrated that microinjection of cytochrome *c*-specific antisera can successfully block apoptosis associated with deregulated expression of c-Myc (Juin *et al.*, 1999).

The examples above clearly attest to the importance of cytochrome *c*—and the molecules and systems that regulate its release—as a unifying element in death signaling pathways. By implication, the down-stream effectors that mediate the cytochrome *c*-induced death are consequently critical in governing the decision as to whether a cell will live or die.

1.8.3. Apaf-1

Exit from mitochondria mediated by any of the mechanisms detailed above, therefore signals a new role for cytochrome *c*, not as a life giver, but as a life-taker. It was initially unclear how cytochrome *c* actually activated caspases (Liu *et al.*, 1996). As it turned out, this connection was very intimate, requiring a series of protein-protein interactions minimally featuring Apafs -1, -2 (or, cytochrome-*c*), and Apaf-3 (Apoptotic Protease Activating Factors).

Fractionation approaches yielded two further activites that were essential for dATP/cytochrome *c*-induced caspase activation. One of these, denoted Apaf-1 was a large protein of a molecular weight of approximately 130 kDa (Zou *et al.*, 1997). Analysis of the Apaf-1 amino acid sequence revealed that the N-terminus of Apaf-1 possesses a CARD motif that was 21% identical to worm CED-3 (Zou *et al.*, 1997) (Figure 9). Furthermore, adjacent to this module was a domain 22% similar to worm CED-4 that included conserved nucleotide binding sites (Figure 9) (Zou *et al.*, 1997). Thus, Apaf-1 appeared to be one of the long sought-after mammalian counterparts of worm CED-4. Based on this similarity, Apaf-1 was predictably a caspase-activating apaptor molecule. In addition to these features shared with CED-4, Apaf-1 possesses a unique C-terminal region, characterized by the presence of multiple tryptophan-aspartate repeats (WDR) (Figure 9) (Zou *et al.*, 1997). Since this domain was not present in CED-4, its role could not be easily anticipated.

Intriguingly, co-immunoprecipitation experiments revealed that Apaf-1 and cytochrome *c* could interact, suggesting that a multimolecular complex may mediate the activation of caspases in this system. However, the exact cytochrome *c* interaction surface on Apaf-1 responsible for this was unknown (Zou *et al.*, 1997). Interestingly, extracts made from cells overexpressing Apaf-1 were more sensitive to caspase-3 activation (Zou *et al.*, 1997). This suggested that Apaf-1 had caspase activating properties attributable to an as yet undefined mechanism. However, since caspase-3 itself lacked the CARD motif present in Apaf-1, it was unlikely that Apaf-1 was responsible for directly activating this caspase. Thus, the search for Apaf-3 was resumed.

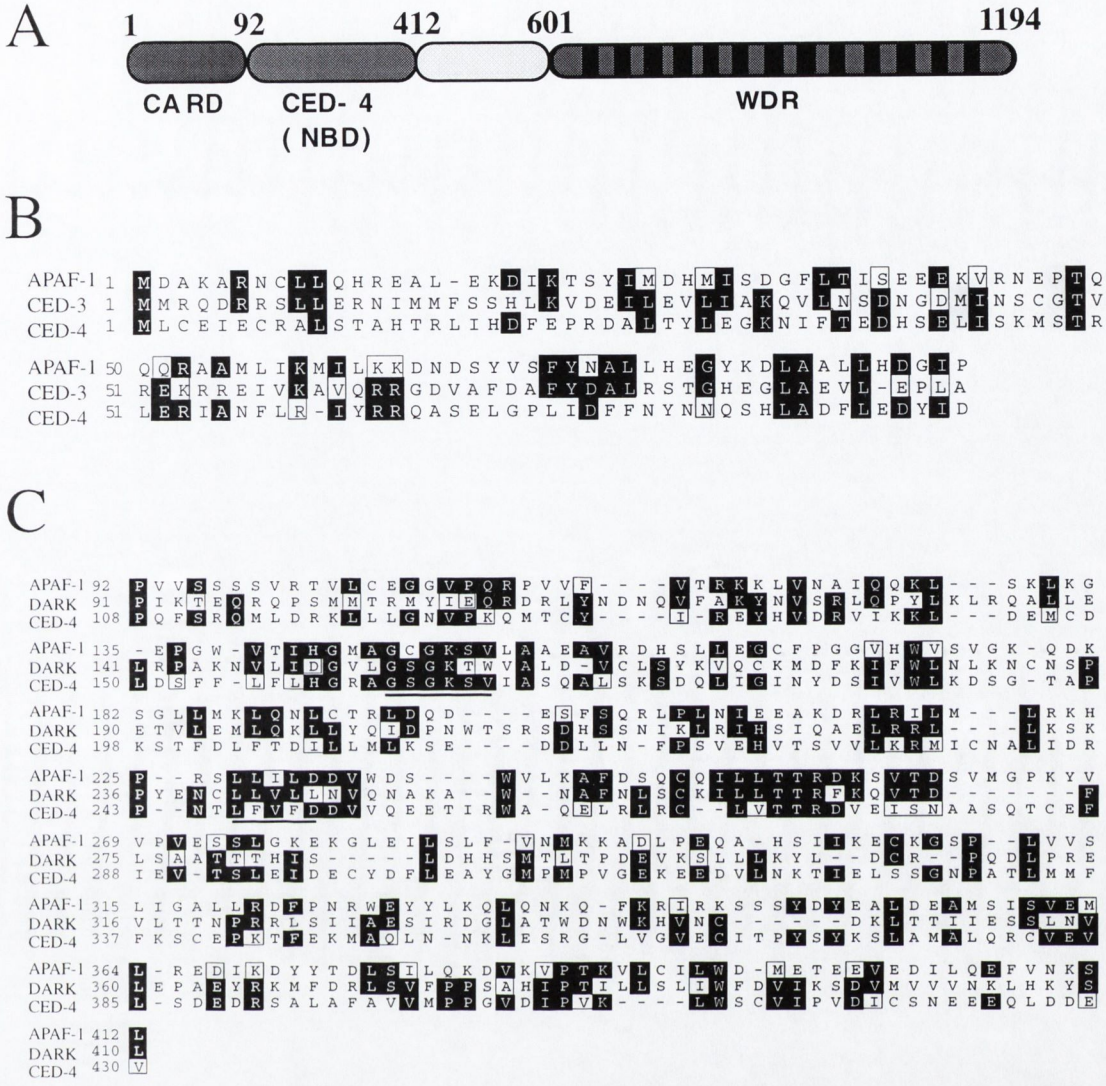

Figure 9

A, Schematic diagram illustrating the modular structure of Apaf-1. Indicated are the CED-3-homologous CARD motif, the CED-4-homologous, nucleotide-binding region and the WD-40 repeat region (WDR). Numbers denote amino acid positions.

B, Alignment of the N-termini of human APAF-1 (Genbank Accession No. AF013263) with those of *C.elegans* CED-3 (Accession No. P42573) and CED-4 (Accession No. S72566) demonstrating possession of the CARD motif.

C, Alignment of the CED-4-homologous portion of human APAF-1 (Genbank Accession No. AF013263) with *C.elegans* CED-4 (Accession No. S72566) and *Drosophila* CED-4 homologue DARK (Accession No. AF162659). Identical amino acids are shaded black; conserved substitutions matching the consensus by three distance units or less are boxed. The Walker's A and B consensus nucleotide binding sites are underlined.

1.8.4. Apaf-1 and Caspase-9

Following a six step purification procedure, the group obtained multiple fractions that possessed Apaf-3 activity (Li *et al.*, 1997). Intriguingly, sequences obtained from tryptic digests revealed that caspase-9 was the missing component of this death-inducing complex (Li *et al.*, 1997). This molecule, previously identified as ICE-LAP6/Mch6 is a member of the long prodomain subfamily of caspases (Duan *et al.*, 1996; Srinivasula *et al.*, 1996). As it transpired, Apaf-1 and caspase-9 interact via their CARD regions (Li *et al.*, 1997). Thus, the collaboration of these molecules was responsible for mediating the effects downstream of cytochrome *c* release. Given the diverse stimuli that converge upon this point, these molecules constitute key cell death effectors.

1.8.5. Apaf-1 and caspase-9: murine knockout studies

The role of Apaf-1/caspase-9 as key cell death effectors was confirmed by murine knockout studies (Cecconi *et al.*, 1998; Yoshida *et al.*, 1998; Hakem *et al.*, 1998; Kuida *et al.*, 1998; Honarpour *et al.*, 2000). Interestingly, these nullizygous phenotypes are very similar, confirming that they participate in a common pathway. Both varieties of knockout mice exhibit perinatal lethality (Cecconi *et al.*, 1998; Yoshida *et al.*, 1998; Hakem *et al.*, 1998; Kuida *et al.*, 1998; Honarpour *et al.*, 2000). These include craniofacial abnormalities and defective brain development, associated with an accumulation of neuroepithelial progenitor cells that should normally be deleted during development (Cecconi *et al.*, 1998; Yoshida *et al.*, 1998; Hakem *et al.*, 1998; Kuida *et al.*, 1998; Honarpour *et al.*, 2000). The deleterious outcome of the loss of either of these molecules is demonstrated by the fact that fewer than 8% of total mice mice born to caspase-$9^{+/-}$ parents are actually homozygotes (Hakem *et al.*, 1998). Similarly, a minority, (approximately 6%) of mice born are *APAF-1* nullizygous (Cecconi *et al.*, 1998; Yoshida *et al.*, 1998).

Dealing with the caspase-9 knockout phenotype, the nullizygous mice that succeed in surviving to birth frequently die post-partum as a result of intracerebral haemhorrage (Hakem *et al.*, 1998). In caspase-9-null homozygotes, by day 10.5 during embryogenesis (E10.5), the animals exhibit

defects in neural tube closure in the hindbrain region. By stage E16.5 of embryonic development, the animals exhibit a prominent extrusion of cranial tissues, including an expanded midbrain (Kuida *et.al.*, 1998). Moreover, examination of brain tissues at a histopathological level reveals that this abnormality relates to an enlarged zone characterized by aberrant proliferation and decreased apoptosis in the forebrain and midbrain of caspase-9 nullizygous mice. This is similarly a feature of Apaf-1 nullizygotes (Cecconi *et al.*, 1998; Yoshida *et al.*, 1998).

Interestingly, the gross morphological phenotype in *APAF-1*$^{-/-}$ animals is somewhat more severe than the *CASP-9*$^{-/-}$ counterparts. For instance, in addition to ectopic protrusions of the forebrain, *APAF-1*$^{-/-}$ mice also exhibit two other major phenotypical differences. In some, but not all animals, these include, a cauliflower-like mass on the face, and a cone-shaped cranial protrusion (Yoshida *et al.*, 1998). Moreover, Apaf-1-null embryos exhibit a delay in the removal of interdigital compared to control littermates (Yoshida *et al.*, 1998; Cecconi *et al.*, 1998). Additional differences include impaired eye development in *APAF-1*$^{-/-}$ animals. In summary, these data suggest that Apaf-1 may regulate one or more initiator caspases, in addition to caspase-9 (Cecconi *et al.*, 1998; Yoshida *et al.*, 1998).

Another interesting feature distinguishes *APAF-1*-null mice from their *CASP-9*-null counterparts. A small proportion of nullizygous mice (some 5%) actually indeed survive to adulthood (Honarpour *et al.*, 2000). Moreover, these mice undergo normal embryonic brain development, suggesting that there are alternative ways of activating caspase-9 in these tissues (Honarpour *et al.*, 2000). Within this context, it is also worth noting that the caspase-9 transcript is expressed most abundantly at embryonic stage E7, whereas Apaf-1 is minimally expressed at this developmental timepoint (Kuida *et al.*, 1998). Correspondingly, the caspase-9 message has a lower expression level at E15 and E17 developmental stages, when significant levels of Apaf-1 continue to be expressed (Kuida *et al.*, 1998). This again suggests that in certain scenarios, these molecules may operate in independent pathways.

In addition to playing an important role in the developing mammalian brain, it is important to note a secondary phenotype shared in both APAF-$1^{-/-}$ and *CASP-*$9^{-/-}$ cells. Both varieties of nullizygous cells are resistant to a range of cytotoxic agents that are known to provoke cytochrome *c* release (Cecconi *et al.*, 1998; Yoshida *et al.*, 1998; Hakem *et al.*, 1998; Kuida *et al.*, 1998). For example, whereas murine thymi develop normally and harbour normal ratios of $CD4^+$:$CD8^+$ cells, thymocytes isolated from these same individuals are resistant to diverse pro-apoptotic stimuli, including etoposide and γ-irradiation (Cecconi *et al.*, 1998; Yoshida *et al.*, 1998; Hakem *et al.*, 1998; Kuida *et al.*, 1998). Thus, Apaf-1 and caspase-9 additionally play important roles in the elimination of cells in pro-pathological settings in mature tissues. This confirms their key role in the mitochondrial/cytochrome *c*-dependent pathways discussed previously.

1.9. AIMS OF THIS THESIS

The paragraphs above therefore highlight the importance of the caspase-9 pathway, not only during mammalian brain development, but also as a key integration point for a variety of cytotoxic stimuli that converge upon mitochondria. For this reason, caspase-9 may represent an important therapeutic target, not only in terms of playing a possible role in neuronal cell death in the adult, but also, by participating in modes of cell death that may be important for anti-cancer strategies. The global aim of this thesis was therefore to examine factors that regulate caspase-9 activation during apoptosis.

In particular, because the majority of apoptotic signalling events involve protein-protein interactions, we dissected the role and function of two caspase-9-binding proteins, Apaf-1 and DRADD. The passages below introduce in brief the key aims of each of the three results chapters.

1.9.1.1. Chapter III: Molecular dissection of Apaf-1 function

Apaf-1 is a caspase-9-activating molecule (Li *et al.*, 1997). However, the precise mechanism of Apaf-1 function remains obscure. Because evidence suggests that some caspases can be activated via an induced-proximity mechanism, we hypothesised that Apaf-1 may act as a caspase-9 aggregating molecule (Salvesen and Dixit, 1997). A key goal was therefore to establish whether Apaf-1 could form oligomers. By extension, we wanted to pinpoint the regions within Apaf-1 that might play a role in regulating this process. A variety of protein-protein interaction assays, including the yeast two-hybrid system, were used to achieve these aims. A further goal was to dissect the role of the C-terminal WDR region in regulating Apaf-1 function. Because this portion of the molecule represents an evolutionary elaboration in comparison to worm CED-4, we speculated that it might have an important regulatory role.

1.9.1.2. Chapter III: Screening for Apaf-1-interacting proteins

A key aim of this chapter involved the use of the yeast two hybrid system to further explore the Apaf-1 pathway by library screening for Apaf-1-binding partners. An overview of this technique is provided in Chapter II. Because

the murine *APAF-1*$^{-/-}$phenotype appears to be more severe than the *CASP-9*$^{-/-}$ mice, we hypothesised that Apaf-1 may bind to and activate additional caspases (Cecconi *et al.*, 1998; Yoshida *et al.*, 1998; Hakem *et al.*, 1998; Kuida *et al.*, 1998). Moreover, returning to the worm CED-3/CED-4/CED-9 paradigm, we speculated that this approach might yield Apaf-1-binding, CED-9 relatives that modulate the ability of Apaf-1 to activate caspase-9.

1.9.3. Chapter IV: Molecular characterization of DRADD, a novel caspase-9-interacting molecule

There is also evidence from the murine knockout studies to suggest that caspase-9 may play a role independent of Apaf-1 in some scenarios. Most notably, a minority of *APAF-1*$^{-/-}$ mice survive into adulthood (Honarpour *et al.*, 2000). We postulated that these mice must possess another means of activating caspase-9 within the embryonic brain. To pursue this hypothesis, a yeast two-hybrid screen was conducted by another laboratory member. Chapter IV describes the molecular characterisation of DRADD, the novel caspase-9-binding partner that this approach revealed. This chapter dissects DRADD function in a number of ways. Firstly, we used a variety of protein-protein interaction assays to characterise the DRADD/caspase-9 interaction and to delineate which region of DRADD is responsible for caspase-9-binding. In addition, we investigated the ability of DRADD to modulate apoptosis in transient overexpression assays. A major priority of this chapter was to investigate what cell death pathway DRADD was involved in. A dominant negative-based approach was adopted to achieve this.

1.9.4. Chapter V: Screening for DRADD-interacting proteins

The dominant negative studies described above failed to reveal a role for DRADD in established cell death pathways. To investigate DRADD binding partners in an objective way, we performed a two-hybrid library screen using DRADD as bait. Chapter V describes the screen and the DRADD-binding partner, DRAMP that was obtained.

CHAPTER II
Materials and Methods

2.1. MATERIALS

2.1.1 Chemicals and general reagents

Unless otherwise stated, reagents were purchased from Sigma-Aldrich, Ireland Ltd.

2.1.2. Enzymes

Unless stated otherwise, enzymes were obtained from New England Biolabs (NEB, UK).

2.1.3. Antibodies

The following antibodies were obtained from the indicated sources

Anti-Gal-4 DB	Santa Cruz, UK
Anti-HA	Santa Cruz, UK
Anti GFP	Clontech, UK
Anti FLAG	Sigma, Ireland
Anti pRb	Santa Cruz
Anti Caspase-9	Provided by Doug Green

2.2. PURIFICATION AND MANIPULATION OF NUCLEIC ACIDS

2.2.1. Bacterial strains used for plasmid isolation purposes

E. coli strain DH5α was routinely used to amplify plasmid DNA.

2.2.2. Preparation of chemically competent cells

Typically, cells were made competent for transformation according to the Inoue protocol (Inoue *et al.*, 1990). Untransformed DH5α was streaked unto LB agar (10g/L tryptone, 5g/L yeast extract, 10g/L NaCl; supplemented with 15g/L agar; pH7.0) lacking antibiotics and a fresh single colony was used to inoculate an overnight 3ml liquid LB starter culture. The following day, 2-3 ml of the saturated overnight culture were diluted into 50 ml of SOB medium lacking

antibiotics (2% bacto tryptone, 0.5% yeast extract, 10mM NaCl, 2.5mM KCl, 10 mM $MgCl_2$, 10 mM $MgSO_4$, pH 7.0; sterilized by autoclaving) and grown at approximately 18°C with rotation at 300 rpm until an OD_{600nm} of 0.4-0.6 was achieved. Cells were harvested by centrifugation at 2,500 g for 10 min at 4°C, resuspended in 20 ml of transformation buffer (10 mM Pipes, 55 mM $MnCl_2$, 15 mM $CaCl_2$, 250 mM KCl, pH 6.7; sterile filtered) and incubated on ice for 10 minutes. Following re-centrifugation, cells were suspended in 4 ml of the same buffer and DMSO was added to a final concentration of 7%. Cells were incubated for a further 10 minutes and 200 µl aliquots were then snap frozen in liquid nitrogen and stored at -70°C.

2.2.3. Transformation of competent DH5α

Frozen competent cells obtained as described above were allowed to defrost on ice. 50 µl aliquots were made for each transformation reaction. Aliquots of 1 µl (approximately 1µg) of plasmid or 2-4 µl of ligation products were mixed with bacteria and incubated on ice for 30 minutes to enable the plasmid to coat the cells. Plasmid uptake was induced by heat-shocking cells at 42°C for 40 seconds followed by recovery on ice for 2 minutes. Following addition of 450 µl of SOC (2% bacto tryptone, 0.5% yeast extract, 10mM NaCl, 2.5mM KCl, 10mM $MgCl_2$, 10mM $MgSO_4$; pH 7.0), cells were incubated for 1 hr with gentle rotation at 220 rpm to allow for expression of the antibiotic resistence gene. Aliquots of 20-250 µl of cells were then spread on LB agar containing either ampicillin (100 µg/ml) or kanamycin (50 µg/ml) to select for transformants harbouring the plasmids.

2.2.4. Plasmid DNA isolation procedures

2.2.4.1. Isolation of plasmid DNA from bacteria: minipreparation procedure

A single bacterial transformant was inoculated into 3 ml of liquid LB medium supplemented with the appropriate selection antibiotic and grown until confluent, approximately 8-12 hours later. 1 ml of culture was then harvested by benchtop centrifugation at 20,000g for 1 minute and the supernatant removed by

aspiration. The cell pellet was resuspended by vigorous vortexing in 100 µl of P1 buffer (50mM Tris-Cl, pH 8, 10 mM EDTA). 200 µl of P2 buffer (0.2M NaOH, 1% SDS) were added and bacteria were lysed by inverting the tube 5-6 times. Following a 1 minute incubation on ice, genomic DNA and SDS-containing complexes were precipitated by the addition of 200 µl of P3 buffer (3M KAc, pH 5.5) and samples were mixed by inversion and allowed incubate on ice for 5 minutes to enhance precipitation. The samples were then centrifuged at 20,000 g for 10 minutes in a microfuge to pellet insoluble material. The supernatant, comprising soluble plasmid DNA was subjected to precipitated by the addition of 0.7 volumes of isopropanol. Following a 30 min incubation at room temperature to promote precipitation, samples were centrifuged for 10 minutes at 20,000 g and the supernatant discarded. Pellets were then washed in 1ml of 70% ice-cold ethanol and allowed to air dry at room temperature for 10 mins. The DNA was dissolved in 20 µl of 0.5X TE pH 8.0 (5mMTris.Cl pH8.0; 0.5 mM EDTA) and a 2 µl sample was analysed by 0.6%-0.8% agarose gel electrophoresis.

2.2.4.2. Isolation of plasmid DNA from bacteria: midiprep procedure

Midipreparations used a scaled-up version of the alkaline lysis procedure described in the procedure above. A starter culture was back-diluted into 50-100 ml of either LB or TB (12g/L tryptone, 24g/L yeast extract, 0.4% glycerol, 17mM KH_2PO_4, 72mM K_2HPO_4). 12-18 hours following inoculation, cultures were harvested by centrifugation at 2,500 g in a Sorvall GSA rotor for 10 minutes at 4°C and the resultant pellets were resuspended in 4 ml of P1 buffer containing 100µg/ml Rnase A (Qiagen, UK). Bacteria were lysed by the addition of 4 ml P2 buffer and samples were inverted 4-5 times to ensure thorough mixing. Following a 5 minute incubation at room temperature to promote lysis, 4 ml of P3 buffer were added and samples were mixed by inversion. A 30 minute incubation period on ice ensured thorough precipitation of SDS-complexes, after which, debris was pelleted for 20 minutes at 15,000 g in a Sorvall SS-34 rotor at 4°C. The resultant supernatant was re-centrifuged if remnants of insoluble debris remained in suspension.

For so-called crude midipreps, the supernatant was precipitated by adding 0.7 volumes of isopropanol, mixed and allowed to incubate for 20 minutes at room temperature. Plasmid DNA was recovered by centrifugation at 15,000 g for 30 minutes in a Sorvall SS-34 rotor and the pellet was washed in 1 ml of ice-cold 70% ethanol and transferred into a 1.5 ml eppendorf. The pellet was re-centrifuged at 15,000 g for 10 minutes, the supernatant discarded and the pellet allowed to air dry before resuspending in 75 µl of distilled H_2O followed by 75 µl of TE pH 8.0 (10mMTris.Cl, pH8.0, 1mM EDTA).

2.2.4.3. Isolation of plasmid DNA from bacteria: phenol/chloroform extraction procedure.

In situations where cleaner DNA preparations were required, DNA samples were further purified by extraction in phenol/chloroform/isoamyl alcohol (25:24:1). The DNA pellet obtained from the procedure described above was initially dissolved in 400 µl of distilled H_2O and a volume of phenol/chloroform/isoamyl alcohol was added. The sample was mixed and centrifuged for 5 minutes at 20,000 g in a microfuge. The upper, aqueous phase was retained and subjected to two further extractions as detailed above. Samples were then subjected to two further extractions in 24:1 chloroform: isoamyl alcohol and plasmid DNA was recovered from the supernatant as described above.

2.2.4.4. Isolation of plasmid DNA from bacteria: Qiagen procedure.

For applications such as transient transfection and *in vitro* coupled transcription and translation (ITT) reactions that required ultrapurified DNA, the Qiagen procedure (Qiagen, UK) was performed. Briefly, the plasmid supernatant obtained following the P1/P2/P3 midiprep procedure was clarified of residual debris by re-centrifugation. The supernatant was then loaded unto a Qiagen Tip-100 column that had been equilibrated by the addition of 4 ml of QBT buffer (750 mM NaCl, 50mM MOPS, pH7.0, 15% isopropanol, 0.15% Triton X-100) and the sample was allowed to run through the column by gravity flow. The column-

immobilized plasmid DNA was then washed in 2 x 10 ml of QC (1.0 M NaCl, 50mM MOPS, pH 7.0, 15% isopropanol) and eluted into 5 ml of QF buffer (1.25M NaCl, 50mM Tris.Cl, pH8.5, 15 % isopropanol). DNA was recovered by isopropanol precipitation.

2.2.5. Agarose gel electrophoresis

This technique was performed routinely following the plasmid isolation procedures and following the restriction digestion and PCR amplification procedures described below. Briefly, an electrophoresis matrix was assembled using a polymer of agarose (0.6%-2.0%) in TAE buffer (40mM Tris base, adjusted to pH 8.0 with acetic acid, 1mM EDTA). The matrix was assembled by melting the agarose/TAE mixture by microwaving and the solution was allowed to cool slightly before casting the gel. As a guideline, a matrix composed of 0.6-0.8% agarose was routinely utilized to resolve most plasmid DNA. For smaller molecular weight DNA molecules, 1.5-2.0% gels were used. To resolve PCR products, a matrix of 0.6-1.0% was used, depending on the anticipated molecular weight of the products and the degree of resolution required between similarly sized molecules.

2.2.6. Quantitation of nucleic acids

To estimate the approximate concentration of ultrapure DNA obtained following the Qiagen plasmid isolation procedure, samples were subjected to spectophotometry. Double-stranded DNA samples were quantitated based on their absorbancy under UV light at 260nm. Typically, the plasmid output of the Qiagen procedure described above was diluted 1:200 prior to this assay and triplicate readings were taken. The DNA concentration in samples was then multiplied by a factor of 50—based on the presumption that an O.D. unit of 1 represents a DNA concentration of 50μg/ml—and extrapolated to include the dilution factor. Similarly, the purity of DNA with respect to co-eluted protein contaminants was obtained by determining the OD_{260}/OD_{280} ratio, with a ratio of greater than 1.8 units constituting ultrapure plasmid DNA.

2.2.7. Genecleaning

2.2.7.1. Genecleaning nucleic acids from suspension

This procedure was used to obtain DNA sufficiently pure to carry out restriction digestion, PCR and automated sequencing reactions and was used as the principal means of purifying nucleic acids during steps involved in cloning procedures. The protocol relies on affinity binding of nucleic acids to a silica matrix in the presence of a chaotropic agent. DNA was purified from solution as follows: three volumes of 6M NaI were added plus 5 µl of Silica (100 mg/ml suspended in 3M NaI) per µg of DNA. Samples were incubated at room temperature with rotation for 5-10 minutes. The silica-bound DNA was pelletted at 20,000 g for 10 seconds and the supernatant discarded. The silica was washed two or three times by resuspending in 500 µl of geneclean wash buffer (10 mM Tris-Cl, pH 7.5, 50 mM NaCl, 2.5 mM EDTA, 50% Ethanol), then re-centrifuged and the supernatant aspirated. The pellet was air-dried for 5 minutes and eluted into distilled water or TE.

2.2.7.2. Genecleaning nucleic acids from agarose gel

The band containing the target DNA stained with ethidium bromide was excised from the gel under UV illumination. Three volumes of 6M NaI were added and the gel slice was incubated for 5-10 minutes to promote dissolution of the agarose. DNA was purified from the solution in the manner described above.

2.2.8. Restriction digestion

Restriction digestions were conducted according to the manufacturer's instructions (NEB, UK).

2.2.9. Ligations

Typically, ligations were setup on a scale of 200 ng of vector and twice the corresponding molar amount of insert, using T4 DNA ligase according to the manufacturer's instructions (NEB, UK).

2.3. PCR

Polymerase chain reaction (PCR) was used to amplify cDNAs possessing flanking restriction sites to enable cloning into plasmid vectors. Typical reaction volumes for cloning purposes were 100 µl. For screening purposes, 25 µl reactions were used. A typical 100 µl reaction included the following components:

- 100-500 ng of genecleaned or Qiagen-cleaned template plasmid DNA.
- dNTPs (dCTP, dATP, dGTP, dUTP) at a final concentration of 200 µm.
- Forward and reverse primers, each at a final concentration of 100 nM.
- 0.5 µl (comprising 2.5 Units) of either Taq (Qiagen) or Vent DNA polymerase (New England Biolabs, UK)

These components were assembled in a final volume of 100 µl including PCR buffer diluted from 10X stocks supplied by the manufacturers. A Mg^{2+} concentration of 1.5 mM (Taq) or 2.0 mM (Vent) was used as a starting point for all PCR reactions. In problematic reactions where longer amplification products were sought, the Mg^{2+} concentration was adjusted between 1.5 and 4.0 mM. The diagram below illustrates a typical PCR program.

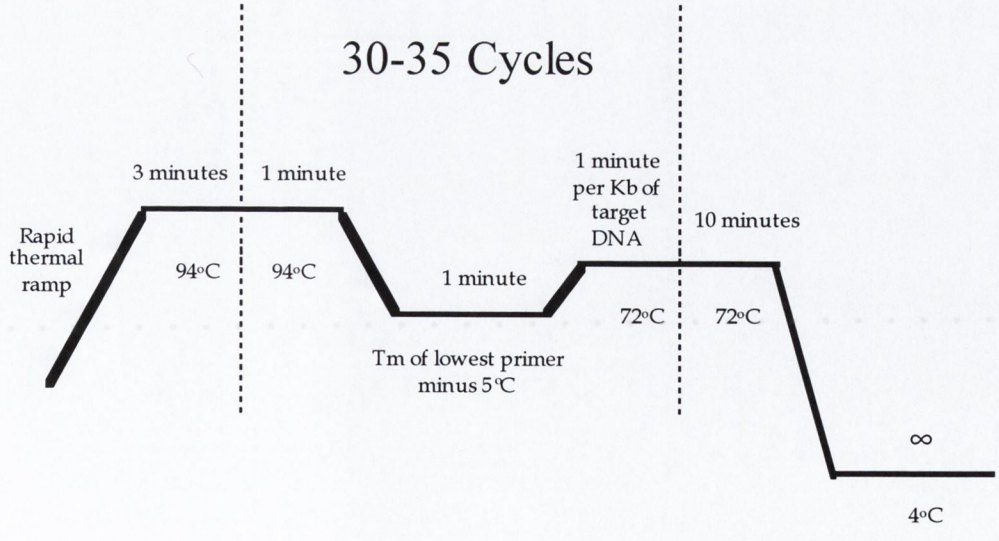

2.4. AUTOMATED DNA SEQUENCING

All sequencing was conducted on an ABI-Prism 310 Genetic Analyser automated DNA sequencer using the ABI-Prism Dye Terminator cycle sequencing ready reaction kit according to the manufacturer's instructions (Perkin Elmer, UK). The amount of template used in thermocycler reactions was 300-500 ng of genecleaned or Qiagen-cleaned plasmid DNA or 30-180 ng of purified PCR products. A 20 µl sequencing reaction comprised the following components:

- 8 µl of ready reaction mix

(incorporating all 4 dNTP-conjugated dye terminators)

- Sequencing primer (4.0 pmoles)
- Distilled H_2O to 20 µl

The thermocycler settings used are illustrated below:

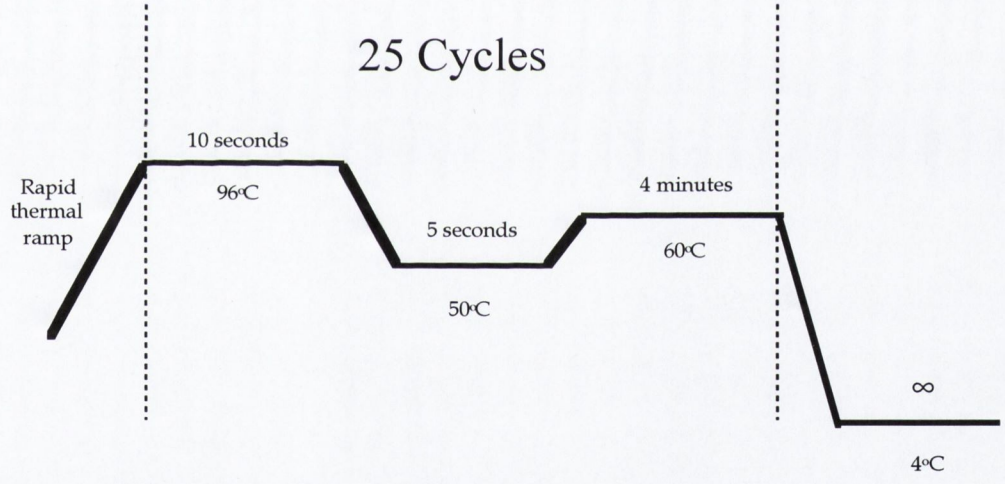

For purification, the thermocycler reaction products were transferred into 1.5 ml eppendorfs and precipitated on ice following the addition of 50 µl of 100% ethanol and 2.0 µl of 3M NaOAc pH 4.6, for no longer than 10 minutes. This avoided excessive precipitation of unincorporated dye terminators. Products were obtained by microcentrifugation at 20,000 g for 30 minutes and the supernatant was carefully aspirated off. The pellet was briefly washed in 250 µl of 70% ethanol and allowed to air dry, then resuspended in template suppression reagent

(Perkin-Elmer, UK). Samples were sequenced on a 50 cm capillary detector under conditions recommended by the manufacturer. Typically, ~450-600 base pairs of good quality sequence were obtained.

2.5. PLASMIDS

A variety of plasmids encoding mutants of Apaf-1 and DRADD were generated by the author. In most cases, this was achieved by PCR-mediated amplification of the relevant coding sequences using primers that incorporated restriction sites flanking the desired coding sequence. Alternatively, some plasmids were generated by sub-cloning an insert directly from one vector to another. For PCR-based cloning, plasmid DNA of the full length molecules was used as a source of cDNA template. PCR-derived inserts were restriction digested as appropriate and ligated into a linearized cloning vector bearing complementary restriction sites. DH5α bacteria were transformed with the ligation products. Recombinant plasmid DNA clones were identified by agarose gel electrophoresis alongside the corresponding empty cloning vector. The authenticity of the plasmids was verified by restriction digestion of the inserts out of the recombinant plasmids as well as by automated DNA sequencing as described above. Details of the plasmids made by the author and the oligonucleotide primers used to generate the inserts by PCR can be found within the appendix (Tables 22-24). The source of a variety of other plasmids not constructed by the author is also acknowledged within the appendix (Table 25).

2.6. PROTEIN PRODUCTION AND ANALYSIS

2.6.1. *In vitro* transcription and translation (ITT)

The production of radiolabeled recombinant proteins was achieved using a coupled *in vitro* transcription and translation (ITT) system from rabbit reticulocyte lysate depleted of amino acids (TNT, Promega, UK). Radiolabelling of target proteins was achieved in the presence of ^{35}S Methionine (10mCi/ml; Amersham, UK) using an RNA polymerase directed against a T7,T3 or SP6 polymerase binding site on the appropriate plasmid cDNA. A typical ITT reactions was comprised as follows:

- 25 µl Reticulocyte lysate
- 2 µl TNT buffer
- 1 µl RNA polymerase
- 1µl RNasin
- 1 µl amino acid mixture (minus methionine)
- 1-2 µl comprising 20-40 µCi translation grade ^{35}S Methionine
- 0.5 - 1.0 µg Qiagen cleaned or genecleaned plasmid DNA
- Nuclease free distilled H_2O to 50 µl.

Translation reactions were typically carried out at 30°C for 1-2 hours, although reactions involving large proteins were occasionally incubated for longer. Translated ^{35}S-labeled proteins were visualized by subjecting 0.5-2.0 µl of ITT products to SDS-PAGE, followed by enhanced fluorography (Amersham, UK).

2.6.2. Induction of GST-fused proteins in bacteria

E. coli DH5α transformants harbouring the pGEX4TK-2 plasmid or its derivatives were induced to express GST or GST-fused proteins by the addition of 100µM IPTG to culture media. Typically, 200 ml of bacteria in LB/ampicillin media were grown to an OD_{600nm} of 0.4-0.6 prior to induction. Following the addition of IPTG, cells were grown at 30°C with rotation at 320 rpm for 2-3 hours. Cells were harvested by centrifugation in a GSA rotor at 2,500 g for 10 minutes at 4°C. To obtain the recombinant proteins, cells partially lysed by one round of freeze-thaw were sonicated on ice for 5 pulses of 30 seconds at 50% duty cycle and 4.0 output following resuspension in lysis buffer (20mMTris.Cl; 100mM NaCl; 1mM EDTA pH8.0; 0.5% NP-40) supplemented with protease inhibitors (100µM PMSF; 10µg/ml leupeptin; 2µg/ml aprotinin). The lysate was then clarified by centrifugation for 15 minutes at 20,000 g. Aliquots of 50µl of Glutathione-

Sepharose beads, prewashed in PBS and suspended as a 50% slurry, were added to each ml of clarified bacterial lysate and GST fusion proteins were captured by continuous rotation for 2-3 hours at 4°C. Beads were washed in 4 x 1ml aliquots of PBS and recovered by centrifugation at 500 g for 5 minutes. Finally, beads were resuspended to a 50% slurry in lysis buffer containing 10% glycerol and supplemented with protease inhibitors as detailed above. The approximate yield of GST protein was determined by electrophoresis alongside known μg amounts of BSA.

2.6.3. SDS-PAGE

Standard SDS-polyacrylamide gel electrophoresis (SDS-PAGE) was carried out as detailed by Sambrook and Maniatis (Sambrook and Maniatis, 1989). 8-12% polyacrylamide gels were typically run at 50V to drive protein samples through the stacking gel, then at 60-90V through the resolving gel. Protein samples were prepared for electrophoresis by denaturing at 90°C for 7 minutes in the presence of SDS loading buffer (2% SDS, 50mM Tris.Cl pH6.8, 10% glycerol, 2.5% β-mercaptoethanol).

2.6.4. Immunoblotting

Following electrophoresis, proteins were transferred onto 0.2 μM nitrocellulose membranes (Biobond-NC, Whatman, UK) for 12 hours at 35-45 mA in transblot buffer (39mM Glycine, 48mM Tris.Cl pH 8.3, 0.037% SDS, 20% Methanol). Prior to immunoblotting with primary antibody, membranes were incubated in blocking solution (10mM Tris.Cl pH8.0, 150 mM NaCl, 0.05% Tween, 5% Non-fat dried milk, 0.05% NaN_3) for 30 minutes. Blots were then heat-sealed inside a polythene bag containing the primary antibody diluted in fresh blocking solution and incubated on a rotating platform for 2 hours. Prior to probing with a secondary antibody, blots were washed in TBST solution (10mM Tris.Cl pH8.0, 150 mM NaCl, 0.05% Tween, 5%). Typically, blots were washed in 3x 100 ml volumes for a total period of 25-30 minutes. For applications involving polyclonal primary antisera, blots were occasionally washed for longer. Blots

were then probed for one hour with a 1:1000 dilution of a horse radish peroxidase-coupled antibody (Amersham, UK) in TBST+5% dried milk. Following a 20 minute wash in TBST, proteins were detected using enhanced chemiluminescence by briefly incubating the blot in equal volumes of Supersignal West Pico Stable Peroxide and Luminol/Enhancer solutions (Pierce, UK). Images were obtained by exposing blots to autoradiography film (Hyperfilm MP, Amersham, UK). On occasions where it was difficult to obtain a signal using regular ECL conditions, the Supersignal West Dura reagent (Pierce, UK) was used to improve sensitivity.

2.6.5. Coomassie staining.

SDS-PAGE-resolved gels were immersed in coomassie staining solution (45% methanol, 10% glacial acetic acid, 0.25% brilliant blue) and incubated with gentle rocking for 4-12 hours. To destain, gels were incubated with gentle rocking in several successive volumes of destaining solution (45% methanol, 10% glacial acetic acid).

2.6.6. Enhanced fluorography.

The presence of ^{35}S radiolabeled proteins in SDS-PAGE gels was detected by enhanced fluorography using Amplify solution (Amersham, UK). Briefly, polyacrylamide gels were fixed for 1-2 hours in autorad fixative solution (45% methanol, 10% glacial acetic acid), then incubated for 20-30 minutes in Amplify. Following a brief wash in distilled H_2O, the polyacrylamide gel was vacuum dried unto blotting paper (Whatman, UK) for 1.5 hours at 80°C on a geldryer (Biorad, UK). To visualize ^{35}S radiolabeled bands, the autorad was exposed to Hyperfilm (Amersham, UK) for 12-36 hours at -70°C.

2.6.7. GST pulldown *in vitro* capture assay

0.5-15 µl aliquots of ITT [^{35}S] methionine-labeled proteins were brought to a total volume of 200 µl in pulldown buffer (50mM Tris, pH7.6, 120mM NaCl, 0.1% CHAPS, 100µM PMSF, 10µg/ml leupeptin, 2µg/ml aprotinin). Aliquots of

approximately 5 µg of bead-immobilized GST or GST-fusions were then added. The total bead volume of pulldown reactions was normalized by the addition of blank glutathione beads that were pre-blocked in a 1% BSA solution. In some instances, cytochrome *c* and dATP were added to pulldown reactions to a final concentration of 50µg/ml and 1mM, respectively. *In vitro* capture reactions were incubated for 2-4 hours at 4°C under constant rotation and bead-associated complexes were washed 3-5 times in pulldown buffer. Captured ^{35}S proteins were detected by SDS-PAGE followed by enhanced fluorography.

2.6.8. Immunoprecipitation

Immunoprecipitations were conducted using lysates derived from 293 or 293T cells overexpressing the appropriate target proteins transfected according to the calcium phosphate precipitation method described below. Typically, cells were lysed in 800 µl of chilled lysis buffer (50mM Tris.Cl pH 8.0, 150mM NaCl, 1% NP-40, 0.5% Sodium deoxycholate, 0.1% SDS) containing 100 µM phenylmethylsulphonyl fluoride, 10 µg/ml leupeptin and 2 µg/ml aprotinin, 24-48 hours post-transfection. Where expression of the target genes resulted in induction of apoptosis, floating dead cells were pooled with adherent cells obtained following trypsinization and centrifuged for 5 minutes at 400 g. The resulting pellet was then disaggregated and resuspended in chilled lysis buffer. Where the transfection conditions did not induce apoptosis, cells were directly lysed in following the aspiration of culture medium. Lysis was allowed to proceed at 4°C for 10 minutes. Prior to immunoprecipitation, lysates were clarified by centrifugation at 20,000g for 10-15 minutes. Typically, lysates derived from the contents of a single confluent 10 cm tissue culture plate were immunoprecipitated using 20-30 µl of agarose-coupled protein A/G (Santa Cruz) and approximately 1 µg of the appropriate antibodies. Reactions were incubated with rotation for 3-6 hours and complexes were washed 3-4 times in lysis buffer containing inhibitors. Immunoprecipitated proteins were visualized by SDS-PAGE and immunoblotting as described above.

2.7. THE YEAST TWO-HYBRID SYSTEM

The yeast two-hybrid system exploits the modular nature of yeast transcription factors (Fields and Song, 1989). The wild type Gal-4 transcription factor is composed of two separate moieties: the DNA binding domain (DB), derived from the N-terminus of the molecule, and the transcriptional activation domain (AD), originally located at the Gal-4 C-terminus (Fields and Song, 1989). In the two-hybrid assay, these modular entities are physically separated and expressed from two individual plasmids, the pAS2-1 and pACT-2 plasmids, encoding the Gal-4 DB and AD modules, respectively. These plasmids also encode nutritional markers (pAS2-1, *TRP1*; pACT-2, *LEU2*). This enables selection of yeast harboring one or both of the plasmids on media lacking tryptophan (for the DB, pAS2-1 plasmid), or leucine (for the AD, pACT-2 plasmid), or for both, on tryptophan/leucine-deficient media. By generating fusions proteins with Gal-4 DB or AD moieties, the system can be used to investigate interactions between known proteins. In addition, DB-"Bait" fusion proteins can be used to screen a Gal-4 AD cDNA library for novel interaction partners.

In the presence of a positive protein-protein interaction, Gal-4 transcriptional activity is reconstituted, enabling reporter gene expression (Figure 10). These are engineered into the *Saccharomyces cerevisiae* genome and contain a Gal-4 responsive Upstream Activating Sequence (UAS) in front of the reporter gene sequence. The *HIS3* histidine synthase gene confers histidine prototrophy in the nutritional selection assay. Yeast co-transformed with DB and AD plasmids encoding Gal-4 fusion proteins can grow on histidine-deficient media only if they harbour interacting pairs. An additional readout is provided by the *LacZ* reporter gene, encoding the β-galactosidase enzyme. This reporter is under the control of a different Gal-4-responsive element than the *HIS3* gene, in order to reduce the number of false positives encountered in the assay arising from proteins that have an ability to bind to DNA. A protein-protein interaction can be measured using the colony lift assay, judged by the conversion of X-Gal to a blue coloured product. For a more quantitative assessment, the *LacZ* liquid ONPG-based assay can be used.

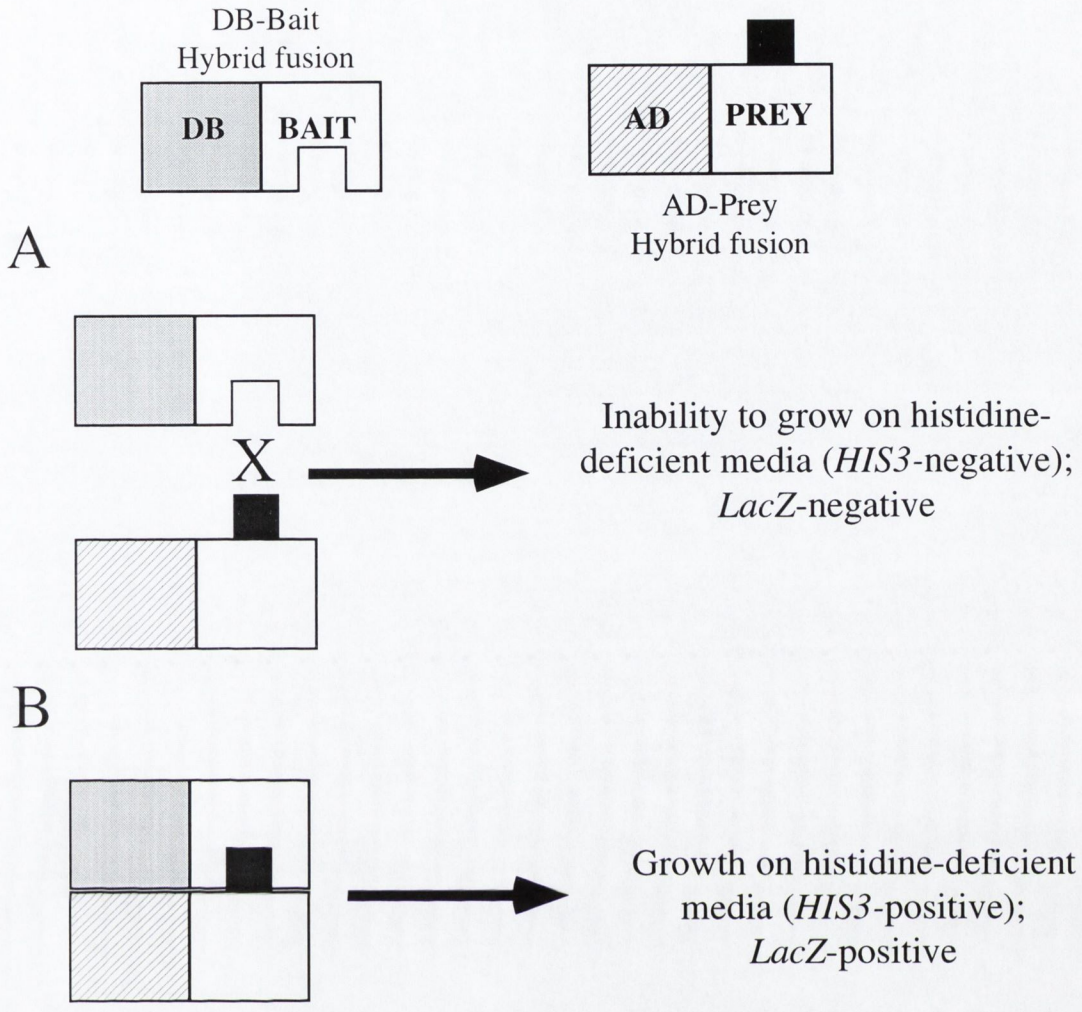

Figure 10

Schematic diagram illustrating the principle of the two hybrid protein-protein interaction assay.

In frame Gal-4 DNA binding domain (DB) and transcriptional activation domain (AD) hybrid fusions are generated with the Bait and Prey proteins respectively. The Prey protein may represent a known protein or alternatively, a variey of anonymous proteins encoded by a cDNA library. Plasmids encoding the Bait and Prey two-hybrid fusions are then co-expressed in a host yeast strain that is auxotrophic for the amino acid histidine. Yeast harbouring positive interacting pairs are selected for by plating on histidine-deficient media.

A, In the absence of a physical interaction between the Bait/Prey proteins, the Gal-4-responsive *HIS3* histidine synthetase gene fails to be transactivated. As a result, yeast cannot grow on histidine-deficient selective media.

B, If the yeast host is harbouring positive interacting Bait/Prey proteins, the activity of the Gal-4 transcription factor is reconstituted, enabling expression of the *HIS3* and *LacZ* reporter genes. *HIS3* expression confers histidine prototrophy, enabling yeast to grow on the selective media. To confirm the interaction, the *LacZ* β-galactosidase assay may be performed on histidine prototrophic yeast colonies.

All two hybrid protein-protein interaction assays and library screenings were conducted using the Matchmaker Two-Hybrid System 2 and Human Leukemia Matchmaker cDNA Jurkat library kits (Clontech, UK). All yeast protocols are derivatives of the manufacturer's instructions (Clontech, UK).

2.7.1. Yeast strains

Yeast strain Y190 (Clontech, UK) was used as a recipient for the Gal-4 AD and DB plasmids. This strain harbours the *leu 2-3, trp 1-901* and *his 3-200* mutations, rendering it auxotrophic for the amino acids leucine, tryptophan and histidine. Y190 harbours both *HIS3* and *LacZ* Gal-4-responsive reporter genes.

2.7.2. Media for maintenance of yeast strains

Recipes for yeast culture media used in the transformation and screening procedures are detailed below:

- YPD liquid medium: 10g/L yeast extract, 20g/L Peptone, 2% dextrose; added from a filter-sterilized 40% stock following autoclaving.
- YPD agar: As above, supplemented with 20g/L Agar.
- Selective Dropout (SD) Liquid media: 6.7 g/L Yeast nitrogen base with ammonium sulphate/without amino acids (DIFCO, UK), 100 ml/L of 10X amino acids stock solution (300 mg/L L-Isoleucine,1500 mg/L L-Valine, 200 mg/L L-Adenine hemisulfate salt, 200 mg/L L-Arginine HCL, 200 mg/L L-Histidine HCL monohydrate, 1000 mg/L L-Leucine, 300 mg/L L-Lysine HCL, 200 mg/L L-Methionine, 500 mg/L L-Phenylalanine, 2000mg/L L-Threonine, 200 mg/L L-Tryptophan, 300 mg/L L-Tyrosine, 200 mg/L L-Uracil), 2% glucose. To select for transformants harbouring pAS2-1 Gal-4 DB plasmids or derivatives, L-Tryptophan was omitted from the mixture; to select for pACT-2 Gal-4 AD plasmids, L-Leucine was omitted. To select for double transformants, both of these amino acids were omitted. In situations where co-transformants were being tested for protein-protein interaction, L-Histidine was additionally omitted and media was

supplemented with 25mM 3-Aminotriazole (3-AT) to attenuate leaky non-specific activation of the Gal-4 reporter gene.

- SD agar: As above, supplemented with 20g/L Agar

2.7.3. Routine yeast culture and inocula for transformation

Yeast were maintained under aerobic growth conditions at 30°C, either under static conditions on agar plates, or in an orbital shaker while in liquid culture. Untransformed Y190 (Clontech, UK) was maintained on YPD agar by routine re-streaking every 3-4 days.

2.7.4. Inoculation of liquid yeast cultures (Starter cultures)

To create an inoculum of untransformed Y190, a single colony obtained from a freshly streaked 2-3 day-old YPD plate was disaggregated by vortexing in 1 ml of liquid YPD medium. This was used to inoculate a 50 ml starter culture in YPD and grown overnight at 30°C in an orbital shaker at 250 rpm. For sequential transformations, pre-transformed host strains harboring a single plasmid of interest were grown in selective dropout (SD) medium. Initially, a large colony or several small colonies grown on SD medium were resuspended by vortexing in 1 ml of SD liquid, then transferred into 4ml of SD liquid medium for overnight growth at 30°C and 250 rpm in an orbital shaker incubator. The following day, the inoculum was back-diluted into a 50 ml selective starter culture of the appropriate SD liquid medium and was allowed grow overnight until stationary phase (OD_{600} ~2.0) had been reached.

2.7.5.1. Midi yeast transformation protocol (Untransformed yeast strains)

This protocol was used either prior to the actual library screening process to obtain yeast transformants harboring a single plasmid directing expression of the bait protein, or to test for an interaction between two known Gal-4 AD/BD-fused proteins or deletion mutants. To obtain yeast for transformation, a starter culture of untransformed Y190 host strain was set up as described above. When the culture had reached stationary phase approximately 12-18 hours later (OD_{600} ~2.0), it was back-diluted 1 in 11 by adding 30 ml of inoculum into 300 ml of fresh YPD.

The culture was allowed to expand for approximately 3 hours until an OD_{600} of ~0.5 ± 0.1 was achieved. Yeast were harvested by centrifugation in 50 ml screw-capped tubes at 1000 g for 5 minutes in a bench-top centrifuge and the supernatant was discarded. The pellet was disaggregated by vortexing and washed in 25 ml of 1x TE at room temperature. Cells were recovered by re-centrifugation in a 25 ml universal tube and the supernatant carefully aspirated off.

To make the yeast competent, the cells were resuspended in 1.5 ml of freshly made LA/TE solution (100mM LiAc, 10mM Tris-Cl, 1mM EDTA pH 7.5) at an approximate density of 10^9 cells/ml. Cells were incubated for 10 minutes at room temperature and were subjected to vigorous vortexing every 2 minutes to ensure adequate disaggregation of yeast clumps. For the transformation phase, aliquots of 1-5 µg of plasmid in a total volume of 5 µl were placed into 1.5 ml eppendorfs and mixed with 100 µg aliquots of herring sperm carrier DNA that was freshly denatured at 100°C for 20 minutes. To this, aliquots of 100µl containing ~10^8 yeast cells were added and the samples vortexed briefly, prior to the addition of 600 µl of 40% PEG 4000 in LA/TE. Samples were then thoroughly mixed by vortexing for 10 seconds before incubation at 30°C and 200 rpm for 30 mins in an orbital shaker. To induce the uptake of plasmid DNA, 70 µl aliquots of DMSO were added and the cells mixed by gently inverting 4-5 times. Cells were then heat-shocked at 42°C for 15 minutes. Following a two minute recovery period on ice, cells were gently transferred into 20 ml of chilled TE and were recovered by centrifugation at 1000g for 5 minutes. Depending on the amount of input DNA and the predicted transformation efficiency, following resuspension in 1ml of TE, 100 µl aliquots of undiluted yeast, or from 1/10, 1/100 and 1/1000 serial dilutions were spread on selective dropout media (SD). For the selection of transformants harboring pAS2-1 Gal-4 DB or pACT-2 AD-based plasmids, cells were spread onto SD medium lacking the amino acids tryptophan or leucine respectively. Alternatively, co-transformants harboring both of these plasmids and their derivatives were selected on double dropout medium lacking both tryptophan and leucine. For protein-protein interaction experiments, cells were additionally

plated unto media additionally lacking histidine and supplemented with 25 mM 3-AT. Under the conditions described above, a tranformation efficiency of approximately $10^5/\mu g$ of input plasmid DNA was achieved for single transformations or $10^4/\mu g$ for transformation of yeast already harbouring one or other of the Gal-4 plasmids.

2.7.5.2. Midi yeast transformation protocol (Sequential transformations).

This protocol was used to maximize the chances of obtaining double transformants as an alternative to co-transformation in situations where simultaneous expression of both plasmids were toxic to host strains. Additionally, yeast single transformants harboring a bait fusion were transformed for library screening purposes using this method. Yeast transformants obtained from the 50 ml selective starter culture described above were back-diluted 1 in 10 by diluting 30 ml of starter culture into 270 ml of non-selective YPD medium, to provide cells with a nutritional boost prior to the transformation process. Cells were grown for 3-6 hours until an OD_{600} of 0.5 +/- 0.1 was reached and were harvested and transformed as described above for untransformed host strains.

2.7.6. Two hybrid protein-protein interaction assays

The ability of Gal-4 AD and DB fusion proteins to physically interact when expressed in yeast was assessed by the transactivation of two independent Gal-4-responsive reporter genes—the *HIS3* histidine synthetase and *LacZ* β-galactosidase reporter genes.

2.7.6.1. *HIS3* nutritional selection assay

For the *HIS3* nutritional selection assay, several colonies of yeast transformants harboring the desired plasmids were picked from SD medium and pooled by suspending in 40 µl of sterile TE. Yeast were then streaked either unto medium lacking tryptophan and leucine as loading controls, or unto medium additionally lacking histidine and supplemented with 25mM 3-AT, to select for positive

interacting pairs. The presence of interacting pairs was judged by the ability to grow on histidine-deficient media 3-5 days following inoculation.

2.7.6.2. *LacZ* colony lift assay.

Positive interacting pairs identified by the *HIS3* nutritional selection assay were also assessed for their ability to transactivate a second independent β-galactosidase, reporter gene. Following selection on histidine-deficient medium supplemented with 25mM 3-AT for 3-5 days, colony lifts were performed by applying 90 mm discs of Whatman No. 5 filter paper on the surface of the agar. Yeast removed from the plate in this way were then subjected to two rounds of freeze thaw at -70°C followed by two incubations at room temperature to lyse the cells. Filters were soaked in Z-Buffer (60 mM Na_2HPO4, 40 mM NaH_2PO_4, 10 m M KCl, 1 mM $MgSO_4$, 0.26% 2-mercaptoethanol) supplemented with 325µg /ml X-Gal (Melford laboratories, UK) and incubated in a sealed chamber for 8 hours. A positive protein-protein interaction was determined by the presence of a blue reaction product.

2.7.6.3. *LacZ* liquid assay

For the liquid β-galactosidase assay, a cell pellet representing 3 OD_{600nm} units of liquid culture was washed briefly, then resuspended in 300 µl of Z-buffer. Triplicate 100 µl aliquots were subjected to several rounds of freeze-thaw in liquid nitrogen, followed by vortexing in the presence of glass beads. 700 µl of Z-buffer were then added to samples, followed by 160µl of ONPG (4mg/ml in Z-buffer). Samples were incubated at 30°C and monitored for the development of a yellow product, typically 20-24 hours later. Reactions were stopped by the addition of 400 µl of Na_2CO_3 and the OD_{420} of the samples determined relative to a blank.

2.7.7. Preparation of Yeast protein lysates for immunoblotting

Yeast transformants were expanded by 1/10 dilution into 50 ml YPD from a overnight selective starter culture until an OD_{600} of 0.4 ± 0.1 was attained. To minimize the risk of yeast protease activity, cells were harvested by decanting cultures into centrifuge tubes partially filled with ice. Cells were pelletted at 1000 g for 5 minutes, washed briefly in ice-cold water and recovered by re-centrifugation. Yeast were snap-frozen in liquid nitrogen then resuspended in ~250 µl of cracking buffer prewarmed to 60°C (35 mM Tris-Cl pH 6.8, 90 µM EDTA, 7M Urea, 4.5% SDS, 0.35 mg/ml bromophenol blue, 125 mM 2-mercaptoethanol) supplemented with protease inhibitors (6 µg/ml pepstatin A, 2 µM Leupeptin; 9 mM benzamidine 20 µg/ml aprotinin, 4.5 mM PMSF). Samples were normalized with respect to cell number by adding additional cracking buffer to take into account differences in culture OD_{600} at harvesting, then heated at 70°C for 10 minutes and vortexed for 1 minute in the presence of 300 mg of acid washed glass beads. Lysates were clarified by centrifugation at 22,000 g for 5 minutes at 4°C then subjected to electrophoresis and western blotting.

2.7.8. Two hybrid library screening

2.7.8.1.Preparation of library plasmid

Approximately 300 µg of pACT-2 Jurkat library plasmid was amplified and purified from stock aliquots obtained from Clontech (Clontech, UK) as follows. Having determined that the library stock titre was in the region of $4.5x10^9$ cfu/ml, approximately 5 million individual bacterial colonies, representing under twice the library complexity, were expanded by plating on a total of 80x15cm LB/ampicillin plates. 24 hours later, colonies were harvested using a cell scraper and purified according to the Qiagen plasmid preparation protocol.

2.7.8.2. Library scale screening

The two library scale screenings that were taken to the DNA sequencing stage were conducted essentially as described in the sequential midi transformation procedure above, only on a larger scale. Briefly, for both screens 100 µg of pACT-2

Jurkat library DNA were transformed in 20 separate reactions employing 10^8 yeast cells and 5µg of library plasmid per reaction. To reflect the saturating amounts of DNA used in the library screening protocol, twice the amount of herring sperm DNA (200µg) was used in each of the 20 transformation reactions. Following the transformation procedure, cells were resuspended in a total of 1 litre of YPD and incubated for ~1 hour with gentle rotation (~200rpm). This provided cells with a nutritional boost prior to plating. 250µl aliquots of cells were plated on a total of 40x15cm histidine-deficient screening plates, supplemented with 3-AT. Parallel aliquots were additionally plated on media containing histidine to determine the approximate scale of the screen. In both screens, approximately 6 million clones, approximately twice the complexity of the library were screened.

2.7.8.3. Plasmid rescue and insert amplification from yeast library clones

To obtain total yeast plasmid from library clones harbouring both the bait and prey plasmids, the pellet derived from a saturated 5 ml leucine-deficient liquid yeast culture was resuspended in plasmid rescue solution (10 mM Tris, pH8.0, 100mM NaCl, 1mM EDTA, 2% Triton X-100, 1% SDS). Yeast were then disrupted in a combination of 200 mg of glass beads (~500 microns diameter) and 200µl of phenol/chloroform/isoamyl alcohol (25:24:1) by vigorous vortexing for 2 minutes. Following centrifugation at top speed for 5 minutes in a microfuge, nucleic acids were precipitated for 20 minutes at -70°C by the addition of 1/10th of a volume of 3M NaOAc and two volumes of absolute ethanol. Precipitated DNA was pelleted at top speed in a microfuge for 20 minutes and washed briefly in 70% ethanol. DNA was dissolved in 20 µl of 10mM Tris.Cl, pH 8.5.

To obtain the library plasmids, leucine auxotrophic *E. coli* strain HB101 was transformed with 1-2 µl of yeast plasmid DNA and plated on leucine-deficient SD media supplemented with ampicillin. In addition, to provide template for DNA sequencing and Alu-1 digestion reactions, the equivalent to 1/8th of a microlitre

of the yeast plasmid prep was used in 50 µl PCR reactions incorporating the pACT-2 Forward and Reverse screening primers (see appendix).

2.8. MAMMALIAN CELL CULTURE

2.8.1. Routine cell culture conditions

Cells were maintained in exponential growth at 37°C and 5% CO_2 by routine passaging every 2-3 days. Complete culture medium was assembled without antibiotics from RPMI supplemented with 5% FCS. Alternatively, DMEM was supplemented with 10% FCS. L-Glutamine was added from 100X stocks to a final concentration of 2mM. Where required for passaging, all centrifugation was done in a swing-bucket centrifuge at 250 g for 5 minutes. Adherent cells were passaged by gently washing monolayers in pre-heated serum-free medium and were dissociated from culture plates by trypsinization in approximately 1-2 ml of Trypsin-EDTA (Gibco-BRL) (0.25% Trypsin, 1mM EDTA·4Na, in Hanks Balanced Salt Solution). Cells were returned to the incubator for a period of 5-10 minutes and dissociation of monolayers was monitored by visual inspection under light microscopy. The trypsin was then neutralized by the addition of approximately 5 ml of complete medium and cells were resuspended in fresh pre-warmed medium following centrifugation in order to remove traces of EDTA.

2.8.2. Cell cryopreservation and thawing

Individual cell-lines in routine culture were maintained in continuous passage for no longer than 2-3 months in order to avoid *in vitro* accumulation of further mutations that might alter the defined characteristics of the line. Upon receipt of a new cell-line, cells of a low passage number were harvested in exponential growth, pelletted by centrifugation and resuspended at a cell density of $1x10^7$/ml in freezing medium (50% FCS; 5% DMSO; 45% RPMI). Aliquots of 500µl of cells were placed in cryogenic storage vials and allowed to freeze slowly in a -70°C freezer. Following freezing, cells were maintained in liquid nitrogen tanks for long-term storage.

To revive frozen stocks, cells were rapidly defrosted by placing storage vials in a 37°C water bath. Complete thawing or warming of aliquots was avoided. The cryopreservative medium was removed by diluting 500 µl of defrosted cells in 20 ml of cold medium, followed by centrifugation at 250g. Cell pellets were then resuspended in 20 ml of cold complete medium to facilitate outgrowth.

2.8.3. Transient Transfection

Cells maintained in exponential growth were passaged approximately 24 hours prior to transfection by either calcium-phosphate precipitation or lipofection-mediated gene transfer.

2.8.3.1. Calcium phosphate precipitation method

Generally, where over-expression of a protein was required for the production of protein lysates, Human Embronic Kidney 293 or 293T fibroblasts cells were plated at a density of 1.5-2.0 x 10^6 cells on 10 cm plates precoated with 0.3% gelatin in a total volume of 10 ml of DMEM/10% FCS. On the day of transfection, calcium phosphate complexes were assembled by diluting a maximum of 20µg of plasmid DNA in a total of 200 µl of sterile dH_2O. 50 µl aliquots of 2.5M $CaCl_2$ were mixed with diluted DNA and added dropwise unto 250 µl aliquots of 2x HBS (280mM NaCl, 10mM KCl, 1.5mM Na_2HPO_4 12mM Dextrose, 50mM Hepes pH 7.1). Complexes were allowed assemble for 20-25 minutes at room temperature, during which time the presence of fine calcium phosphate/DNA precipitates was monitored by microscopy. 500 µl aliquots of complexes were added dropwise unto culture plates. On some occasions, complexes were removed 12 hours post-transfection. Cells were harvested 24-36 hours following transfection.

2.8.3.2. Liposome-mediated transient transfection.

For transient overexpression-based cell death assays, MCF-7 (Human Breast Adenocarcinoma) cells or HeLa (Human Epitheloid Cervical carcinoma) cells were plated at a density of 1x10^5 cells per well in 6-well plates in 2ml of RPMI/5%

FCS. 24 hours later, cells were transfected using the Fugene-6 (Roche Molecular Biochemicals) lipofection reagent. The effect of transient over-expression of the target gene was monitored by co-transfection with a limiting amount of the β-galactosidase (pCMVβ) reporter plasmid or the pEGFPC3 (GFP) plasmid. A ratio of at least 4:1 of assay plasmid: reporter gene was maintained to ensure that there was a statistically higher liklihood that β-galactosidase-positive cells also expressed the gene of interest. Typically, a mastermix was assembled in a 25 ml universal by diluting 2µl of Fugene-6 per treatment into a total volume of 100µl (per treatment) of RPMI. The Fugene-6 was added dropwise into RPMI. Following a 5 minute incubation, 100 µl of diluted Fugene-6 were added dropwise unto a maximum of 1 µg of plasmid DNA in a 96-well TC plate. The mixes were tapped gently and incubated for 20 minutes at room temperature. Complexes were pipetted gently prior to adding to cells. Approximately 2-6 hours following addition of complexes, cells were washed in 2 mls of pre-warmed serum-free medium and fresh RPMI/5% FCS was added. Assays were typically conducted for 24-48 hours. Cells were fixed in 1 ml of β-Galactosidase fixative solution (2% Paraformaldehyde, 0.2% Gluteraldehyde, in PBS pH 7.2 at 4°C for 5 minutes. Following rehydration in 2 ml of ice-cold PBS, 800 µl aliquots of X-Gal (20mg/ml, dissolved in dimethylformamide) diluted to 1mg/ml in β-gal staining solution (5mM $KFe_3(CN)_6$, 5mM $KFe_4(CN)_6$, 2mM $MgCl_2$, 0.01% SDS, 0.02% NP-40 in PBS pH 7.2) were added. Culture plates were incubated at 37°C to allow the development of blue (β-gal positive cells). The percentage of apoptotic cells was scored based on a morphological assessment of blue cells under standard light microscopy. Alternatively, cells transfected using with the GFP reporter plasmid were fixed in 4% paraformaldehyde for 5 minutes, rehydrated in ice cold PBS pH7.2 and mounted for examination under UV microscopy in mounting solution (98% Glycerol, 2% PBS). GFP-positive apoptotic cells were enumerated. A vector-transfected well was included to indicate the proportion of cells that underwent apoptosis as a result of the transfection regime.

2.8.4. Subcellular localization analysis

The subcellular distribution of overexpressed GFP-fusions of DRADD and its mutant derivatives was determined by transient transfection of MCF-7 cells plated on autoclaved glass coverslips at a density of $3x10^5$ in 6-well plates. One day following plating, cells were transfected using Fugene-6 as described previously. Typically, 500 ng of pEGFPC3 based plasmids encoding GFP or GFP-DRADD and its derivatives were transfected per treatment. Cells were washed briefly in prewarmed serum-free RPMI 3-5 hours post-transfection and media was replaced. Approximately 18 hours post-transfection, cells were fixed for 5 minutes at 4°C in 4% paraformaldehyde in PBS, pH7.2, then allowed to rehydrate for 10 minutes in PBS. Coverslips were then mounted (Glycerol/2% PBS) and examined under UV microscopy using a FITC filter.

2.8.5. Jurkat cell free extracts

Where *in vitro* reactions employed Jurkat cell free extracts, aliquots prepared as described were obtained from Dr. Liz Slee (Slee *et al.*, 1999b).

2.8.6. Trypan blue exclusion and Hoechst cell viability assays.

These were conducted as described by Cotter and Martin, 1996.

CHAPTER III:
Molecular dissection of Apaf-1 function

3.1. INTRODUCTION

As was discussed in Chapter I, a large body of evidence supports a role for mitochondria as key regulators of caspase activation, through the release into the cytosol of pro-apoptotic molecules such as cytochrome c and Smac/Diablo (Liu *et al.*, 1996; Verhagen *et al.*, 2000; Du *et al.*, 2000; Adrain and Martin, 2000; Green, 2000). The importance of Apaf-1/caspase-9 as key effectors of this pathway, has already been discussed. To reiterate briefly, both *APAF-1* and *CASP-9* murine knockout models demonstrate that this pathway plays a critical role during the development of the embryonic brain, acting as a negative regulator of neuronal populations (Cecconi *et al.*, 1998; Yoshida *et al.*, 1998; Hakem *et al.*, 1998; Kuida *et al.*, 1998; Honarpour *et al.*, 2000). Although it has yet to be demonstrated, it is therefore plausible that Apaf-1 may also play a role in regulating neuronal lifespans in the adult. In addition, Apaf-1 is a key downstream regulator of deaths provoked by a number of diverse cytotoxic stimuli (Cecconi *et al.*, 1998; Yoshida *et al.,1998*). As a result, Apaf-1 constitutes a very attractive target molecule, particularly relevant in the treatment of neoplastic disease. Thus, for all of these reasons, it is desirable to elucidate the function of Apaf-1 as a caspase activating molecule.

Structurally, Apaf-1 bears striking resemblance to worm CED-4, possessing both an N-terminal CARD motif known to mediate interaction with caspase-9, as well as a CED-4-homologous region that includes conserved nucleotide binding motifs (Figure 11) (Zou *et al.*, 1997). In addition to the domains that exhibit obvious similarity to nematode CED-4, Apaf-1 also possesses a module comprising twelve tryptophan/aspartate repeats, known as WD-40 repeats (WDR) (Figure 11), that are not present in CED-4. These modules play diverse roles in numerous cellular signal transduction pathways, making it difficult to speculate as to the role of this portion of Apaf-1. However, a consensus is that WDRs may mediate protein-protein interactions (van de Voorn and Ploegh, 1992; Neer *et al.*, 1994). While it has yet to be determined what functional role this region plays in the regulation of Apaf-1-mediated activation of caspase-9, it is postulated that cytochrome c may

A

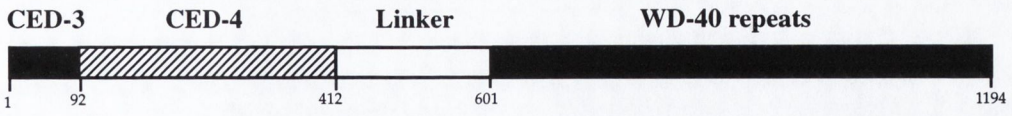

B

```
MDAKARNCLLQHREALEKDIKTSYIMDHMISDGFLTISEEEKVRNEPTQQ   50
QRAAMLIKMILKKDNDSYVSFYNALLHEGYKDLAALLHDGIPVVSSSSVR  100
TVLCEGGVPQRPVVFVTRKKLVNAIQQKLSKLKGEPGWVTIHGMAGCGKS  150
VLAAEAVRDHSLLEGCFPGGVHWVSVGKQDKSGLLMKLQNLCTRLDQDES  200
FSQRLPLNIEEAKDRLRILMLRKHPRSLLILDDVWDSWVLKAFDSQCQIL  250
LTTRDKSVTDSVMGPKYVVPVESSLGKEKGLEILSLFVNMKKADLPEQAH  300
SIIKECKGSPLVVSLIGALLRDFPNRWEYYLKQLQNKQFKRIRKSSSYDY  350
EALDEAMSISVEMLREDIKDYYTDLSILQKDVKVPTKVLCILWDMETEEV  400
EDILQEFVNKSLLFCDRNGKSFRYYLHDLQVDFLTEKNCSQLQDLHKKII  450
TQFQRYHQPHTLSPDQEDCMYWYNFLAYHMASAKMHKELCALMFSLDWIK  500
AKTELVGPAHLIHEFVEYRHILDEKDCAVSENFQEFLSLNGHLLGRQPFP  550
NIVQLGLCEPETSEVYQQAKLQAKQEVDNGMLYLEWINKKNITNLSRLVV  600
RPHTDAVYHACFSEDGQRIASCGADKTLQVFKAETGEKLLEIKAHEDEVL  650
CCAFSTDDRFIATCSVDKKVKIWNSMTGELVHTYDEHSEQVNCCHFTNSS  700
HHLLLATGSSDCFLKLWDLNQKECRNTMFGHTNSVNHCRFSPDDKLLASC  750
SADGTLKLWDATSANERKSINVKQFFLNLEDPQEDMEVIVKCCSWSADGA  800
RIMVAAKNKIFLWNTDSRSKVADCRGHLSWVHGVMFSPDGSSFLTSSDDQ  850
TIRLWETKKVCKNSAVMLKQEVDVVFQENEVMVLAVDHIRRLQLINGRTG  900
QIDYLTEAQVSCCCLSPHLQYIAFGDENGAIEILELVNNRIFQSRFQHKK  950
TVWHIQFTADEKTLISSSDDAEIQVWNWQLDKCIFLRGHQETVKDFRLLK 1000
NSRLLSWSFDGTVKVWNIITGNKEKDFVCHQGTVLSCDISHDATKFSSTS 1050
ADKTAKIWSFDLLLPLHELRGHNGCVRCSAFSVDSTLLATGDDNGEIRIW 1100
NVSNGELLHLCAPLSEEGAATHGGWVTDLCFSPDGKMLISAGGYIKWWNV 1150
VTGESSQTFYTNGTNLKKIHVSPDFKTYVTVDNLGILYILQTLE       1194
```

Figure 11

The modular structure of Apaf-1

A, Schematic diagram illustrating the domain structure of human Apaf-1 S isoform (Genbank Accession number AF013263). Indicated are the CED-3 -homologous, CED-4-homologous, linker and WD40-repeat containing portions of the molecule. Numbers denote amino acid positions.

B, Amino acid sequence of Apaf-1. The dashed underlining highlights the CARD motif, the CED-4-homologous domain is emboldened and the WDR region is enclosed by shading. Walkers A and B box consensus nucleotide binding sites within the CED-4 domain are underlined.

C

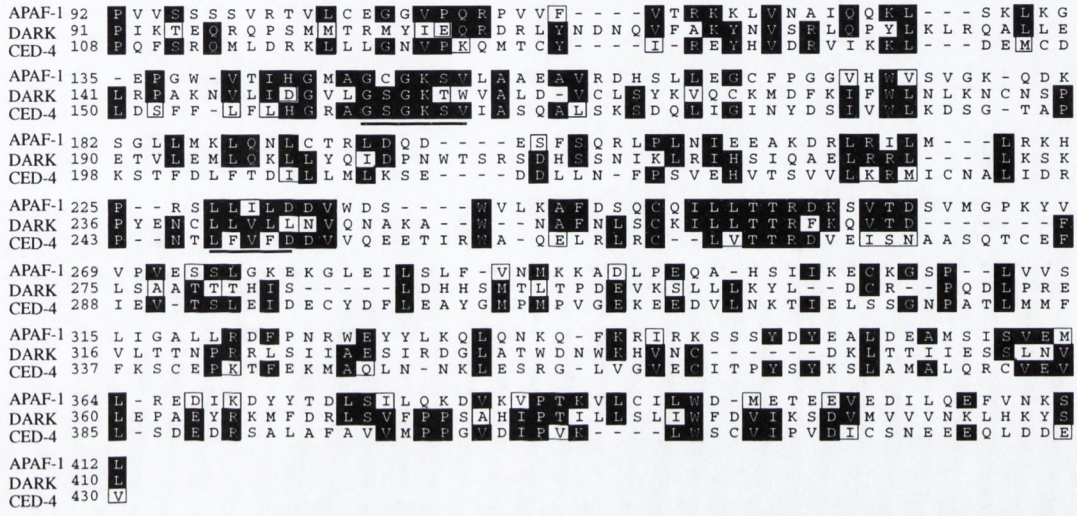

Figure 11

The modular structure of Apaf-1 (continued)

C, Alignment of the CED-4-homologous portion of human Apaf-1 (Genbank Accession No. AF013263) with *C.elegans* CED-4 (Accession No. S72566) and *Drosophila* CED-4 homologue DARK (Accession No. AF162659). Identical amino acids are shaded black; conserved substitutions matching the consensus by three distance units or less are boxed. The Walker's A and B consensus nucleotide binding sites are underlined.

bind to Apaf-1 in this area and potentially unlock the death inducing properties of the molecule (Li *et al.*, 1997)

Given the similarity between worm CED-4 and human Apaf-1, a key question is whether human Apaf-1 regulates caspase activation in a similar fashion to worm CED-4. Certainly, evidence suggests that Apaf-1 does indeed bind to and activate its cognate protease, caspase-9 (Li *et al.*, 1997; Slee *et al.*, 1999b). These data concur with the worm apoptosome framework, whereby CED-4 recruits and activates CED-3 (Chinnaiyan *et al.*, 1997a, b).

The death-inducing properties of the worm apoptosome are nullified by CED-9 binding to CED-4 (Chinnaiyan *et al.*, 1997b; Wu *et al.*, 1997a). However, it is unclear whether human CED-9 relatives Bcl-x and Boo/Diva block apoptosis by binding to Apaf-1, since there are conflicting reports concerning whether these interactions occur (Pan *et al.*, 1998b; Hu *et al.*, 1998a; Inohara *et al.*, 1998; Song *et al.*, 1999; Moriishi *et al.*, 1999; Newmeyer *et al.*, 2000).

3.2. CHAPTER AIMS

The global aim for this phase of the project was to explore the mechanism of Apaf-1 function. In particular, the hypothesis that Apaf-1 may act as a caspase-9 aggregating molecule was tested. Similar to worm CED-4, preliminary observations have suggested that Apaf-1 can self-associate in co-immunoprecipitation assays (Yang *et al.*, 1998a; Srinivasula *et al.*, 1998). However, it is unclear whether this is achieved directly through an intrinsic oligomerization mechanism specific to Apaf-1 molecules, or whether this is dependent upon other adaptor molecules. We therefore sought to discriminate between these two possibilities. To address this question we examined Apaf-1 within the context of two independent protein-protein interaction tests: the Yeast two-hybrid interaction trap assay and GST-pulldowns.

We also used the same protein-protein interaction assays to map the domains of Apaf-1 that may participate in the formation of oligomers. This was achieved through the generation of Apaf-1 deletion mutants possessing minimally defined structural modules. In particular, the conserved CED-4-homologous domain was scrutinized in this regard, given its evolutionary conservation between human and worm. In addition, given the presence of the WDR module on human Apaf-1 and its conspicuous absence in worm CED-4, we also explored the role this module in the regulation of the pro-apoptotic activity of Apaf-1.

The final part of this portion of the study attempted to extrapolate observations made from the protein-protein interaction assays into a functional cell death consequence. This was achieved using a mammalian transient transfection-based expression system to examine the ability of Apaf-1 deletion mutants to modulate apoptosis.

We also sought to identify novel Apaf-1 interaction partners using the two-hybrid screening procedure. The background to this technique is described in Chapter II. There were several justifications for this approach. First, differences between the *APAF-1* and *CASP-9* knockout phenotypes (see Chapter I, section

1.8.5.) suggest that other molecules—possibly caspases—may be regulated by Apaf-1 (Cecconi *et al.*, 1998; Yoshida *et al.*, 1998; Hakem *et al.*, 1998; Kuida *et al.*, 1998; Honarpour *et al.*, 2000). However, work by others in the laboratory (Slee *et al.*, 1999b) suggests that none of the currently identified human caspases can interact with Apaf-1 with an affinity comparable to the Apaf-1/caspase-9 interaction. We therefore reasoned a two hybrid screening approach would be required to identify these binding partners of Apaf-1. Moreover, we hoped that establishing the network of Apaf-1 interactors, even as part of a blind survey would undoubtedly further our understanding of Apaf-1 and the pathway(s) within which it operates. Finally, since the binding of CED-9 homologues to Apaf-1 is currently controversial, we hypothesized that a two-hybrid screen may help to resolve this debate (Pan *et al.*, 1998; Hu *et al.*, 1998; Inohara *et al.*, 1998; Song *et al.*, 1999; Moriishi *et al.*, 1999; Newmeyer *et al.*, 2000).

3.3. RESULTS

3.3.1. Design and generation of Apaf-1 two-hybrid deletion mutants

To investigate whether Apaf-1 can self-associate independently of other putative mammalian adaptor proteins, we designed and generated a series of Apaf-1 deletion mutants (Figure 12A). To test for Apaf-1 self-association we used the Gal-4-based Yeast two-hybrid protein-protein interaction assay (Fields and Song, 1989). Because Apaf-1 exhibits extensive sequence similarity to the worm CED-4 adaptor within the CED-4-homologous portion of the molecule, we reasoned that the portion of the molecule spanning the CED-4-homologous domain might be important for Apaf-1 self-association.

As illustrated in Figure 12A, we created a series of Apaf-1 deletion mutants by standard PCR amplification of the relevant coding sequences using primers specific to human Apaf-1 S (Accession No. AF013263) and inserted these into the pACT-2 plasmid. This generated in-frame N-terminal fusions between the various Apaf-1 truncations and the transcriptional Activation Domain (AD) moiety of the Gal-4 transcription factor. The plasmids were constructed as described in Chapter II and were subjected to digestion to confirm the presence of an insert flanked by the appropriate restriction sites.

We then confirmed expression of the Gal-4 AD-Apaf-1 fusion proteins in yeast ("Prey" proteins) by transforming yeast host strain Y190 with the appropriate Apaf-1 expression plasmids. Yeast protein extracts were then analyzed by SDS-PAGE analysis and following western blotting, were probed with an antibody directed towards the HA epitope present upstream of the pACT-2 Gal-4 sequence. Figure 12B demonstrates that yeast transformants harboring the various Gal-4-AD-Apaf-1 mutants expressed recombinant proteins of the predicted molecular weights.

A

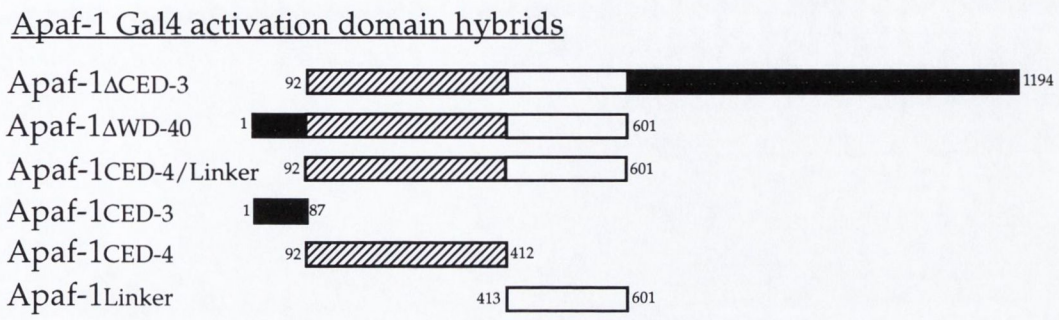

B

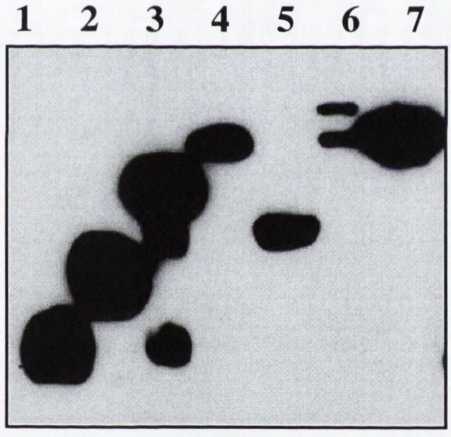

Activation domain hybrids:

1. Gal4AD
2. Gal4AD-Apaf-1 CED-3
3. Gal4AD-Apaf-1 CED-4
4. Gal4AD-Apaf-1 CED-4/linker
5. Gal4AD-Apaf-1 linker
6. Gal4AD-Apaf-1 ΔCED-3
7. Gal4AD-Apaf-1 ΔWD-40

Figure 12

Generation and expression of Apaf-1 two-hybrid deletion mutants

A, Schematic diagrams illustrating the two-hybrid activation domain (AD) Apaf-1 deletion mutants that were generated for protein-protein interaction analysis.

B, Immunoblot of lysates derived from yeast Y190 transformants overexpressing the indicated Gal-4 AD-Apaf-1deletion mutants. Proteins were detected by immunoblotting with a polyclonal antibody directed towards the HA epitope present within the N-termini of the fusion proteins. The image shown is over-exposed to reveal detection of the Apaf-1 ΔCED-3 mutant (lane-6).

3.3.2. Detection of Apaf-1 self-association by two-hybrid analysis

We then used this panel of AD-Apaf-1 deletion mutants to test for interaction with a Gal-4 DNA binding domain (DB) fusion of Apaf-1 (amino acids 92-601) spanning the CED-4-homologous and adjacent linker regions of the molecule: denoted DB-CED-4/Linker: the "Bait" (Figure 13A). To this end, we generated Y190 yeast co-transformants expressing the DB-Apaf-1 CED-4/Linker mutant in combination with the various AD-Apaf-1 deletion mutants illustrated in Figure 12A.

Following transformation, yeast co-transformants harboring both pAS2-1 and pACT-2 plasmids or their derivatives were identified by growth on SD medium lacking the amino acids tryptophan and leucine, to select for transformants harbouring the DB and AD plasmids respectively. To assay for protein-protein interactions, we took several representative colonies of each of the yeast transformant combinations plus yeast transformants harboring the DB-Apaf-1 CED-4/linker mutant alongside the pACT-2 AD vector as a control. Yeast were streaked on selective media that additionally lacked the amino acid histidine (Figure 13B, right panel). As a control, we also streaked the same yeast transformants on plates lacking only tryptophan and leucine to demonstrate that equal numbers of live yeast were loaded into each sector of both plates (Figure 13B, left panel).

This analysis revealed that the bait protein alone failed to transactivate the *HIS3* histidine synthase reporter gene when co-expressed with the pACT-2 AD empty vector (Figure 13B, right panel). However, yeast transformants expressing prey fusions of either Apaf-1ΔWD-40 or Apaf-1CED-4/linker alongside the CED-4/linker Bait, transactivated the GAL-4-responsive histidine synthase (*HIS3*) reporter, as judged by their ability to grow on histidine-deficient media, indicative of a positive protein-protein interaction (Figure 13B, right panel). This result suggested that Apaf-1 can homodimerize and that this interaction occurs minimally between the CED-4/linker portions of the Apaf-1 molecule, since the yeast transformants harboring the Apaf-1 CED-4 domain-only, or the linker

A

B

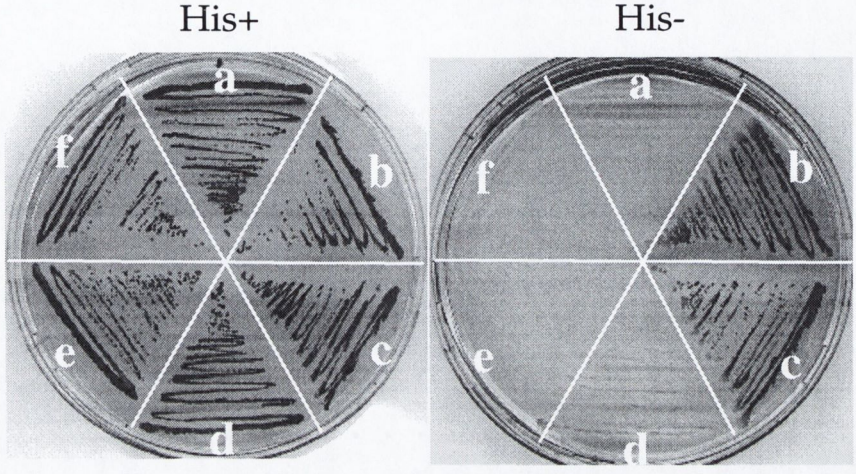

DB hybrid: Apaf-1CED-4/linker

AD hybrids:

a None
b Apaf-1ΔWD-40
c Apaf-1CED-4/linker
d Apaf-1CED-4
e Apaf-1Linker
f Apaf-1ΔCED-3

Figure 13

Yeast Two-hybrid protein-protein interaction assay illustrating Apaf-1 dimerization

A, Schematic representation of the DB-Apaf-1 CED-4/Linker deletion mutant that was transformed alongside a panel of Gal-4 AD Apaf-1 deletion mutants.

B, Interactions between Gal-4-DB-Apaf-1 CED-4/linker and transcriptional activation domain (AD) fusions of the indicated proteins were determined by the yeast two-hybrid assay. The presence of interacting pairs was indicated by transactivation of the *HIS3* reporter gene in the yeast, which confers an ability to grow on medium lacking histidine. Left, control plates showing equal loading of yeast; right, the same transformants growing on plates lacking histidine where colony growth indicates an interaction. Data shown are representative of at least three independent experiments.

domain only AD fusions, failed to activate the reporter system when co-expressed with the Apaf-1-CED-4/linker (Figure 13B, right panel). Strikingly, the Apaf-1ΔCED-3 mutant, encompassing the CED-4/linker portions but additionally, possessing the WDRs (Figure 12A) failed to associate with the Apaf-1CED-4/linker mutant (Figure 13B, right panel). This interesting result strongly suggested that Apaf-1 self-association was repressed by the presence of the WDR module. The results obtained using the *HIS3* reporter system were verified using a second independent *LacZ* β-galactosidase colony lift assay (Table 4). As anticipated from the nutritional selection assay, Apaf-1 readily self-associated via the CED-4/linker portions of the molecule, with a *LacZ* signal intensity similar to the Apaf-1/caspase-9 interaction. The outcomes of both the *HIS3* and *LacZ* assays are summarized in Table 4.

3.3.3. Generation of GST-Apaf-1 fusions and ^{35}S-labeled *in vitro* translated (ITT) Apaf-1 mutants for *in vitro* pulldown analysis

We next sought to verify Apaf-1 self-association using an *in vitro* protein-protein interaction assay. To this end, we generated plasmid derivatives of the pGEX4TK2 bacterial expression vector encoding GST-Apaf-1 fusions of either amino acids 1-412 or amino acids 1-601 (See schematic representations, Figure 14 A, B). Recombinant GST-Apaf-1^{1-412}, GST-Apaf-1^{1-601} or GST, were affinity purified from bacterial lysates. Purification of GST-Apaf-1^{1-412} and GST-Apaf-1^{1-601} of the approximate predicted molecular weight was confirmed by SDS-PAGE analysis and coomassie staining (Figure 14C, left and right panels).

As an interaction partner for these GST-Apaf-1 fusions, we generated pcDNA3-based mammalian expression plasmids encoding various Apaf-1 deletion mutants and a pBluescript II plasmid encoding Apaf-1 92-1194 (ΔCED-3 mutant) (Figure 15A). Using the T7 RNA polymerase binding site upstream of the multiple cloning site, we generated ^{35}S-radiolabeled Apaf-1 mutant proteins using a rabbit reticulocyte lysate-based coupled *in vitro* transcription and translation (ITT) expression system. We then used SDS-PAGE followed by fluorography to

Table 4

Summary of all the two-hybrid Apaf-1/Apaf-1 combinations tested in the *HIS3* and *LacZ* β-galactosidase assays

"-" denotes no growth; -/+, weak growth. ND, not determined. The caspase-9/Apaf-1 interaction is included as a positive control.

BD hybrid	AD hybrid	Growth on His-	β-gal assay
CED-4/linker	none	-	-
CED-4/linker	CED-4	-/+ (weak)	++
CED-4/linker	linker	-	-
CED-4/linker	CED-4/linker	+++	+++
CED-4/linker	ΔWD-40	+++	+++
CED-4/linker	ΔCED-3	-	-
CED-4	CED-4	-	ND
CED-4	ΔWD-40	-	ND
Caspase-9pro	ΔWD-40	+++	+++

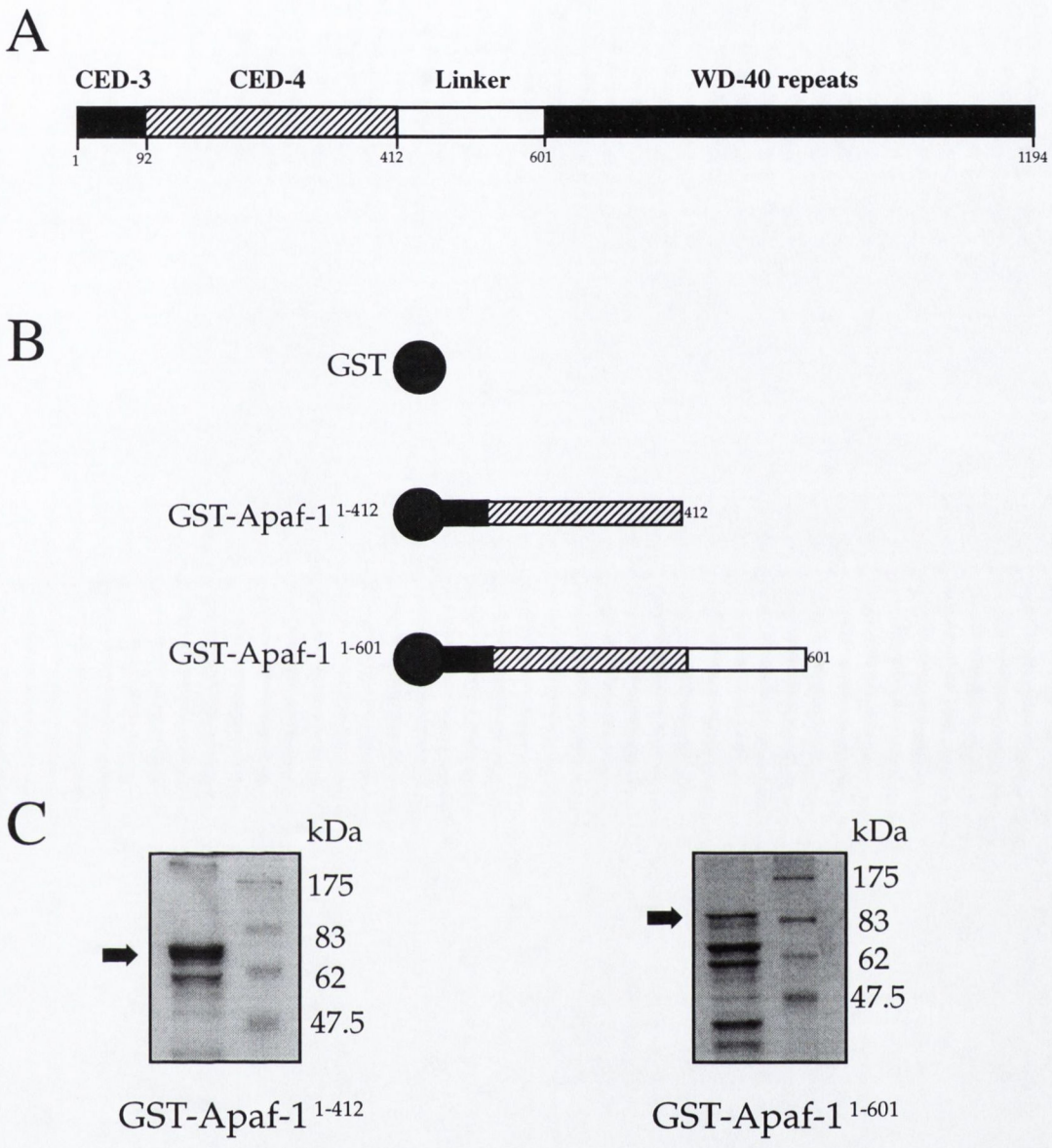

Figure 14

Purification of recombinant GST-Apaf-1 fusion proteins

A, Schematic representation of full-length Apaf-1. Indicated are the CED-3-homologous, CED-4-homologous, linker and WDR regions of the molecule.

B, Schematic representation of GST, GST-Apaf-1^{1-412} and GST-Apaf-1^{1-601}.

C, Images of coomassie stained, SDS-PAGE-resolved, GST-Apaf-1^{1-412} and GST-Apaf-1^{1-601}. Arrows indicate the position of the purified recombinant proteins. The additional bands likely represent degradation products of the Apaf-1 recombinant proteins.

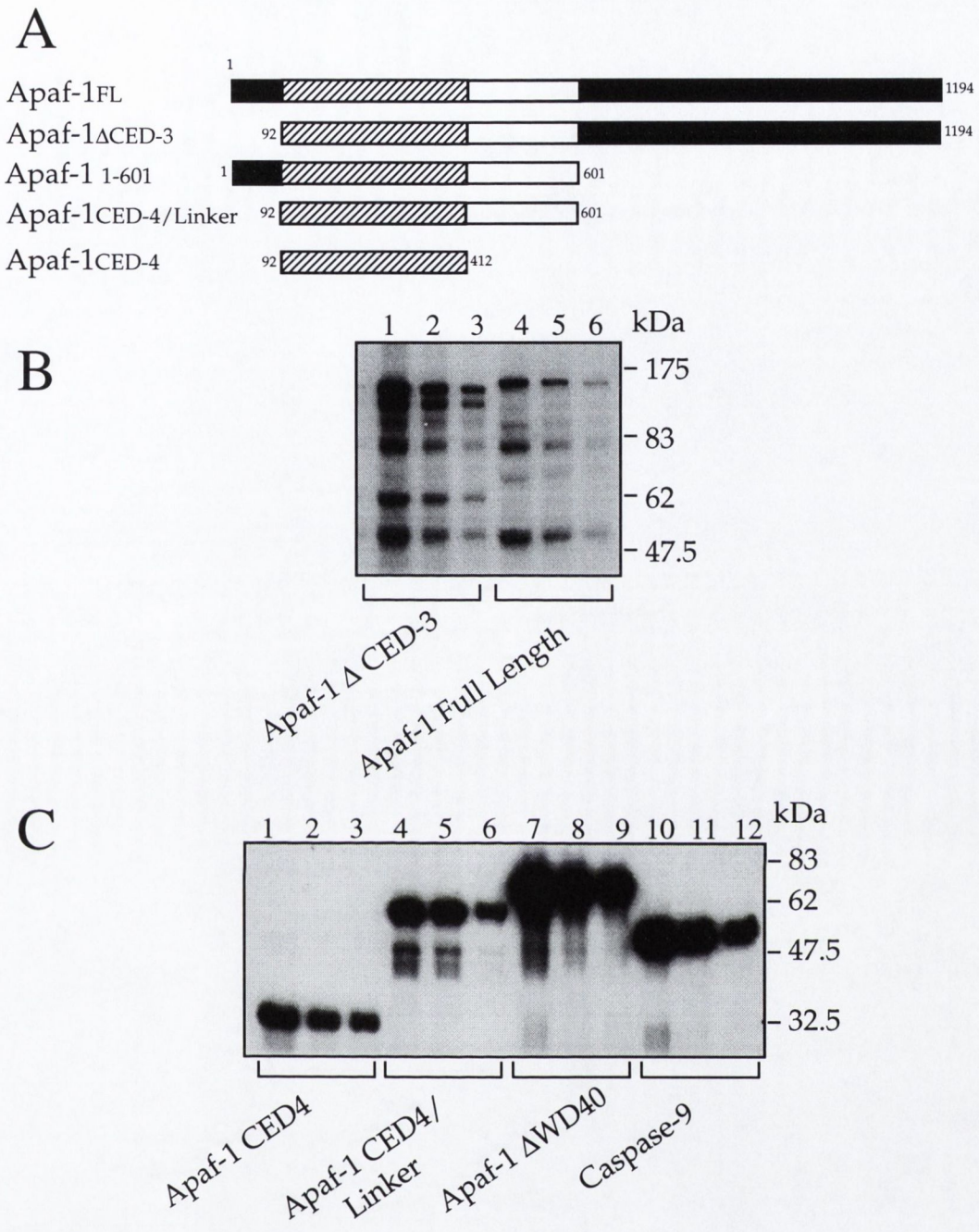

Figure 15

Design and production of radiolabeled Apaf-1 deletion mutant proteins

A, Schematic representation of pcDNA3-derived full length Apaf-1 and its associated deletion mutants that were generated for *in vitro* transcription and translation (ITT) and mammalian expression.

B, Aliquots of 2 µl, 1µl and 0.5 µl of ITT ^{35}S-labeled Apaf-1ΔCED-3 (lanes 1-3), or full length Apaf-1 (lanes 4-6) were subjected to 8% SDS-PAGE followed by fluorography.

C, Aliquots of 2 µl, 1µl and 0.5 µl of ITT ^{35}S-labeled Apaf-1 CED-4 (lanes1-3), CED-4/linker (lanes 4-6), ΔWD40 (lanes 7-9) and full length caspase-9 (lanes10-12) were subjected to 10% SDS-PAGE followed by fluorography. Both images represent 12 hour exposures.

verify that the constructs directed expression of proteins of the predicted molecular weights (Figure 15B, C). We also produced radiolabeled ^{35}S caspase-9 as a positive control for Apaf-1 binding under our GST-pulldown conditions (Figure 15c).

3.3.4. Detection of Apaf-1 self-association by GST pulldown analysis

To verify our two-hybrid observations using an independent assay, we used the reagents described above to determine whether GST fusions of Apaf-1 mutants could specifically capture their radiolabeled counterparts in GST-pulldown assays (Figure 16). Aliquots of approximately 5 μg of GST or GST-Apaf-1^{1-412} or GST-Apaf$^{1-601}$ were typically used in pulldown reactions.

In agreement with the results obtained using the two-hybrid deletion mutants, we consistently observed enhanced capture of ^{35}S-Apaf-CED-4/linker and ^{35}S-Apaf-ΔWD40 by the GST-Apaf-1^{1-601} compared to GST alone (Figure 16B, left panel). Interestingly, the GST-Apaf-1^{1-412} mutant failed to efficiently capture the CED-4/linker protein, again highlighting that efficient Apaf-1 self-association required both the CED-4 and adjacent linker portions of the molecule (data not shown). Strikingly, in experiments employing either GST-Apaf-1 fusion, the *in vitro* translated caspase-9 used as a positive control in this assay bound to bead-immobilized Apaf-1 with a considerably higher affinity than the Apaf-1 self association interaction (Figure 16B, left panel and data not shown).

3.3.5. The WDR inhibits Apaf-1 self-association

Since a primary difference between Apaf-1 and worm CED-4 is the presence of the C-terminal WDR region in Apaf-1, we next sought to examine whether the WDR played a role in regulating Apaf-1 self-association. Since the Apaf-1ΔCED-3 deletion mutant failed to associate with the Apaf-1-CED4-/linker mutant in yeast (Figure 13 and Table 4) this strongly suggested that the WDR region inhibited oligomerization. We first attempted to repeat this striking result by pulldown analysis (Figure 17A, B). In agreement with the results encountered in yeast,

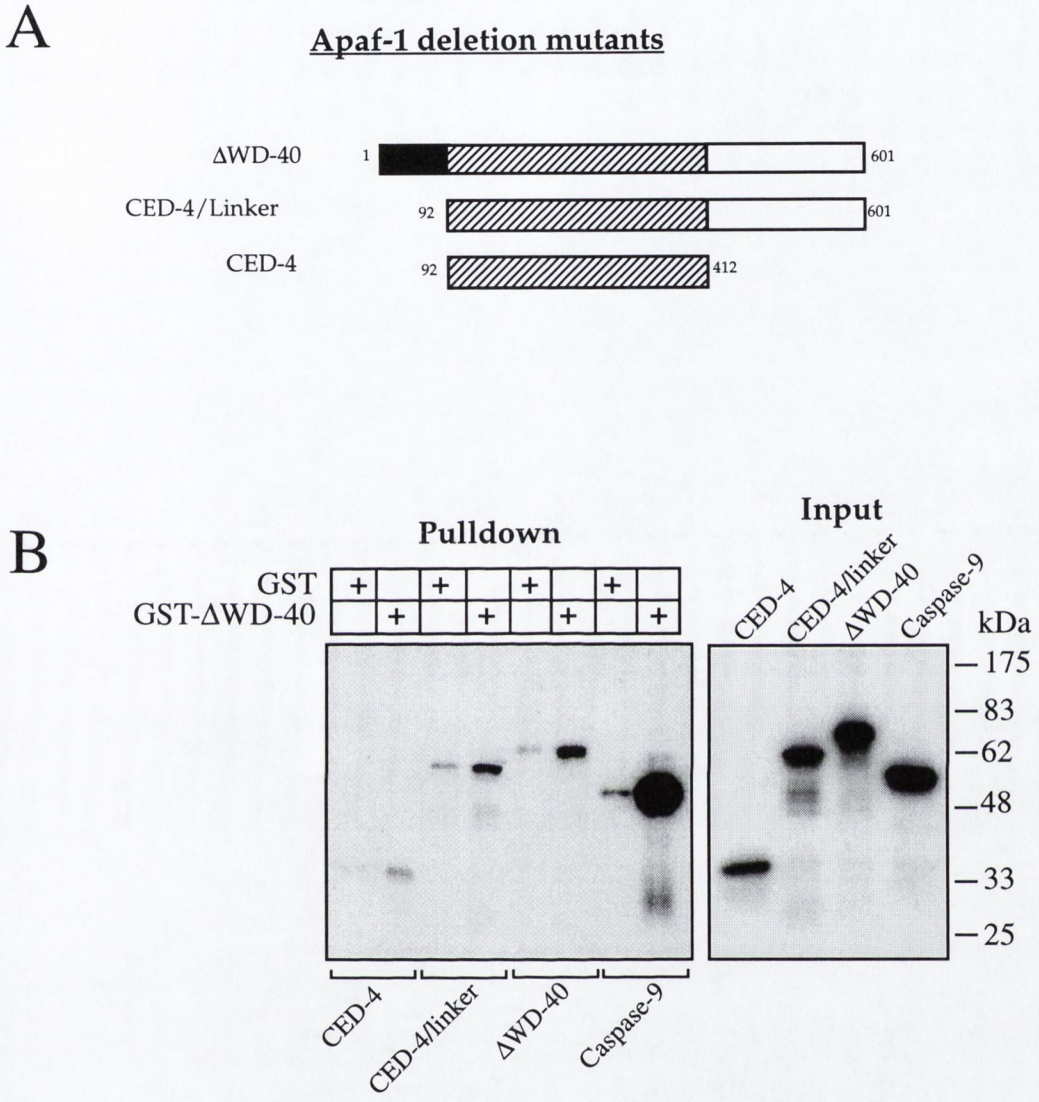

Figure 16

Detection of Apaf-1 self-association using GST-pulldowns

A, Schematic representation of *in vitro* translated ^{35}S radiolabeled Apaf-1 ΔWD40, CED-4/linker and CED-4 deletion mutants that were subjected to the *in vitro* capture assay.

B, Left panel, fluorogram illustrating GST-Apaf-$1^{1\text{-}601}$pulldown capture of ITT ^{35}S-labeled Apaf-1 mutants; right, fluorogram illustrating 10% of the amounts of radiolabeled proteins added to pulldown reactions. Input amounts of radiolabeled proteins were normalized by signal intensity.

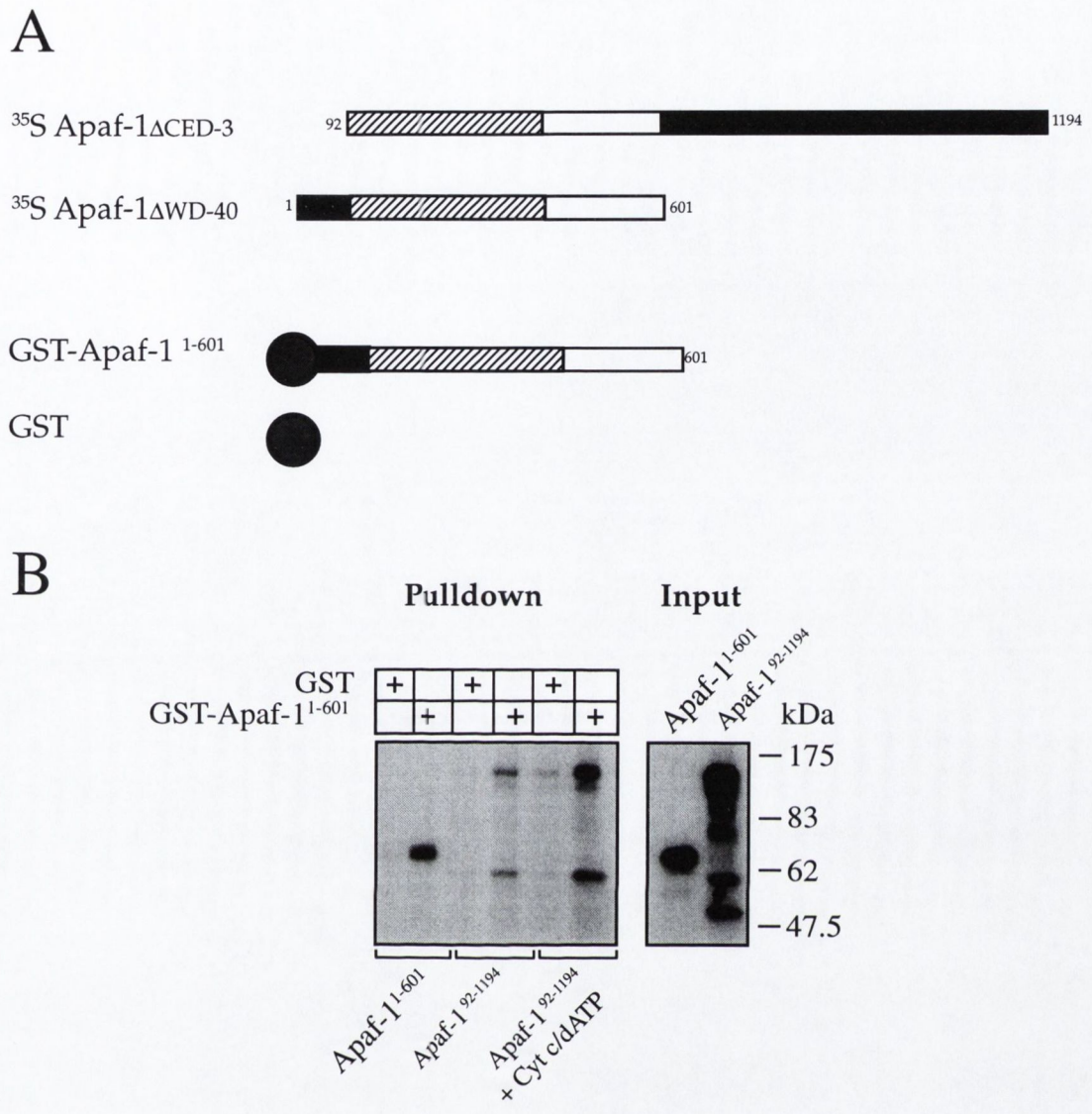

Figure 17

The WDR region of Apaf-1 inhibits self-association in *in vitro* GST pulldown assays

A, Schematic representation of the ^{35}S-labeled and GST-fused Apaf-1 deletion mutants generated for the *in vitro* capture assay; schematic representation of GST-Apaf-1$^{1-601}$ and GST.

B, GST-pulldown illustrating specific capture of the Apaf-1ΔCED-3 mutant by GST-Apaf-1$^{1-601}$ in the presence of cytochrome c (50μg/ml) and dATP (1mM). Left panel, fluorogram of GST pulldown capture assay; right, fluorogram illustrating 10% of the total amount of radiolabeled proteins used in the pulldown reaction. Input amounts of radiolabeled proteins were normalized by signal intensity.

whereas the ^{35}S-labeled Apaf-1 ΔWD40 mutant was readily captured by its GST-fused counterpart, the Apaf-1ΔCED-3 radiolabeled mutant bound GST-Apaf-1^{1-601} with a considerably lower affinity (Figure 16B). These results confirmed our suspicion that the C-terminal WDR plays an important role in inhibiting the ability of Apaf-1 to form oligomers.

3.3.6. Cytochrome *c*/dATP overcome the inhibitory effect of the WDR

Since Apaf-1 was identified by Wang and colleagues as a factor that collaborated with cytosolic cytochrome *c* to modulate apoptosis (Zou *et al.*, 1997), we next examined whether cytochrome *c* could regulate the assembly of Apaf-1 oligomers. While it has yet to be demonstrated directly, it is believed that cytochrome *c* binds to Apaf-1 somewhere within the WDR of the molecule. Since we have observed that the WDR of Apaf-1 seems to exert an inhibitory effect over the formation of oligomers (Figures -13 and -17; Table 4), we reasoned that cytochrome *c* might be a good candidate for a regulator of WDR function. To this end, we added cytochrome *c* and dATP to pulldown reactions and assessed the ability of GST-Apaf-1^{1-601} to capture Apaf-1ΔCED-3 under these conditions (Figure 17B). Surprisingly, in comparison to pulldown reactions lacking cytochrome *c*/dATP, Apaf-1ΔCED-3 was readily captured by GST-Apaf-1^{1-601} with an affinity similar that of the ^{35}S Apaf-1ΔWD40 mutant. These data strongly suggest that the inhibitory properties of the WDR can be overcome by cytochrome *c*/dATP (Figure 17B).

3.3.7. Caspase-9 recruitment of Apaf-1 is negatively regulated by the WDR

Having observed that the WDR plays an important role in the regulation of the ability of Apaf-1 to form oligomers, we next examined the effect that this module has upon the recruitment of caspase-9. To this end, we generated a plasmid encoding GST fused to the N-terminal CARD domain present within the caspase-9 prodomain (GST-Caspase-9^{CARD}) and induced *E.coli* DH5α to express the recombinant protein. This portion of caspase-9 has been demonstrated to be necessary and sufficient for the binding of Apaf-1 to caspase-9 (Slee *et al.*, 1999b).

Figure 18A shows purified GST-caspase-9^{CARD} alongside an aliquot of unfused GST.

We then set up pulldown reactions to assess the ability of similar amounts of bead-immobilized GST or GST-Caspase-9^{CARD} to specifically capture either full length in vitro translated ^{35}S-labeled Apaf-1 or a deletion mutant lacking the inhibitory C-terminal WDR (Figure 18B). Surprisingly, whereas GST-Caspase-9^{CARD} readily captured ^{35}S-labeled Apaf-1ΔWD40, albeit to a slightly more modest extent than the reciprocal of this interaction demonstrated above (Figure 16B), equivalent amounts of full length Apaf-1 failed to be captured in parallel pulldown reactions (Figure 18B). Surprisingly, this suggested that the WDR not only regulates Apaf-1 at the level of formation of oligomers, but critically, also at the level of recruitment of caspase-9 by Apaf-1.

3.3.8. Deletion of the WDR renders Apaf-1 constitutively pro-apoptotic

If removal of the WDR enables spontaneous Apaf-1 oligomerization and caspase-9 recruitment, this would predict that the Apaf-1ΔWD40 mutant ought to be constitutively pro-apoptotic in the absence of cytochrome *c*. To test this hypothesis, we used a transient overexpression system based on lipofection-mediated transient transfection of MCF-7 breast adenocarcinoma cells to evaluate the effect of ectopic expression of the Apaf-1ΔWD40 deletion mutant in mammalian cells (Figure 19). We used pcDNA3-derived mammalian expression plasmids of Apaf-1 and its deletion mutants in these experiments. For comparison, the established pro-apoptotic molecule FADD was used as a positive control. To determine the population of cells that received plasmid, we co-transfected cells with the pCMVβ β-galactosidase reporter plasmid. 48 hours following transfection, cells were stained for β-galactosidase activity in order to identify transfected (blue) cells. Figure 19 illustrates that whereas expression of the pcDNA3 vector provoked minimal apoptosis when transfected into these cells, FADD dramatically attenuated cell survival. Similarly, transfection of a plasmid encoding Apaf-1ΔWD40 resulted in a substantial reduction in the

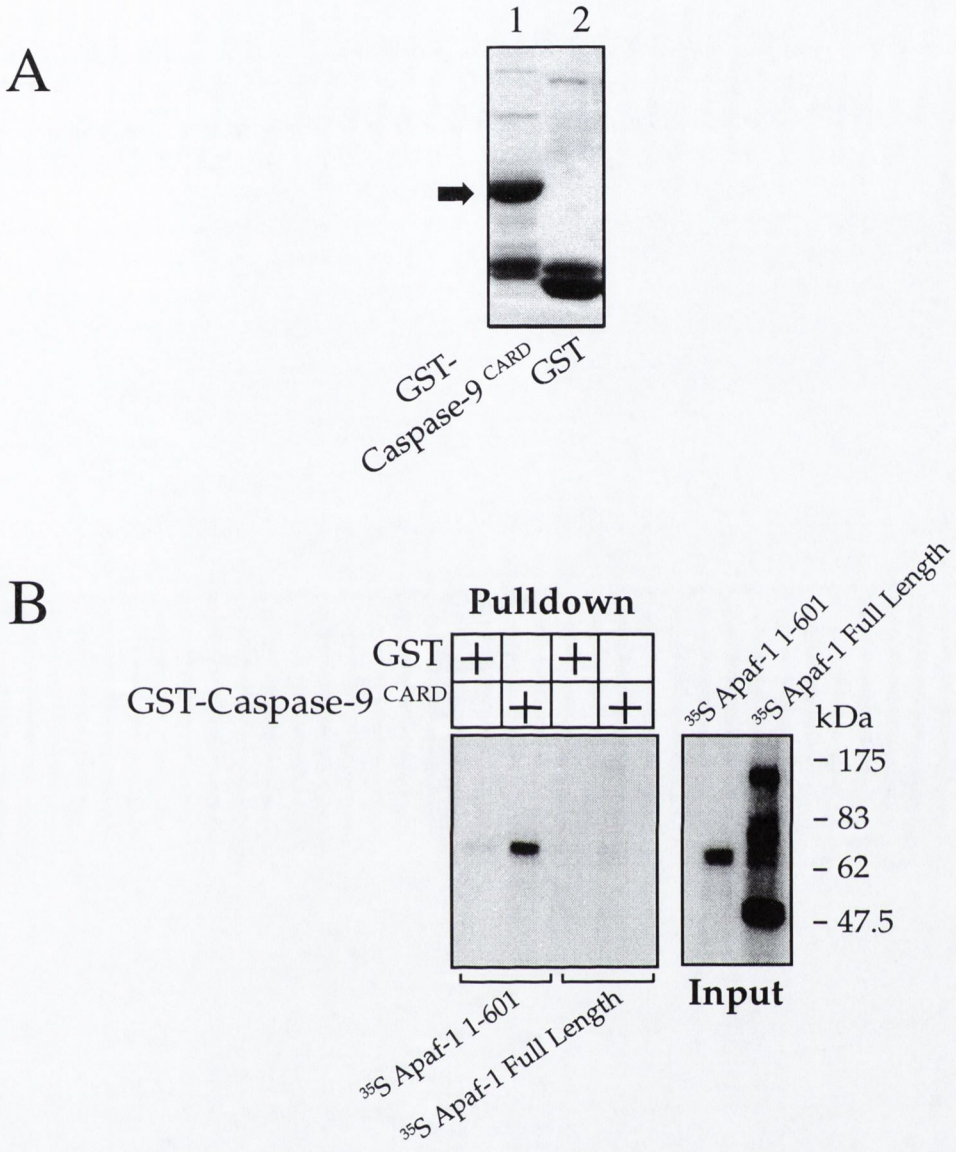

Figure 18

Detection of caspase-9^{CARD} recruitment of radiolabeled Apaf-1 by the GST pulldown *in vitro* capture assay

A,Coomassie stained SDS-PAGE gel illustrating affinity purified GST- caspase-9^{CARD} (lane 1) or GST alone (lane 2). Purified recombinant caspase-9^{CARD} protein is indicated with an arrow. The GST-caspase-9^{CARD} plasmid was made by Mary Harte.

B, GST-pulldown capture assay illustrating that full length Apaf-1 cannot bind GST-Caspase-9^{CARD}. Left panel, fluorogram of pulldown; right, fluorogram illustrating 10% of the total amount of radiolabeled proteins used in the pulldown reaction. Input amounts of radiolabeled proteins were normalized by signal intensity. Results are representative of two independent experiments.

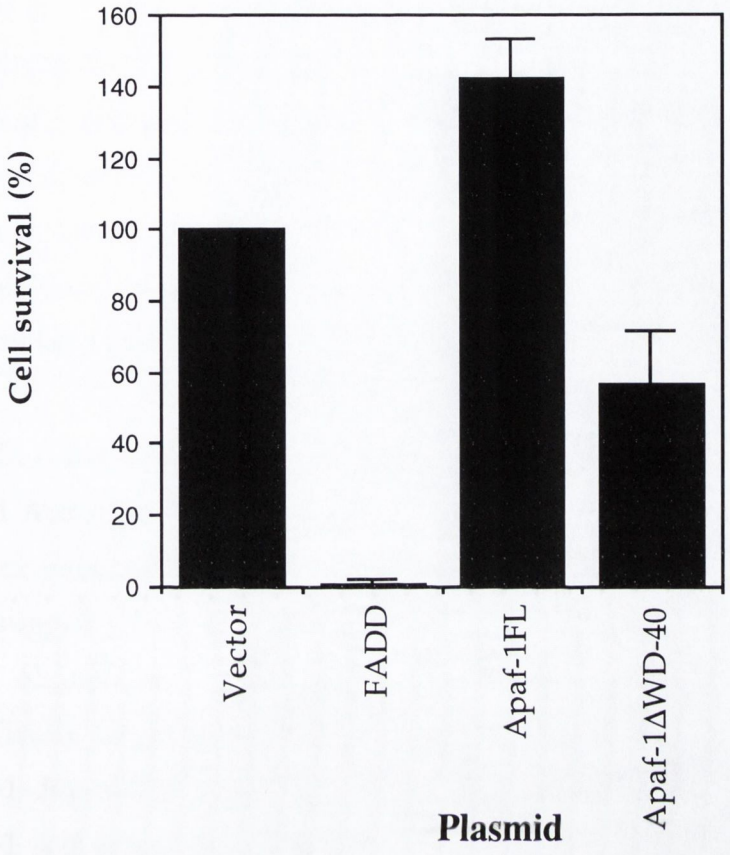

Figure 19

Evaluation of apoptosis associated with forced Apaf-1 expression

MCF-7 human breast adenocarcinoma cells were transiently transfected with 2.5 μg of the indicated pcDNA3-derived plasmids encoding either Apaf-1 full length (F.L.), an Apaf-1 deletion mutant lacking the WDR (ΔWD40), FADD or pcDNA3 vector alongside limiting amounts (500ng) of the pCMVβ reporter plasmid. Cells were fixed and stained for β-galactosidase activity 48 hours post-transfection as described in the Materials and Methods section. Cell survival was determined as the percentage of transfected (blue) cells for each treatment. All treatments were normalized with respect to the background cell death associated with transfection of pcDNA3 vector, expressed as 100% cell survival. A minimum of 3 fields of 100 cells were counted for each treatment. Results represent the mean of three independent experiments +/- SEM. The experiment was carried out in collaboration with Elizabeth Slee.

number of live blue cells, albeit to a more modest degree in comparison with FADD (Figure 19). Interestingly, overexpression of full length Apaf-1 failed to kill cells (Figure 19), consistent with the inability of mutants possessing the WDR to self-associate or recruit caspase-9^{CARD} (Figures -13, -17, -18; Table 4). Thus, there is a clear correlation between the ability of the WDRs to repress dimerization/caspase-9 recruitment and the ability of this region to repress the death promoting activities of Apaf-1. This indeed suggests that the inhibitory properties of the WDR must be neutralized in order to unlock the pro-apoptotic activity of Apaf-1.

3.3.9 *In vitro* modulation of caspase-9 activity

3.3.9.1 Attempts to recapitulate caspase-9 activation *in vitro*

As was detailed previously, Apaf-1 is a very attractive therapeutical target. Our data suggests that the pro-apoptotic activity of Apaf-1 derives from its ability to form oligomers. Thus, we suggest that therapeutic intervention ought to specifically target this oligomerization mechanism, either to repress or promote Apaf-1-dependent apoptosis. In addition we reasoned that an *in vitro* readout of Apaf-1 self-association would be very valuable assay to employ in screening for drugs that repress or promote oligomerization.

We initially determined whether these mutants could activate caspase-9 *in vitro*, since the development of this assay might enable screening for peptide inhibitors of Apaf-1-mediated caspase-9 activation. To this end, we incubated ^{35}S-Caspase-9 with aliquots of GST-Apaf-1^{1-412}, GST-Apaf-1^{1-601} or GST alone, at 37°C in the presence of a buffer containing 1mM DTT in order to stabilize the thiol group in the active site of caspase-9 (Figure 20A). Unfortunately, whereas both of these mutants readily captured caspase-9 in pulldown reactions (Figure 16 and data not shown), they failed to promote the maturation of caspase-9 (Figure 20A).

Since we considered this an important question, as an alternative approach we examined the ability of radiolabeled ITT Apaf-1ΔWD40 to promote maturation of endogenous caspase-9, within the context of reactions incorporating Jurkat cell

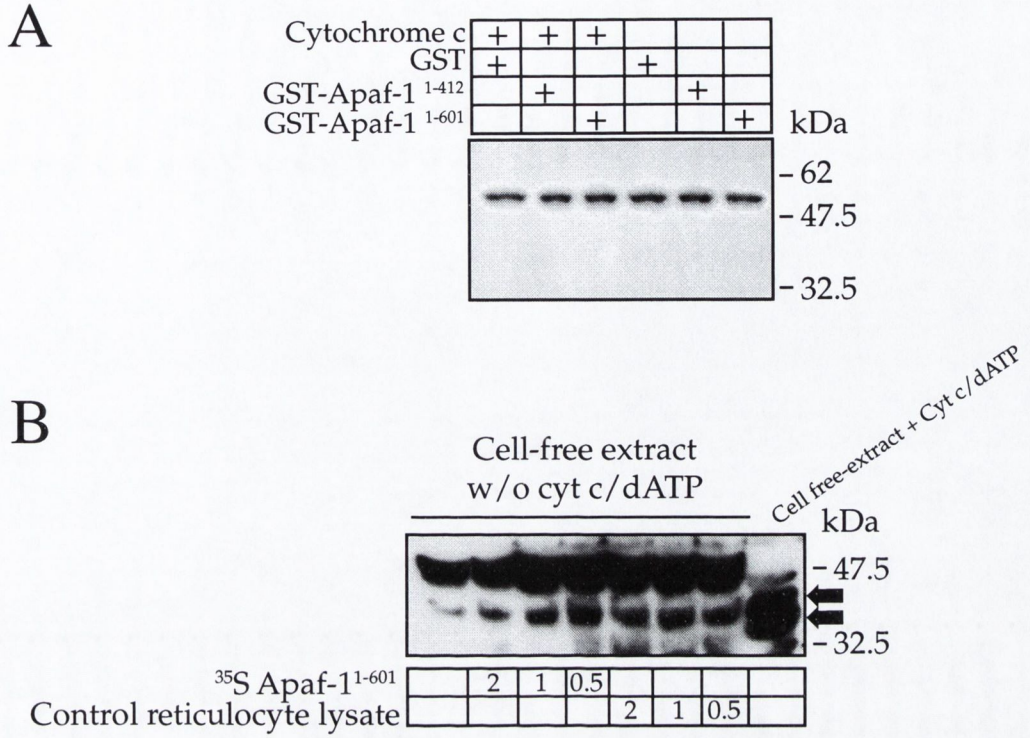

Figure 20

Attempts to modulate caspase-9 activation using recombinant Apaf-1

A, Fluorogram illustrating the inability of GST-Apaf-1^{1-412} or GST-Apaf-1^{1-601} to activate ^{35}S radiolabeled caspase-9 *in vitro*. Aliquots of approximately 5µg of GST, GST-Apaf-1^{1-412} or GST-Apaf-1^{1-601}, pre-washed in WCEB buffer containing 1mM DTT, were incubated in 10µl reactions containing 1mM DTT supplemented with 50µg/ml cytochrome c/1mM dATP containing 1 µl of ^{35}S radiolabeled caspase-9. Samples were incubated for 2 hours at 37°C, followed by subjection to 10% SDS-PAGE and fluorography.

B, Anti-caspase-9 immunoblot illustrating the inability of a ^{35}S-labeled Apaf-1 deletion mutant lacking the WDR (Apaf-1 ΔWD40) to activate endogenous caspase-9 in cell free extracts. Aliquots of either 2, 1 or 0.5 µl of ^{35}S-Apaf-1 ΔWD40 or equivalent amounts of control rabbit reticulocyte lysate were added to Jurkat S-15 cell-free extracts containing 1mM DTT in a total reaction size of 10µl. Samples were incubated at 37°C for 2 hours and subsequently subjected to 10% SDS-PAGE and immunoblotting with an anti-caspase-9 polyclonal antibody. The reaction indicated by the lane on the extreme right was supplemented with 50µg/ml cytochrome c and 1mM dATP and serves as a positive control for caspase-9 activation. The arrows denote the processed form of caspase-9.

free extract. As is illustrated in Figure 20B, a control reaction comprising extract treated with cytochrome *c*/dATP to trigger the apoptotic program, induced maturation of caspase-9 into the p35/p37 active subunits, as assessed by immunoblotting of endogenous caspase-9 in extracts using a caspase-9-specific polyclonal antibody. In contrast, extracts treated with ^{35}S-labeled Apaf-1ΔWD40 failed to propagate caspase activation (Figure 20B).

3.3.9.2. Attempts to repress caspase-9 activation *in vitro*

To address the problem from a different angle, we speculated that the CED-4/linker mutant may be able to interfere with endogenous Apaf-1 activity by binding to endogenous Apaf-1 and preventing the formation of caspase-9-activating complexes. This mutant lacks the N-terminal caspase-9 recruitment motif and therefore can form oligomers, but cannot bind to caspase-9 (Figure 21A). To test this, we incubated ^{35}S-labeled Apaf-1CED-4/linker with Jurkat S-15 cytosolic extracts activated by the addition of cytochrome *c* and dATP. Reactions were analyzed at relatively short endpoints, in order to observe any subtle or transient inhibitory effect that might occur. Unfortunately, we were unable to observe any inhibitory effect attributable to the addition of Apaf-1CED-4/linker as judged by detection of radiolabeled caspase-9 added exogenously to extracts (Figure 21B).

3.4. Two-hybrid Screening for Apaf-1 interactors

We next sought to identify novel Apaf-1 binding partners as a means to further dissecting the role of the molecule during apoptosis. As described in section 3.2. of this chapter, it is likely that molecules including novel caspases and CED-9 homologues may bind to Apaf-1. Moreover, as a result of our observations concerning the ability of Apaf-1 to dimerize, we were keen to investigate whether novel interacting partners might inhibit or promote this mechanism by binding to Apaf-1.

Since the Apaf-1 protein is a multi-modular molecule, possessing at least three clearly defined structural entities (Figure 22A), we reasoned that screening with

Figure 21

Attempt to repress in vitro activation of caspase-9 using recombinant Apaf-1

A, Schematic representation of the ^{35}S radiolabeled Apaf-1 CED-4/linker deletion mutant used to attempt to inhibit *in vitro* activation of caspase-9.

B, Fluorogram illustrating the inability of ^{35}S Apaf-1 CED-4/linker to inhibit *in vitro* caspase-9 activation. Aliquots of 1 µl of ^{35}S Caspase-9 plus 5 µl of Jurkat S-15 cell free extract (CFE) were incubated in buffer containing 1mM DTT alongside either 2, 1 or 0.5 µl of ^{35}S Apaf-1 CED-4/linker. Where indicated, samples were treated by the addition of cytochrome c (50µg/ml) and dATP(1mM) to initiate Apaf-1-dependent activation of caspases. Samples were incubated at 37^{o}C for the ind icated timepoints and reactions were stopped by the addition of an equal volume of 2x SDS-PAGE loading buffer. Samples were then subjected to 10% SDS-PAGE and fluorography. The image shown represents a 12 hour exposure. Control treatments incorporating 2 µl of rabbit reticulocyte lysate were included for both of the indicated timepoints. The solid line indicates unprocessed caspase-9, the arrows denote the caspase-9 cleavage product. ^{35}S Apaf-1 CED-4/linker protein is indicated by an asterisk.

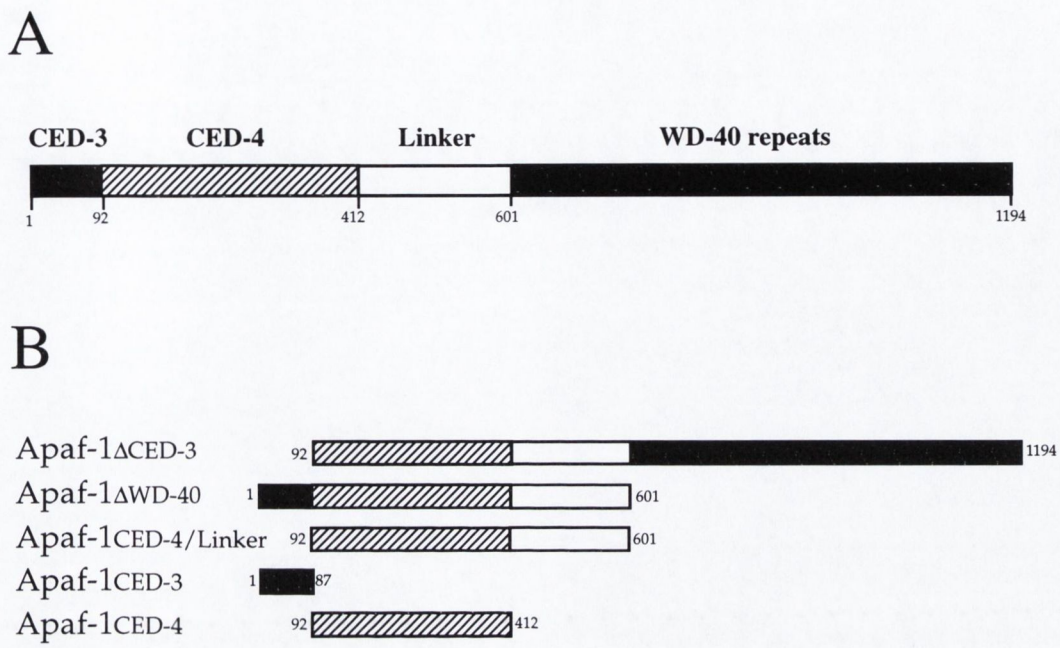

Figure 22

Selection of an Apaf-1 Gal-4 DB mutant suitable for screening purposes

A, Schematic representation of full length Apaf-1 protein. Indicated are the CED-3-homologous, CED-4-homologous, Linker and WD-40 repeat regions of the molecule.

B, Schematic representation of the Two-Hybrid Gal-4 DNA binding domain (DB) fusion proteins of Apaf-1 mutants that were preliminarily tested for the screening procedure.

Table 5

Summary of the suitability of the Two-Hybrid Apaf-1 DB mutants for screening purposes.

Apaf-1 DB-Fusion	Comment	Suitability for Screening
pAS2-1 ΔCED-3	Toxic when expressed in yeast	No
pAS2-1 ΔWD40	Autoactivates reporter systems	No
pAS2-1 CED-3	Autoactivates reporter systems	No
pAS2-1 CED-4/Linker	Toxic	No
pAS2-1 CED-4	Mildly Toxic	No
pGBT-8 CED-4	Non-Toxic	Yes

the full length molecule would offer the greatest chance of success in retrieving an interaction partner. However, we were concerned about the use of the full length protein as a screening bait for two reasons. Firstly, during the earlier studies, we had observed that expression of the Apaf-1ΔCED-3 contruct was in fact considerably toxic to yeast, thus rendering it unsuitable for screening purposes (See Table 5). By extension, it was likely that the full length protein would similarly prove toxic when expressed in yeast. Moreover, because the actual function of the WDR region of Apaf-1 was unknown, it thus constituted an attractive screening target. However, we were concerned that because of the relatively ubiquitous presence of WDR modules in numerous other cellular proteins, the screen might retrieve many non-specific WDR-binding molecules that did not have a genuine specificity for Apaf-1.

On this basis, we considered that it was most logical to screen with the Apaf-1 ΔWD40 mutant, since this truncation possessed both CARD and CED-4 motifs. This offered two potential interaction faces with which to retrieve binding partners. Moreover, in earlier analyses, we observed that this mutant could readily dimerize; thus, screening with this portion of the molecule may yield interactors that promote or repress dimerization. To this end, we designed and generated a pAS2-1-derived plasmid encoding an in-frame fusion with the coding sequence of amino acids 1-601 of Apaf-1 (designated DB-Apaf-1 ΔWD40; Figure 22 and Table 5). To obtain a yeast transformant for screening purposes, we transformed the host strain Y190 with the DB-Apaf-1ΔWD40 plasmid, according to the lithium acetate technique described in Chapter II. To select for transformants harboring the pAS2-1-derived Gal-4 DB-Apaf-1 plasmid, yeast were plated on SD media lacking the amino acid tryptophan.

Before progressing towards the screening procedure, Y190 host strain was additionally transformed with the DB-Apaf-1ΔWD40 construct together with the pACT-2 AD empty vector to ensure that expression of the recombinant Apaf-1 molecule did not autonomously autoactivate the reporter genes. These

transformants were plated on media lacking tryptophan and leucine to select for the presence of the DB and AD-encoding plasmids, respectively. In order to test for auto-activation, representative colonies were then retreaked on media additionally lacking the amino acid histidine. Only yeast transformants harboring positive interacting pairs—or an autoactivating bait fusion protein—should be able to grow on this media, as a result of transactivation of the *HIS3* histidine synthetase gene under control of a Gal-4-responsive Upstream Activating Sequence (UAS). Unfortunately, preliminary analysis revealed that the DB Apaf-1 ΔWD40 mutant did indeed autoactivate the *HIS3* reporter gene (Table 5). Moreover, this mutant also transactivated the second, *LacZ* reporter gene in β-galactosidase colony lift assays (Table 5). As a compromise strategy, we contemplated using a DB-Apaf-1 CED-3-only mutant, encoding a fusion of the Apaf-1 CARD. However, this construct also autonomously transactivated both reporter genes, thus preventing it from being used in the screening procedure (Table 5).

We next re-directed our focus towards screening for Apaf-1 CED-4-domain interactors. Since the previous analyses demonstrated that the Apaf-1 CED-4/Linker mutant readily self associated in yeast and did not autoactivate the reporter systems (Figure 13 and Table 4), we decided this was a suitable candidate for screening. However, consistent with a report concerning the toxicity of worm CED-4 protein when expressed in yeast, expression of this construct was similarly toxic (James *et al.*, 1997). We therefore opted to screen with the DB-CED-4 domain-only mutant, encoded by amino acids 92-412 of the full-length Apaf-1 protein (Figure 22A and Table 5). Since this mutant possessed the minimally-defined, conserved CED-4-homologous region and retained an albeit weak self-association ability, we decided to to seek interacting proteins that might modulate Apaf-1 self-association.

As a prelude to screening, we generated Y190 yeast transformants of the pAS2-1 DB Apaf-1 CED-4 plasmid in the manner described above. In order to determine

whether this mutant was suitably non-toxic for efficient screening purposes, we then conducted a series of test sequential transformations, by transforming the Y190 DB-Apaf-1 CED-4 host with pACT-2 jurkat cDNA library plasmid intended for the library screening procedure. For comparison, host strain Y190 and a Y190 mutant expressing the unfused Gal-4 DB protein were included as controls for these test transformations. The outcome of these experiments is summarized in Table 6. Untransformed Y190 yeast regularly yielded in the region of ~10^5 transformants/μg of input library DNA, and Y190 overexpressing the unfused DB moiety yielded approximately one log fewer transformants than this. Unfortunately, the Y190 Apaf-1 CED-4 mutant generally yielded in the region of $5x10^3$ transformants/μg of DNA (Table 6). Since substantial subsequent efforts designed to optimize screening with this construct failed to measurably improve the transformation efficiency, we decided to proceed into a screen, albeit with a reduced efficiency.

As a guideline, information concerning the technicalities of the screen is provided in Table 7. As is illustrated, an attempt to screen one complexity of the pACT-2 Jurkat cDNA library, some $3x10^6$ individual library clones, would have required using 600 μg of library plasmid. As a compromise, we opted to screen 500 μg of plasmid: aiming to cover in the region of $2.5x10^6$ cfu, or some ~80% of the total library complexity. As a further necessary compromise, we increased the plating density of yeast by five-fold, thus using 80, rather than the required 400, 15 cm screening plates (Table 7).

The screening procedure was performed as detailed in the Chapter II. To determine the transformation efficiency of the screen, we plated identical aliquots of library-transformed yeast onto control plates composed of leucine and tryptophan-deficient SD media. This revealed that the actual efficiency of the screen was only in the region of ~$3.0x10^2$/μg of DNA, predicting that approximately $1.5x10^5$ individual library clones had been screened. Unsurprisingly given the paucity of clones screened in this attempt—

Table 6

Table illustrating a comparison in the average transformation efficiency of yeast strains Y190, Y190 DB empty vector and Y190 Apaf-1 CED-4 when transformed with pACT-2 library plasmid.

Yeast Host Strain	Average Transformation Efficiency/μg of pACT-2 library DNA
Y190	$1.4x10^5$
Y190-pAS2-1 Vector	$1.6x10^4$
Y190-pAS2-1 Apaf-1 CED-4	$5.6x10^3$

Table 7

Table illustrating the relationship between yeast transformation efficiency and the scale of library screening undertaken.

Predicted Screening Efficiency	~$5x10^3$/μg library DNA
Library Complexity	~$3x10^6$ Independent Clones
No. μg required to screen 1 library Complexity	$3x10^6/5x10^3$ =600 μg
No. μg required to screen ~80% Complexity	2. $5x10^6/5x10^3$ = 500 μg
Maximum DNA amount transformable	5μg/10^8 yeast cells
No. yeast cells required for 500 μg	$1.0x10^{10}$ cells
Recommended plating density	$2.5x10^7$ cells/ 15 cm plate
Total plates required	$1.0x10^{10}/2.5x10^7$ = 400 plates
Total plates required at 5X normal density	80 plates

Table 8

Table illustrating a comparison between the library transformation efficiency of Y190 pGBT-8 empty vector and that of the Y190 pGBT-8 Apaf-1 CED-4 strain.

	Mean Transformation Efficiency/μg library DNA	
Yeast Strain	Experiment #1	Experiment #2
Y190 pGBT-8 DB empty vector	$1.1x10^5$	$5.1x10^4$
Y190 pGBT-8 Apaf-1 CED-4	$1.2x10^5$	$5.9x10^4$

representing approximately only 5% of the total library complexity—this screening procedure failed to reveal any significant candidate clones, as judged by a lack of histidine prototroph colonies 10-14 days following plating. Thus, due to the toxicity of this molecule as well as possible compromization of the screen because of plating the yeast at a higher than recommended screening density, this approach was unsuccessful in retrieving Apaf-1 binding partners.

Since our failure to conduct a library screen related to a toxic effect of the overexpressed DB-Apaf-1CED-4 protein, we reasoned that reducing expression levels of the protein might reduce toxicity, making this molecule more amenable for screening. To explore this possibility, we obtained the pGBT-8 Gal-4 DB-encoding plasmid. This progenitor of the more modern pAS2-1 plasmid encodes the same sized Gal-4 DB moiety, the first N-terminal 147 amino acids of the wild-type transcription factor. However, it possesses a weaker promoter than its pAS2-1 derivative. It was correspondingly likely that the expression levels of the resultant fusion protein would be lower than those obtained from the pAS2-1 vector.

To see if reduced expression levels of our toxic bait could remedy the transformation efficiency problem, we subcloned the Apaf-1 CED-4 insert directly from the pAS2-1 DB Apaf-1 CED-4 plasmid used in the failed screen. The insert was excised, as described in Chapter II, using the restriction enzymes Sma-1 and Sal-1 and then ligated into the linearized pGBT-8 empty vector bearing complementary restriction sites. Following screening for recombinant clones that possessed the insert flanked by the appropriate restriction sites, Y190 yeast host was transformed with the pGBT-8 Apaf-1CED-4 plasmid, alongside the corresponding pGBT-8 empty vector as a control. Strikingly, both of these plasmids transformed with a similar efficiency/μg, suggesting that the DB-Apaf-1CED4 was less toxic than its predecessor. This probably related to reduced expression levels of both the Gal-4 DB protein and its Apaf-1 mutant derivative.

On the basis of this encouraging result, we then proceeded to test the Y190 DB-Apaf-1CED-4 mutant to determine whether the sequential transformation efficiency was also much improved due to reduced toxicity levels. As is detailed in Table 8, these experiments revealed that the pGBT-8-based Apaf-1 mutant was readily transformable with pACT-2 jurkat library DNA, with an efficiency ranging between ~$6x10^4$-$1x10^5$. Thus, on this basis it was decided to proceed with the screening procedure, the toxicity problem having been solved by switching expression vectors.

We embarked upon a second two-hybrid screen, this time using 100μg of library DNA to screen a predicted $5x10^6$ individual library molecules, assuming an efficiency of $5x10^4$ cfu/μg of DNA. The screening procedure was conducted as detailed within Chapter II. Briefly, based on control platings, we screened some $6x10^6$ clones, approximately twice the complexity of the library. These were plated on a total of 40x15 cm plates lacking the amino acids histidine, leucine and tryptophan, supplemented with 25mM 3-AT to dampen down leaky expression of the reporter genes, according to the manufacturer's protocol. Visual inspection of the screening plates 9 days later revealed the presence of many small candidate histidine prototrophs. These were re-streaked on fresh histidine-deficient media to assess their ability to grow on media that did not initially have a covering of dead yeast.

The pGBT-8 plasmid features a lower expression level than its pAS2-1 derivative. We therefore reasoned that it might be difficult to make a decisive assessment as to the preferential candidacy of specific putative interactors based on the *LacZ* colony lift assay, since the extent of blue colour development may have been hampered by the low cellular levels of the protein. Thus, some 80 of the clones that regrew upon restreaking on fresh histidine-deficient media were subjected to further analysis, independent of an assessment of *LacZ* activity. To this end, we created inocula of the candidate clones and grew these in liquid selective media in order to obtain yeast pellets for the isolation of total yeast plasmid DNA. We

used a mixture of phenol and glass beads to achieve disruption/isolation of the yeast, as described in Chapter II. As is described therein, plasmid obtained in this procedure was used as template for PCR-based insert screening reactions, incorporating primers that flank the pGBT-8 multiple cloning site.

In an attempt to collapse these candidate clones into more managable putative subgroups, we next performed Alu-1 restriction digest analysis on the PCR products amplified from the yeast plasmid template. Since this enzyme is a frequent cutter, library clones harbouring contiguous portions of the same gene therefore ought to exhibit similar hallmark Alu-1 banding patterns. Disconcertingly, in spite of our having screened approximately twice the compexity of the library, this analysis failed to reveal any striking similarity in Alu-1 banding patterns. As a result, approximately the first forty of these clones were arbitrarily chosen for sequencing.

To reveal the identity of some of the putative Apaf-1 interactors, we used the PCR products described above as template for automated DNA sequencing reactions, as described in Chapter II. The samples were then subjected to automated sequencing using a Perkin Elmer ABI-PRISM 310 Genetic Analyzer automated sequencer, according to the manufacturer's instructions. The resultant nucleotide sequences were stripped of any vector-specific DNA and subjected to database interrogation using the BLASTN and BLASTX algorithms, accessed via the NCBI web interface. These algorithms were used to search the non-redundant database for similarities to human and non-human genes. The BLASTN algorithm directly interrogates nucleotide sequences, whereas the BLASTX algorithm performs a conceptual amino acid translation of a nucleotide sequence in all three reading frames and then probes a protein database.
Unfortunately, interrogation of the non-redundant NCBI database revealed the screen to be a failure, as judged by the lack of multiple copies of any particular molecule. On this basis, the screening procedure was abandoned as a means of retrieving Apaf-1 interactors. For reference, the identity of some of the library clones is recorded in Tables-9 and -10.

TABLE 9

Table illustrating clones obtained from the Apaf-1 Yeast-Two–hybrid Screen identified by DNA sequencing followed by BLAST database searching

Clone No.	Identity/ Similarity	Accession No.	Species	E-Value (BLASTN)	E-Value (BLASTX)
1B	Human p311	U30521	*Homo sapiens*	0.030	
1D	SWI/SNF complex 170kDa subunit	U66616	*Homo sapiens*	8e-55	
2A	Sequence from cosmid L60G9B, Huntington's Disease Region	Z69363	*Homo sapiens*	0.0	
2D	Proteasome Iota Chain	P34062	*Homo sapiens*		9e-34
2E	Prolyl 4-hydroxylase alpha subunit	M24487	*Homo sapiens*	0.0	
2F	Tyrosine phosphoprotein SLP-76	A56110	*Homo sapiens*		9e-80
3A	Ubiquitin fusion degradation protein homolog	AF059906	*S. pombe*		4.8
3B	Alu subfamily SB warning entry	P39189	*Homo sapiens*		4e-04
3D	Human rac protein kinase alpha mRNA	M63167	*Homo sapiens*	0.0	
3E	Mammary tumour-associated protein INT-6	U94174	*Homo sapiens*		2e-47
4A	Cytoskeletal gamma-actin	X04098	*Homo sapiens*	0.0	
6A	Ribosomal protein L30	M94314	*Homo sapiens*	e-179	
6B	Heat shock factor binding protein	AFO68754	*Homo sapiens*	0.0	
8C	18S ribosomal RNA	L15195	*Byblis liniflora*	0.42	
9C	SSR alpha subunit	Z12830	*Homo sapiens*	7e-18	
14B	Mucin 5AC	S53363	*Homo sapiens*		0.001
15B	COX17 mRNA	L77701	*Homo sapiens*	0.0	

TABLE 10

Table illustrating clones obtained from the Apaf-1 Yeast-Two–hybrid Screen identified by DNA sequencing followed by BLAST database searching

Clone No.	Identity/Similarity	Accession No.	Species	E-Value (BLASTN)	E-Value (BLASTX)
18A	Carnitine palmitoyltransferase II precursor	U09646	*Homo sapiens*	e-110	
19A	Mus musculus mbac6, complete sequence	AC004407	*Mus musculus*	0.10	
19B	Chromosome 17, clone HRPC1169K15	AC003963	*Homo sapiens*	0.027	
19D	Ribosomal protein S3a	M77234	*Homo sapiens*	0.0	
21A	60S ribosomal protein	P52859	*Rattus norvegicus*		5e-44
21B	SEC14L mRNA	D67029	*Homo sapiens*	e-173	
21C	Hypothetical protein	AL022245	*S. pombe*		6.1
23A	ribosomal protein L7a (surf 3)	M36072	*Homo sapiens*	0.0	
23D	Replication factor C	M87339	*Homo sapiens*	e-111	
26A	DNA sequence from cosmid U84B10	Z70274	*Homo sapiens*	5e-07	
34A	Streptomyces cyaneus plasmid pSA1.1	AB010724	*Streptomyces cyaneus*	0.46	
37A	Immunoglobulin gamma chain	M81769	*Sus scrofa*		169
37B	PIG-L	D88364	*Rattus norvegicus*		4e-24
38A	60s ribosomal protein L23	P23131	*Homo sapiens*		5e-34
39A	KIAA0005 gene	D13630	*Homo sapiens*	0.0	
40C	C37E2.2	Z81046	*C. elegans*		8.5
41B	DNA sequence from BAC 1216H12 on chromosome 22q12	AL008715	*Homo sapiens*	0.12	

3.5. DISCUSSION

3.5.1. Summary

In this study, we have identified the WDR region as a critical regulator of Apaf-1 function, dually in terms of the ability of this molecule to self-associate, as well as by modulating caspase-9 recruitment. Using two-hybrid and GST pulldown deletional analyses, we have demonstrated that Apaf-1 is capable of direct self-association in the absence of other cytosolic adaptor molecules. Moreover, we have pinpointed the CED-4 and adjacent linker domains of the molecule as the oligomerization surfaces necessary and sufficient for the formation of Apaf-1/Apaf-1 complexes.

3.5.2. Apaf-1 functions via an induced proximity mechanism

Our observation that Apaf-1 is capable of self-association further supports the "induced proximity" model of caspase activation (Salvesen and Dixit, 1999) whereby inactive procaspase zymogens become converted into their mature enzymatically active forms via an aggregation-dependent mechanism. It is thus tempting to speculate that Apaf-1 acts primarily as a procaspase-9-aggregating molecule. As a result, negative regulation ought to act at the level of restricting the ability of the molecule to form oligomers. Herein, we have demonstrated that the WDR region of Apaf-1 performs this role. Interestingly, a report has suggested that artificially induced aggregation of procaspase-9 is sufficient to promote its autocatalytic processing (Srinivasula *et al.*, 1998). Within this context, it is also interesting to note a report that suggests that nematode CED-4 activates its cognate caspase, CED-3, via a similar clustering mechanism (Yang *et. al.*, 1998a). Indeed, this study reveals a direct correlation between the ability of nematode CED-4 to oligomerize and its ability activate the CED-3 caspase, since oligomerization-dead CED-4 mutants fail to have CED-3 activating properties (Yang *et. al.*, 1998a). Thus, Apaf-1 and CED-4 share a conserved induced proximity caspase-activating mechanism.

3.5.3. Apaf-1 oligomerization requires the CED-4-homologous domain

These data therefore imply that human Apaf-1 and worm CED-4 share not only a common ability to self associate in order to activate their respective target caspase, but moreover, that they possess an evolutionarily conserved oligomerization surface: the CED-4 domain. Interestingly, the CED-4-homologous region of *Drosophila* Apaf-1 relative, DARK is similarly well conserved (Figure 11C) (Rodriguez *et al.*, 1999).

While our analyses reveal that oligomerization of human Apaf-1 is dependent on the CED-4-homologous domain, the results suggest that optimal Apaf-1 self-association additionally requires the so-called "linker" region. The requirement for the latter in human Apaf-1 oligomerization may represent a divergence in the components of the oligomerization surface between human Apaf-1 and worm CED-4. It is more likely however, that the presence of this additional motif in the CED-4/linker deletion mutants may stabilize the folding of this artificially truncated mutant. However, it is nonetheless interesting to note that several other groups have reported a similar requirement for both the CED-4 domain as well as portions of the adjacent "linker domain" for maximal formation of oligomers (Hu *et al.*, 1998b; Srinivasula *et al.*, 1998). Clearly however, since the linker region alone is insufficient to mediate even a weak degree of self-association (Figure 13 and Table 4), these data suggest that the evolutionarily conserved CED-4-homologous region plays an essential role in Apaf-1 oligomerization.

3.5.4. The WDR plays a dual role in regulating Apaf-1 activity

Clearly, human Apaf-1 and nematode CED-4 differ considerably with respect to the presence of multiple WDRs in the former. Our results reveal the critical role of the WDRs within human Apaf-1 as a means of safely muzzling inappropriate Apaf-1 activity in the absence of cytosolic cytochrome *c*, since the Apaf-1ΔCED-3 mutant lacks spontaneous oligomerization/caspase-9 binding abilities. We have demonstrated that the WDRs act as a death-repressing module via two important and distinct mechanisms.

Under normal conditions, Apaf-1 is prevented from self-association by the presence of the WDR. From our data, we predict that the removal of the WDR mimics the *in vivo* binding of cytosolic cytochrome *c* to Apaf-1. Using GST pulldown analysis, we have demonstrated that cytochrome *c* and dATP can overcome the block that the WDRs exert on Apaf-1 oligomerization. Whereas the ΔCED-3 mutant failed to be captured by GST-Apaf-1 1-601 in the absence of cytochrome *c*, addition of this molecule to pulldown reactions enabled self-association of Apaf-1 with an affinity similar to the WDR-deficient Apaf-1ΔWD40 mutant.

Importantly, we provide additional evidence for the WDRs as a regulator of caspase-9/Apaf-1 interaction. Whereas the ΔWD40 mutant that was capable of self-association was readily captured by GST-caspase-9^{CARD}, full-length Apaf-1 failed to be recruited under similar conditions. Given this, it is tempting to speculate that cytochrome *c* binding to the WDR may overcome this block on procaspase-9 recruitment.

These data therefore highlight the critical importance of the WDR as a regulator of Apaf-1 activity and suggest that the binding of cytochrome *c* to Apaf-1, presumably within the WDR, may induce a conformational change in the molecule that has long-range effects, influencing both the formation of oligomers as well as the recruitment of procaspase-9.

3.5.5. The WDR represses the pro-apoptotic activity of Apaf-1

In this study, we have demonstrated a functional correlation between the ability of Apaf-1 mutants to spontaneously oligomerize/recruit caspase-9 and their ability to induce apoptosis in the absence of a cytochrome *c*-mediated death signal. Whereas transiently overexpressed Apaf-1 failed to provoke apoptosis and moreover, elicited a slight pro-survival effect (Figure 19), the ΔWD40 mutant autonomously initiated apoptosis. These data therefore highlight the critical

importance of both Apaf-1 oligomerization and the recruitment of caspase-9 during Apaf-1-mediated apoptotic signal transduction. Further studies will be required to determine whether caspase-9 recruitment and the formation of oligomers occur simultaneously upon the binding of cytochrome *c*, or whether one of these steps occurs following the other.

In this study, we have not examined the role of dATP either with respect to its influence upon the formation of oligomers or the binding of caspase-9 to Apaf-1. Moreover, we have not discriminated between cytochrome *c* and dATP-mediated effects upon the WDR. However, on the basis that mutation of the P-loop in worm CED-4 abrogates its CED-3 activating activity, it is likely that dATP binding/hydrolysis is important for human Apaf-1 function (Chaudhary *et al.*, 1998).

3.5.6. Screening for Apaf-1-interacting proteins

In this study we have attempted to further elucidate the Apaf-1 pathway using a two-hybrid approach to identify novel Apaf-1 interacting molecules. Unfortunately, due to technical difficulties, relating to the toxicity of the molecule, this approach has been unsuccessful. Interestingly, our observation that Apaf-1 expression is toxic in yeast concurs with a report concerning the toxicity of *C. elegans* CED-4 (James *et al.*, 1997). It is unlikely in either of these cases that CED-4 or its human relative can trigger a specific death program in yeast, most obviously since no caspase homologues have been identified in these primitive eukaryotes. It is nonetheless interesting to note that the nucleotide binding motif, or P-loop can be found conserved amongst a family of plant genes that play a role in host defense, the *R*—or resistance—genes. In particular, this family of plant proteins regulate the so-called hypersensitive response, whereby a plant will mount a localized suicide response to the invasion of a pathogen (Van der Biezen and Jones, 1998; Ellis and Jones, 1998).

3.5.7. Modulation of Apaf-1 oligomerization represents an important therapeutic target

The relevance of Apaf-1 as a therapeutic target has already been discussed. Our observation that oligomerization is critical for Apaf-1 function suggests that a key means of modulating Apaf-1 activity would involve promoting or repressing dimerization. Our *in vitro* capture assay could be applied to an automated screening procedure designed to identify candidate molecules capable of preventing the formation of productive Apaf-1 oligomers. Equally, drugs directed towards promoting the spontaneous aggregation of Apaf-1, independent of cytochrome *c*, may be one possible option to artificially promote cell death in neoplastic tissue.

Unfortunately, our preliminary attempts to modulate Apaf-1-mediated caspase-9 activation have been unsuccessful. However, because of the potential value of intervening in Apaf-1 mediated apoptosis, future work may apply the *in vitro* assay as a means for finding peptide inhibitors or promoters of Apaf-1-mediated caspase-9 activation.

The discussion section above primarily places the results of our study within the context of published observations that were undertaken concurrently by other groups. For a more global, up-to-date appraisal of our observations within the context of significant recent developments in this area, the reader is directed towards the General Discussion in Chapter VI.

CHAPTER IV:
Molecular characterization of DRADD, a novel caspase-9-interacting molecule

4.1. INTRODUCTION AND AIMS

This chapter deals with the molecular characterization of DRADD, a novel caspase-9-interacting molecule that was identified as a result of a two-hybrid screen previously conducted in the laboratory. As was detailed in Chapter I, there are some obvious differences between the *CASP-9*$^{-/-}$ and *APAF-1*$^{-/-}$ murine knockout phenotypes. The survival of a fraction of *APAF-1*-nullizygous animals into adulthood (~5%) indicates that there are certain genetic contexts, admittedly, thusfar obscure, within which other caspase-activating adaptor molecules may substitute for the loss of Apaf-1 function (Honarpour *et al.*, 2000). Intriguingly, apart from male sterility, these *APAF-1*-nullizygous mice are healthy and exhibit few defects in cell death regulation (Honarpour *et al.*, 2000). Therefore, we reasoned that there might be other caspase-9-interacting adaptor molecules that substitute for Apaf-1 function in the minority of *APAF-1*-null mice that survive into adulthood. The sections below that describe the screening and subsequent identification of DRADD as a caspase-9-selective molecule are initially written in the passive tense. This is to demarcate work that the author did not participate in, that is included so as to place DRADD within the context which it was cloned.

4.2.1 Identification of DRADD as a caspase-9-selective interaction partner by yeast two-hybrid screening

To search for interaction partners that may potentially regulate the activity of caspase-9 during apoptosis, a two hybrid screen was conducted in the laboratory using the N-terminal pro-domain (amino acids 1-130) encompassing the caspase-9 CARD motif (Figure 23A, B). As was demonstrated in Chapter III, this portion of caspase-9 is sufficient for mediating the CARD/CARD interaction with caspase-9 adaptor molecule Apaf-1, making it likely that it would also be sufficient for CARD-based interactions with other caspase-9-interacting molecules.

For screening purposes, a Gal-4 DB fusion incorporating amino acids 1-130 of the caspase-9 CARD (designated DB-Caspase-9^{CARD}; Figure 23B) was transformed into yeast Y190 host strain. After verifying that the hybrid protein was suitably non-toxic and did not autonomously autoactivate the two-hybrid reporter genes, a

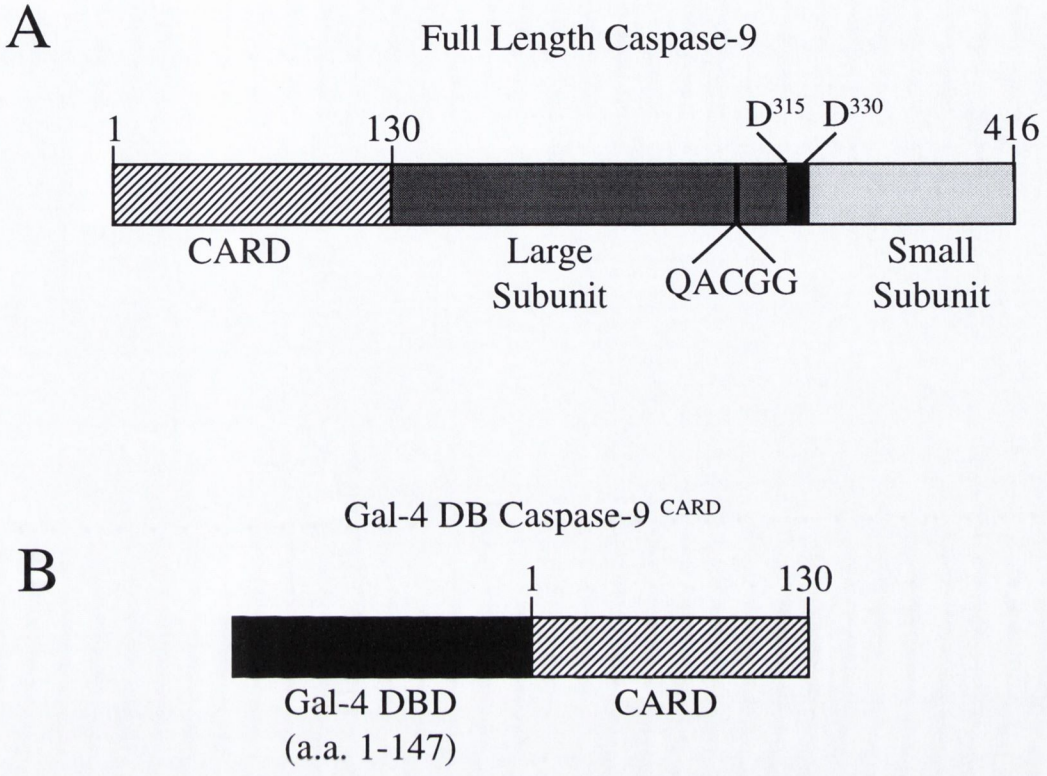

Figure 23

Illustration of the caspase-9^{CARD} bait used for two-hybrid library screening

A, Schematic representation of the domain structure of full length procaspase-9. Indicated are the CARD motif, and the large and small subunits of the molecule. The active site QACGG motif is indicated within the large subunit. Also shown are the P4 Aspartate positions of sites cleaved by caspase-9 (Asp 315) and caspase-3 (Asp 330) during activation of the molecule. Numbers denote amino acid positions; amino acids are represented using the single letter code.

B, Schematic representation of the Gal-4 DNA binding domain (DB) fusion with the caspase-9 CARD motif (the "Bait") that was used in the 2-Hybrid screening procedure.

library screen was conducted. This involved the sequential transformation of the DB-Caspase-9^{CARD} Y190 transformant with pACT-2 AD Jurkat cell cDNA library plasmids (Clontech). Figure 24 provides a summary of the steps that were undertaken during the screening procedure.

Briefly, yeast co-transformants expressing both bait and library plasmids were plated on histidine-deficient medium supplemented with 25 mM 3-Aminotriazole (3-AT) to select for bait-interacting proteins. From an estimated pool of 1.3×10^7 library clones, multiple candidate colonies were found to grow on the original histidine-deficient screening plates, potentially indicating an interaction with the DB-Caspase-9^{CARD} bait (Figure 24). Of these, some 79 individual yeast colonies survived a second round of histidine-deficient selection when streaked on fresh selective plates, by transactivating the *HIS3* reporter gene. Candidate interactors were then subjected to a further round of screening, judged by the ability to transactivate a second Gal-4-responsive reporter gene (*lacZ*) in the colony lift assay. Of the original 79 colonies, 63 of these were found to transactivate both Gal-4 reporter genes and these were subjected to further analysis.

Yeast transformants harboring the putative positive interacting clones were then subjected to a plasmid isolation procedure (see Chapter II) and the resultant pACT-2-derived library clones were partially sequenced. Analysis of the nucleotide sequences obtained revealed the presence of 15 clones encoding overlapping portions of an identical open reading frame (ORF). The identity of several of these overlapping candidate clones was revealed by BLASTX database searching against the public databases at the NCBI (www.ncbi.nlm.nih.gov/BLAST/). This algorithm performs a conceptual translation of an input nucleotide query in all three possible reading frames and this information was used to probe the non-redundant (nr) NCBI protein database. Database interrogation revealed that the candidate clones were identical in the regions tested to an 84 kDa protein of unknown function, designated p84 (Genbank accession No. AAA53571), that had previously been identified by two-

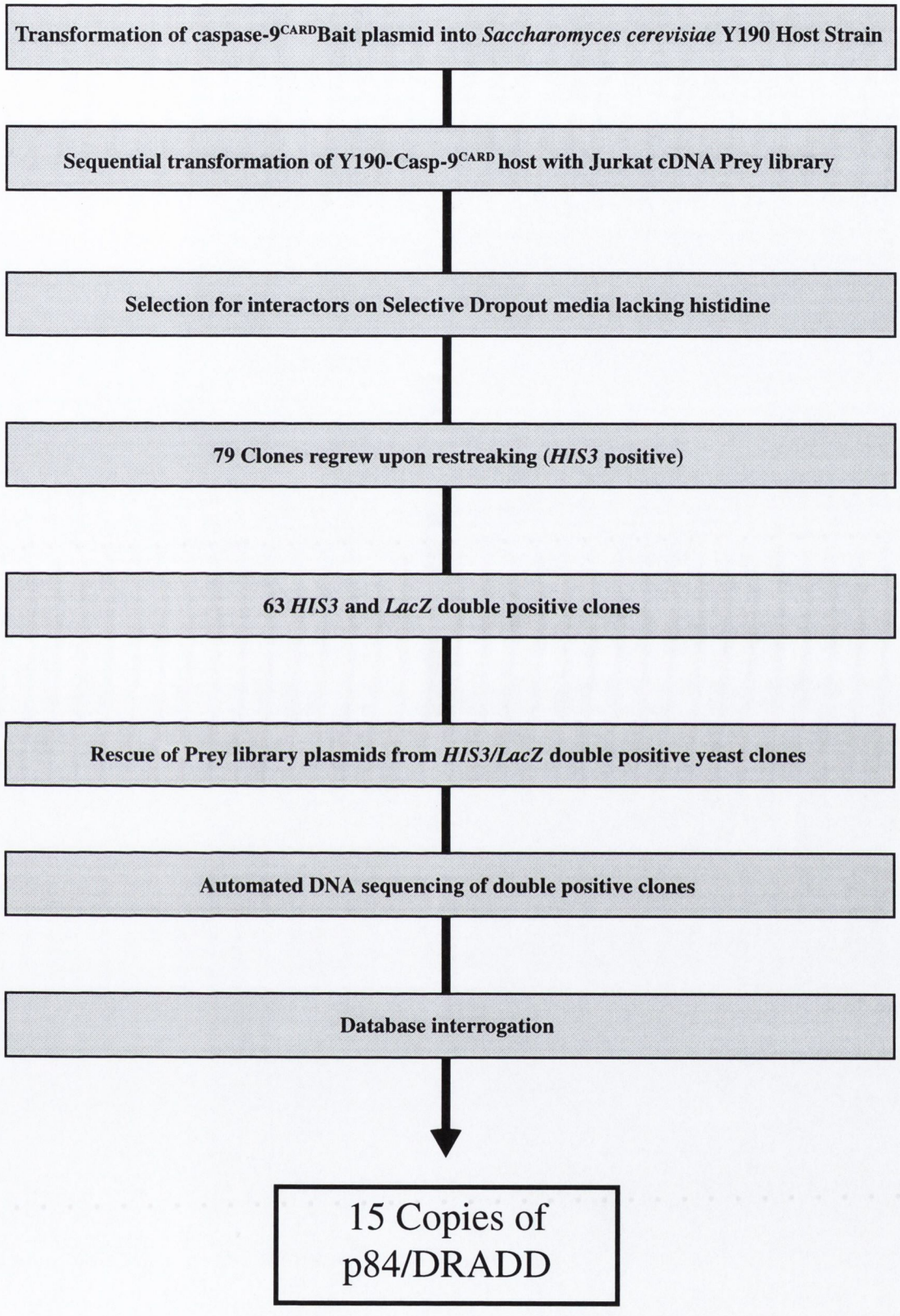

Figure 24

Flow diagram illustrating the stages involved in the identification of DRADD as a caspase-9 interacting protein

hybrid screening using the N-terminus of pRb as bait (Durfee *et al.*, 1994). The published sequence of p84 is illustrated in Figure 26A.

4.2.2 p84 binds specifically to caspase-9^{CARD}

A preliminary two-hybrid protein-protein interaction assay was then conducted to investigate the specificity of the full-length library clones for caspase-9 (Figure 25). Full length AD-p84 failed to interact with the N-terminal moieties of either caspases -7, -8, -10 or the Gal-4 DB alone, as judged by the ability to transactivate the *HIS3* reporter gene. In contrast, AD-p84 specifically bound to the DB-caspase-9^{CARD} bait protein, enabling yeast transformants to grow on histidine-deficient media (Figure 25). The previously reported interaction between p84 and the N-terminal 300 amino acids of pRb (Durfee *et al.*, 1994) was included as a positive control in this assay (Figure 25).

4.2.3. Domain structure of p84

Given the specificity of the interaction between p84 and the caspase-9 CARD bait, the amino acid sequence of p84 (Genbank accession No. AAA53571; Figure 26A) was subjected to further inspection using the BLASTP algorithm at the NCBI database. Strikingly, systematic database analysis of truncated portions of the published amino acid sequence of p84 revealed a region in the C-terminus of the molecule (amino acids 585-649; Figure 26B, D) that resembled a death domain. This module is commonly used during apoptotic signaling by the TNF family of death receptors and their associated adaptor proteins (Ashkenazi and Dixit, 1998). Moreover, further BLASTP analysis revealed the presence of a leucine-rich region located towards the centre of the molecule with similarities to the CARD motif (Hofmann *et al.*, 1997) (amino acids 296-384; Figure 26B, C). The CARD-like and death domain regions of DRADD are aligned for comparison with other molecules that have been established to possess these apoptotic signaling motifs (Figure 26B, C).

Given the domain structure of this molecule in terms of the possession of two hallmark apoptotic signaling modules, and its abilty to regulate apoptosis (see

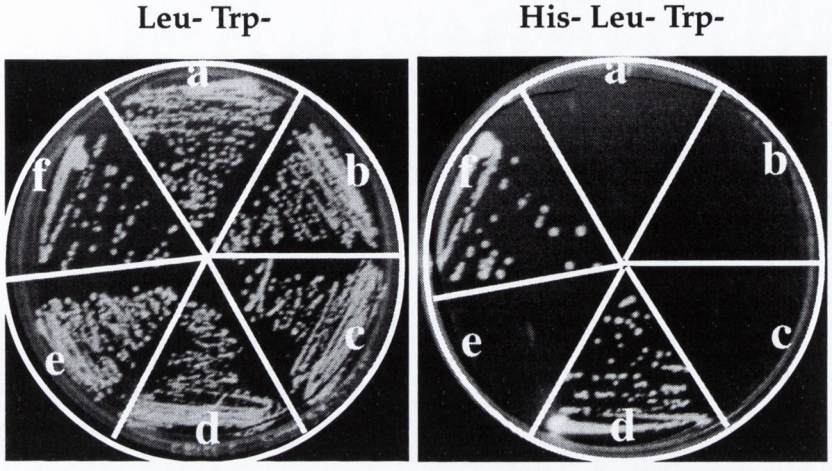

DB-hybrids

a Gal-4 DB only
b Caspase-7^{pro}
c Caspase-8^{pro}
d Caspase-9^{pro}
e Caspase-10^{pro}
f pRB-NT

Figure 25

***HIS3* yeast Two-Hybrid protein-protein interaction assay illustrating the selectivity of DRADD binding for caspase-9^{CARD}.**

Interactions between a Gal-4 Activation Domain (AD) fusion of DRADD and the indicated Gal-4 DNA binding domain fusions of the indicated proteins were determined using the Two-hybrid assay. The presence of interacting pairs was identified through the ability to transactivate the *HIS3* reporter gene. Left, control plates illustrating equal loading of yeast transformants; right, positive interacting pairs exhibit the ability to grow on histidine-deficient media. The experiment was conducted by Mary Harte and Helen Egan.

A

```
MSPTPPLFSLPEARTRFTKSTREALNNKNIKPLLSTFSQVPGSENEKKCT  50
LDQAFRGILEEEIINHSSCENVLAIISLAIGGVTEGICTASTPFVLLGDV  100
LDCLPLDQCDTIFTFVEKNVATWKSNTFYAAGKNYLLRMCNDLLRRLSKS  150
QNTVFCGRIQLFLARLFPLSEKSGLNLQSQFNLENVTVFNTNEQESTLGQ  200
KHTEDREEGMDVEEGEMGDEEAPTTCSIPIDYNLYRKFWSLQDYFRNPVQ  250
CYEKISWKTFLKYSEEVLAVFKSYKLDDTQASRKKMEELKTGGEHVYFAK  300
FLTSEKLMDLQLSDSNFRRHILLQYLILFQYLKGQVKFKSSNYVLTDEQS  350
LWIEDTTKSVYQLLSENPPDGERFSKMVEHILNTEENWNSWKNEGCPSFV  400
KERTSDTKPTRIIRKRTAPEDFLGKGPTKKILTGNEELTRLWNLCPDNME  450
ACKSETREHMPTLEEFFEEAIEQADPENMAENEYKAMNNSNYGWRALKLL  500
ARRSPHFFQPTNQQFKSLQEYLENMVIKLAKELPPPSEEIKTGEDEDEED  550
NDALLKENESPDVRRDKPVTGEQIEVFANKLGEQWKILAPYLEMKDSEIR  600
QIECDSEDMKMRAKQLLVAWQDQEGVHATPENLINALNKSGLSDLAESLT  650
NDNETNS                                              657
```

B

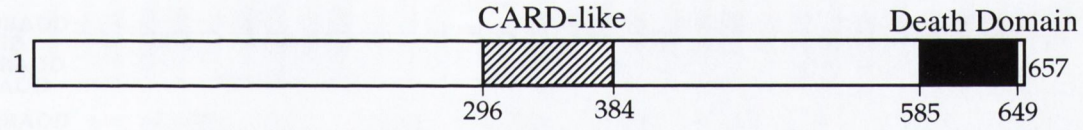

Figure 26

Identification of DRADD

A, The published amino acid sequence of p84/DRADD (Accession No. AAA53571). The areas shaded and underlined respectively denote the CARD-like and Death Domain modules in the molecule.

B, Schematic representation of full length DRADD protein. The CARD-like and Death Domain modules are indicated.

below), we refined the previous designated of this protein to $p84^{DRADD}$ (Death-inducing Rb-Associated Death Domain protein).

4.2.4. Identification of DRADD homologues

We characterized DRADD in terms of its similarity to other non-mammalian eukaryotic proteins contained within the public databases, accessed via the NCBI BLAST web interface. Interestingly, using TBLASTN searches based on the full-length nucleotide sequence of one of the DRADD AD library clones, we identified putative homologues of DRADD in *Caenorhabditis elegans* (Accession No. AAF39962; 25% identity), *Drosophila melanogaster* (Accession No. AAF51946; 33% identity) and intriguingly, *Schizosaccharomyces pombe* (Accession no. CAB62828; 24% identity). These respective hypothetical protein sequences are aligned alongside the full length DRADD sequence for comparison (Figure 27). Interestingly, several regions of DRADD were well conserved in the sequences of both *C.elegans* and *Drosophila*, including several remarkably well conserved regions within the N-terminus and centre of the molecules (Figure 27). Significantly, the region of human DRADD homologous to the CARD motif (amino acids 296-384) was found to be highly conserved in the fly and worm sequences (Figure 27). In contrast, some amino acids within the death domain homology region were poorly conserved in worm and fly DRADD. However, low stringency BLASTP database searches using the death domain-like regions of these proteins were successful in retrieving the death domains of human RAIDD as well as human DRADD.

4.2.5. A CARD-like region within DRADD is responsible for caspase-9 binding

Given the specificity of DRADD for the CARD of caspase-9, we next undertook a two-hybrid deletional analysis in order to identify the region of DRADD that interacted with DB caspase-9^{CARD}. To this end, we designed a series of DRADD deletion mutants (Figure 28A) that were generated by PCR using primers that incorporated flanking Sma-1/BamH-1 restriction enzyme sites, using the full length AD-DRADD library clone as a source of template. The primers were designed to allow insertion of DRADD deletion mutants into both AD and DB-

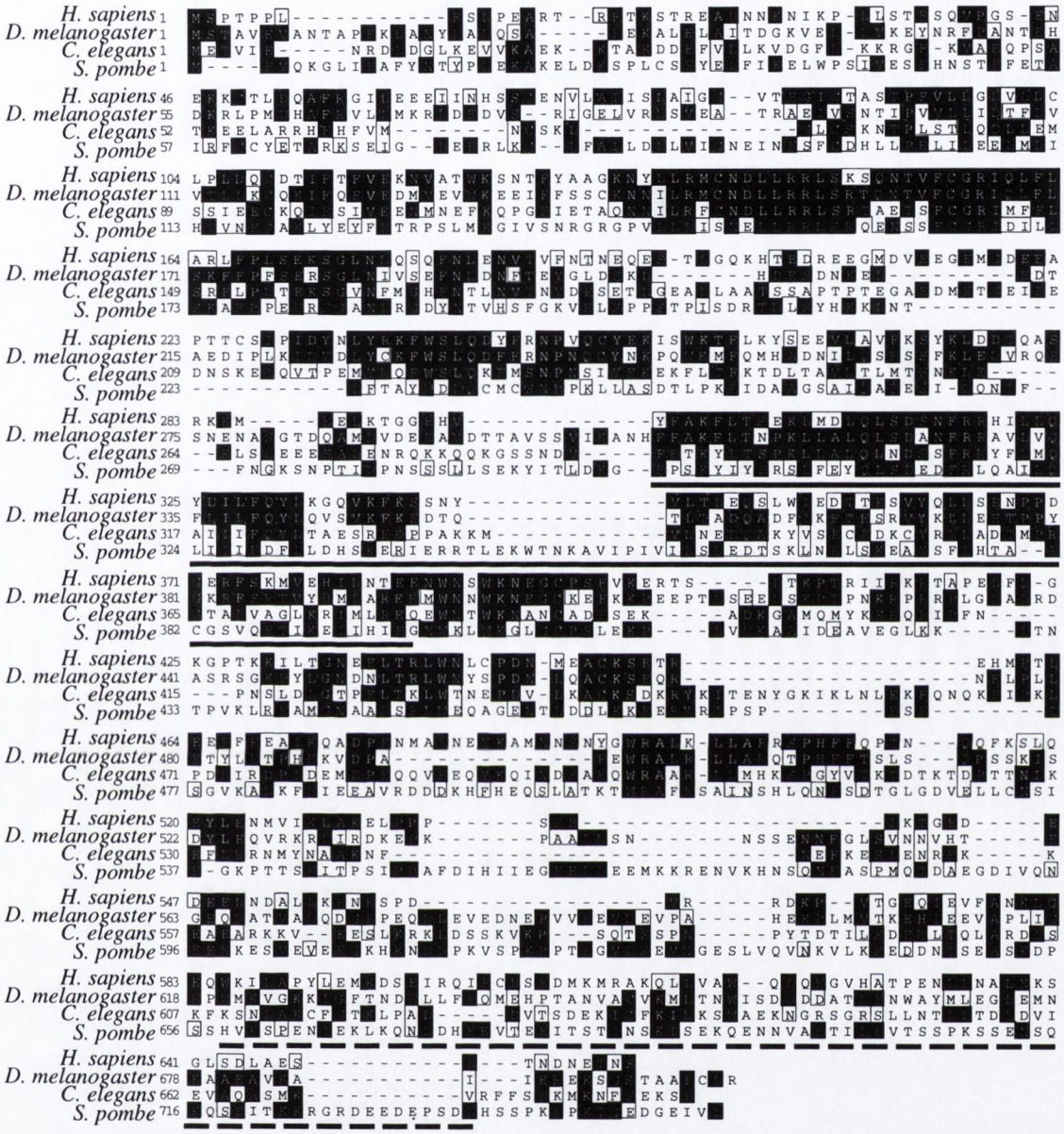

Figure 27

Identification of DRADD homologues

Alignment of human DRADD with homologous non-human sequences retrieved following BLAST interrogation of the non-redundant NCBI database (Human p84, Genbank Accession No. AAA53571; *Drosophila* protein, Accession No. AAF51946; *C.elegans* protein, Genbank Accession No. AAF39962; *Schizosaccaromyces pombe* protein, Genbank Accession No. CAB62828). The CARD-like and Death Domain regions in human DRADD are indicated on the alignment by hatched and solid lines respectively.

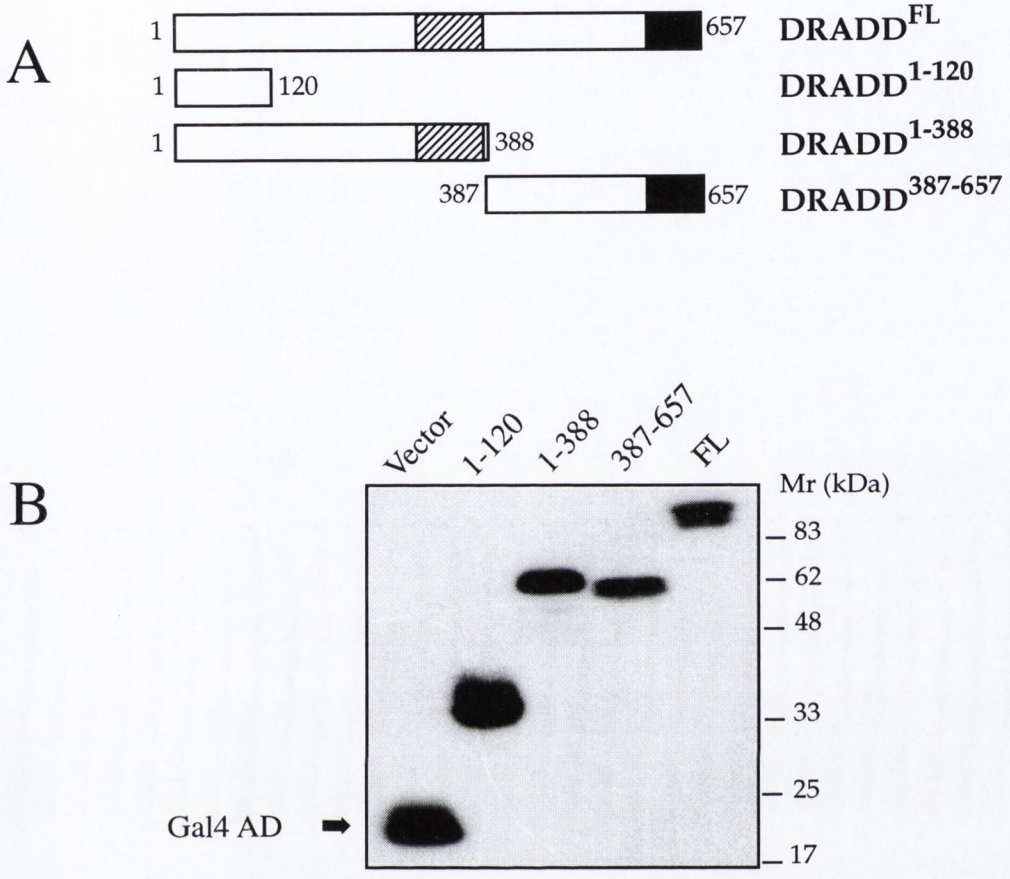

Figure 28

Deletional analysis of DRADD/caspase-9 interaction in yeast

A, Schematic representation of Gal4-AD fusions of DRADD^{FL} and the indicated DRADD deletion mutants. The CARD-like region and Death Domain are indicated by hatched and black shading respectively. Numbers refer to amino acid positions.

B, Western blot analysis of protein lysates from Y190 yeast transformed with either pACT2 empty vector (lane 1), pACT2-DRADD$^{1-120}$ (lane 2), pACT2-DRADD$^{1-388}$ (lane 3), pACT2-DRADD$^{387-657}$ (lane 4), or pACT2-DRADD^{FL} (lane 5), demonstrating expression of Gal4-AD (lane 1) and the indicated Gal4-AD-DRADD fusions—revealed by blotting with an anti-HA antibody. The experiment was conducted in collaboration with Helen Egan.

encoding two-hybrid vectors. The expression of Gal-4 AD-DRADD mutant proteins of the predicted molecular weights was confirmed by immunoblotting of lysates derived from Y190 transformants (Figure 28B).

The AD-DRADD mutants illustrated in Figure 28 were then screened for interaction against the DB-caspase-9^{CARD} used in the original two-hybrid screen. The N-terminal CARD domain of Apaf-1 (Apaf-1^{1-87}) was included as a caspase-9-interacting positive control for the *HIS3* nutritional selection assay. As expected, full length DRADD readily interacted with DB-caspase-9^{CARD}, as judged both by the *HIS3* reporter assay (Figure 28C) and the *LacZ* liquid β-galactosidase assay (Figure 28D). The DRADD deletion mutants spanning either the N-terminal 1-120 amino acids or the C-terminal deletion mutant encoding the putative death domain (amino acids 387-657) failed to interact with caspase-9^{CARD}, as judged by both assays (Figure 28C, D). In contrast, the AD-$DRADD^{1-388}$ mutant, spanning the putative CARD-like region of DRADD, bound specifically to caspase-9^{CARD} (Figure 28C, D). Moreover, analysis of this interaction using the *LacZ* liquid assay revealed that the $DRADD^{1-388}$ mutant containing the CARD-like region interacted with a substantially stronger affinity than full length DRADD. This was measured by arbitrary OD_{420} units indicative of the conversion of the ONPG substrate to a coloured product by the *LacZ* enzyme (Figure 28D). These data therefore suggested that DRADD and caspase-9 bind via a homophilic CARD/CARD interaction, much in the same manner as other caspases and their cognate adaptors such as Apaf-1/Caspase-9, FADD/Caspase-8 and RAIDD/Caspase-2 (Li *et al.*, 1997; Boldin *et al.*, 1996; Duan and Dixit, 1997).

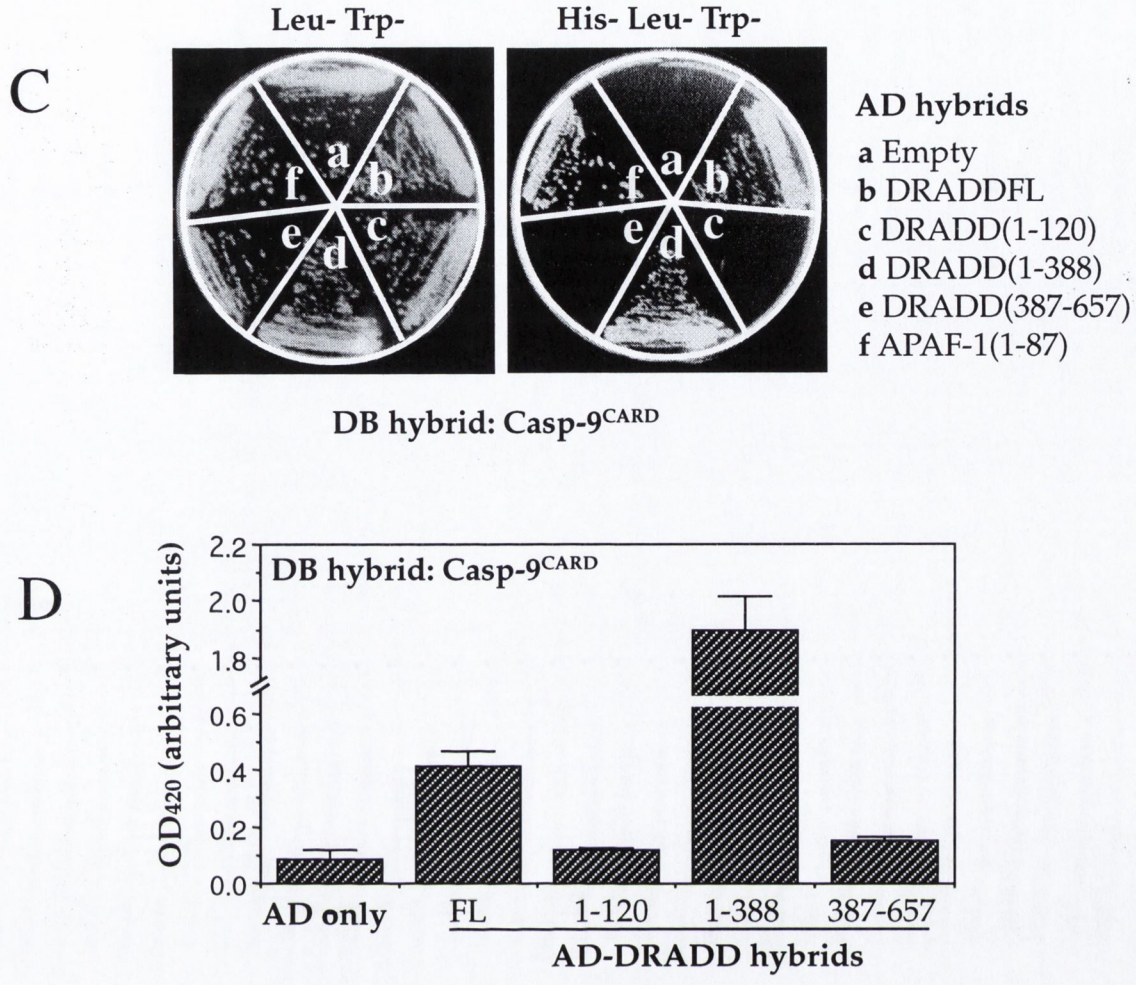

Figure 28

Deletional analysis of DRADD/caspase-9 interaction in yeast (Continued).

C, Yeast two-hybrid assay illustrating interaction between Gal4-DB-Caspase-9^{CARD} (amino acids 1-130) and the indicated Gal4-AD-DRADD truncations. Left, control plates showing equal loading of yeast; Right, the same transformants growing on plates lacking histidine where colony growth indicates an interaction.

D, Two-hybrid *lacZ* liquid assay. Yeast transformants co-expressing Gal4-DB-Caspase-9^{CARD} plus Gal4-AD alone, or the indicated Gal4-AD-DRADD truncations, were assessed for their ability to transactivate the *lacZ* reporter, as indicated by the conversion of ONPG to a coloured product that absorbs at 420 nm. Data are representative of three replicate experiments, each carried out in triplicate. The Histogram illustrates a comparison in arbitary units of OD_{420} readings. The experiment was conducted in collaboration with Helen Egan.

4.2.6. Detection of DRADD/caspase-9 association by a GST *in vitro* capture assay

We next verified the two-hybrid interactions within the context of other established protein-protein interaction assays. We also needed to ascertain whether full length caspase-9 could interact with DRADD. Moreover, we had thusfar utilized only the N-terminal CARD region of caspase-9 in our analyses and it was therefore critical to establish that full length caspase-9 could also interact with DRADD. Initially, to address the question of the specificity of DRADD for other caspases, we designed and contructed a Glutathione S-transferase (GST)-fused deletion mutant, $DRADD^{289-657}$, a truncation that spans both the CARD-like and death domain regions of the molecule. (Figure 29A). We assessed the ability of GST-$DRADD^{289-657}$, or GST alone, to specifically capture various ^{35}S-labeled caspases (Figure 29B). As is illustrated in Figure 29B, GST-$DRADD^{289-657}$ specifically captured ^{35}S-labeled caspase-9, while caspases-2 and -8 failed to be captured in parallel treatments. Under the same conditions, GST alone failed to capture significant amouts of any of these caspases (Figure 29B).

4.2.7. DRADD and caspase-9 interact in mammalian cells

To determine whether the DRADD/caspase-9 interaction takes place within the more physiologically relevant context of mammalian cells, we designed and made a series of Green Fluorescent Protein (GFP)-epitope tagged $DRADD^{FL}$ and DRADD deletion mutants (Figure 29D). The GFP epitope was fused to the N-terminus of DRADD or its deletion mutants in all cases. The mutants were generated as described in Chapter II. Expression of these fusions was verified by calcium phosphate-mediated transfection of HEK 293T cells and subsequent immunoblotting with a GFP-specific monoclonal antibody. This analysis revealed expression of GFP-$DRADD^{FL}$ or its derivatives of the predicted molecular weights (Figure 29E, lower panel).

To investigate DRADD binding to full length caspase-9 within the context of mammalian cells, we transfected HEK 293T cells with GFP vector, GFP-$DRADD^{FL}$ or its derivatives alongside a pcDNA3-derived plasmid encoding full-length caspase-9 (Figure 29E). We then used a monoclonal αGFP antibody to

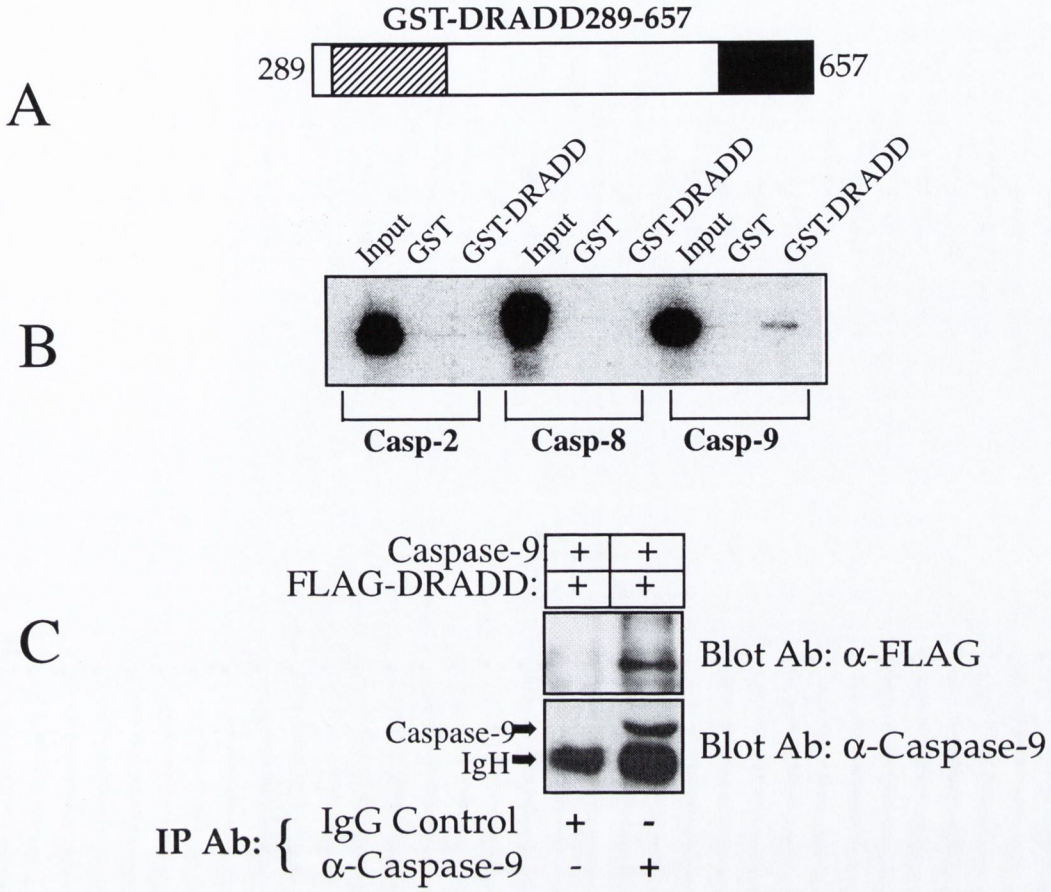

Figure 29

DRADD interacts with caspase-9 *in vitro* and in mammalian cells.

A, Schematic diagram of the GST-DRADD$^{289-657}$ mutant used in the *in vitro* capture assay.

B, Fluorogram illustrating that GST-DRADD$^{289-657}$ selectively binds caspase-9 in pulldown assays. Aliquots (2 μg) of bacterially expressed, affinity purified GST, or GST-tagged DRADD (amino acids 289-657), immobilized on glutathione beads were incubated with ^{35}S-labeled *in vitro* transcribed and translated caspases -2, -8 and -9. Bead-associated caspases were then visualized by SDS-PAGE and enhanced fluorography. The experiment was conducted by Helen Egan.

C, Co-immunoprecipitation of FLAG-DRADD with caspase-9 from HEK293T cells. HEK293T cells were transfected with 7.5 μg of pcDNA3-FLAG-DRADD plus 7.5 μg of pcDNA3-Caspase-9. Lysates were made 48 h post-transfection and immunoprecipitates prepared with 30 μl of protein A/G agarose beads plus 4 μl of polyclonal caspase-9 antibody, or an equivalent amount of control pre-immune (PI) antisera. Following extensive washing, samples were electrophoresed and immunoblotted using a FLAG-specific monoclonal antibody (Clone M2, Sigma). The lower panel indicates the amount of caspase-9 specifically captured during the immunoprecipitation. The experiment was conducted by Mary Harte.

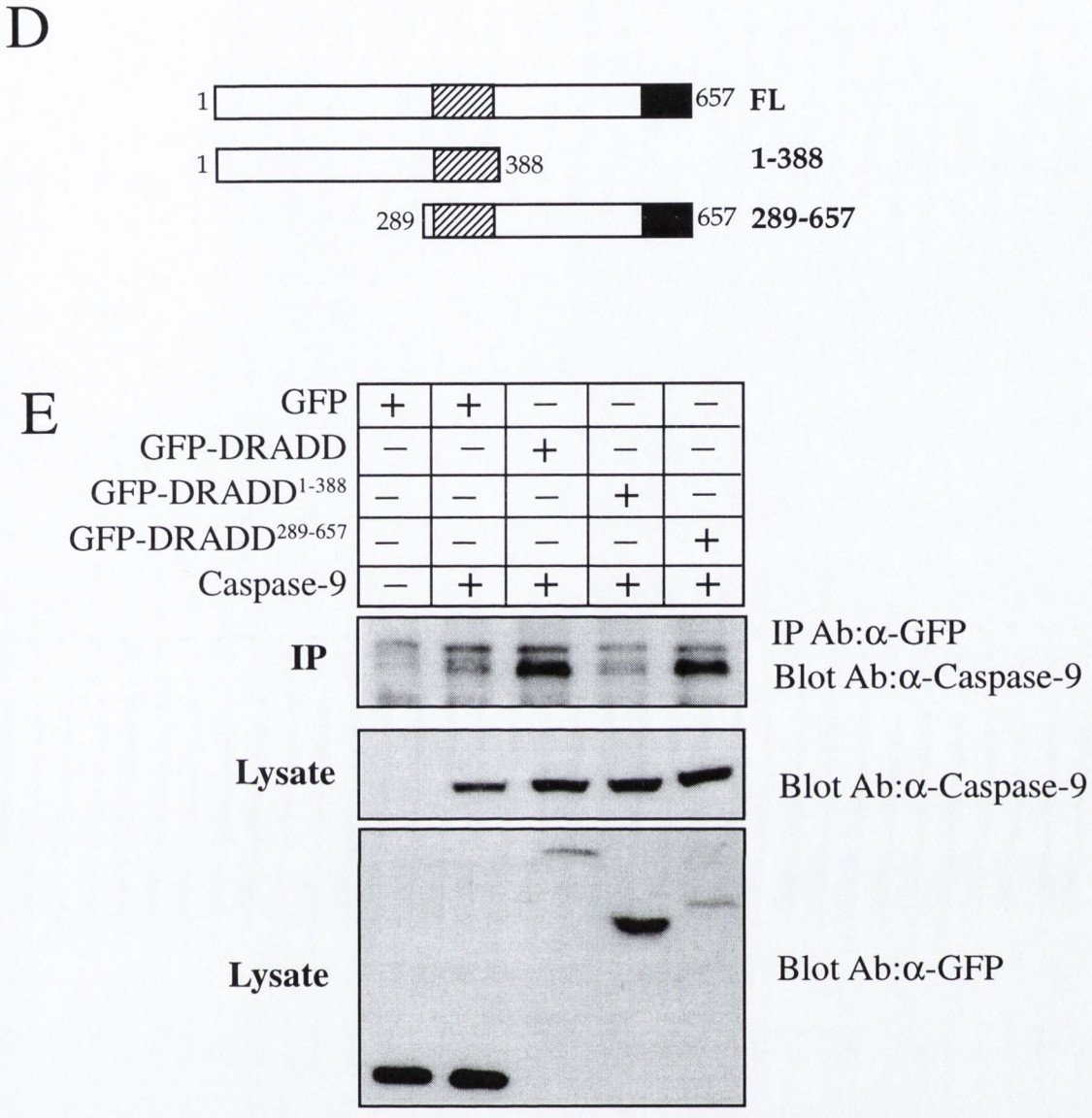

Figure 29

DRADD interacts with caspase-9 *in vitro* and in mammalian cells

D, Schematic diagram of the GFP-epitope tagged DRADD mutants used in co-immunoprecipitation analysis.

E, Co-immunoprecipitation of caspase-9 with GFP-DRADD from HEK293T cells. HEK293T cells were transiently transfected with 10 μg of pEGFP-C3 plasmid encoding GFP, or the indicated GFP-DRADD deletion mutants, along with 10 μg of pcDNA3 Caspase-9. Lysates were made 24 h post-transfection and immunoprecipitations were conducted using 1 μg of monoclonal anti-GFP antibody plus 20μl of protein A/G agarose. The presence of caspase-9 in immunoprecipitates was detected by immunoblotting using a rabbit polyclonal antibody specific to caspase-9 (upper panel). The middle and bottom panels illustrate 10% of total input amounts of caspase-9, GFP, or GFP-DRADD deletion mutants.

immunoprecipitate GFP-tagged proteins from cell lysates. We typically used a lysis buffer that incorporates 0.1% SDS in order to ensure maximal lysis of all cellular organelles/compartments in which DRADD may reside. Following extensive washing, bead-immobilized immunoprecipitates were subjected to SDS-PAGE followed by immunoblotting with a caspase-9-specific polyclonal antibody (Figure 29E). This analysis revealed the ability of full length DRADD to interact with full length caspase-9, whereas bead immobilized GFP alone failed to capture caspase-9 in parallel reactions (Figure 29E).

To confirm the reciprocal of this interaction, HEK 293 cells were transfected with similar amounts of FLAG-epitope tagged DRADD and the same caspase-9-encoding plamid as was used above. Using polyclonal anti-caspase-9-specific antisera as the immunoprecipitant, capture of FLAG-DRADD was consistently observed, whereas an isotype control IgG antibody failed to mediate capture of DRADD (Figure 29C). The lower panel of this figure illustrates that capture of DRADD was indeed dependent of the presence of caspase-9 in immunoprecipitates (Figure 29C).

We then determined the ability of the GFP-DRADD deletion mutants to interact with caspase-9 in the same assay. Surprisingly, whereas the Gal-4 AD DRADD$^{1-388}$ mutant readily bound to its DB-caspase-9^{CARD} counterpart in the yeast two-hybrid assay (Figure 28), the GFP-DRADD$^{1-388}$ mutant was unable to capture caspase-9 in immunoprecipitation reactions (Figure 29D), possibly because of incorrect protein folding in the context of the ~29 kDa GFP epitope. However, the GFP-DRADD$^{289-657}$ mutant readily bound caspase-9 in the same experiment, confirming the result obtained by GST-DRADD pulldown analysis (Figure 29B, D). Taken together, these data suggest that the caspase-9-interacting region of DRADD lies within the CARD-containing motif spanning amino acids 289-388 (Figure 26B). This is compatible with a direct CARD/CARD-based interaction between these two molecules. Further deletional studies will be required to demonstrate conclusively that conserved CARD consensus residues within DRADD critically mediate this interaction.

4.2.8. Detection of DRADD oligomerization

A wide body evidence suggests that the so-called initiator—or CARD domain-containing long prodomain caspases—become activated via an oligomerization-dependent mechanism (Salvesen and Dixit, 1999) (reviewed in Chapter I). This is probably achieved through the clustering action of an associated adaptor molecule such as Apaf-1 (Adrain *et al.*, 1999), or through aggregation via a death receptor/adaptor complex, such as Fas/TNFR-1 and FADD (Muzio *et al.*, 1996). To investigate whether DRADD can dimerize independently of other putative mammalian accessory proteins, we used the panel of two-hybrid deletion mutants described previously (Figure 28A) to test for DRADD self-association (Table 11). Interestingly, whereas full length DRADD was observed to dimerize only very weakly within the context of the *HIS3* and *LacZ* reporter assays, both the N-terminal deletion mutants, $DRADD^{1-120}$ and $DRADD^{1-388}$ amino acids readily dimerized, as judged by the *LacZ* colony lift assay (Table 11). Since the $DRADD^{1-120}$ mutant could self-associate, as well as binding to the FL and $DRADD^{1-388}$ hybrid proteins, we concluded that a region within the extreme N-terminus of DRADD may mediate self-association of the molecule (Table 11). These data suggest that DRADD and Apaf-1 may share a common caspase-9 activating mechanism, achieved through direct self-association of these adaptor molecules. Interestingly, since full length DRADD failed to self-associate substantially (reminiscent of Apaf-1), we postulated that the binding of a protein cofactor, or some form of post-translational modification, may be required to unlock the ability of DRADD to form oligomers.

4.2.9. DRADD interacts with pRb in yeast

Because preliminary two-hybrid analysis confirmed the previously reported interaction between DRADD and the retinoblastoma protein, pRb (Figure 25) (Durfee *et al.*, 1994), we next sought to further evaluate this interaction within the context of the AD-DRADD mutants used for two-hybrid-based caspase-9^{CARD} interaction analysis. To this end, yeast host strain Y190 was co-transformed with the panel of DRADD deletion mutants alongside a DB fusion of the N-terminal

Table 11

Detection of DRADD self-association in yeast

Yeast Two-Hybrid assay. Y190 yeast transformants expressing the indicated DRADD Gal-4 DB and AD fusions were streaked on selective media lacking histidine and grown for 5 days prior to the assay. Streaking on control non selective media plates indicated equal loadings of each yeast transformant. Histidine prototrophs were then subjected to the β-galactosidase filter lift assay. The development of a blue colony colour, indicative of the presence of positive interacting pairs, was monitored and the relative intensity of blue colour in each treatment was scored at a 5 hour endpoint.

DB HYBRID	AB HYBRID	Relative β-galactosidase Signal
Vector	DRADD Full Length	-
DRADD 1-120	DRADD Full Length	+
DRADD 1-388	DRADD Full Length	++
DRADD 387-657	DRADD Full Length	Autoactivation
DRADD Full Length	DRADD Full Length	-
DRADD 1-388	Vector	-
DRADD 1-388	DRADD 1-120	++++
DRADD 1-388	DRADD 1-388	++++
DRADD 1-388	DRADD 387-657	-
DRADD 1-388	DRADD Full Length	+
Caspase-9 CARD	DRADD Full Length	+++

300 amino acids of Rb (Figure 30B, C). Interestingly, this portion of pRb (Figure 30A) has been speculated to play a role in the oligomerization of the molecule (Hensey *et al.*, 1994). The established Rb interaction partner SV40 large T antigen was included as a positive control for the assays. Whereas the N-terminal deletion mutants $DRADD^{1-120}$ and $DRADD^{1-388}$ failed to interact with Rb, both full length DRADD and the C-terminal deletion mutant $DRADD^{387-657}$ bound to Rb. This was assessed by growth on histidine-deficient plates as well as by the *LacZ* ONPG liquid assay (Figure 30C, D). Moreover, analysis of the interaction using the semi-quantative *LacZ* liquid assay revealed that the C-terminal $DRADD^{387-657}$ mutant bound Rb with a substantially higher affinity than full length DRADD (Figure 30D). Intriguingly, these data suggest that the Rb interaction motif lies within the region that includes the death domain of DRADD (Figure 26B). Moreover, because Rb interacts with DRADD within a region outside the caspase-9 binding motif, a complex involving all three of these molecules may occur under certain conditions.

4.2.10. DRADD interacts with pRb in mammalian cells

We then confirmed the binding of DRADD/Rb within the context of mammalian cells (Figure 30E). To achieve this, we transfected HEK 293T cells using the calcium phosphate-based transfection protocol to overexpress either GFP-$DRADD^{FL}$ alone, or in combination with Rb. Overexpressed GFP was included as a specificity control (Figure 30E). Cell lysates were generated as described above and GFP or GFP-DRADD, were immunoprecipitated with αGFP antibody coupled to protein A/G-agarose beads. As is indicated in Figure 30E, whereas relatively similar input amounts of both GFP proteins (Figure 30E, lower panel) and Rb (middle panel) were incorporated into co-immunoprecipitation experiments, immunoblotting of bead complexes with an Rb-specific monoclonal antibody revealed that Rb was present only in GFP-DRADD immunoprecipitates (Figure 30E). Collectively these data confirm the DRADD/Rb interaction and moreover, imply that the region containing the DRADD death domain may be responsible for Rb binding (Figure 30).

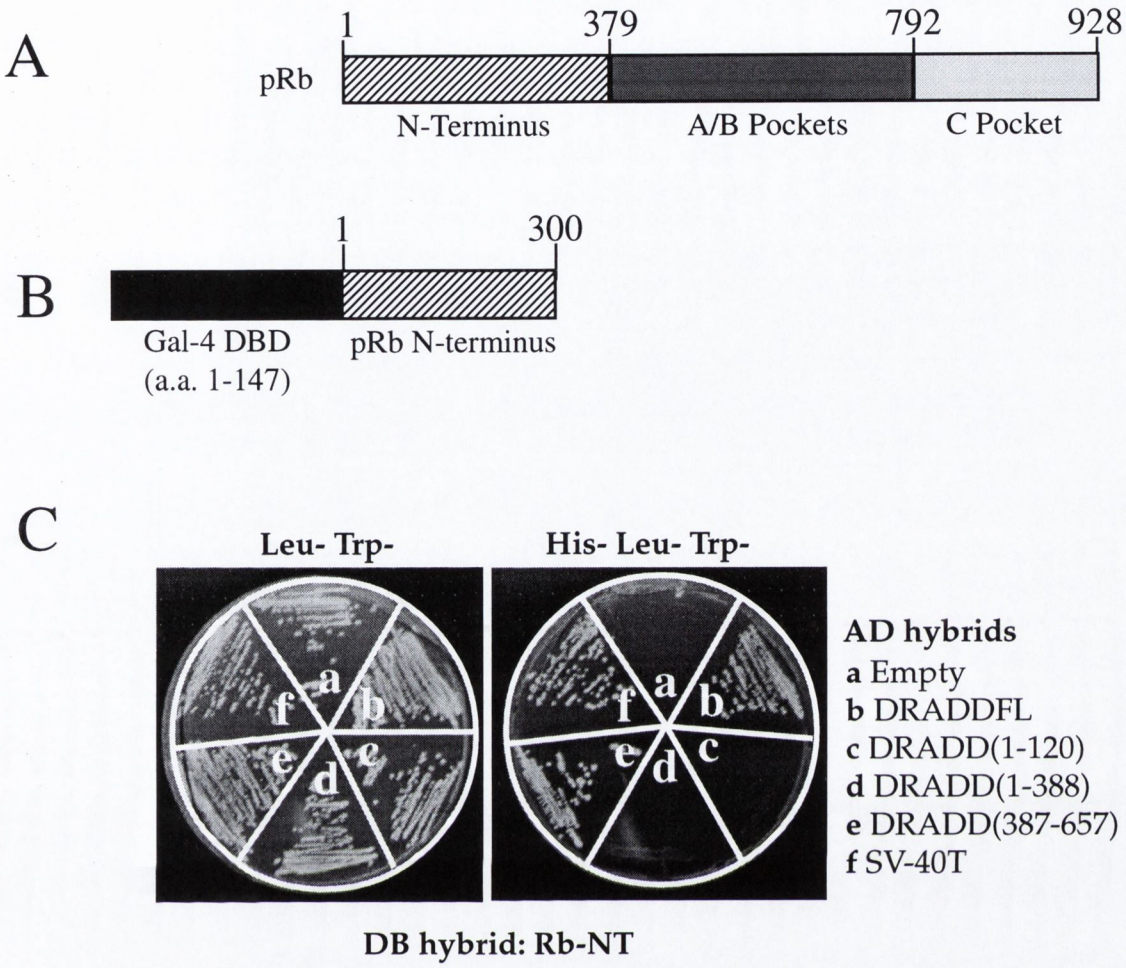

Figure 30

DRADD interacts with the retinoblastoma protein, pRb

A, Schematic diagram illustrating the domain structure of the retinoblastoma gene product. The N-terminus, A, B and C pocket modules are illustrated. Numbers denote amino acid positions

B, Schematic diagram illustrating the Gal-4 DB fusion with the pRb N-terminal deletion mutant (DB-pRb$^{1-300}$).

C, Yeast two-hybrid assay. The indicated Gal4-AD fusions were tested for interaction with the DB-pRb$^{1-300}$ mutant shown above. Left, control plate illustrating equal loading of yeast co-transformants; Right, the same transformants growing on plates lacking histidine, where colony growth indicates an interaction. The pRb-interactor SV-40 Large T antigen, is included as a positive control. The experiment was conducted in collaboration with Liam Carlin.

D

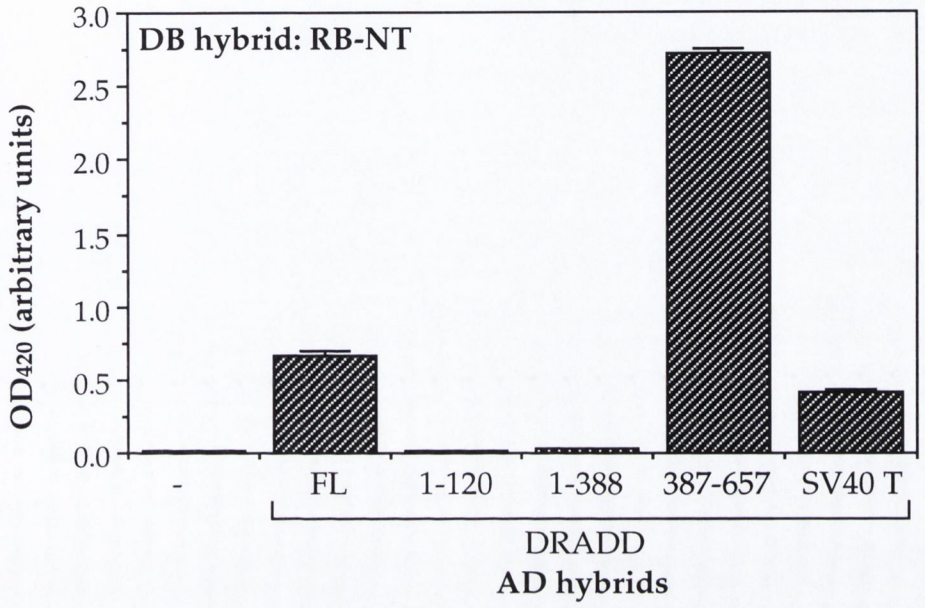

Figure 30

DRADD interacts with the Retinoblastoma protein pRb (continued)

D, Two-hybrid *lac Z* liquid assay. Yeast transformants co-expressing Gal4-DB-Rb^{1-300} plus Gal4-AD alone, the indicated Gal4-AD-DRADD truncations, or Gal4-AD-SV40T, were assessed for their ability to transactivate the *lacZ* reporter, as indicated by the conversion of ONPG to a coloured product that absorbs at 420 nm. Data are representative of three replicate experiments, each carried out in triplicate. The Histogram illustrates a comparison in arbitary units of OD_{420} readings. The experiment was conducted in collaboration with Liam Carlin.

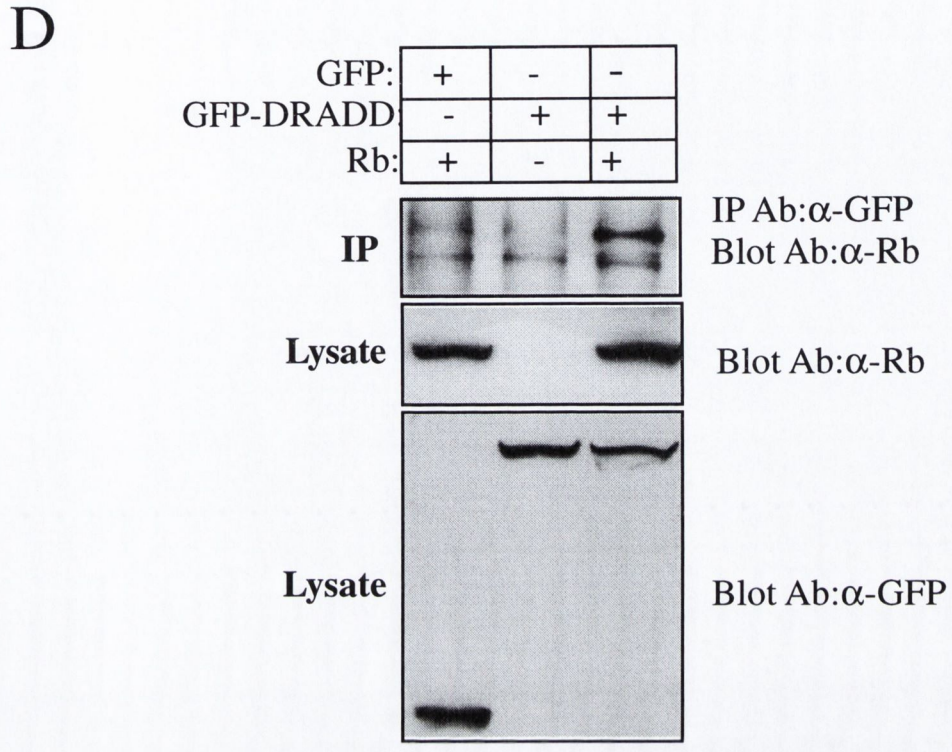

Figure 30

DRADD interacts with Retinoblastoma protein pRb (continued)

E, Co-immunoprecipitation of Rb with GFP-tagged DRADD. HEK293 cells were transiently transfected with 10 μg of pEGFP-C3 plasmid encoding GFP alone, or GFP-DRADD, along with 10 μg of pCMV-Rb, as indicated. Lysates were made ~24 h post-transfection and immunoprecipitates were prepared using 1 μg of monoclonal anti-GFP antibody (Clontech) coupled to protein A/G agarose beads. The presence of Rb in immunoprecipitates was detected by immunoblotting using a monoclonal anti-Rb antibody (Santa Cruz). The middle and bottom immunoblots illustrate 10% of total input amounts of Rb, GFP, and GFP-DRADD respectively.

4.2.11. DRADD is a nuclear protein

The subcellular localization of classical death domain-containing molecules such as FADD, TRADD or RIP is cytosolic, consistent with the role of these molecules as adaptors for transmembrane receptors. Thus, we were intrigued by the observation that DRADD can interact with the nuclear-localized phosphoprotein pRb. Moreover, analysis of the amino acid sequence of DRADD using the PSORT II algorithm revealed the presence of two putative nuclear localization signals (NLSs) within the C-terminus of DRADD (amino acids 409-416 and 561-567) (Nakai and Horton, 1999; www.psort.nibb.ac.jp). This suggested that the protein may be unique among death domain family members in terms of its subcellular distribution (Figure 31A; Table 12). As is shown in Table 12, the more C-terminally localized putative NLS exactly matches the *Pat-7* class of NLS consensus, characterized by a sequence starting with a proline and followed within three residues by a peptide motif of basic residues containing 3 K or R residues out of a total of four (PXXRRXK; amino acids 561-567) (Figure 31A; Table 12). The other, more N-terminal putative NLS (PXRXXRKR; amino acids 409-416) shared several hallmarks of classical NLSs, including a proline residue and several basic (R or K) residues (Table 12).

To establish the subcellular localization of DRADD, we used the panel of GFP-DRADD deletion mutants previously described, alongside an additional death-domain-containing truncation encoding DRADD amino acids 441-657 to examine the subcellular distribution of DRADD and its truncated derivatives. Figure 31B shows a schematic representation of all of the GFP-fused deletion mutants used in the analysis. Expression of all of these mutants was confirmed by calcium phosphate-mediated expression in HEK 293T cells and subsequent immunoblotting with a GFP-specific antibody (Figure 31C).

We then used a lipofection-based transfection system (see Chapter II) to transiently overexpress these mutants in MCF-7 human breast adenocarcinoma cells (Figure 31D). Cells transfected with plasmids directing expression of the

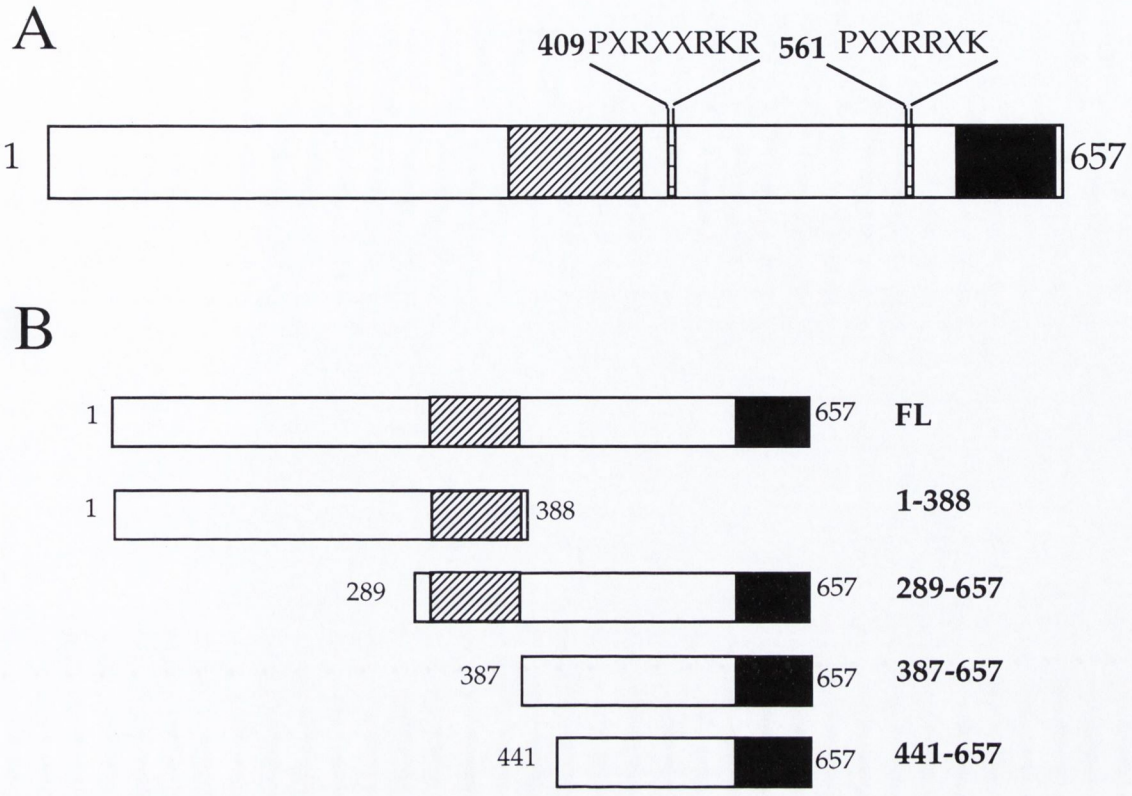

Figure 31

DRADD sublocalizes to the nucleus

A, Schematic diagram illustrating the position of putative nuclear localization signals within DRADD. The single letter amino acid sequences representing putative nuclear localization consensus sequences are indicated; 'X' denotes any amino acid.

B, Schematic diagrams of the pEGFP-C3-derived GFP epitope tagged DRADD and DRADD deletion mutant constructs that were used in the sublocalization experiments. The CARD-like and Death Domain regions of the molecule are denoted by hatching and shading respectively. Numbers denote amino acid positions.

Table 12

The position of putative NLSs within DRADD

Table illustrating the DRADD peptide sequences that represent candidate NLS sequences. Numbers represent amino acid positions.

DRADD Peptide	Significant residues	Comment
409-PTRII**RKR**-416	**PXRXXRKR**	Proline followed by four basic residues
561-PDVRR**DK**-567	**PXXRRXK**	Matches pat7 NLS consensus

C

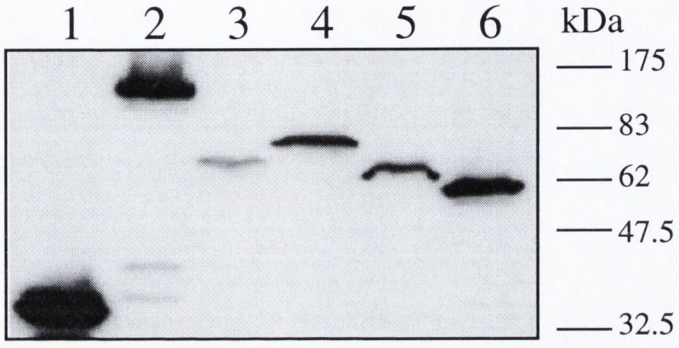

Key:

1. GFP

2. GFP-DRADD Full Length

3. GFP-DRADD 1-388

4. GFP-DRADD 289-657

5. GFP-DRADD 387-657

6. GFP-DRADD 441-657

Figure 31

DRADD sublocalizes to the nucleus

C, Expression of the GFP-epitope tagged DRADD proteins used in the subcellular localization analysis. Protein samples from HEK 293T cells transiently transfected with the indicated pEGFP-C3 derived plasmids were obtained 45 hours post-transfection and subjected to SDS-PAGE followed by immunoblotting with an αGFP antibody (Clontech).

indicated GFP-fused mutants were fixed approximately 18 hours post-transfection and images were captured using a digital camera fitted to a UV microscope. Cells expressing unfused GFP protein exhibited fluorescence in all cellular compartments, including both the nucleus and cytosol. In sharp contrast, cells transfected with GFP-DRADD plasmid exhibited fluorescence only within the nuclear compartment, implying that overexpressed GFP-DRADD was sharply confined within the nucleus (Figure 31D).

We next studied the subcellular distribution of the overexpressed GFP-tagged DRADD deletion mutants in an attempt to pinpoint the NLS within DRADD that was directing the nuclear import of the molecule. In keeping with the predicted NLSs being localized to the C-terminus of DRADD, the DRADD$^{1-388}$ mutant failed to be restricted within the nucleus and exhibited a distribution similar to GFP alone (Figure 31D). However, overexpression of the GFP-DRADD$^{289-657}$ and GFP-DRADD$^{387-657}$ mutants exhibited a distinctive nuclear localization, consistent with the presence of both of the putative NLSs in the C-termini of these truncations (Figure 31A). Strikingly, however, the GFP-DRADD$^{441-657}$ deletion mutant exhibited a distinctive cytosolic sublocalization and in fact this protein appeared to be excluded from the nuclear compartment (Figure 31D). These data suggest that the putative NLS most adjacent to the DRADD N-terminus (409-416; PXRXXRKR) was active in directing nuclear import (Figure 31A).
The exclusion of the DRADD$^{441-657}$ mutant suggests that DRADD may also possess a motif containing a nuclear exclusion signal (NES) that was activated because of the folding of the DRADD$^{441-657}$ mutant, or because of loss of the putative NLS region.

4.2.12. Forced DRADD expression induces apoptosis

Given the interesting modular structure of DRADD in terms of it possessing both DD and CARD-like apoptotic signaling modules, we were keen to investigate the role of DRADD as a modulator of apoptosis. To this end, a variety of pcDNA3-derived mammalian expression plamids were made, encoding full length DRADD, or its deletion mutant derivatives (Figure 32A). To explore the role of

D

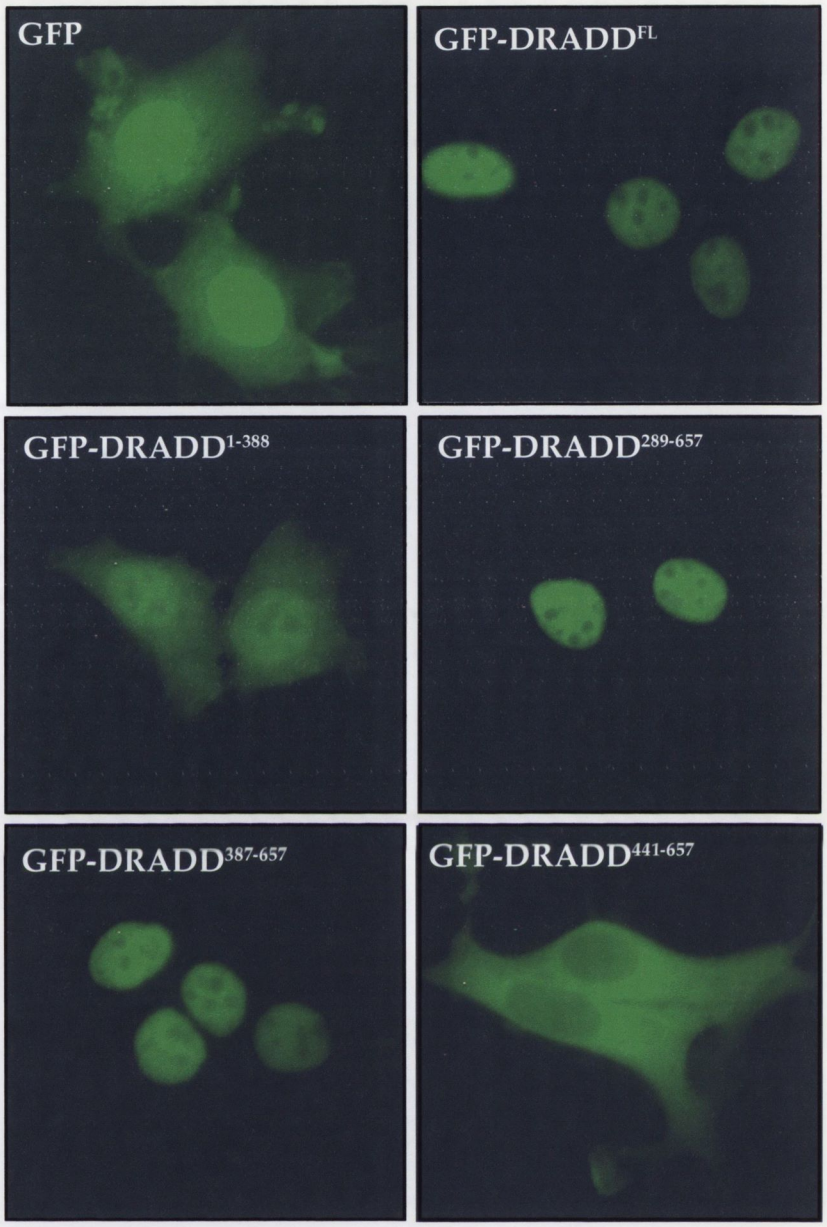

Figure 31

DRADD sublocalizes to the nucleus.

D, MCF-7 human breast carcinoma cells were transiently transfected with 500 ng of pEGFP-C3-based expression plasmids encoding GFP alone, GFP-DRADD, or the indicated GFP-DRADD deletion mutants. Cells were fixed 18 hours post-transfection in 4% paraformaldehyde/PBS, pH 7.2, followed by rehydration in PBS and mounting in glycerol/2% PBS. Cells were photographed under UV microscopy using a FITC filter. Images shown were obtained using a 40x objective lens.

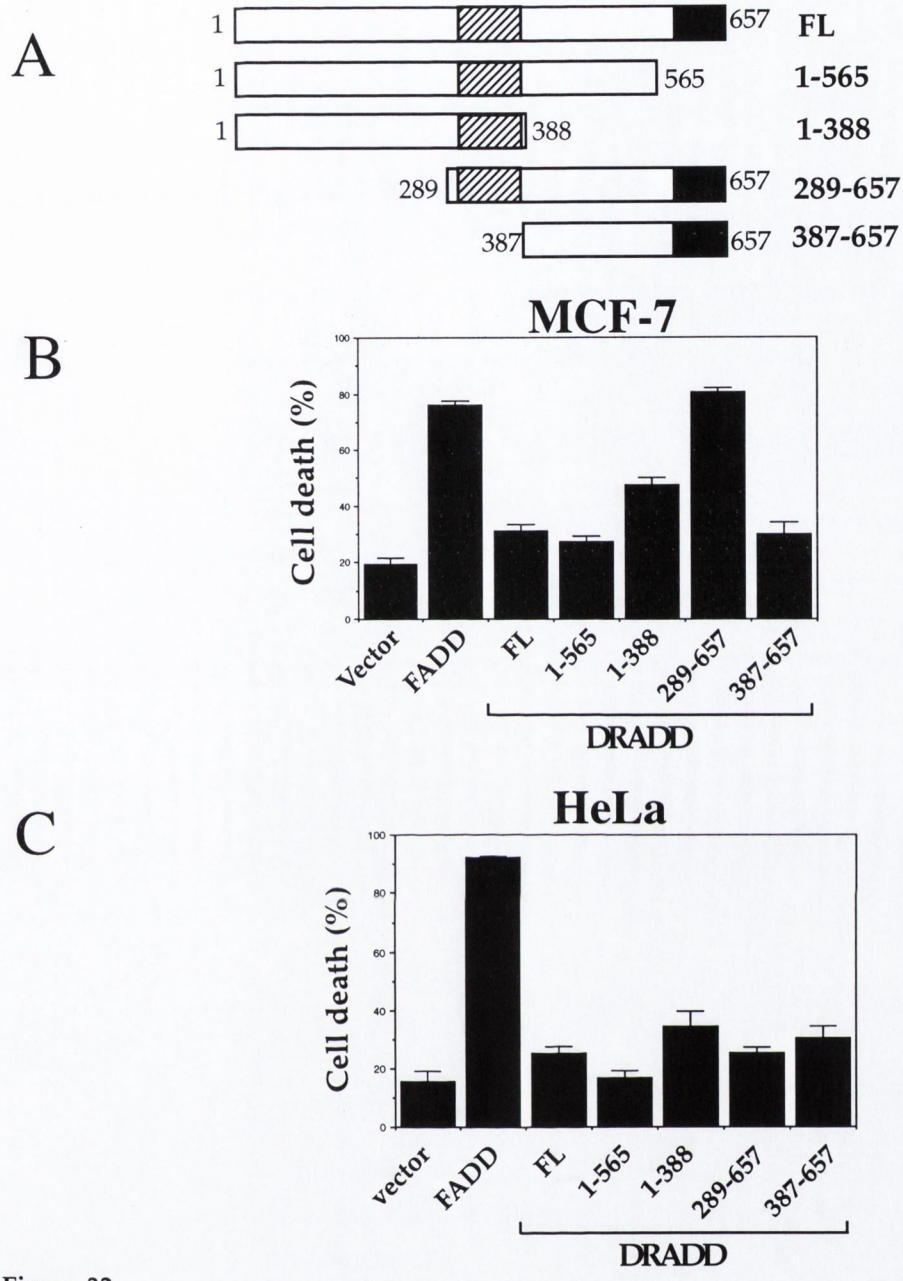

Figure 32

Evaluation of apoptosis associated with DRADD overexpression

A, Schematic representation of the DRADD pcDNA3-based mammalian expression constructs used in the assay. The CARD-like and Death Domain regions are indicated by hatched and black shading respectively. Numbers denote amino acid positions.

B and **C**, MCF-7 cells (B) or Hela cells (C) were transiently transfected with 500 ng of the indicated plasmids plus 100 ng of the pCMVβ β-galactosidase reporter plasmid using the Fugene-6 lipofection-based transfection reagent according to the manufacturers instructions. Cells were fixed and stained for β-galactosidase activity 46 hours (B) or 24 hours (C) following transfection and the percentage of β-galactosidase-positive (blue) cells exhibiting apoptotic features was determined from three separate fields of at least 100 cells. Error bars denote the standard error of the mean of three independent replicate experiments. Overexpressed FADD is included as a positive control.

DRADD in apoptosis, we transiently overexpressed DRADD and its truncations in MCF-7 human breast adenocarcinoma cells (Figure 32B). To identify cells that were transfected with target plasmids, we included limiting amounts of the pCMVβ reporter plasmid that directs expression of the β-galactosidase enzyme. The percentage of β-galactosidase-positive (blue) cells exhibiting typical apoptotic features including plasma membrane blebbing, nuclear condensation and rounding up from the culture dish, was then enumerated. These experiments revealed that full-length DRADD did not provoke apoptosis, since levels of cell death resulting from overexpression of this plasmid were similar to background levels associated with transfection of the empty pcDNA3 vector as a control (Figure 32B, C).

Given our observation that overexpressed full length Apaf-1 fails to promote apoptosis, whereas the Apaf-1ΔWD40 was active in this regard, we next examined the DRADD deletion mutants for cytotoxic effects upon overexpression (Figure 32B). Whereas full length DRADD, a mutant lacking the C-terminal death domain ($DRADD^{1-565}$), and a death domain only mutant ($DRADD^{387-657}$) minimally provoked apoptosis, expression of CARD-containing mutants, most notably, $DRADD^{289-657}$, but also $DRADD^{1-388}$, initiated apoptosis in MCF-7 cells (Figure 32B).

Next we evaluated the ability of these molecules to induce apoptosis in other mammalian tumor cell lines. Figure 32C illustrates a similar transfection experiment performed in HeLa cells. Consistent with the effect observed in MCF-7 cells, full-length DRADD failed to provoke apoptosis when overexpressed. However, whereas the $DRADD^{289-657}$ mutant failed to kill that cell-line, the $DRADD^{1-388}$ mutant was very weakly pro-apoptotic, similar to observations made with MCF-7 cells (Figure 32B, C). We additionally evaluated the effect of overexpression of DRADD in 293T cells. However, consistent with reports concerning the relative resistance of these cells to a variety of pro-apoptotic stimuli that potently initiate apoposis in other non-fibroblast transformed lines,

overexpression of either full-length DRADD or its derivative mutants failed to provoke apoptosis in this context (data not shown).

4.2.13. DRADD-associated cell death is caspase-9-dependent

We next further characterized apoptosis induced by the DRADD$^{289-657}$ mutant upon overexpression in MCF-7 cells (Figure 32D). Transfection of MCF-7 cells with this DRADD deletion mutant resulted in apoptosis that was readily inhibitable by the addition of the pancaspase inhibitor Z-VAD-fmk to culture medium several hours post-transfection. This confirmed that the mode of cell death observed was caspase-dependent (Figure 32D). We then examined the ability of catalytically inactive caspase-3 and caspase-9 cysteine>alanine (C>A) active site mutants to modulate DRADD-induced apoptosis (Figure 32E). Whereas a caspase-3 dominant negative mutant failed to block apoptosis induced by either overexpression of DRADD$^{289-657}$ or caspase-8-specific adaptor FADD, a caspase-9 active site mutant attenuated apoptosis induced by both of these proteins (Figure 32E). In summary, these data suggest that DRADD$^{289-657}$ overexpression can promote caspase-9-dependent apoptosis (Figure 32).

We next examined the ability of a two apoptosis inhibitory proteins, CrmA and Bcl-x, to modulate apoptosis associated with overexpression of DRADD$^{289-657}$ and caspase-8 adaptor, FADD (Figure 32E, F). Interestingly, whereas Bcl-x effectively attenuated apoptosis associated with both FADD and DRADD overexpression, crmA proved to be a poor inhibitor of DRADD-associated apoptosis, while potently reducing the cytotoxic effects associated with FADD overexpression (Figure 32E, F). These data therefore suggest that the cognate caspase activated in reponse to DRADD overexpression is unlikely to be amongst the caspases that can be inhibited by crmA, including caspases-1 and -8 (Zhou *et al.*, 1998).

4.2.14. DRADD dominant negative studies

Given the propensity of DRADD CARD-containing truncations to promote apoptosis upon overexpression, we speculated that DRADD may act as a caspase-9-specific adaptor molecule within the context of a novel pro-apoptotic signaling

D

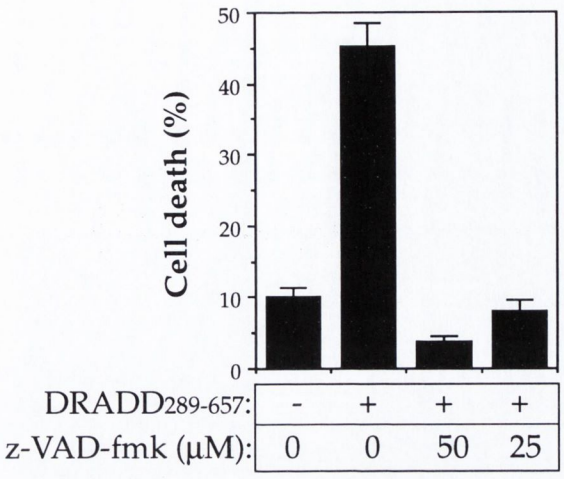

E

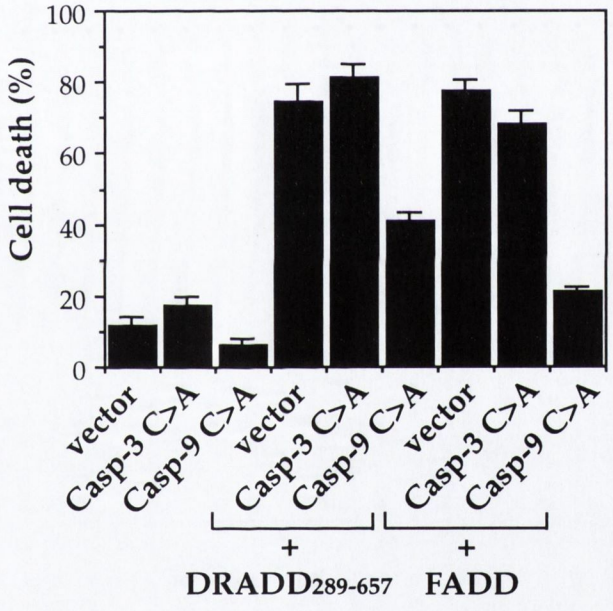

Figure 32

Evaluation of apoptosis associated with DRADD overexpression (continued)

D, MCF-7 cells were transfected with 400 ng of pcDNA3-DRADD$^{289-657}$ in combination with limiting amounts of the pCMVβ reporter plasmid, as detailed previously. Where indicated, Z-VAD-fmk was added to culture medium 5 hours post-transfection. The percentage of apoptotic cells among the transfected population was evaluated 48 hours post-transfection. **E,** MCF-7 cells were transfected with either 200 ng of pcDNA3-DRADD$^{289-657}$, or pcDNA3-FADD, plus 200 ng of plasmids encoding catalytically inactive mutants of caspase-3 (Casp-3 C>A) or caspase-9 (Casp-9 C>A), as indicated. Apoptosis was evaluated 36 hours post-transfection, as detailed previously.

F

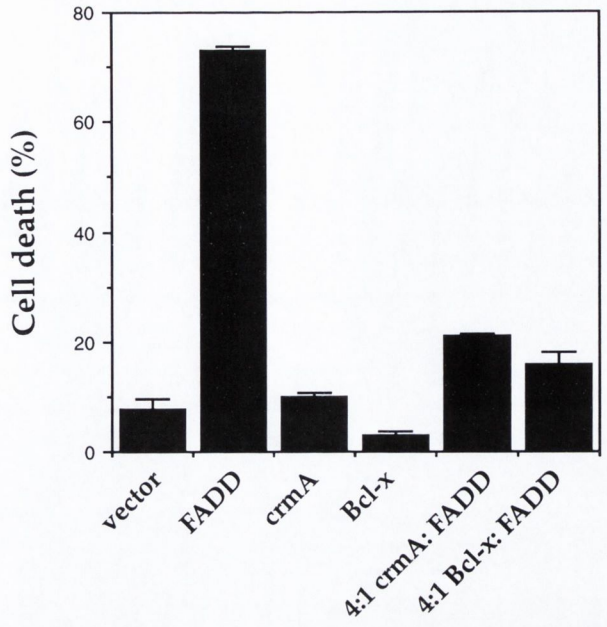

G

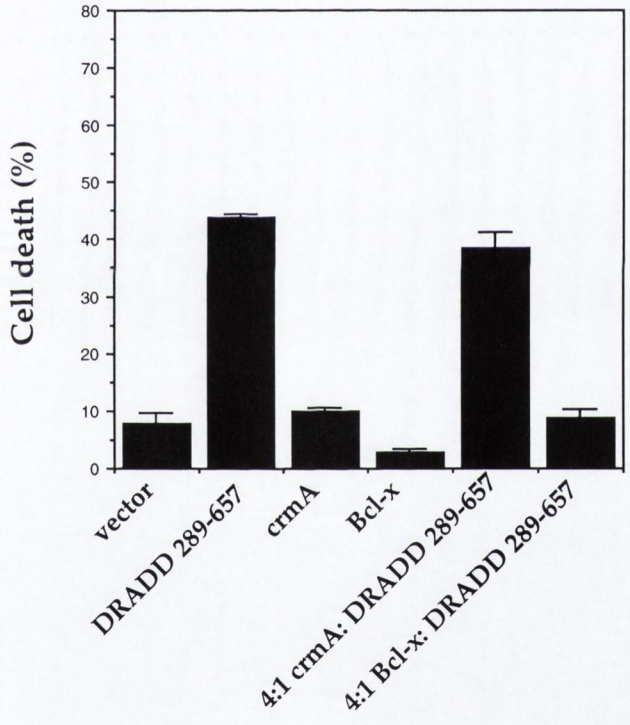

Figure 32

Evaluation of apoptosis associated with DRADD overexpression

F, MCF-7 cells were transfected with 100 ng of pcDNA3-FADD in combination with 400 ng of plasmid encoding either vector alone, crmA or Bcl-x alongside limiting amounts of the pCMVβ reporter plasmid. The percentage of apoptotic cells among the transfected population was evaluated 24 hours post-transfection.

G, MCF-7 cells were transfected with 100 ng of pcDNA3-DRADD$^{289\text{-}657}$ in combination with 400 ng of plasmid encoding either vector alone, crmA or Bcl-x alongside limiting amounts of the pCMVβ reporter plasmid. The percentage of apoptotic cells among the transfected population was evaluated 24 hours post-transfection.

pathway. Because DRADD contains a well-conserved death domain motif within its C-terminus, we decided to examine whether DRADD could collaborate with other established DD-containing species to modulate apoptosis. However, since we had observed that DRADD is unique amongst death domain-containing species in terms of its nuclear location (Figure 31) as well as its ability to interact with nuclear protein Rb (Figure 30), we considered it unlikely that DRADD may function as a typical cytosolic adaptor for the transmembrane death receptors.

Since a truncation of FADD lacking the caspase-8 interaction motif but retaining the death receptor-interacting DD module can successfully block death signals potentiated by its cognate death receptors Fas and TNFR-1 (Chinnaiyan *et al.*, 1996b), we reasoned that a similar dominant negative-based approach may reveal the putative death domain containing partners of DRADD. To achieve this, we used DRADD$^{387-657}$ and DRADD$^{356-657}$ mutants modelled on dominant negative FADD in that the caspase-9 interaction motif was either partially (DRADD$^{356-657}$) or wholly (DRADD$^{387-657}$) removed, leaving only the death domain module (Figure 33). We reasoned that this mutant should block any DRADD-dependent signaling pathway by binding to a DD-containing interaction partner. By sequestering this DD partner from endogenous full length DRADD, this would likely prevent caspase-9 recruitment and activation as a result of incorporation into a DISC-like complex composed of a receptor aggregate of DRADD and caspase-9 (Figure 33).

4.2.14.1. DRADD-DN does not potentiate death receptor-associated apoptosis

Using this aproach, we investigated whether DRADD plays a role in apoptosis initiated by any of the known death receptors. To ascertain whether this experiment was feasible, we first examined whether two tumor lines, MCF-7 and HeLa were sensitive to overexpression of the various death receptors (Figure 34A, B). As is illustrated, whereas expression of the full length versions of DR-4 and DR-5 potently induced apoptosis upon transfection into both of these cell lines, the plasmid constructs encoding the intracellular death domain moieties,

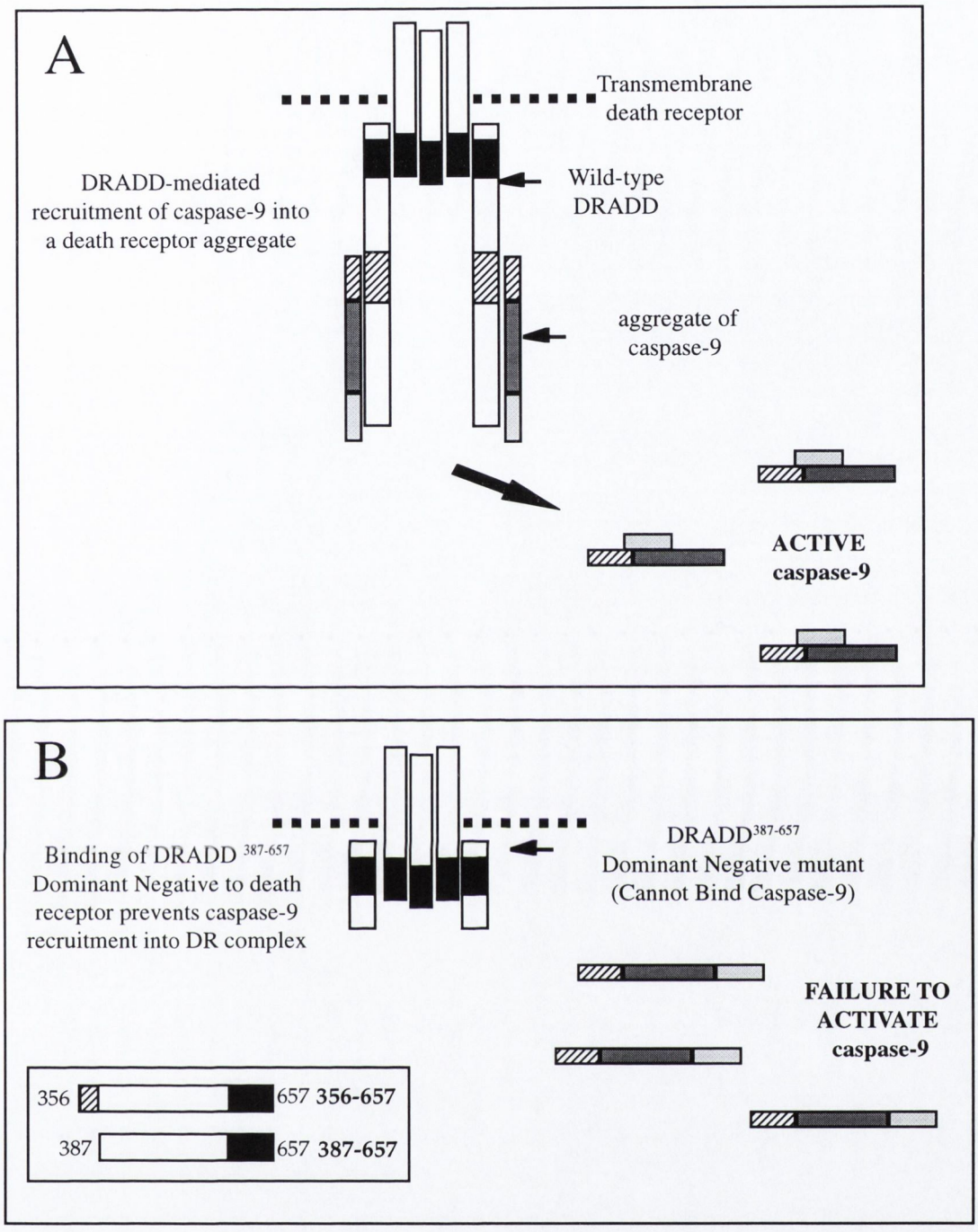

Figure 33

Investigation of DRADD function using a dominant negative-based approach

A, Schematic diagram illustrating a scenario whereby full length wild-type DRADD recruits procaspase-9 into a death receptor aggregate, resulting in active caspase-9, provoking death, mediated by an unknown death receptor stimulus.

B, Schematic diagram illustrating a scenario whereby overexpressed DRADD$^{387\text{-}657}$ dominant negative (DN) mutant interferes with wild type DRADD function by blocking death receptor signal transduction. DN-DRADD binding to the death receptor complex via the death domain of the molecule, prevents wild type DRADD from recruiting caspase-9 into the complex, thus frustrating activation of the caspase and blocking apoptosis. Schematic diagrams of the DRADD$^{387\text{-}657}$ and DRADD$^{356\text{-}657}$ DN deletion mutants are included within the boxed inset.

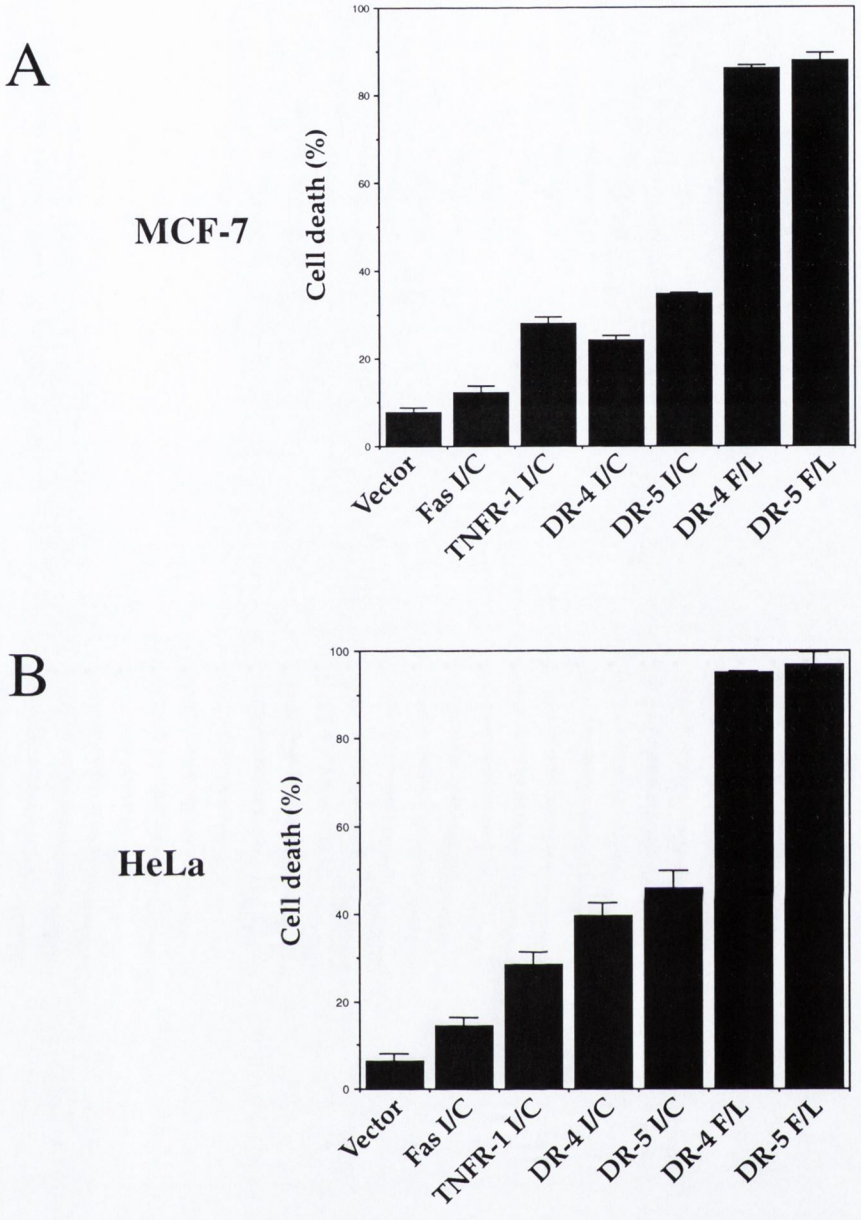

Figure 34

Evaluation of apoptosis associated with transient overexpression of death receptors or their intracellular death domain-containing moieties

A and **B**, MCF-7 (**A**) or HeLa cells (**B**) were transiently transfected with 200 ng of the indicated plasmids encoding the intracellular portion (I/C, intracellular) or Full Length (F/L) proteins, as indicated, of the Fas and TNFR-1, DR-4 and DR-5 receptors, alongside limiting amounts of the pCMVβ reporter plasmid. Cells were transfected using the Fugene-6 lipofection reagent according to the manufacturers instructions. The percentage cell death among transfected cells was evaluated as described previously approximately 44 hours post-transfection.

specifically of the Fas and TNF receptors, only modestly provoked apoptosis (Figure 34A, B).

Since the Fas and TNFR receptors use FADD as a death adaptor, we considered it unlikely that DRADD played a role in these pathways (Boldin *et al.*, 1995). Nonetheless, in order to exclude this possibility we used the putative dominant negative-DRADD (DN) constructs described above to explore a role for DRADD within these pathways. As anticipated, DN-DRADD failed to block apoptosis resulting from either overexpression of the intracellular death domain portion of the Fas receptor, or from death resulting from addition of an agonistic anti-Fas antibody to cells transiently overexpressing DN-DRADD (Figure 34C, D). However, cells treated with anti-Fas antibody could be rescued by expression of the caspase-8 inhibitor crmA and a caspase-9 cysteine-alanine (Caspase-9-DN) active site mutant, proving that the death stimulus used was suitably subtle not to overwhelm DN-DRADD-mediated inhibition (Figure 34D).

We next examined a role for DRADD within the context of TNFR-dependent death signaling (Figure 34E, F). Interestingly, transient co-expression of DN-DRADD at both 2:1 and 3:1 ratios alongside the TNFR-1 intracellular truncation modestly inhibited apoptosis induced by this death receptor molecule (Figure 34E). We tried to verify this observation within the context of addition of agonistic anti-TNFR-1 antibodies to the culture medium of MCF-7 cells overexpressing DN-DRADD (Figure 34F). It is well established that stimulation of TNFR-1 dually engages both pro-apoptotic and survival signals (Van Antwerp *et al.*, 1996). We therefore repressed the NFκB-related survival outcome of receptor ligation by the addition of cycloheximide to the culture medium in order to inhibit the synthesis of cellular survival factors. However, using this approach, we were unable to recapitulate the modest inhibitory effect encountered in the first cell death assay, suggesting that the original observation may have been artifactual (Figure 34F).

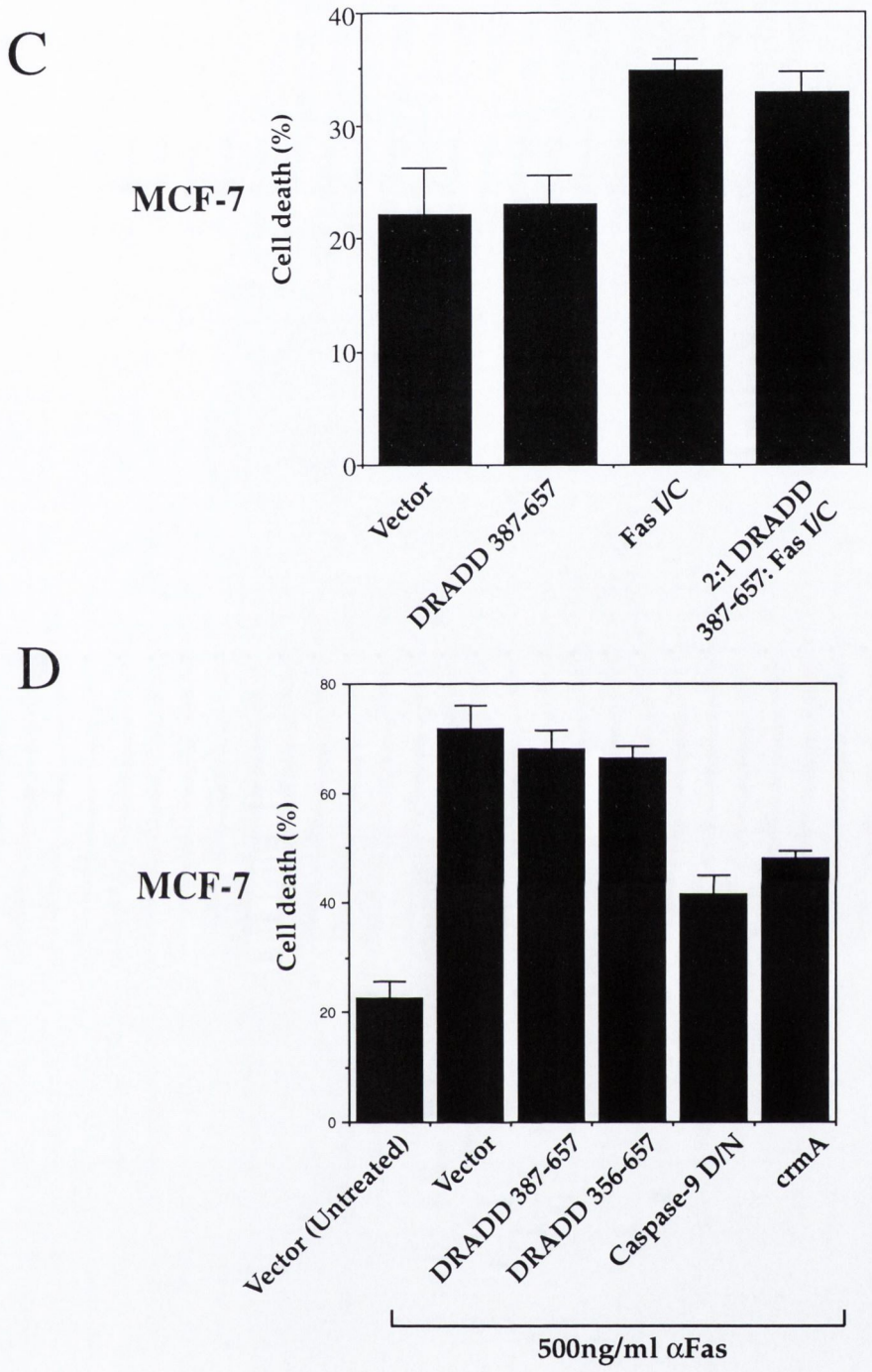

Figure 34

DRADD DN fails to block Fas-associated apoptosis

C, MCF-7 cells were transfected with 200 ng of plasmid encoding Fas I/C, alongside a 2:1 ratio (400ng) of DRADD$^{387-657}$ DN. Cells were assessed for apoptotic features as previously described 46 hours post-transfection.

D, MCF-7 cells were transfected with 800 ng of the indicated plasmids. 14 hours post-transfection, cells were treated as indicated with 500 ng/ml agonistic αFas mAb CH-11 (Upstate Biotechnology). The percentage of apoptotic transfected cells was determined 44 hours post-transfection.

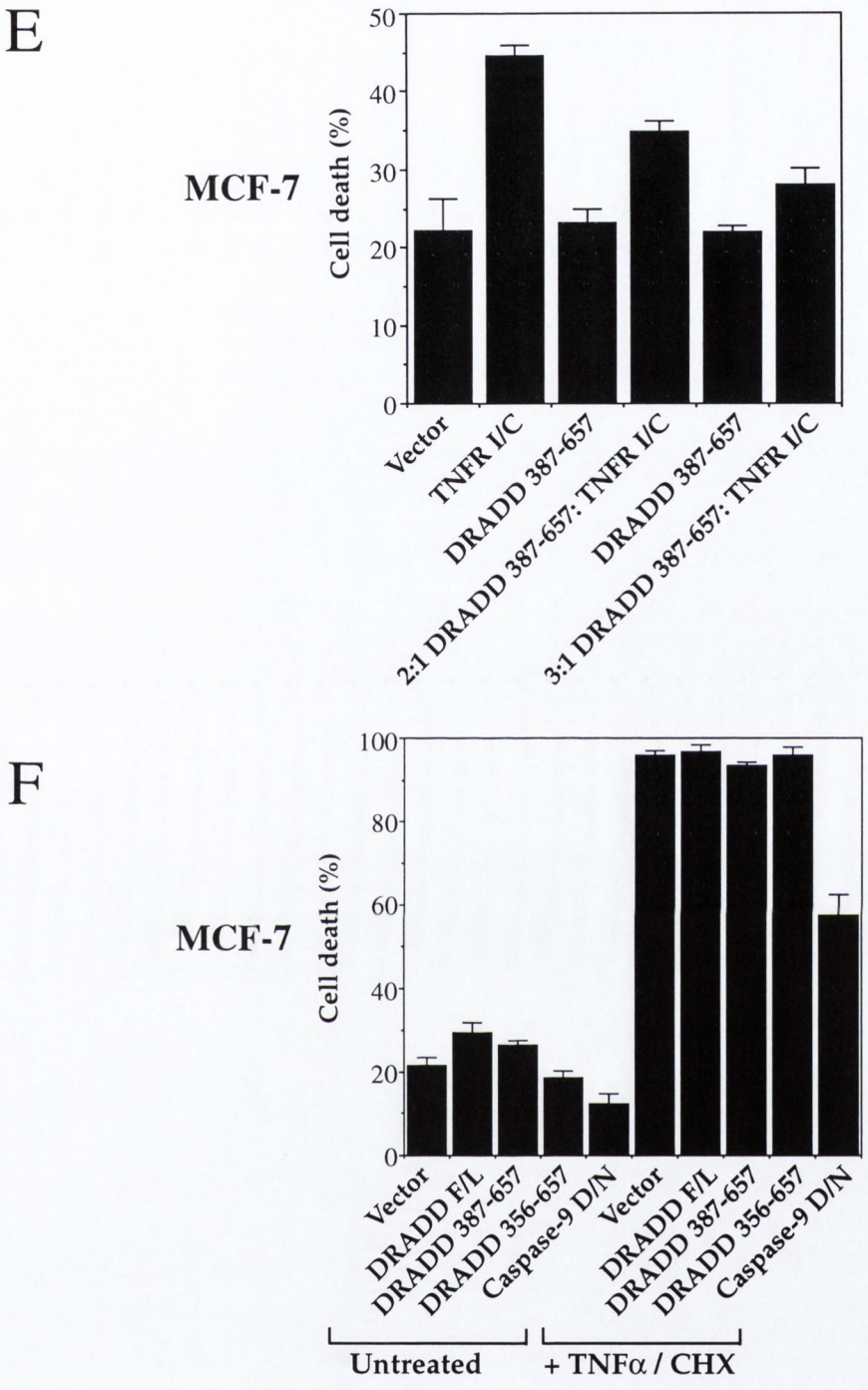

Figure 34

DRADD DN fails to block TNFR-associated apoptosis

E, MCF-7 cells were transfected with 200 ng of plasmid encoding Fas I/C, alongside a 2:1 ratio (400ng) or 3:1 ratio (600ng) of DRADD$^{387\text{-}657}$ DN. Cells were assessed for apoptotic features as previously described 46 hours post-transfection.

F, MCF-7 cells were transfected with 800 ng of the indicated plasmids. 20 hours post-transfection, cells were treated as indicated with 50 ng/ml TNFα The percentage of apoptotic transfected cells was determined 40 hours post-transfection.

Since overexpression of both of the cognate receptors of the TNF family member ligand TRAIL (DR-4/TRAILR-1 and DR-5/TRAILR-2) readily provoked apoptosis in our transient transfection-based model (Figure 34A, B), we next tested the ability of DRADD to potentiate apoptosis associated with ectopic expression of these death receptors (Figure 34G). However, expression of a 2:1 ratio of DN-DRADD failed to rescue cells transfected with either of these death receptors, suggesting that DRADD does not function as a specific adaptor in TRAIL death signaling (Figure 34G).

4.2.14.2. DRADD-DN does not potentiate death adaptor-associated apoptosis

Finally, since we observed that ectopic expression of death domain-containing adaptor molecules FADD, TRADD and RIP potently induce apoptosis in our MCF-7 model, we next evaluated a role for DRADD in these pathways. To this end, we transfected MCF-7 cells with plasmids encoding a 2:1 ratio of DN-DRADD$^{387-657}$ together with plasmids directing expression of either death adaptors FADD, TRADD or RIP. As is illustrated in Figure 34H, DN-DRADD failed to repress apoptosis induced by either of these molecules.

In summary, from these studies we thus concluded that DRADD did not play a role as a death adaptor molecule for any of the known transmembrane death receptors or their cognate adaptors tested: an outcome consistent with the subcellular localization of DRADD.

4.2.14.3. DRADD-DN does not potentiate genotoxic stress-associated apoptosis

We next directed our attention towards other pro-apoptotic stimuli that might require DRADD to engage caspase-9. Since DRADD expression is largely restricted to the nuclear compartment, we reasoned that stimuli that impinge upon this organelle—in particular, by inducing DNA damage, interfering with DNA replication, gene expression or cell cycle regulation—may provoke DRADD-dependent apoptosis. Moreover, *CASP-9*$^{-/-}$ mice are resistent to a variety of genotoxic agents, strongly suggesting that these provoke a caspase-9-dependent death pathway (Hakem *et al.*, 1998; Kuida *et al.*, 1998). To investigate this

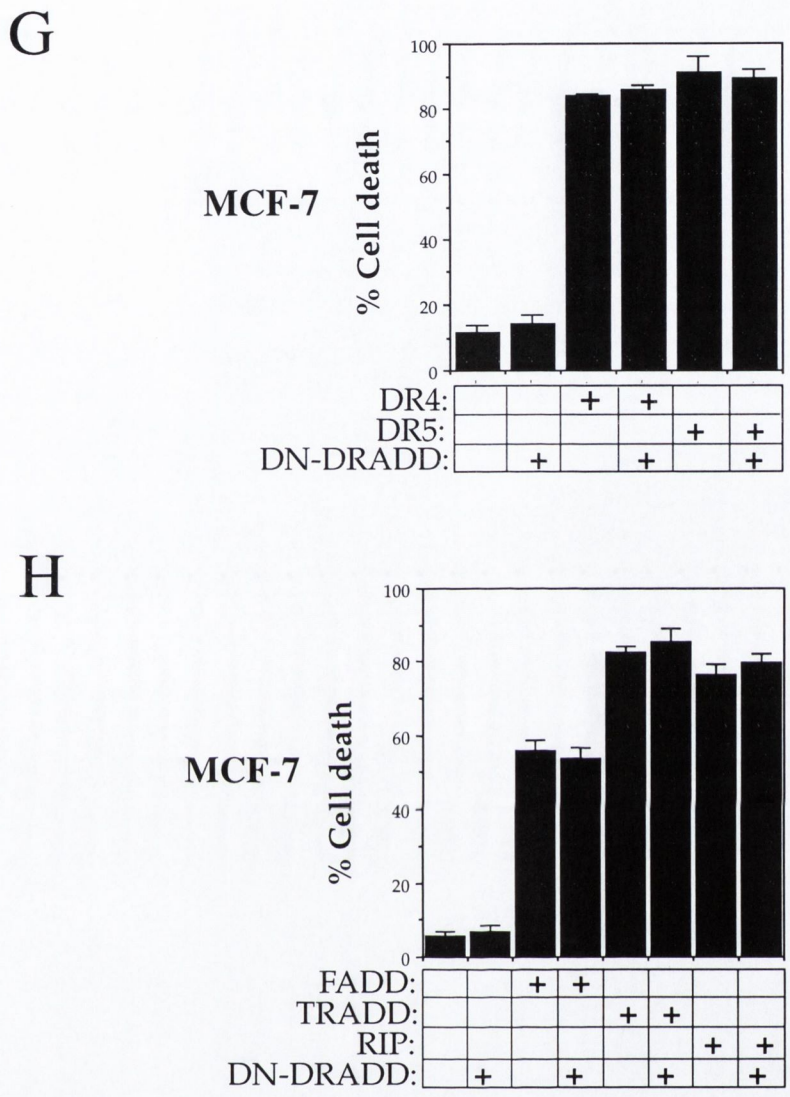

Figure 34

Dominant Negative DRADD Fails to antagonize DR-4/TRAILR-1, DR-5/TRAILR-2 and death adaptor-mediated apoptosis

G, MCF-7 cells transfected with 400 ng of pcDNA3-DRADD$^{387-657}$ plus 200 ng of either pcDNA3-DR-4/TRAILR-1 or pcDNA3-DR-5/TRAILR-2 were assessed for apoptotic features 60 hours post-transfection as described previously

H, MCF-7 cells were transfected with 200ng of CMV-based plasmids encoding death domain adaptors FADD, TRADD or RIP plus 400 ng of pcDNA3-based dominant negative (DN) DRADD$^{387-657}$, as indicated. Cells were assessed for apoptotic features 46 hours post-transfection.

possibility, we used the dominant negative approach described previously (Figure 33) in an attempt to block apoptosis provoked by a range of genotoxic stimuli (Figure 35). MCF-7 cells transfected with DN-DRADD as described for the death receptor experiments, were challenged with various genotoxic stimuli (Figure 35). However, initial observations using both UV-irradiation and the topoisomerase-inhibiting drug etoposide as a source of nuclear stress revealed that both of the DRADD-DN constructs were incapable of blocking apotosis (Figure 35). In contrast, cells expressing the caspase-9 DN active site mutant were considerably more refractile to these stimuli than their DRADD or vector-transfected counterparts, suggesting that apoptosis induced by these stimuli was caspase-9-dependent, though seemingly, not DRADD-dependent (Figure 35).

Artificially truncated proteins may be subject to proteolytic degradation as a result of mis-folding due to novel steric constraints enforced by fusion to, or removal of, essential domains from the full length molecule. However, in the absence of DRADD-specific antisera, we were unable to verify whether the pcDNA3-derived untagged DRADD-DN mutants were expressed. Because earlier experiments with the GFP-fused DRADD deletion mutants had demonstrated that GFP-DRADD$^{387-657}$ and DRADD$^{441-657}$ DD mutants were readily expressed, we decided to employ these in the dominant negative studies. To this end, we transfected MCF-7 cells with GFP-DRADD^{FL} or the GFP-DRADD deletion mutants described previously and then challenged the cells with various genotoxic stimuli (Figure 35C-E). Interestingly, these experiments suggested that all of the GFP-DRADD proteins tested, including full length DRADD, afforded a modest protective effect against UV-irradiation and drugs cisplatin and actinomycin-D (Figure 35C-E). In contrast, parallel-treated GFP transfectants died more readily in these experiments (Figure 35C-E). However, a further experiment aimed at establishing the background levels of death associated with expression of each of these proteins in cells untreated with genotoxic stimuli revealed that expression of the unfused GFP protein appeared to be somewhat more toxic than its DRADD-fused counterparts (Figure 35F). Thus, the apparently increased refractility of GFP-DRADD transfectants to these genotoxic agents may have related to this phenomenon

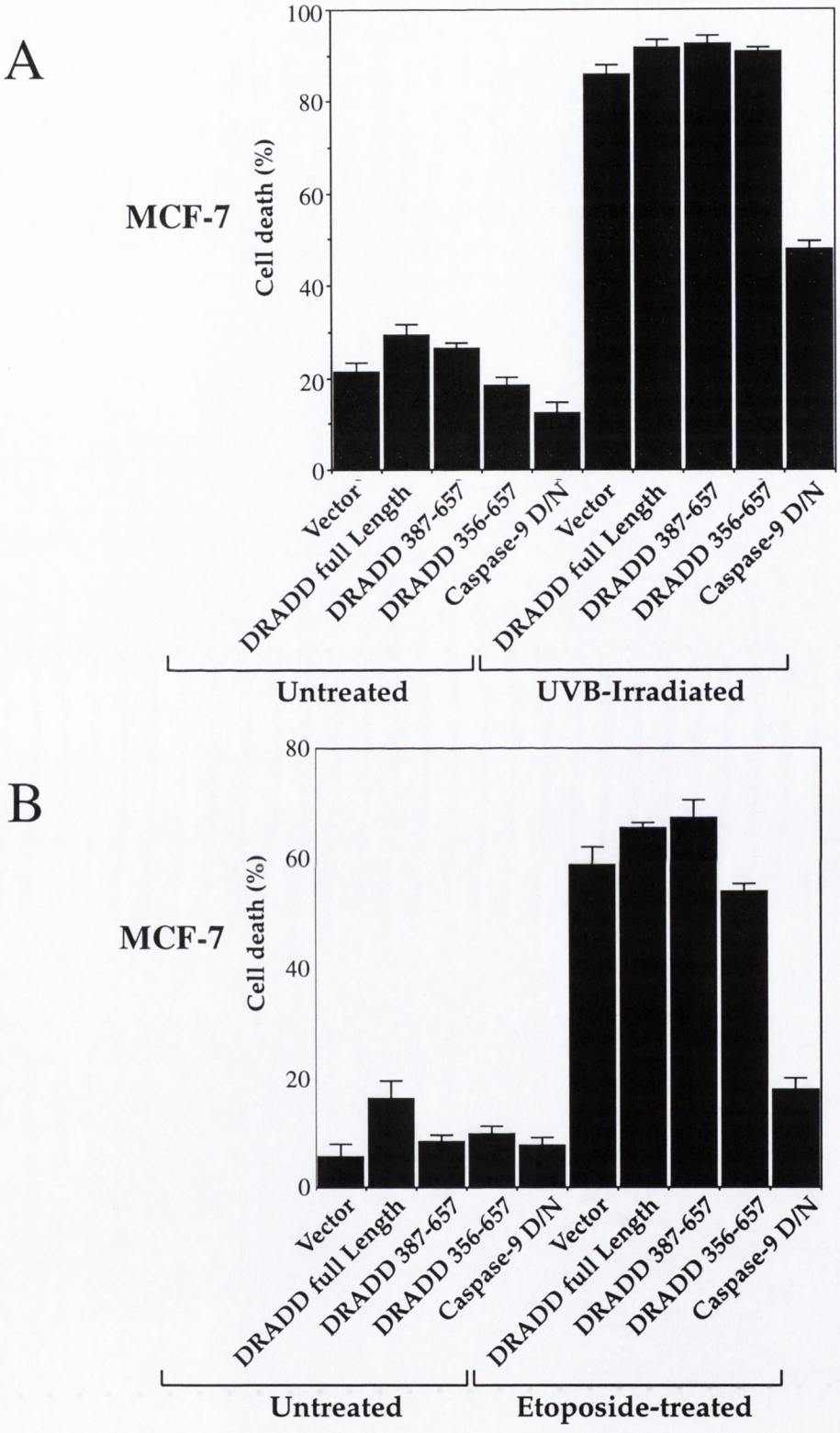

Figure 35

DRADD DN fails to block genotoxic stress-associated apoptosis

A and **B**, MCF-7 cells were transfected with 800 ng of the indicated plasmids alongside limiting amounts of the pCMVβ reporter plasmid. 24 hours post-transfection, cells were treated with UV irradiation for 5 minutes (**A**) or with 200μM Etoposide (**B**). Untreated controls for both experiments are indicated. The percentage apoptosis in the transfected cell population was determined approximately 48 hours post-transfection.

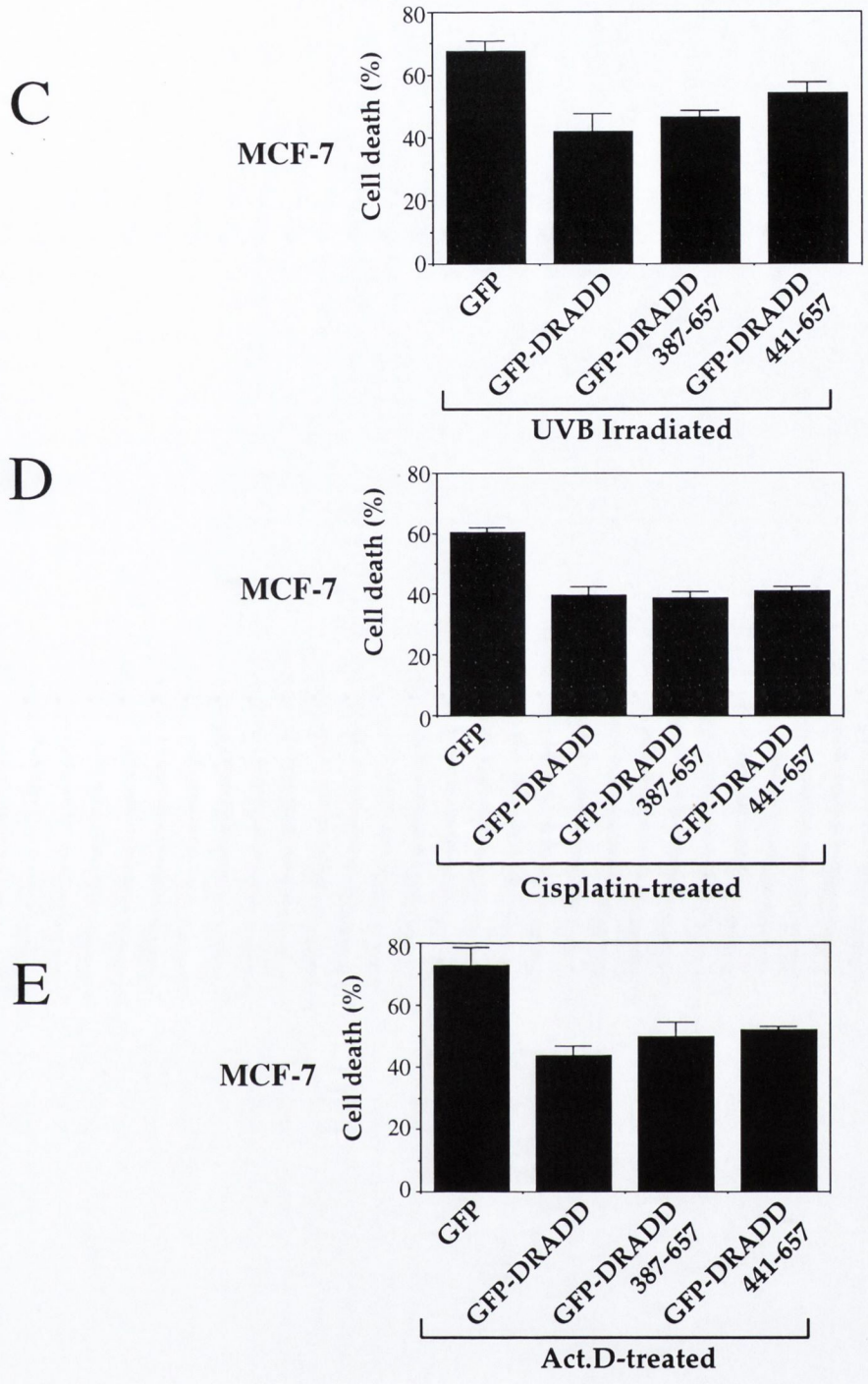

Figure 35

The effect of DRADD DN on genotoxic stress-associated apoptosis

MCF-7 cells were transfected with 500 ng of the indicated GFP or GFP-DRADD plasmids alongside limiting amounts of the pCMVβ reporter plasmid.

C, 20 hours post-transfection, cells were treated with UV irradiation for 30 seconds and the percentage apoptosis in the transfected cell population was determined approximately 12 hours later.

D, 20 hours post-transfection, cells were treated with 30 μM cisplatin and the percentage of apoptotic transfected cells was determined 32 hours later.

E, 12 hours post-transfection, cells were treated with 2 μM Actinomycin-D (Act.D) and the percentage of apoptotic transfected cells was determined 12 hours later.

F

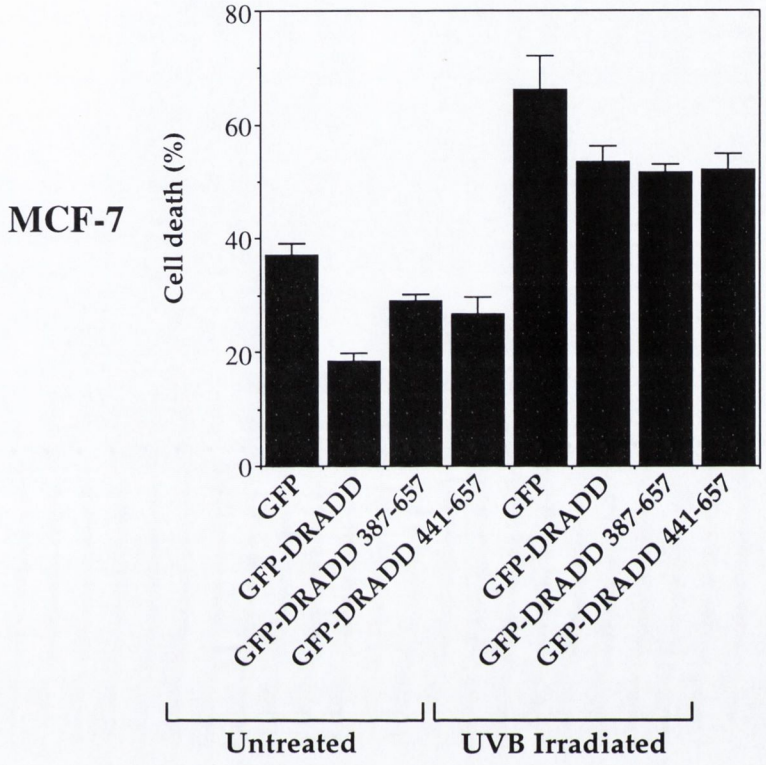

Figure 35

The effect of DRADD DN on genotoxic stress-associated apoptosis

F, MCF-7 cells were transfected with 400 ng of the indicated GFP or GFP-DRADD plasmids alongside limiting amounts of the pCMVβ reporter plasmid. 18 hours post-transfection, cells were subjected to UVB irradiation for 30 seconds and the percentage apoptotic transfected cells was determined 9 hours later. A similarly transfected but untreated cohort of cells serve as a control.

(Figure 35), possibly as a result of co-expression with the β-galactosidase reporter gene.

4.2.15. Generation of a stable GFP-DRADD dominant negative cell line

Since our attempts to elucidate the function of DRADD using the MCF-7-based transient overexpression system had been unsuccessful, we decided to create stable DRADD DN-overexpressing cell lines. With a stable cell line, a bulk population can be more easily analyzed for subtle effects than only a subproportion of transfected cells arising from a transient expression-based approach. Unfortunately, an initial attempt to make a stable HeLa cell line based on FLAG epitope-tagged DN-DRADD was unsuccessful. Since a plausible explanation for this failure may be that long-term DRADD expression in this cell line may have elicited cytotoxic or cytostatic effects, through interaction with caspase-9 or with pRb, respectively, we decided to repeat the procedure using a different cell line.

We next chose Jurkat cells as a recipient for stable DN-DRADD expression. Because the initial two-hybrid screen obtained multiple DRADD clones from a Jurkat cDNA library, we reasoned that the other components of a DRADD-specific pathway might be expressed in these cells, potentially making it more likely that we might be able to find a dominant negative effect. Since we could readily detect expression of GFP-DRADD^{FL} (Figure 31D), we chose to make GFP, GFP-DRADD^{FL} and GFP-DRADD$^{387-657}$ overexpressing lines. As a prelude to generating a stable jurkat line we first had to ascertain the dose of G418 selection drug required to kill untransfected cells not harbouring the GFP plasmid that conferred drug resistance. To this end we set up a titration of various concentrations of the drug in untransfected jurkat cell cultures, with a view to finding a dose that killed ~100% of the cells over approximately 7 days. On the basis of these assays (Figure 36A, B) a dose of 1.6 mg/ml was chosen for the selection of transfected cells.

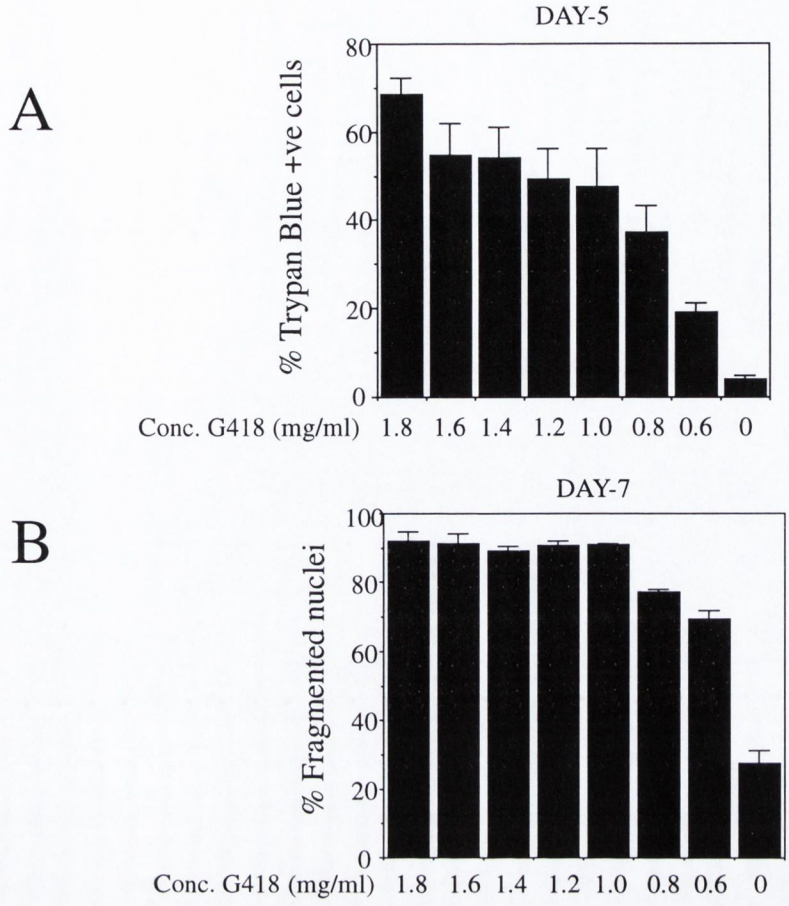

Figure 36

Determining the electroporation conditions required for the generation of stable Jurkat GFP, GFP-DRADD and GFP-DRADD 387-657-overexpressing cells

A, Graph illustrating % cell death as assessed by trypan blue staining of G418-treated Jurkat cell cultures at a 5-day timepoint. Cells that failed to exclude the dye were scored as dead. **B**, Graph illustrating % cell death as assessed by Hoechst staining of G418-treated Jurkat cell cultures at a 7-day timepoint. Cells exhibiting marginated chromatin and/or fragmented nuclei were scored as apoptotic. Indicated beneath both graphs are the G418 concentrations used in the titration.

Table 13

Table illustrating the electroporation parameters tested in order to optimize the efficiency of transfection of Jurkat cells. The % cell survival and % of GFP-positive cells obtained from each experimental setting are indicated.

Treatment	% Cell survival	Total No. GFP +ve cells
0.5 kV/950μF	4.0	8.9×10^3
0.4 kV/950μF	9.5	1.5×10^4
0.3 kV/950μF	43.2	7.0×10^4
0.2 kV/950μF	74.4	3.6×10^4

We next optimized the parameters involved in the transfer of plasmid DNA into recipient cells. To this end, we electroporated Jurkat cells with GFP plasmid under various voltage settings and determined the extent of cell survival of the bulk population as well as the total number of GFP-positive transfected cells (Table 13). This analysis revealed that the 0.3kV setting that killed just over half of the total population, yielded the maximum number of GFP-positive cells (Table 13). Since it is well established that linearized DNA is more recombinogenic than circular plasmid, the constructs were linearized by restriction endonuclease digestion of the pEGFP-C3 vector within a site that does not effect gene expression, prior to electroporation. At the time of writing, G418-resistant clones of GFP, GFP-DRADD and GFP-DRADD$^{387-657}$ are outgrowing in culture.

4.2.16. DRADD does not translocate from the nucleus upon induction of the death program

It is well established that several key regulators of apoptosis, including Bid and cytochrome c, translocate from one cellular compartment to another in order to realize their death-inducing abilities (Liu *et al.*, 1996; Li *et al.*, 1998; Luo *et al.*, 1998; Adrain and Martin, 2001; Green 2000). Thus, we hypothesized that DRADD may exit the nucleus in response to specific death-inducing stimuli, as part of a DRADD-dependent death program. Identification of the stimulus responsible for DRADD translocation may yield clues about the apoptotic signaling pathway within which DRADD may operate.

To investigate this possibility, we transfected MCF-7 cells with GFP-DRADD^{FL} as described previously, then challenged the GFP-DRADD^{FL} transfectants with a variety of pro-apoptotic stimuli (Figure 37). While GFP-DRADD transfectants treated with a variety of cytotoxic stimuli continued to retain the majority of GFP-DRADD within the nuclear compartment, cells treated with several stimuli including UV irradiation and cisplatin exhibited a condensed, granular/punctate DRADD distribution within the nucleus (Figure 37). Interestingly, in UV-treated transfectants, GFP-DRADD fluorescence exhibited a particularly punctate pattern,

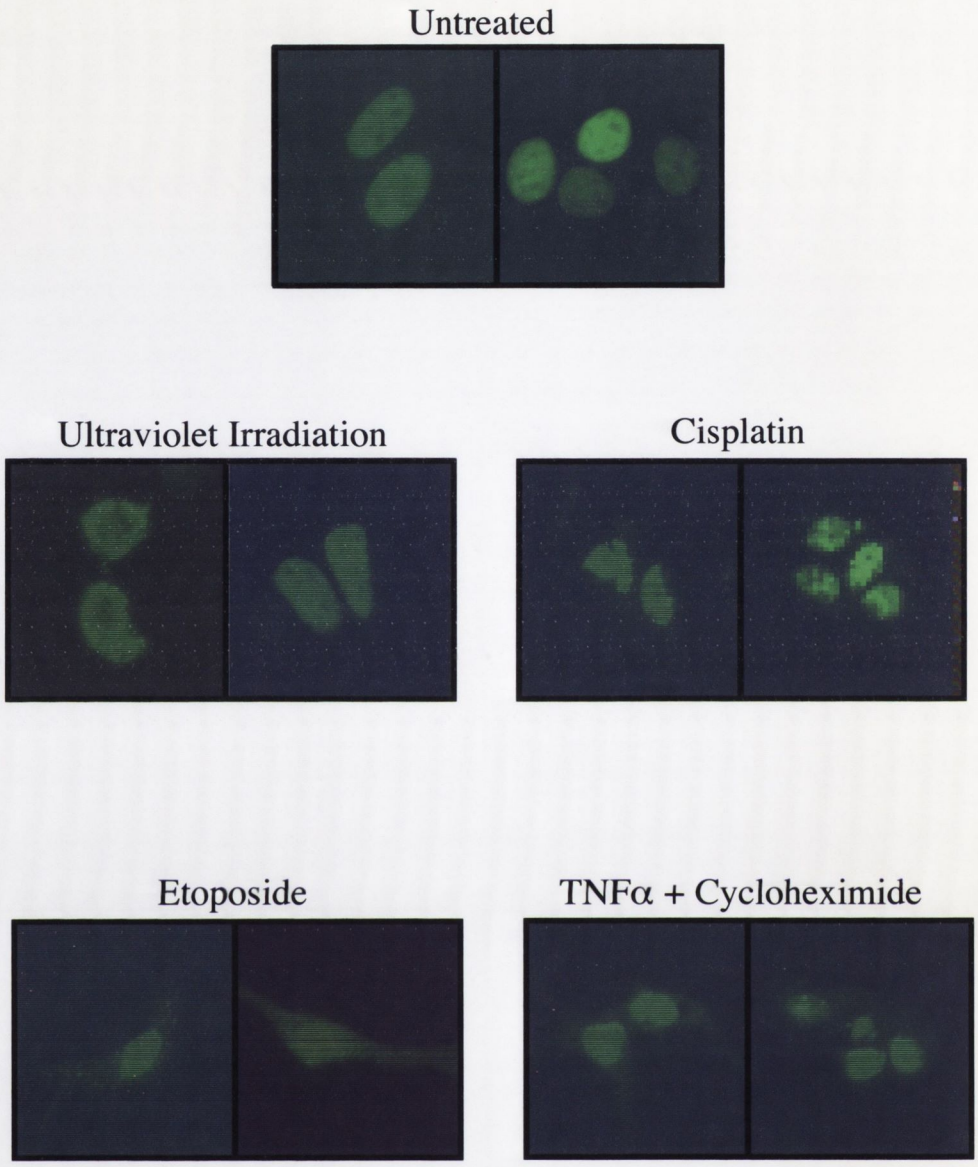

Figure 37

DRADD does not undergo redistribution from the nucleus in dying cells

MCF-7 cells growing on coverslips were transfected with 400 ng of GFP-DRADD. 20 hours post transfection, cells were treated with the following cytotoxic stimuli:
UV-irradiation (30 seconds), Cisplatin (40μM), Etoposide (200μM) and TNFα/Cycloheximide (25 ng/ml ; 1μM). 24 hours later, cells were fixed, rehydrated in PBS and mounted in glycerol for inspection under UV illumination using a FITC filter to visualize GFP-positive cells. Representative images of apoptotic GFP-DRADD-positive nuclei were captured under X40 magnification. GFP-DRADD transfected, untreated cells serve as a control.

with numerous small GFP-DRADD-positive foci (Figure 37, middle panel). Cells treated with cisplatin exhibited a similar punctate DRADD distribution, albeit with fewer, larger GFP-DRADD-positive nuclear foci (Figure 37, middle panel). In contrast, cells dying in response to TNFα/cycloheximide treatment exhibited a more condensed but less punctate DRADD-labeled nuclear morphology (Figure 37, bottom panel). These subtle differences are interesting, especially since UV-irradiation and cisplatin are nuclear damaging agents, whereas TNFα clearly exerts its pro-apoptotic effects at the level of death receptor ligation. However, an important caveat to note is that cells treated with different stimuli were dying asychronously, with the onset of classical apoptotic features varying amongst different treatments. Thus, it is possible that the apparent differences in DRADD sublocalization in response to different treatments may reflect different stages of nuclear attack during apoptosis.

However, some stimuli, most notably etoposide (and also actinomycin D, data not shown) elicited a somewhat different DRADD distribution in dying cells (Figure 37, bottom panel). In contrast to dying cells that retained substantial amounts of DRADD within the nucleus when treated with the stimuli discussed above, a substantial proportion of the population of etoposide-treated transfectants exhibited a striking loss of nuclear GFP-DRADD^{FL} fluorescense. Moreover, many of these cells exhibited weak fluorescence in punctate, discrete localities within the cytosol, perhaps consistent with a mitochondrial sublocalization (Figure 37, bottom panel). However, in spite of the distinct loss of nuclear DRADD, the appearance of GFP-DRADD^{FL} fluorescence within the cytosol was too weak to support the notion of a simple bulk movement of DRADD from the nucleus into the cytosolic compartment. Interestingly, certain cells exhibited both a substantial nuclear GFP-DRADD^{FL} fluorescence as well as a weak punctate fluorescence throughout the cytosol (Figure 37). However, for the reasons stated above, the significance of this observation within the context of cells treated with diverse stimuli progressing through the death program asychronously, remains to be seen. In summary, in response to most cytotoxic agents, the majority of

GFP-DRADD remains within the nucleus (Figure 37). These data may therefore suggest that DRADD exerts its pro-apoptotic effects from within the nucleus. Within this context, it is interesting to note a recent report that suggests that a substantial portion of the caspase-9 cellular pool colocalizes to nuclei (Ritter *et al.*, 2000). Thus, all of the hitherto identified DRADD-interacting molecules are indeed present within the nuclear compartment.

4.2.17. Detection of stimulus-specific DRADD cleavage

Proteolysis, like phosphorylation, represents an important means of switching on or off the function of a protein. For instance, ICAD, the inhibitor of the caspase-activated DNase, gets cleaved during apoptosis, thus enabling the DNase activites of the CAD enzyme through its subsequent shuttling into the nucleus (Sakahira *et al.*, 1998). In another example, cleavage of Bid by caspase-8 during death-receptor-induced apoptosis enables its pro-apoptotic activity, channelled via the mitochondrion (Luo *et al.*, 1998; Li *et al.*, 1998; Gross *et al.*, 1999). To determine if DRADD undergoes proteolytic cleavage during apoptosis, we transfected 293T cells with GFP-DRADD alongside plasmids under the control of a CMV-based promoter expressing a variety of known pro-apoptotic proteins as a means of inducing the death program in DRADD-overexpressing cells (Figure 38). Intriguingly, in cells dying as a result of expression of the death agonist molecule Bax, GFP-DRADD was completely converted from its full length form to a ~30kDa cleavage product (Figure 38). In contrast, cells overexpressing other proapoptotic proteins retained substantial amounts of full length GFP-DRADD (Figure 38). Since the approximate proportion of cells undergoing apoptosis as a result of expression of these other death-inducing molecules was the same, or greater than Bax-transfectants, this suggested that cells dying in response to Bax overexpression were not simply undergoing cleavage of the GFP moiety of GFP-DRADD^{FL} in a non specific manner. Clearly, further investigation will be required to determine whether the putative candidacy of DRADD as a substrate for Bax-associated apoptosis relates to unlocking its cell death regulatory ability, or alternatively, simply relates to DRADD being a passive caspase substrate under these conditions.

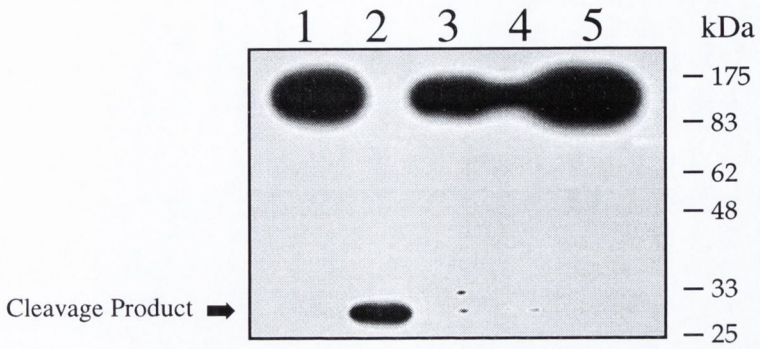

Key:

1. GFP-DRADD alone
2. GFP-DRADD + Bax
3. GFP-DRADD + Caspase-8
4. GFP-DRADD + Rip
5. GFP-DRADD + TRADD

Figure 38

Cleavage of DRADD specific to Bax-induced apoptosis

293T cells were transiently transfected with 2 μg of GFP-DRADD plus 18 μg of CMV-based plasmids encoding the indicated pro-apoptotic proteins. 48 hours post-transfection, live and floating cells were collected and lysed in 1x SDS-PAGE loading buffer. Samples were subjected to SDS-PAGE followed by immunoblotting with an GFP-specific antibody. The arrow illustrates the GFP-reactive cleavage product that was observed specifically in response to co expression with death agonist molecule, Bax.

4.2.18. Ectopic expression of pRb induces apoptosis

We next directed our attention towards elucidating a role for Rb as a regulator of DRADD. The role of Rb as a tumor suppressor has been well established. Indeed, this molecule is second only to p53 in terms of the frequency of mutatation of this gene in a wide variety of human cancers (Weinberg, 1995). The role of the latter as a key mediator of both cell cycle arrest and apoptosis, has been well established within the context of stimuli that provoke nuclear damage (Choisy-Rossi and Yonish-Rouach, 1998). In contrast, the role of Rb as a modulator of apoptosis has yet to be fully elucidated. Somewhat confusingly at odds with its established role as a tumor suppressor, targeted deletion of this gene in *RB* $^{-/-}$ mice suggests a role for Rb as a negative regulator of apoptosis, since Rb-deficient animals exhibit increased apoptosis in both the central nervous system (CNS) and peripheral nervous system (PNS) (Macleod *et al.*, 1996). Because we have demonstrated that Rb interacts with DRADD we wondered whether Rb could modulate the ability of this molecule to regulate apoptosis.

Within this context, we initially determined whether ectopic expression of Rb alone could modulate apoptosis. Thus, we transiently overexpressed a CMV-based Rb expression plasmid alongside an expression plasmid encoding the well established tumor suppressor, p53, together with the pCMVβ reporter plasmid and examined cells for typical apoptotic features 1-2 days post-transfection (Figure 39). This analysis revealed that in agreement with a recently published report (Hsieh *et al.*, 1999), ectopic expression of Rb modestly provoked apoptosis in these cells (Figure 39). However, at both of the endpoints tested, the tumor suppressor p53 proved more potent in this regard (Figure 39). To illustrate the apoptotic phenotype induced by forced expression of both these tumor suppressors, albeit in a non-quantitative manner, we captured images of Rb or p53-transfected apoptotic cells alongside vector-transfected cells under standard light microscopy using a 40x lens (Figure 39B). As can be seen, blue-staining (transfected) cells treated with either Rb or p53 exhibited a rounded and condensed morphology

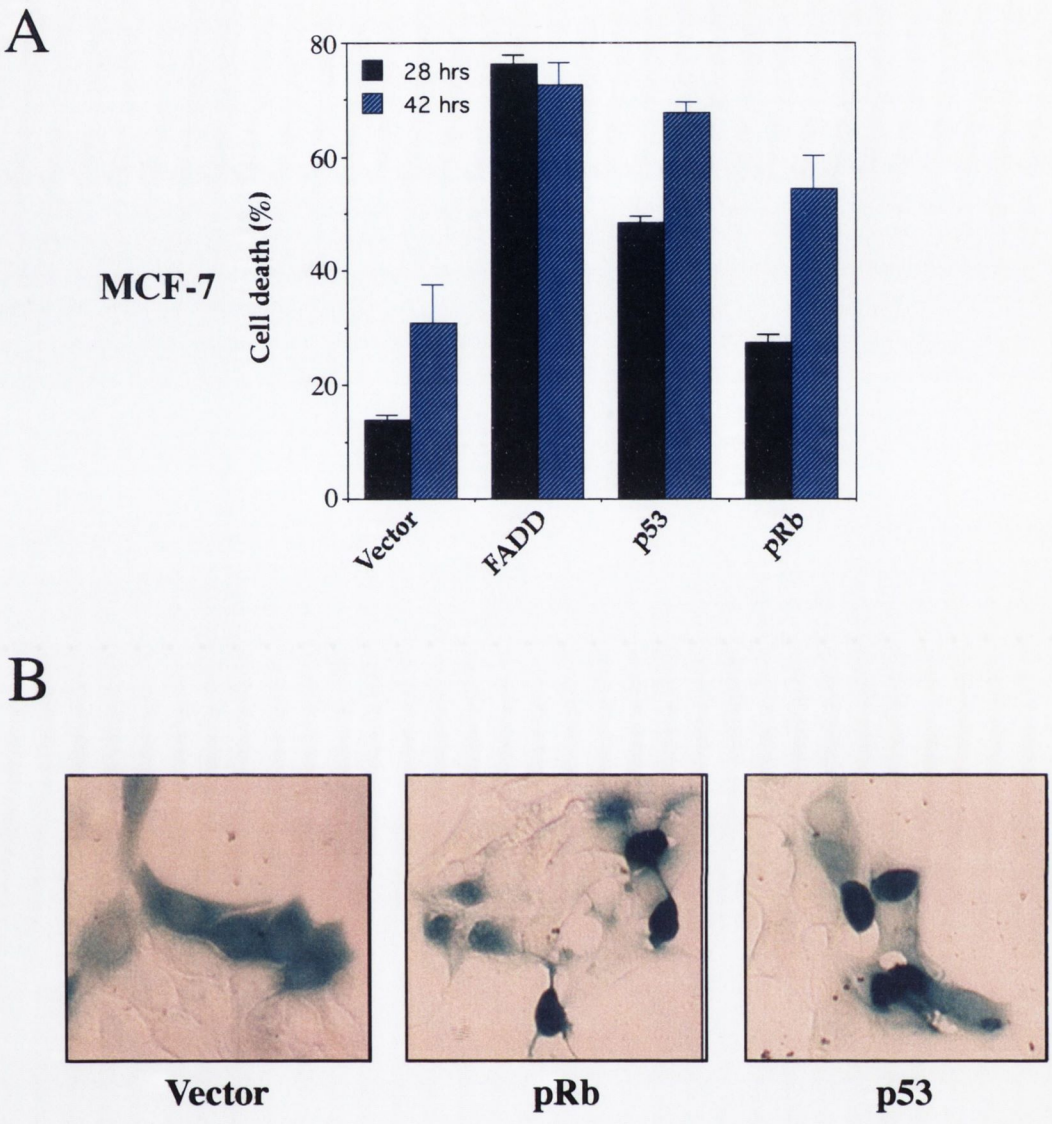

Figure 39

Ectopic expression of pRb induces apoptosis

A, MCF-7 cells were transfected with 800 ng of the indicated plasmids alongside limiting amounts of the pCMVβ reporter plasmid. 28 or 42 hours post-transfection, cells were fixed and stained for β-galactosidase activity and the percentage of apoptotic transfected cells was determined. **B**, Images captured using a x40 lens of cells transfected with either pcDNA3 vector or CMV-based plasmids encoding pRb or p53. Images are intended to represent the morphology of transfected (blue) cells, but do not reflect a quantitative assessment of % death attributable to each treatment.

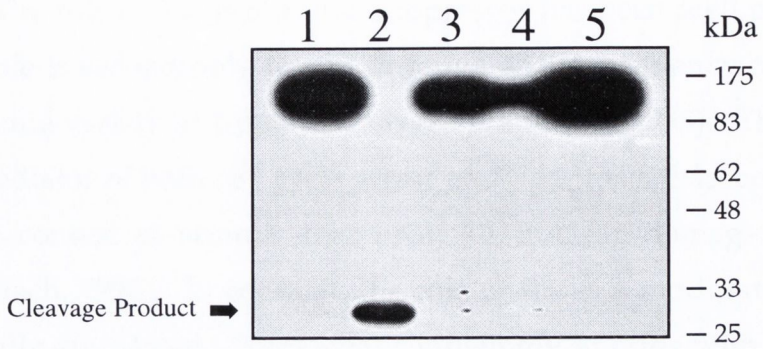

Key:

1. GFP-DRADD alone
2. GFP-DRADD + Bax
3. GFP-DRADD + Caspase-8
4. GFP-DRADD + Rip
5. GFP-DRADD + TRADD

Figure 38

Cleavage of DRADD specific to Bax-induced apoptosis

293T cells were transiently transfected with 2 μg of GFP-DRADD plus 18 μg of CMV-based plasmids encoding the indicated pro-apoptotic proteins. 48 hours post-transfection, live and floating cells were collected and lysed in 1x SDS-PAGE loading buffer. Samples were subjected to SDS-PAGE followed by immunoblotting with an GFP-specific antibody. The arrow illustrates the GFP-reactive cleavage product that was observed specifically in response to co expression with death agonist molecule, Bax.

typical of apoptosis, whereas blue cells transfected with the pcDNA3 vector exhibited a fully spread, viable morphology (Figure 39B).

4.2.19. pRb and DRADD collaborate to induce apoptosis

We next examined whether the ability of Rb to modulate apoptosis was related to its association with DRADD. To achieve this, we co-expressed Rb with either GFP-DRADD or a GFP-DRADD$^{387\text{-}657}$ deletion mutant, under conditions where overexpression of Rb alone provoked minimal apoptosis (Figure 39C). In this context we used GFP-positive nuclei to identify GFP-DRADD^{FL}-transfected cells. Strikingly, whereas expression of either DRADD or Rb alone elicited a similar minimal degree of apoptosis as that encountered through transfection of the vector, co-expression of Rb and DRADD resulted in a significant increase in the number of cells exhibiting typical apoptotic features, most notably including fragmented and condensed nuclei (Figure 39D). In contrast, co-expression of Rb with the DRADD$^{387\text{-}657}$ mutant that lacks the caspase-9-binding site but retains the Rb-interaction motif, failed to elicit this effect. These data suggest that DRADD may couple Rb to the death machinery under conditions where Rb activity is impaired or deregulated.

4.2.20. Generation of DRADD antisera

Studies conducted on DRADD had thusfar utilized either overexpressed epitope-tagged or recombinant bacterial proteins. To investigate protein-protein interactions using endogenous levels of DRADD, we decided to generate a DRADD-specific antibody. This was critically important since investigating protein-protein interactions using endogenous levels of untagged DRADD protein is clearly more informative than within the context of the greatly increased levels of protein associated with transient overexpression studies. Additionally, the use of epitopes of any variety clearly risks impairing the activity of the target protein by changing protein folding or occluding vital protein-protein interaction motifs. Moreover, it was desirable to verify our data concerning the observed subcellular localization of DRADD within the context of endogenous protein levels.

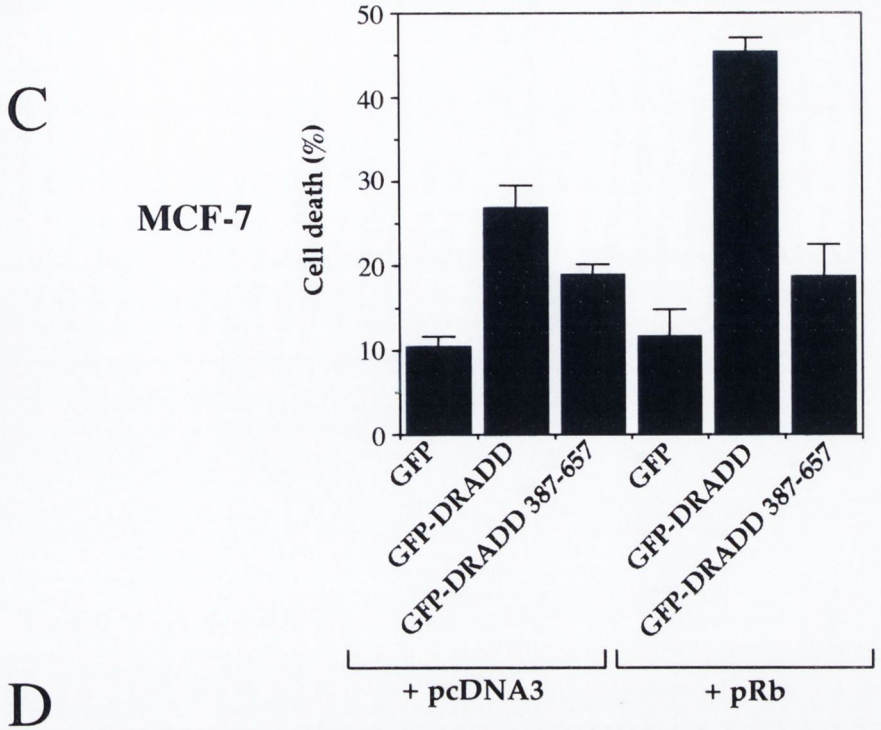

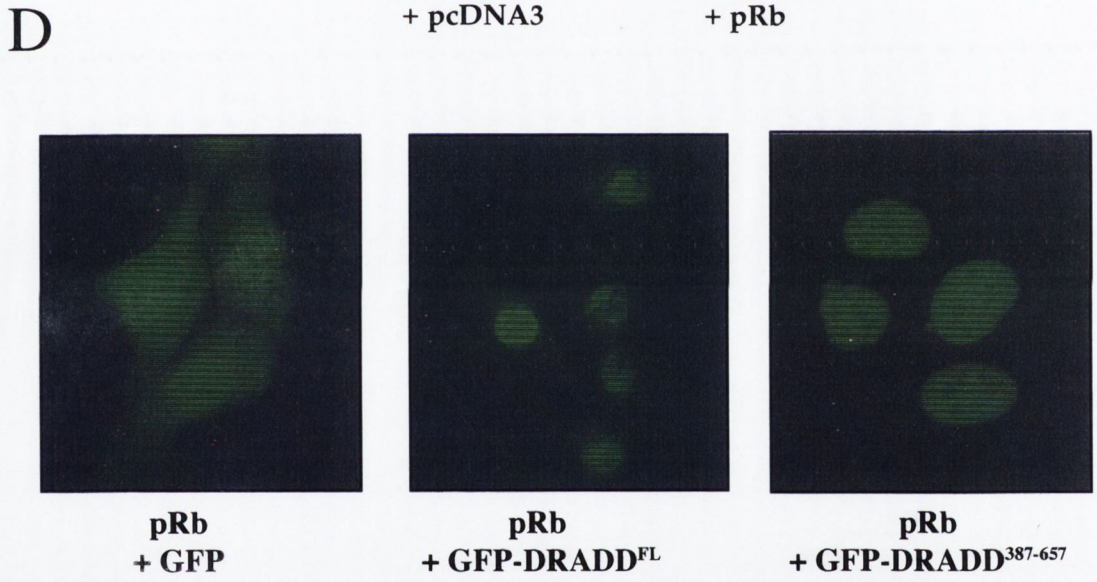

Figure 39

pRb augments DRADD-associated apoptosis

C, MCF-7 cells were transiently transfected with 700 ng of pEGFP-C3-based plasmid encoding either GFP, GFP-DRADD^{FL}, GFP-DRADD$^{387-657}$ plus 700 ng of pCMV-Rb, where indicated. An equal plasmid amount in each well was maintained by the addition of pcDNA3 vector plasmid to appropriate wells. The percentage of GFP-positive apoptotic cells was assessed under fluorescence microscopy 44 hours post-transfection. Data shown are representative of at least three independent replicate experiments. Error bars represent standard error of the mean derived from 3 independent fields of at least 100 cells.

D, Images captured using a x40 lens of cells transfected with pRb together with either GFP alone or the indicated GFP-DRADD fusion proteins. Images are intended to represent the morphology of GFP-positive cells, but do not reflect a quantitative assessment of % death attributable to each treatment.

To this end, the amino acid sequence of DRADD was subjected to inspection using the Protean program from the Lazergene suite of sequence analysis software in order to select a peptide for immunization and production of polyclonal DRADD antisera. This analysis revealed a candidate region (Figure 40 A) that was a suitable antigen, since this peptide sequence was hydrophilic and therefore had a high surface probability, as predicted by the algorithms of Kyte and Doolittle and Emini respectively (Figure 40A). In addition, the Jameson-Wolf algorithm predicted this area to possess a high probability of antigenicity. Finally, inspection of a 20 amino acid peptide chosen from this region (Figure 40B) by database interrogation revealed that the peptide chosen bore no resemblance to other identified human proteins. The antibody produced was therefore less likely to cross-react with other human protein species in cell lysates.

The peptide chosen was synthesized with a cysteine residue at the N-terminus in order to facilitate coupling to Keyhole Limpet Haemocyanin (KLH) to confer immunogenicity (Figure 40B). The process of peptide production, rabbit immunization and serum harvesting was carried out commercially (Genosys, UK) according to standard procedures. Upon obtaining the terminal bleed, we tested the sera from both rabbits (denoted 'A' and 'B') for reactivity against endogenous DRADD in cell lysates derived from a variety of tumour lines. However, by immunoblot analysis, we were unable to detect DRADD-reactive bands. Moreover, further attempts to analyze the antisera with respect to immunoblots of lysates derived from cells overexpressing either untagged pcDNA3 DRADD or epitope tagged pcDNA3 FLAG-DRADD again failed to reveal the presence of DRADD-reactive bands.

As a final attempt, we then probed immunoblots derived from 293T cell lysates overexpressing GFP or GFP-DRADD^{FL} and its derivatives with a 1:50 dilution of aliquots of antibodies 'A' and 'B' (Figure 40C). Surprisingly, whereas the same dilutions of antibody failed to detect overexpressed untagged or FLAG-tagged DRADD, antibody obtained from both rabbits proved reactive against GFP-

A

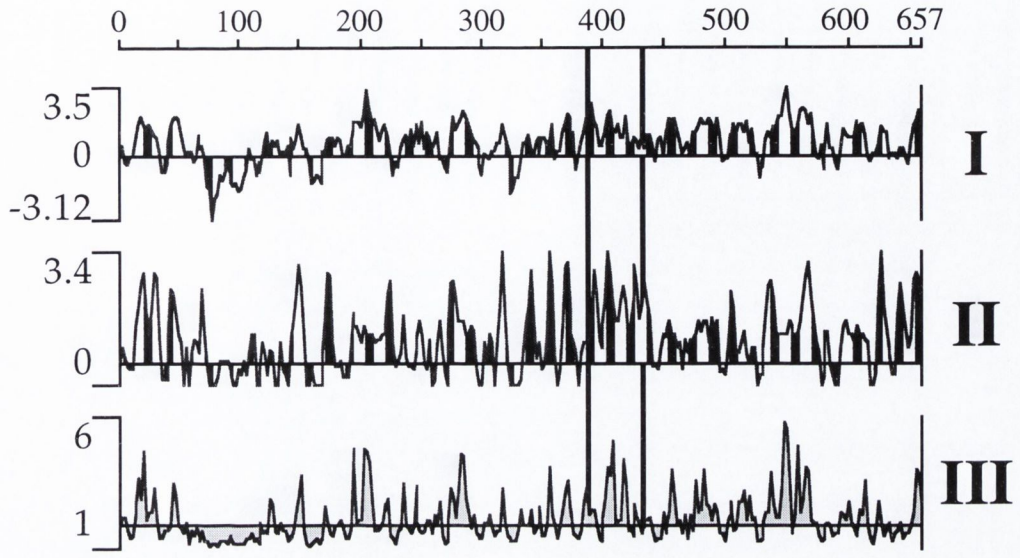

B

402-(C)**ERTSDTKPTRIIRKRTAPED**-421

Figure 40

Identification of an antigenic region in DRADD suitable for antibody generation

A, The DRADD amino acid sequence was analyzed using Protean program from the Lazergene software suite. A candidate antigenic peptide was chosen based on prediction of (**I**) hydrophilicity based a plot obtained using the the Kyte and Doolittle angorithm, (**II**) the Jameson-Wolf antigenic index prediction and (**III**) a surface probability plot, based on the Emini algorithm. The candidate antigenic region of molecule is enclosed by the vertical bars. The scale above the plots denotes amino acid positions in the full length DRADD sequence.

B, The DRADD peptide from the region indicated in (A) that was chosen for immunization. The peptide was synthesized with a cysteine residue (C) included at the amino terminus of the peptide, to facilitate coupling to Keyhole Limpet Haemocyanin (KLH) prior to immunization. The numbers denote amino acid positions in the full length DRADD sequence

C

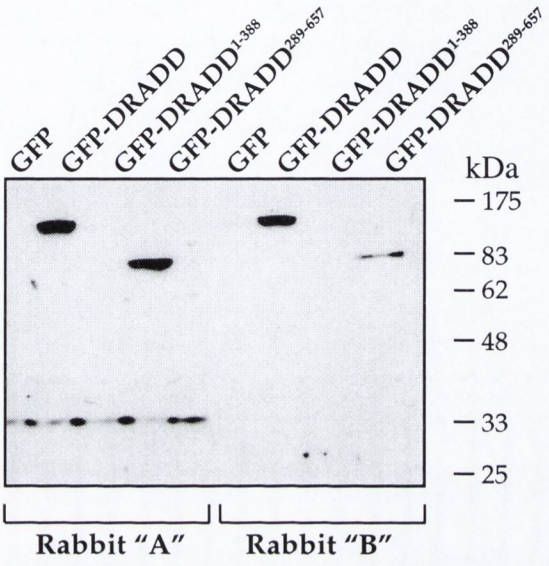

Figure 40

Verification of the specificity and reactivity of DRADD antisera

C, 293T cells were transiently transfected with plasmids encoding GFP or the indicated GFP-DRADD deletion mutants. Lysates derived from these cells were subjected to SDS PAGE followed by immunoblotting with a 1:50 dilution of DRADD polyclonal antisera derived from two individual rabbits. Consistent with the position of the C-terminal DRADD epitope used for immunization, the $DRADD^{1-388}$ mutant fails to be detected by the antisera, as does overexpressed unfused GFP.

DRADD (Figure 40C). The specificity of the GFP-DRADD-reactive bands was demonstrated by the failure of the antisera to reveal a specific band for GFP alone (Figure 40C). Moreover, although equivalent input amounts of GFP-DRADD$^{1-388}$ were loaded alongside aliquots of GFP-DRADD full length or GFP-DRADD$^{289-657}$, the antibody failed to detect DRADD-reactive bands in this lane (Figure 40C). Since the N-terminal DRADD$^{1-388}$ mutant lacks the epitope site chosen for immunization, this confirmed the specificity of the antisera.

These data revealed that the antibody was clearly reactive, although the titre was clearly too low to detect endogenous levels of proteins. Future work will thus utlilize affinity chromatography as a means of increasing the DRADD-specific titre in these sera. Importantly, these data also reveal that the protein levels of overexpressed GFP-DRADD were considerably higher than either untagged or FLAG-tagged. This implies that either GFP-based expression vectors facilitate higher expression levels than other comparable CMV-based expression vectors, or, that DRADD is normally targeted for proteolytic degradation—that is somehow prevented by the fusion of the GFP-epitope to the DRADD N-terminus. The provision of DRADD-specific antisera will enable us to investigate the expression levels of DRADD in response to particular stimuli.

4.3. DISCUSSION

4.3.1. Summary

In this chapter we report the identification of a novel caspase-9-specific putative death adaptor protein we have called DRADD. Notably, sequence analysis of DRADD revealed the presence of classical apoptotic signaling modules, namely a death domain (DD) and a region bearing substantial homology to the CARD motif, strongly suggesting that DRADD may function as a caspase adaptor protein. In support of this, through an extensive deletional analysis of the molecule, we have demonstrated that DRADD binds caspase-9 through the putative CARD-like motif. Moreover, transient overexpression of CARD-containing DRADD deletion mutants provokes caspase-9-dependent apoptosis, suggesting a role for DRADD as a caspase-9 adaptor.

4.3.2. DRADD does not potentiate death receptor-associated apoptosis

Given the presence of the death domain within the C-terminus of DRADD, we have attempted to identify a role for DRADD within death domain-dependent apoptotic signaling pathways. The established paradigm is that death domain modules participate in signal transduction via a homophilic interaction with other death domain-containing molecules (Ashkenazi and Dixit, 1998). Based on this principle, we have eliminated a role for DRADD as a proximal signaling adaptor in death receptor pathways Fas, TNFR-1, DR-4/TRAILR-1 and DR-5/TRAILR-2 using a dominant negative-based approach. Because proximal death receptor signaling events occur at the plasma membrane, whereas DRADD is nuclear in distribution, it is not surprising that we have been unable to place DRADD within these pathways.

4.3.4. DRADD interacts with cell cycle regulator, pRb

Consistent with the work of others (Durfee *et al*, 1994) we have demonstrated that DRADD interacts with the tumor suppressor and key cell cycle regulator, Rb, a molecule which functions from within the nuclear compartment. Intriguingly, deletional analysis of the DRADD/Rb interaction revealed that the C-terminal moiety of DRADD, encompassing the death domain motif, mediates binding to

the Rb N-terminus. While Rb is frequently the target of tumourigenic mutations, the majority of these involve the A and B pocket regions of the molecule required for transcription factor E2F and viral oncogene binding (Weinberg, 1995). However, given that caspase adaptor DRADD binds to the Rb N-terminus, it is interesting to note reports of mutations detected in human retinoblastoma tumours, specifically within the N-terminus of the molecule (Hogg *et al,* 1993). Within this context, it would be interesting to determine if the tumorigenicity of this mutation correlates with an inability to interact with DRADD. Moreover, a study by Hensey and colleagues suggests that the N-terminus of Rb is required for the formation of oligomers via interaction with the C-terminus of the molecule (Hensey *et al,* 1994). While the significance of oligomerization of Rb is as yet unappreciated, this feature of Rb may provide a mechanism for clustering DRADD under specific conditions.

The phosphorylation status of Rb dictates its ability to interact with binding partners that regulate cell cycle progression (Weinberg, 1995). It is interesting to note a report by Durfee and colleagues that suggests a cell cycle-specific interaction between Rb and p84 (DRADD) (Durfee *et al,* 1994). The authors state that these molecules associate during the G1 phase of the cell cycle, when Rb is hypophosphorylated and is therefore actively inhibiting cell cycle progression (Durfee *et al,* 1994; Weinberg, 1995). Thus, the function of Rb as a tumour suppressor may relate not only to its ability to provide a brake on mitosis, but also by regulating cell death via DRADD. Thus, in a manner similar to that of tumour suppressor p53, Rb may have cell cycle and cell death regulatory abilities.

Several lines of evidence place tumor suppressor Rb at the hub of a network of proteins that modulate apoptosis. Indeed, consistent with the work of others (Hsieh *et al,* 1999), we observed that overexpressed Rb is modestly proapoptotic. Rb can physically associate with the anti-apoptotic ubiquitin ligase MDM-2, thereby neutralizing the ability of this molecule to downregulate p53-dependent transcription through proteasome-mediated degradation of the latter (Hsieh *et al,* 1999). Additionally, the Rb-interacting tyrosine kinase cAbl can collaborate with

p53 homologue p73 to mediate apoptosis provoked by specific genotoxic stimuli (Gong *et al*, 1999; Agami *et al*, 1999; Yuan *et al*, 1999). Moreover, Rb is an important regulator of the E2F family of transcription factors critically required to promote mitogenesis via transcriptional targets required for progression through S phase of the cell cycle (Weinberg, 1995). Interestingly, ectopic expression of E2F provokes apoptosis (Qin *et al*, 1994). In addition, Rb has been demonstrated to interact with the c-Myc oncogene (Rustgi *et al*, 1991). Deregulated c-Myc activity results in both aberrant cellular proliferation as well as sensitizing cells to apoptosis (Evan *et al*, 1992).

Critically, we provide preliminary evidence for a novel role for Rb as a tumour suppressor, specifically as a direct regulator of caspase activation within the nuclear compartment. Whereas ectopic expression of both DRADD and sublethal amounts of Rb provoked minimal apoptosis in transient overexpression studies, we consistently observe a significant increase in the percentage of cells exhibiting hallmarks of apoptosis, including nuclear condensation and fragmentation, when these molecules are co-expressed. These data suggest a novel, intimate connection between a key cell cycle regulator and the caspase arm of the cell death machinery.

4.3.5. DRADD is a nuclear protein

Intriguingly, DRADD appears unique in comparison with other DD-containing species in that its expression is largely restricted to within the nuclear compartment. We have identified two putative nuclear localization signals within the C-terminus of the molecule, one of which we have demonstrated to mediate the nuclear import of DRADD. While overexpressed GFP-DRADD exhibits a relatively homogeneous distribution within the nucleus, this is probably attributable to the overflow of DRADD from its natural subnuclear compartment as a result of enhanced expression levels of the protein. Further studies will use purified DRADD antisera to examine the specific subnuclear localization of endogenous DRADD.

Within this context, it is interesting to note reports suggesting that other apoptosis-associated molecules may reside within the nuclear compartment. For instance, the CARD-containing protein ASC (Masumoto *et al,* 1999) has been demonstrated to inducibly localize to speck-like foci within the nuclear matrix during apoptosis. Additionally, the caspase-8-interacting protein DEDD appears to enter the nuclear compartment following death receptor stimulation (Stegh *et al,* 1998). Several reports suggest a nuclear sublocalization for caspase-2, consistent with the identification of putative NLSs within the prodomain of the molecule (Colussi *et al,* 1998). We have excluded the possibility that DRADD acts as an adaptor for caspase-2, since it failed to bind caspase-2 in the GST *in vitro* capture assay.

4.3.6. Does DRADD participate in a caspase activating pathway within the nucleus?

It has long been appreciated that chemotherapeutic drugs and genotoxic stimuli such as γ-irradiation, provoke programmed cell death primarily through damage inflicted upon the nuclear compartment (Choisy-Rossi and Yonish-Rouach, 1998). As described within Chapter I, some cell deaths initiated by nuclear damage utilize p53-dependent transcriptional targets. However, surprisingly given the nuclear origin of the stimuli, transcriptional targets of p53, including death agonist genes such as Bax and Noxa actually exert their death-inducing functions at the level of regulating cytochrome *c* release from mitochondria (Oda *et al,* 2000; Jurgensmeier *et al,* 1998). Thus, events that originate within the nuclear compartment seemingly invoke an Apaf-1-dependent cell death pathway that takes place within the cytosol. Moreover, the p53-inducible death receptor DR-5/Killer (Wu *et al,* 1999) also receives death signals at the level of the plasma membrane at a site distinct from the nuclear origin of the death signal. While a novel p53-inducible death domain-containing molecule, PIDD, has recently been identified, further studies are required to determine the subcellular compartment where this molecule exerts its role (Lin *et al,* 2000). Finally, the human homologue of yeast Rad-9 promotes DNA damage-mediated apoptosis via its

ability to neutralize the prosurvival effects of Bcl-2 and Bcl-X (Komatsu *et al*, 2000).

Our identification of DRADD as a nuclear death adaptor protein thus represents a novel class of caspase activating mechanism that may actually transduce death signals to caspases from within the nucleus. Thus, by analogy with caspase activating complexes within the cytosol, DRADD may represent a novel "nuclear apoptosome". Moreover, while a substantial subset of genotoxic stress-associated cells deaths clearly owe their origins to the transcriptional activity of p53, evidence suggests that there are also transcriptionally-independent, as well as p53-independent means of achieving cell suicide within the context of nuclear damage (Caelles *et al*, 1994). Thus, a subset of cell deaths derived from nuclear stimuli may rely on direct protein-protein interactions rather than gene expression to modulate the apoptotic signal.

4.3.7. DRADD remains within the nucleus in dying cells

Certain apoptotic signaling events require death agonist molecules to translocate from one cellular compartment to another (Porter, 1999). For instance, the caspase-8 interacting death effector domain protein DEDD translocates from the cytosol to the nucleus in response to Fas/CD95 stimulation (Stegh *et al*, 1998). Within similar contexts, cleaved Bid (tBid) shuttles from the cytosol to the mitochondrial membrane. In this study we examined whether DRADD can be induced to translocate from the nucleus in response to various stimuli that elicit nuclear damage. However, apart from a general loss of fluoresence, albeit with a weak punctate cytosolic fluorescence in response to some treatments, we were generally unable to detect an overt bulk movement of DRADD from the nucleus into another cellular compartment. These data suggest that DRADD exerts its cell death role within the nuclear compartment.

A recent study suggests that a substantial proportion of the zymogen form of caspase-9 actually resides within the nucleus (Ritter *et al*, 1999). Therefore, all of the DRADD-interacting components thusfar identified reside within the nuclear

compartment. This again supports the notion of a so-called nuclear apoptosome, discussed above.

Of interest within this context, targeted deletion studies have established caspase-9 as an essential mediator of programmed cell death in response to diverse genotoxic stimuli. Notably, several cell types including embryonic stem (ES) cells and fibroblasts isolated from caspase-9-null embryos exhibit resistance to anti-neoplastic stimuli including adriamycin, etoposide and γ-irradiation (Kuida *et al*, 1998; Hakem *et al*, 1998). Our identification of DRADD as a nuclear-localized, caspase-9-selective adaptor molecule may shed some light as to how nuclear-damaging stimuli achieve caspase activation. Targeted deletion of cytosolic caspase-9 adaptor, *APAF-1* in mice results in a phenotype that is relatively similar to those encountered in *CASP-9*-null cells (Cecconi *et al*, 1998; Yoshida *et al*, 1998; Hakem *et al*, 1998; Kuida *et al*, 1998; Honarpour *et al*, 2000). However, further studies will be required to establish whether Apaf-1 is actually required in all instances where caspase-9 plays an apical role in apoptotic signaling provoked by genotoxic damage. Moreover, certain cell types actually engage Apaf-1 downstream of apical signaling events such as death receptor ligation (Li *et al.*, 1998; Luo *et al.*, 1998). Thus there may be instances where Apaf-1 plays a non-redundant role in cell death, not as an instigator of apical caspase activation, but as a critical distal amplification mechanism. Further studies will evaluate the role of DRADD as a caspase-9 adaptor within the context of stimuli that provoke damage within the nuclear compartment. Indeed, studies using *APAF-1*$^{-/-}$ cells will enable the specific role of DRADD as a caspase-9 adaptor protein to be further elucidated.

4.3.8. DRADD undergoes proteolytic cleavage during Bax-mediated apoptosis

During a survey of a panel of death-inducing agents, we observed proteolytic cleavage of GFP-DRADD in cells co-expressing death agonist molecule, Bax. Intriguingly, this cleavage event appeared specific, since GFP-DRADD remained largely intact in cells expressing other death-inducing molecules. Moreover, unfused GFP was not cleaved under these conditions, suggesting that it was not

mediated by a fortuitous caspase cleavage site within the GFP epitope. This observation must be verified by detection of endogenous DRADD. However, it is interesting to note the observation of several groups that Bax can be found within the nuclear matrix, as well as sublocalized to the nuclear membrane in several cell types (Gajkowska *et al.*, 2000). Thus, in certain contexts Bax may provoke cell death independently of its role as a cytochrome *c*-releasing agent, by impinging upon the nucleus in some manner.

Assuming that there is some functional significance to this cleavage event, one possible explanation for this phenomenon may be to provide a DRADD-mediated caspase activating amplification loop to promote or enhance proteolysis of substrates with the nuclear compartment. While DRADD cleavage is clearly not a proximal apoptotic signaling event, this does not preclude a caspase-catalysed functional role for the molecule. For instance, DEDD translocation from the cytosol to the nucleolus is caspase-dependent (Stegh *et al,* 1998). This molecule is speculated to be involved in modulating the shutdown of cellular biosynthetic activities within the nucleolus. Moreover, hepatocytes derived from *BID* $^{-/-}$ mice are resistant to Fas receptor ligation, demonstrating the requirement for this caspase-initiated amplification loop (Yin *et al.*, 1999). Thus, situations may exist where a DRADD-dependent amplification loop may occur. The functional significance of this observation could be further evaluated by generating a non-cleavable DRADD mutant.

4.3.9. Concluding remarks

Much of this study has been directed towards elucidating a functional role for DRADD as a caspase-9-binding adaptor molecule. In this study we have relied upon a dominant negative DRADD modelled on DN-FADD, in terms of a death domain-only mutant that is incapable of caspase-9 binding. Using this approach we anticipated that DN-DRADD would bind to a death domain species dependent upon DRADD signaling and thus frustrate the ability of endogenous DRADD to recruit and activate caspase-9. DRADD clearly differs substantially from other death domain species in that it resides predominantly within the nucleus, where it interacts with a key cell cycle regulator, Rb. One obvious caveat in this regard concerns whether the death domain mutant of this molecule actually constitutes a dominant negative DRADD in the same manner as would be anticipated for the other adaptors. Moreover, given the DRADD/Rb interaction, an obvious concern relates to the fact that this approach involves overexpression of an Rb-binding protein: given the diverse network of proteins that Rb controls, it is difficult to predict the knock-on effects on other cell cycle regulators and upon E2F family-mediated gene expression.

An additional reason for our failure to find a pathway for DRADD may simply relate to not having uncovered the appropriate death-inducing stimuli that engage DRADD. Another reason may relate to the limited transfection efficiency of the overexpression system used in these dominant negative experiments. Clearly, some inhibitory effects are subtle in their nature and may only reveal themselves within a transient window of time. When using a system in which only a fraction of the cells actually take up the plasmid, it becomes difficult to evaluate the significance of an effect as viewed from the perspective of a whole cell population, a minority of which are actually participants in the experiment. Thus, this approach has its limitations with respect to rapid screening of a wide range of diverse cytotoxic agents required in order to uncover an appropriate death-inducing agent. We have sought to counteract this problem through the generation of stable DRADD-overexpressing cell lines. This approach offers the advantage that all of the cells will be expressing DRADD, making it possible to

analyze bulk populations for signs of resistance to death stimuli. This also allows cells to be analyzed using flow cytometry, enabling more quantitative data to be gathered.

An additional advantage of the approach regards the fact that DRADD was cloned from a Jurkat cDNA library. Thus, these cells are more likely to express the other signaling components required for a DRADD-dependent death pathway. This may not have been the case in the cell types we used in the transient overexpression assays. Finally, DRADD may participate in a redundant death signaling pathway, making it difficult to elucidate function using a dominant negative-based approach.

A further departure we have undertaken to elucidate DRADD function regards the generation of DRADD antisera. Clearly, an overexpression-based approach risks usurping a molecule from its normal endogenous context, allowing it to cross-react with signaling pathways it may not normally engage. Purified DRADD antisera will enable us to confirm the DRADD interactions reported in this study, using endogenous protein levels. In addition, it will enable us to evaluate whether DRADD expression levels change in response to specific pro-apoptotic stimuli, particularly DNA damaging agents.

CHAPTER V:
Cloning of DRADD-interacting molecules by yeast-two hybrid screening

5.1. INTRODUCTION

As is detailed in Chapter IV, a dominant-negative-based approach failed to determine a functional role for DRADD within a variety of known apoptotic signaling pathways. To address this important question from a different perspective, we decided to undertake a two-hybrid screen with DRADD as bait to identify putative DRADD-interacting partners that might regulate its pro-apoptotic activity. Because numerous signaling pathways rely heavily on protein-protein interactions as a means of transducing specific stimuli, we reasoned that identification of DRADD-interacting molecules may guide us to the specific pathway(s) within which DRADD is operative.

5.2. RESULTS

5.2.1. Design and generation of DRADD two-hybrid bait proteins

As has been previously discussed, DD molecules frequently mediate pro-apoptotic signaling events through homophilic interactions with other DD species (Ashkenazi and Dixit, 1998). We therefore reasoned that screening with the $DRADD^{387-657}$ DD mutant would be a likely means of retrieving a DD-containing molecule that utilizes a DRADD-dependent pathway. To this end, we generated a Gal-4 DB fusion encoding the $DRADD^{387-657}$ DD mutant identical to the truncation used in the dominant negative studies (Figure 41A). Unfortunately, preliminary analysis revealed that this fusion protein autoactivated both the *HIS3* and *LacZ* reporter systems when co-expressed with the unfused AD moiety of Gal-4 (Table 14). As a result, this mutant was deemed unsuitable for screening.

Since we were concerned with identifying novel proteins that interact with the DRADD C-terminus, we decided to use full length DRADD as a bait for two-hybrid screening. To this end, we subcloned the original pACT-2 AD library insert encoding full length DRADD into the pAS2-1 vector, in frame with the Gal-4 DB. The resultant plasmid was transformed into *Saccharomyces cerevisiae* host strain Y190 according to the lithium acetate transformation procedure previously described (Adrain *et al.*, 1999). Transformants harboring the pAS2-1 DB-$DRADD^{FL}$ plasmid were selected by plating on SD medium lacking tryptophan. Immunoblotting of yeast protein lysates derived from these transformants with a Gal-4 DB-specific antibody confirmed expression of the fusion protein (Figure 41B). Moreover, preliminary testing revealed that this Bait protein did not autoactivate the two-hybrid reporter genes (Table 14).

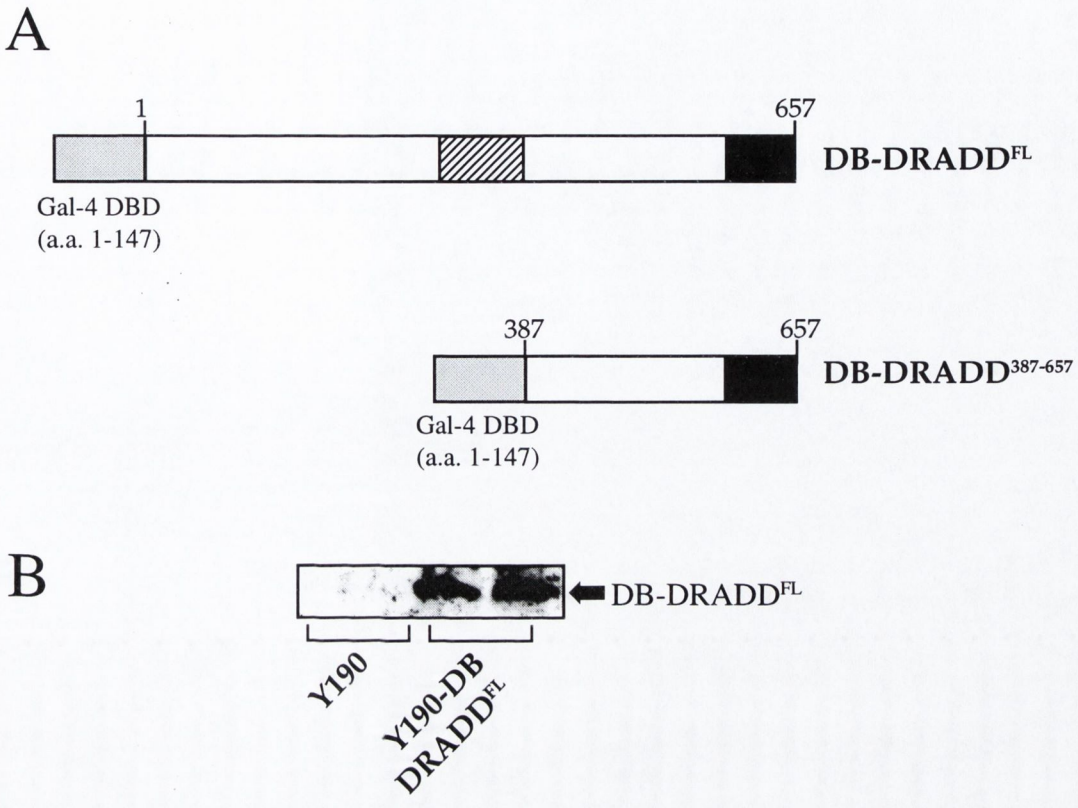

Figure 41

Selection of the DB-DRADD bait protein for 2-hybrid screening.

A, Schematic diagrams illustrating the DB-DRADD^{FL} (full length) and DB-DRADD$^{387-657}$ bait fusions that were considered for library screening. The CARD-like and Death Domain regions are indicated by hatched and black shading respectively.

B, Immunoblot demonstrating expression of the DB-DRADD^{FL} hybrid fusion protein. Yeast protein lysates derived from untransformed Y190 strain or from the Y190 transformant expressing the DB-DRADD^{FL} protein were subjected to SDS-PAGE followed by immunoblotting with a Gal-4 DB-specific monoclonal antibody.

Table 14

Table illustrating that the DB-DRADD$^{387-657}$ mutant autoactivates the *HIS3* and *LacZ* reporter genes when co-expressed with the unfused Gal-4 AD.

DB Hybrid protein	AD Hybrid protein	*HIS3* status	*LacZ* status
DRADD Full Length	Vector	—	—
DRADD 387-657	Vector	+	+

5.2.2. Toxicity tesing of the DB-DRADD^{FL} bait plasmid

We next determined whether expression of the DB-DRADD^{FL} protein was sufficiently non-toxic to enable a two-hybrid library screening of at least one library complexity (approximately $3x10^6$ independent clones). To this end, we conducted small-scale test-transformations using the Y190-DB-DRADD^{FL} transformant as a recipient for library plasmid. Encouragingly, sequential transformation of the DRADD-overexpressing host with pACT-2 cDNA Jurkat plasmids consistently yielded at least $1x10^4$ yeast co-transformants per µg of library plasmid DNA. On this basis, we decided to proceed with large-scale library screening.

5.2.3. Library screening with DB-DRADD^{FL}

The flow diagram in Figure 42 outlines the procedure that was adopted, from library screening to DNA sequencing and BLAST-search based identification of clones. The screening and clone isolation procedures are detailed within Chapter II. Briefly, yeast Y190 transformants harboring the BD-DRADD^{FL} fusion protein were inoculated into liquid SD media and grown overnight. The following day, cells were expanded in YPD media to provide a nutritional boost immediately prior to the transformation phase. Yeast transformants growing in log phase were harvested, transformed with a total of 100 µg of pACT-2 library prey plasmids, and plated on 40 x 15 cm plates containing media lacking the amino acids histidine, leucine and tryptophan supplemented with 25mM 3-AT (to quench leaky reporter gene expression). This allowed selection for yeast transformants harboring putative interacting bait/prey pairs.

To determine the transformation efficiency of the screen, aliquots of yeast were also plated on media lacking leucine and tryptophan to select for the bait and library plasmids. Determining the average colony count from four replicate plates revealed that cells had been transformed with an approximate efficiency of $6.3x10^4$ colony forming units/µg library plasmid, suggesting that approximately

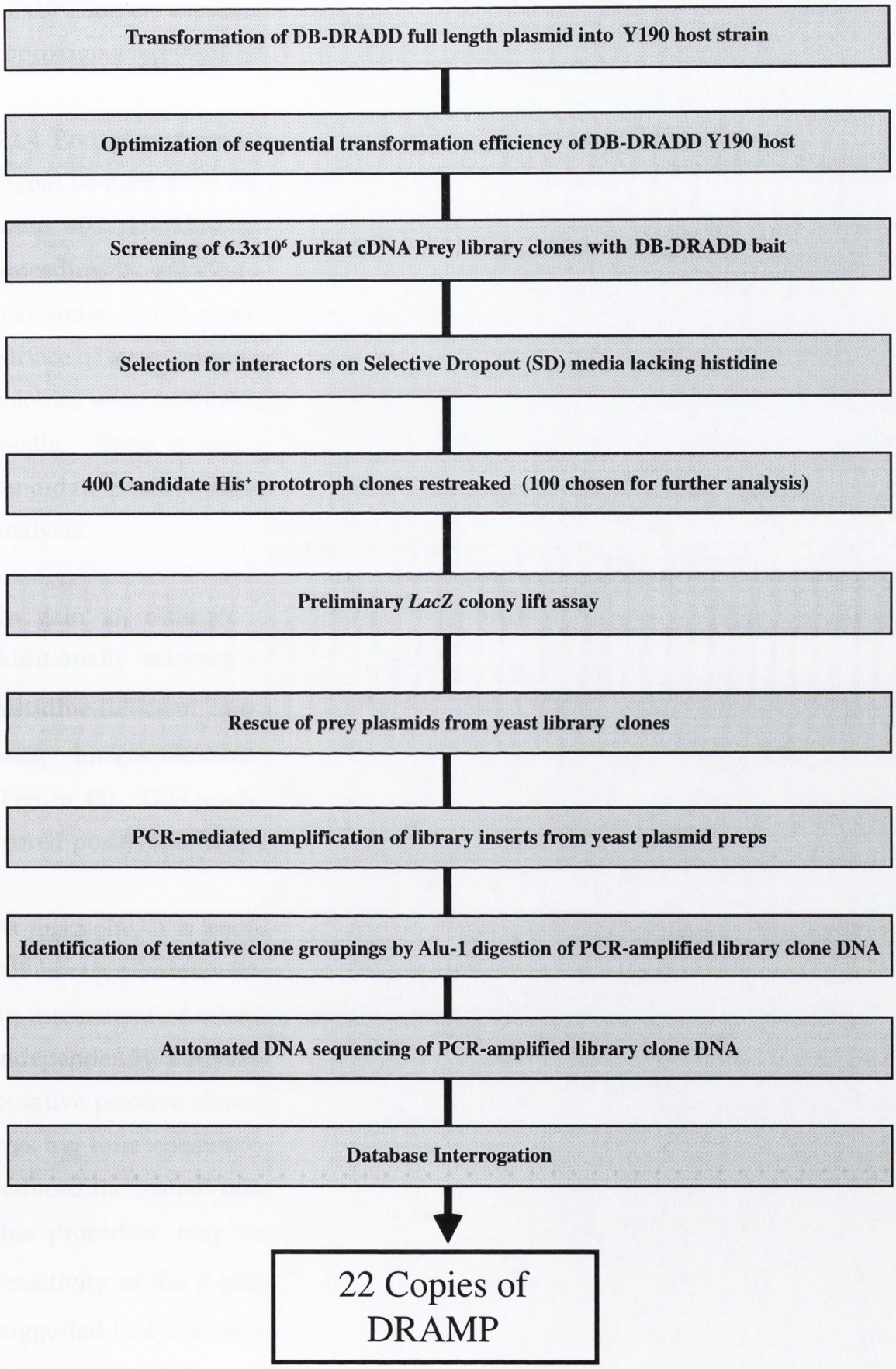

Figure 42

Flow chart illustrating the stages involved in the identification of DRAMP as a DRADD-interacting protein using Two-Hybrid library screening

$6.3x10^6$ library clones had been screened. On this basis, we estimated that approximately twice the library complexity was successfully screened.

5.2.4. Preliminary outcome of the DB-DRADD^{FL} screen

Visual inspection of library screening plates 8 days later revealed the presence of some 400 candidate clones. These fulfilled the first stage of the screening procedure by growing on histidine-deficient media. To exclude the possibility that some of the candidate clones may have been growing fortuitously on the surface of agar containing a high density of dead yeast, the first 400 of these yeast colonies were restreaked onto gridded master plates containing identical selective media. Since it was considered impossible to process all 400 of the original candidate positive clones, the first 100 of these were carried forward for further analysis.

To gain an estimate of the proportion of the putative positive clones that additionally transactivated the *LacZ* reporter gene, yeast clones from parallel histidine-deficient master plates were subjected to the β-galactosidase colony lift assay. Images illustrating *LacZ* (blue) and *HIS3* double positive clones are shown (Figure 43). This analysis revealed that approximately 70% of the clones tested scored positive in both assays.

At this point, it is traditional in two-hybrid screening procedures to segregate the AD library plasmids from *HIS3/LacZ* double positive library clones. This enables an assessment of whether the clones are *bona fide* interactors, or whether they independently autoactivate the reporter genes. However, given the number of putative positive clones obtained at the nutritional selection stage, this procedure was too time consuming. Whereas choosing double positive clones may have reduced the overall number subjected to further analysis, we were concerned that this procedure may result in missing weak interactors that were beyond the sensitivity of the β-galactosidase filter lift assay. Moreover, several reports have suggested that overexpression of cell death regulators including caspases and Bcl-

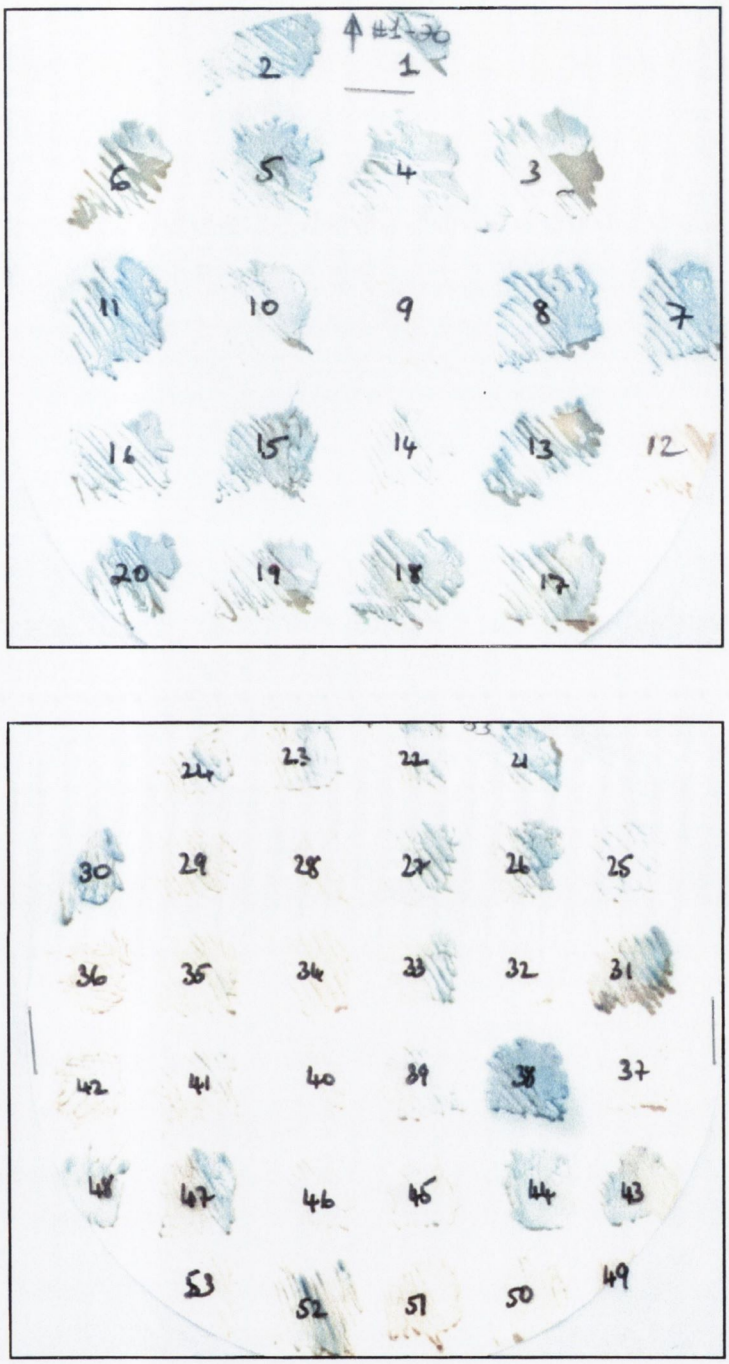

Figure 43

LacZ two-hybrid colony lift assay of putative DRADD-interacting clones.

Yeast *HIS3* prototrophs obtained from the screen were re-streaked on fresh histidine-deficient media and grown at 30°C. 5 days later, colonies were subjected to the *LacZ* filter lift assay as described in the materials and methods section. A blue colony colour is indicative of transactivation of the *LacZ* reporter gene and may denote a postive interaction between the library clone and the DB-DRADD bait protein.

2 related death agonists may be toxic to yeast (James *et al.*, 1997; Xu and Reed, 1998). On this basis, we were anxious to avoid excluding clones that were weakly *HIS3/LacZ* positive as a result of retarded growth, since these may have been genuine, cell death regulatory, DRADD-interactors.

5.2.5. Alu-1 digestion of DB-DRADD^{FL}-interacting library clones

To collapse the first 100 clones into smaller subgroups, we performed Alu-1 restriction digest analysis on PCR products amplified from the library plasmids. To this end, clones were expanded in liquid SD medium lacking leucine/tryptophan and total yeast plasmid DNA was isolated from the yeast as described in Chapter II. Plasmid was used as a template for PCR reactions incorporating primers that flanked the 5' and 3' termini of the pACT-2 multiple cloning site. Following agarose gel electrophoresis, we observed that the modal library insert size of the PCR products was approximately 1.5 Kb, with individual inserts ranging in size from 0.6-3.0 Kb. Following purification of the PCR products, Alu-1 restriction digests were performed. Since this enzyme is a frequent cutter, the banding patterns obtained by digestion ought to reveal sequence similarities between overlapping clones encoding the same molecule.

Intriguingly, characterization of the Alu-1 digest products by agarose gel electrophoresis revealed that many of the clones could be subdivided into distinctive groups based on their banding patterns. This strongly suggested the presence of multiple copies of overlapping portions of at least one gene (Table 15 and Figure 44). Based on this analysis, many of the library clones fell into 7 distinct groups, denoted A-G. This information is summarized in Table 15. Of particular significance, a large grouping of 12 clones that possessed common digestion products in the ranges ~ 550, 400, 200, 150 and 100 kb was designated Group 'A' (Table 15). The banding patterns characteristic of these clones is shown in Figure 44. Since this constituted the largest single grouping, several clones were chosen for further analysis.

Table-15

Table summarizing the individual groups of that shared common Alu-1 restriction digest banding patterns.

Group	No. Clones	Approximate size of Alu-1 digestion fragments	Clone Numbers
A	**12**	550, 400, 200, 150, 100, 50	04, 10, 16, 18, 22, 24, 29, 43, 50, 57, 59, 78
B	**3**	550,75	23, 33, 45
C	**2**	800, 550, 375, 225, 150, 110, 75	64,66
D	**3**	400, 300, 250,150, 100	37, 40, 67
E	**3**	900, 650, 500, 400, 225,150,100	25, 39, 44
F	**2**	550, 450, 175, 125, 100	17, 26
G	**2**	750, 600, 450, 525, 350, 300, 275, 150, 75	61, 71

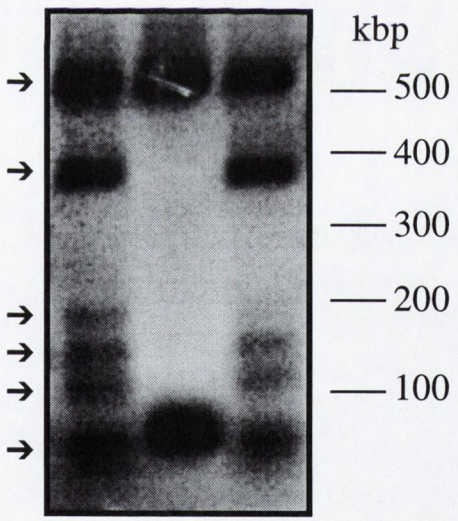

Figure 44

Designation of library clones into groups on the basis of Alu-1 digestion patterns

Image of an ethidium bromide-stained agarose gel illustrating a typical banding pattern (indicated by arrows) shared by the 12 clones that were designated to group A.

5.2.6. DNA sequence analysis of clones

We next determined the identity of the multiple and single copy clones by automated DNA sequencing and database interrogation. To this end, the PCR products amplified from the library plasmids were used as a template. Reactions employed the pACT-2 Forward Screen F oligonucleotide as a sequencing primer, as described in Chapter II. To sequence as many of the original 100 clones as possible, only one or two representative members from each of the major groupings were sequenced. The remainder of the candidates sequenced were single copy clones. In spite of the fact that this placed a bias on sequencing single copy clones, this approach avoided overlooking clones that may have a low abundance in the cell type that the library was derived from, that might nonetheless be genuine DRADD-interacting partners.

Following the removal of pACT-2 vector-specific sequences, the identity of the clones was determined by database interrogation, using the BLAST program, accessed via the NCBI web interface (www.ncbi.nlm.nih.gov/BLAST/). The similarity of the clones to human nucleotide or amino acid sequences deposited in the non-redundant (nr) database was determined by BLASTN and BLASTX interrogation respectively. Analysis of sequences obtained from clones that were present in single copy number only revealed that the majority of these clones were indeed unique. The identity of these clones can be found in Tables 16 and 17. In addition, database analysis revealed that several library clones were represented in two copies, most of which were not predicted from Alu-1 banding patterns (Table 18).

5.2.7. The identity of the DRADD^{FL}-interacting library clones

Intriguingly, analysis of clones that were sequenced as representatives from not only from group A, but also, groups B and C (Table 15) revealed that these clones encoded overlapping portions of a single open reading frame. The gene encoded by these clones was identical to a molecule variously described in the non-redundant human database database as Motor Protein (Accession No. D21094); Transmembrane Protein (Accession No. L42572) and Mitofilin (Accession No.

Table 16

Table illustrating the identity of single copy clones, as revealed by DNA sequencing and subsequent database interrogation

Clone No.	Identity/ Similarity	Accession No.	Species	E-Value (BLASTN)	E-Value (BLASTX)
#01	RNA polymerase II termination factor	AF073771	*Homo sapiens*		35
#03	Protein phosphatase 2A B-56 delta	L76702	*Homo sapiens*		8e-16
#06	Non histone chromatin protein HMG1	U51677	*Homo sapiens*	4e-60	
#08	Zinc finger protein EZNF	AF116030	*Homo sapiens*		1.2
#11	Adrenal mRNA for ubiquitin-52	HSUBA52 A	*Homo sapiens*	e-145	
#12	p53-Binding protein	Q12888	*Homo sapiens*		15
#13	Proteasome activator hPA28 subunit beta	I53518	*Homo sapiens*		8.5
#17	Chromatin assembly factor I p150 chain	A56731	*Homo sapiens*		1e-06
#25	C1D protein	CAA64845	*Homo sapiens*		2e-33
#26	Differentiation factor	S51027	*Homo sapiens*		9e-12
#27	Elongation factor-1 alpha 2	Q05639	*Homo sapiens*		2e-41
#28	Possible global transcription activator	P28370	*Homo sapiens*		8e-42
#30	Similar to salivary proline-rich protein	D89501	*Homo sapiens*		22
#31	Glyceraldehyde 3-phosphate dehydrogenase	P04406	*Homo sapiens*		9e-30
#32	26S Proteasome regulatory subunit S14	P48556	*Homo sapiens*		2e-85
#34	Polypeptide BM28	X67334	*Homo sapiens*		6.5
#36	E2F-1	Q01094	*Homo sapiens*		118
#42	Gene MM1 protein	I52685	*Homo sapiens*		0.37
#46	FLAP Endonuclease-1	P39748	*Homo sapiens*		7e-33
#49	Human mRNA for KIAA0169 gene	D79991	*Homo sapiens*	0.0	
#54	Mesothelin or CAK1 antigen precursor	U40434	*Homo sapiens*		22
#60	Trophoblast STAT utron mRNA	AF080092	*Homo sapiens*	4e-09	

Table 17

Table illustrating the identity of single copy clones, as revealed by DNA sequencing and subsequent database interrogation.

Clone No.	Identity/ Similarity	Accession No.	Species	E-Value (BLASTN)	E-Value (BLASTX)
#63	Oviduct-specific glycoprotein precursor	Q12889	*Homo sapiens*		14
#68	Full length insert cDNA clone ZD69A07	AF086377	*Homo sapiens*	1e-58	
#69	GOK (stromal interaction molecule 1)	U52426	*Homo sapiens*		5e-27
#72	KIAA0465 protein	AB007934	*Homo sapiens*		8e-69
#75	Succinate dehydrogenase iron protein subunit B	U17886	*Homo sapiens*		1e-47
#76	ZFP-36 mRNA for a zinc finger protein	X51760	*Homo sapiens*	e-110	
#80	KIAA0197 protein	D83781	*Homo sapiens*		0.0
#81	Presenilin I-374	S63684	*Homo sapiens*		0.056
#82	S164	AF109907	*Homo sapiens*		5.6
#83	Unknown protein (Similarity to transcription factors)	AF072242	*Homo sapiens*		1e-05
#86	Nuclear protein SDK3	Y10351	*Homo sapiens*		0.006
#87	Special AT-rich sequence binding protein 1 (binds to nuclear matrix /scaffold associating DNAs)	M97287	*Homo sapiens*		37
#88	KIAA0410 Protein	AB007870	*Homo sapiens*		3.0
#90	Tic	U63127	*Homo sapiens*		165
#94	Progestin-induced protein	AF006010	*Homo sapiens*		8e-22
#97	Regulatory factor X, 1	A20498	*Homo sapiens*	0.0	
#98	mRNA for MACH-beta-3 protein	X98177	*Homo sapiens*	0.0	

Table 18

Table illustrating clones obtained from the DRADD two-hybrid screen of which two copies were identified following DNA sequencing and subsequent database interrogation.

Clone No.	Identity/ Similarity	Accession No.	Species	E-Value (BLASTN)	E-Value (BLASTX)
#58	X-linked anhidroitic ectoderm...	AF003528	*Homo sapiens*	0.003	
#100	X-linked anhidroitic ectoderm...	AF003528	*Homo sapiens*	1.0	
#61	ZNF74-1 zinc finger protein	X71623	*Homo sapiens*	0.0	
#71	ZNF74-1 zinc finger protein	X71623	*Homo sapiens*	0.0	
#07	Chromosome 14 PAC RPC14-794B2	AC005924	*Homo sapiens*	0.0	
#65	Chromosome 14 PAC RPC14-794B2	AC005924	*Homo sapiens*	0.0	
#07	Paraneoplastic neuronal antigen MA1	AF037364	*Homo sapiens*	0.003	
#65	Paraneoplastic neuronal antigen MM2	AF037365	*Homo sapiens*	0.014	
#09	Chromosome 21q22.3 PAC 39C17	AF043945	*Homo sapiens*	0.62	
#55	Chromosome 21q22.3 PAC 39C17	AF043945	*Homo sapiens*	0.92	
#09	Nucleophosmin	P06748	*Homo sapiens*		3.3
#55	Nucleophosmin	P06748	*Homo sapiens*		1.8
#21	DNA Replication licensing factor MCM7	P33993	*Homo sapiens*		2e-37
#48	DNA Replication licensing factor MCM7	P33993	*Homo sapiens*		0.0
#20	Signal recognition particle 72	AF069765	*Homo sapiens*	0.0	4e-45
#74	Signal recognition particle 72	AF069765	*Homo sapiens*	0.0	4e-47
#47	Protein regulating Cytokinesis 1 (PRC-1)	AF044588	*Homo sapiens*	0.0	1e-60
#51	Protein regulating Cytokinesis 1 (PRC-1)	AF044588	*Homo sapiens*	0.0	8e-33

AF148646) (Icho *et al.*, 1994; Odgren *et al.*, 1996; Gieffers *et al.*, 1997). Moreover, in addition to the 17 copies identified by collapsing the contents of Alu-1 Groups A, B and C, further sequencing analysis of some of the single copy clones revealed that a further 5 clones (#35, #41, #52, #73 and #91) of this molecule that were not readily identified based on initial banding pattern analysis, were also identical to this gene. Thus, since our screening had obtained a total of 22 copies, representing 1/5 th of the total number of clones examined, this molecule was chosen for further analysis. This information is summarized in Table 19. Given the similarity between the molecule encoded by our library clone and the molecular motor, myosin (see below) we therefore denoted this molecule DRAMP (DRADD-Asssociated Myosin-like Protein).

5.2.8. Analysis of the DRAMP amino acid sequence

To characterize DRAMP, we subjected the 758 amino acid sequence of the gene previously described as Motor Protein (Accession number D21094; Icho *et al.*, 1994) to database analysis (Figure 45A). Analysis using the PSORT II web-based program (http://psort.nibb.ac.jp; Nakai and Horton, 1999) predicted that the DRAMP protein possessed a coiled-coil motif within the centre of the molecule (Figure 45B), that is commonly observed in a range of proteins including transcription factors, the myosins and several large structural proteins (Lupas, 1996). Moreover, analysis using this software revealed the presence of a putative bipartite-class of NLS within the coiled-coil region of the molecule, suggesting that under certain conditions, this protein may be targeted to the nucleus (Figure 45B). Further analysis of the DRAMP amino acid sequence using the Hopp and Woods prediction of hydrophilicity from the DNASIS software revealed the presence of two hydrophobic, putative transmembrane stretches, at the N- and C-termini of the molecule, implying that the molecule may be tethered to organelle membranes (Figure 45C).

We next used BLAST interrogation to determine the similarity that this molecule shared with other human and non-human proteins within the non-redundant NCBI database. Interestingly, BLASTP analysis based on the full length DRAMP

Table 19

Table summarizing the mode of identification of all 22 of the DRAMP clones, including those identified initially by Alu-1 restriction endonuclease digestion, as well as those only subsequently identified by automated DNA sequencing.

Clone No.	Grouping based on Alu-1 Digestion	Sequenced (Y/N)
04	A	Y
10	A	N
16	A	Y
18	A	N
22	A	N
24	A	N
29	A	N
43	A	N
50	A	N
57	A	N
59	A	N
78	A	N
64	B	Y
66	B	N
		N
23	C	N
33	C	Y
45	C	N
35	Ungrouped based on banding patterns	Y
41	Ungrouped based on banding patterns	Y
52	Ungrouped based on banding patterns	Y
73	Ungrouped based on banding patterns	Y
91	Ungrouped based on banding patterns	Y

A

```
MLRACQLSGVTAAAQSCLCGKFVLRPLRPCRRYSTSGSSGLTTGKIAGAG  50
LLFVGGGIGGTILYAKWDSHFRESVEKTIPYSDKLFEMVLGPAAYNVPLP  100
KKSIQSGPLKISSVSEVMKESKQPASQLQKQKGDTPASATAPTEAAQIIS  150
AAGDTLSVPAPAVQPEESLKTDHPEIGEGKPTPALSEEASSSSIRERPPE  200
EVAARLAQQEKQEQVKIESLAKSLEDALRQTASVTLQAIAAQNAAVQAVN  250
AHSNILKAAMDNSEIAGEKKSAQWRTVEGALKERRKAVDEAADALLKAKE  300
ELEKMKSVIENAKKKEVAGAKPHITAAEGKLHNMIVDLDNVVKKVQAAQS  350
EAKVVSQYHELVVQARDDFKRELDSITPEVLPGWKGMSVSDLADKLSTDD  400
LNSLIAHAHRRIDQLNRELAEQKATEKQHITLALEKQKLEEKRAFDSAVA  450
KALEHHRSEIQAEQDRKIEEVRDAMENEMRTQLRRQAAAHTDHLRDVLRV  500
QEQELKSEFEQNLSEKLSEQELQFRRLSQEQVDNFTLDINTAYARLRGIE  550
QAVQSHAVAEEEARKAHQLWLSVEALKYSMKTSSAETPTIPLGSAVEAIK  600
ANCSDNEFTQALTAAIPPESLTRGVYSEETLRARFYAVQKLARRVAMIDE  650
TRNSLYQYFLSYLQSLLLFPPQQLKPPPELCPEDINTFKLLSYASYCIEH  700
GDLELAAKFVNQLKGESRRVAQDWLKEARMTLETKQIVEILTAYASAVGI  750
GTTQVQPE                                             758
```

B

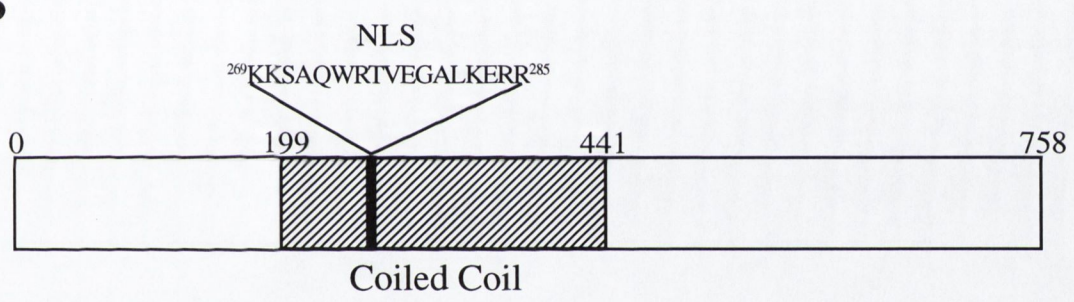

Figure 45

Characterization of the DRAMP amino acid sequence

A, Amino acid sequence of human Motor Protein (Genbank Accession No. D21094) that was found to be identical to the DRAMP sequence. Numbers denote amino acid positions. **B**, Schematic representation of Full Length DRAMP protein. The central coiled-coil region is indicated by hatched shading. The peptide sequence of the putative NLS is indicated. Numbers denote amino acid positions.

C

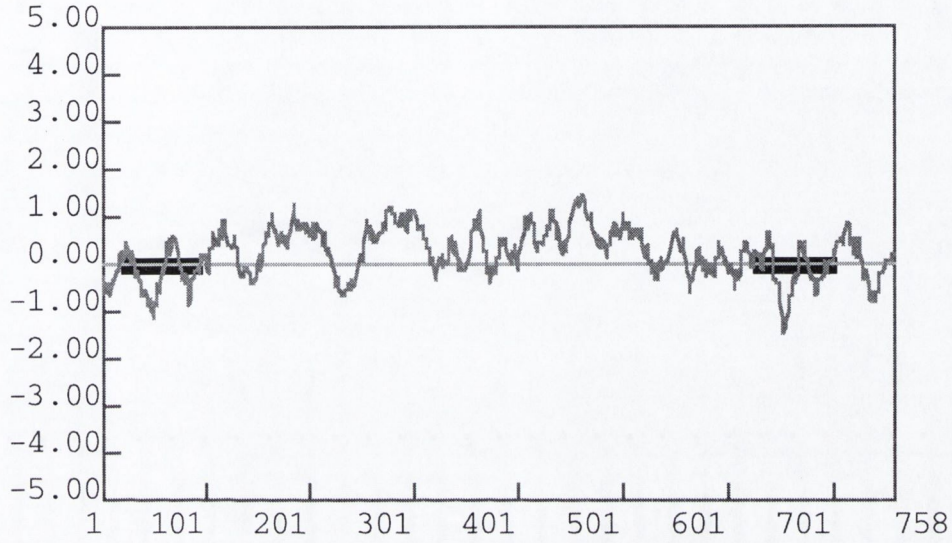

Figure 45

Characterization of the DRAMP amino acid sequence

C, A prediction of the hydrophobicity of amino acid residues within the Full Length DRAMP sequence, as judged by the Hopp and Woods algorithm. The two hydrophobic, putative transmembrane stretches at the N- and C- termini are indicated by the black lines.

sequence revealed that this molecule exhibited substantial similarity to several coiled-coil motif containing proteins. In particular, virtually all of the DRAMP sequence, with the exception of the N-terminal 100 amino acids was found to resemble multiple portions of large coiled coil proteins, most notably Nuclear Mitotic Apparatus Protein-1 (NuMA, Accession No. Z11584); the nucleoprotein Tpr, (Accession No. X63105) as well as Plectin (Accession No. U53204). Typically, portions of these molecules of some 300-600 amino acid stretches that resembled DRAMP, shared in the region of ~20% identity. In broad agreement with the name ascribed to this molecule by another group, DRAMP also exhibited significant homology to the myosins (Myosin Heavy Chain, Accession No. Y00821) and a protein called Kinesin family member 5C (Accession No. AB011103), again within the area including the putative coiled coil region of DRAMP (Icho *et al.*, 1994).

5.2.9. Identification of DRAMP homologues

We next searched for a similarity between human DRAMP and proteins in other organisms. Interestingly, this analysis revealed hypothetical proteins in both the *Drosophila* (Accession no. AAD38598; 26% identity; expect value =8e-47) and *C. elegans* (Accession No. T29795; 26% identity; expect value = 1e-62) databases that were similar to human DRAMP throughout most regions of the molecules (Figure 46).

5.2.10. Preliminary analysis of the DRADD/DRAMP interaction

To verify that the interaction between DRADD and DRAMP was not due to autoactivation of the two-hybrid reporter genes, we obtained the pACT-2 library plasmids for DRAMP clones #04 and #33, representing the longest and shortest clones from the screen. To retrieve the library plasmids, bacterial host strain HB101 was transformed with whole yeast plasmid DNA isolated from the original candidate library clones. This bacterial strain harbours a *LeuB* mutation that renders it auxotrophic for the amino acid leucine that can be complemented by the yeast *LEU2* gene encoded by the pACT-2 plasmid. We selectively rescued the pACT-2 library plasmids from a mixed background of pAS2-1 DB-DRADD and

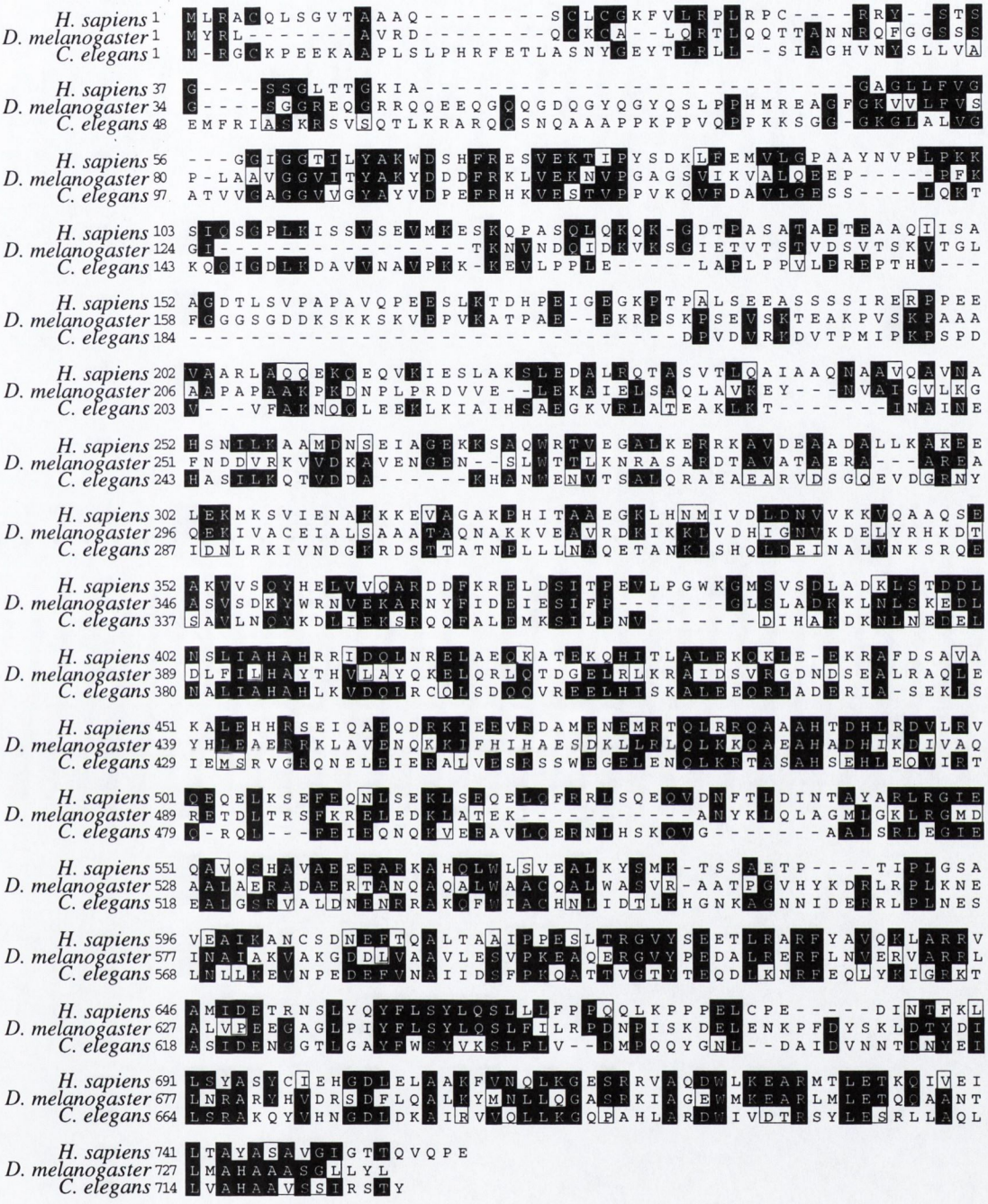

Figure 46

Identification of non-human DRAMP homologues

Alignment of Human DRAMP with homologous sequences retrieved following interrogation of the non-redundant NCBI database with the DRAMP amino acid sequence using the BLASTP algorithm. (Motor Protein, Accession No. D21094; homologous *Drosophila* protein, Accession No. AAD38598; homologous *C.elegans* hypothetical protein, Accession No. T29795)

pACT-2 library plasmids by selecting bacterial transformants on media lacking leucine. The library plasmids were then re-transformed alongside either the full length DB-DRADD bait fusion or the empty pAS2-1 Gal-4 DB vector (Figure 47).

Both DRAMP clones failed to activate the reporter genes in conjunction with the unfused Gal-4 DB. However, when these mutants were co-expressed within the context of DB-DRADD, both reporter genes were readily activated, as judged by nutritional selection on histidine-deficient media as well as by the β-galactosidase colony lift assay shown in Figure 47. These data suggested a genuine interaction with DRADD. Moreover, the DRADD/DRAMP interaction may be of a higher affinity than the DRADD/Caspase-9 interaction, since histidine prototroph colonies co-expressing these molecules failed to assume a substantial blue colony colour at a endpoint when DRADD/DRAMP transformant colonies readily exhibited a striking blue colour in the *LacZ* assay (Figure 47).

5.2.11. The minimal DRADD interaction motif of DRAMP

Since the interaction between DRADD and DRAMP is therefore specific, we next determined the minimal motif required to mediate this interaction based on the information obtained from the sequence of DRAMP library clones. This information revealed that the smallest clone (#33) obtained from the screening encoded a truncation of DRAMP that began at amino acid 639 (Table 20). On this basis, the portion of DRAMP required for interaction with DRADD lies within the C-terminus of the molecule (Figure 48A). Interestingly, further inspection of the sequence within this portion of the molecule revealed a leucine-rich region that weakly resembled the CARD motif (Figure 48) (Hofmann *et al.*, 1997).

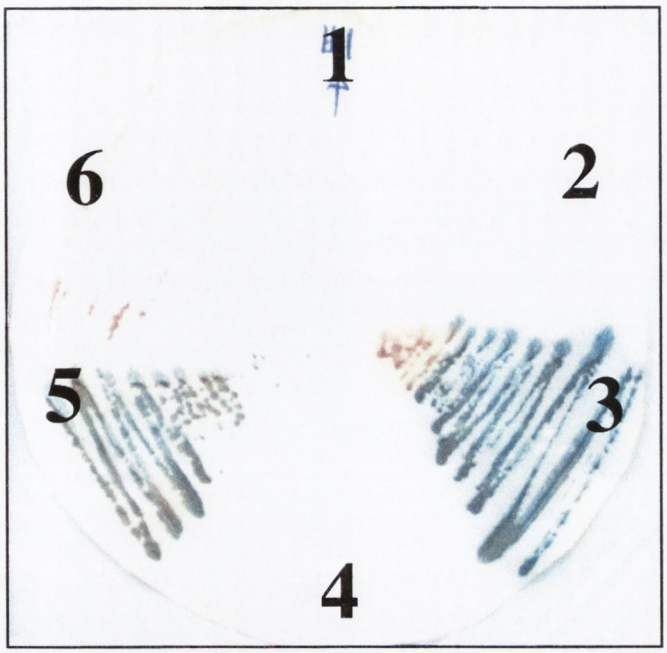

Key:

	AD Hybrid	DB Hybrid
1	Vector	DRADD F.L.
2	Clone #04	Vector
3	Clone #04	DRADD F.L.
4	Clone #33	Vector
5	Clone #33	DRADD F.L.
6	DRADD F.L.	Caspase-9 CARD

Figure 47

Two-hybrid *LacZ* colony lift assay illustrating interaction between DRAMP library clones and DRADD in yeast.

Yeast transformants expressing DRAMP library clones #04 or #33 in combination with the indicated DB fusions were streaked on histidine-deficient media. Five days later, *HIS3*-positive colonies growing on selective dropout media were subjected to the *LacZ* colony lift assay as described in the materials and methods section. A positive protein-protein interaction due to transactivation of the *LacZ* reporter gene is indicated by blue colony colour. The DRADD/Caspase-9^{CARD} interaction is included as a positive control.

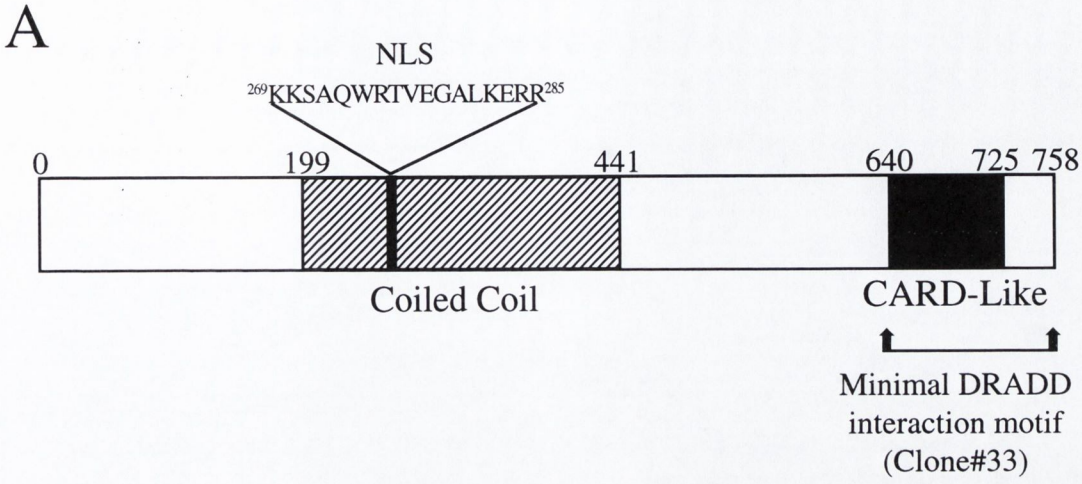

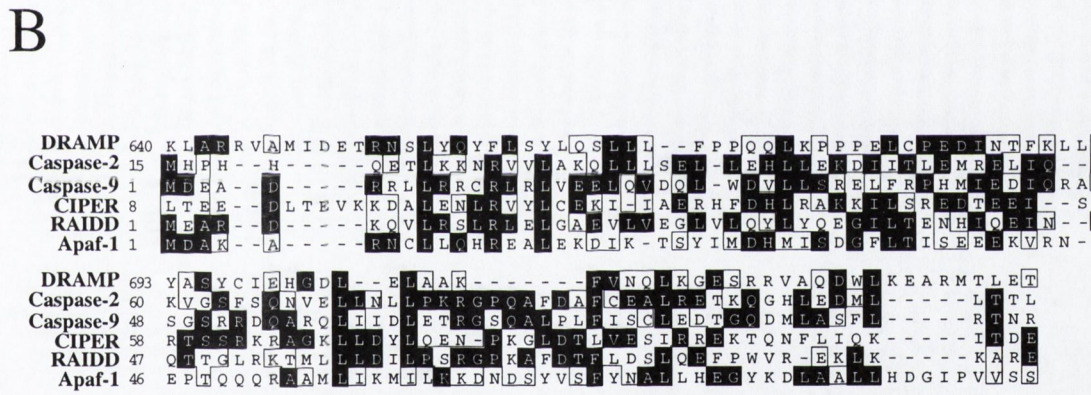

Figure 48

The minimal DRADD-interacting motif of DRAMP coincidentally encodes a weak CARD-like motif.

A, Schematic diagram illustrating the position of the minimal DRADD-interacting motif within DRAMP, as judged from the shortest Two-Hybrid screen library clone (#33). The CARD-like portion of the molecule that begins in this minimal interacting region is shaded. Numbers denote amino acid positions.

B, Multiple alignment of the CARD-like region of DRAMP with the CARD domains of several CARD-containing molecules (Caspase-2, Accession No. P42575; Caspase-9, Accession No. NP001220; CIPER, Accession No. AAD15800; RAIDD, Accession No. P78560; Apaf-1, Accession No. AF013263). Solid shading denotes residues that share the consensus; boxed residues match the consensus by 3 distance units or less.

Table 20

Table illustrating the starting amino acid position of DRAMP clones.

Clone No.	Approx. size in kilobases	Starting amino acid position relative to accession number D21094
#4	2.3	Position 228
#16	1.5	Position 437
#33	0.9	Position 639
#35	1.3	Position 534
#41		Position 534
#52		Position 419
#64	2.2	Position 428
#73		Position 515
#91		Position 471

5.2.12. DRAMP binds to the DRADD N-terminus

We characterized the DRADD/DRAMP interaction with respect to the specific portion of DRADD required for association with DRAMP. To this end, we transformed the longest (#4) and shortest (#33) of the DRAMP library clones alongside the panel of DB-fused versions of the DRADD deletion mutants that were previously described (Figure 28). Yeast transformants expressing either $DRADD^{FL}$ or its associated deletion mutants were then tested for an ability to associate with DRAMP as judged by the *LacZ* liquid two-hybrid interaction assay (Figure 49). As expected, co-expression of DRAMP with the Gal-4 DB vector provoked only mininal expression of the *LacZ* reporter gene, however, both DRAMP clones readily associated with full length DRADD (Figure 49). Interestingly, this analysis revealed that DRAMP readily associated with the N-terminal moiety of DRADD spanning amino acids 1-388, that includes the putative CARD-like region of DRADD. In addition, the DRADD 1-120 region modestly interacted with DRAMP, particularly with the shorter clone #33. Furthermore, a comparison of the relative binding efficiencies of the longest versus the shortest clones revealed that the longest DRAMP clone more readily associated with DRADD, as judged by the liquid assay (Figure 49). These data may suggest that there are multiple regions within DRAMP responsible for DRADD binding that are not included in the shorter library clone, or may relate to the relative stability or folding of one DRAMP truncation versus another.

5.2.13. Verifying the molecular weight of DRAMP protein

Since DRADD and DRAMP readily associated in two-hybrid assays, we wanted to verify this interaction within the context of the full length DRAMP protein. To this end, we designed primers flanking the full length published sequence of Motor Protein (Accession No. D21094; Icho *et al.*, 1994) to generate a pcDNA3-based DRAMP expression plasmid. Preliminary analysis revealed that full length DRAMP encoded a protein of appproximately 80 kDa, as judged by SDS-PAGE and fluorography of *in vitro* translated ^{35}S-labeled DRAMP (Figure 50). Future work will use this contruct to examine the interaction with DRADD within the context of the full length DRAMP molecule.

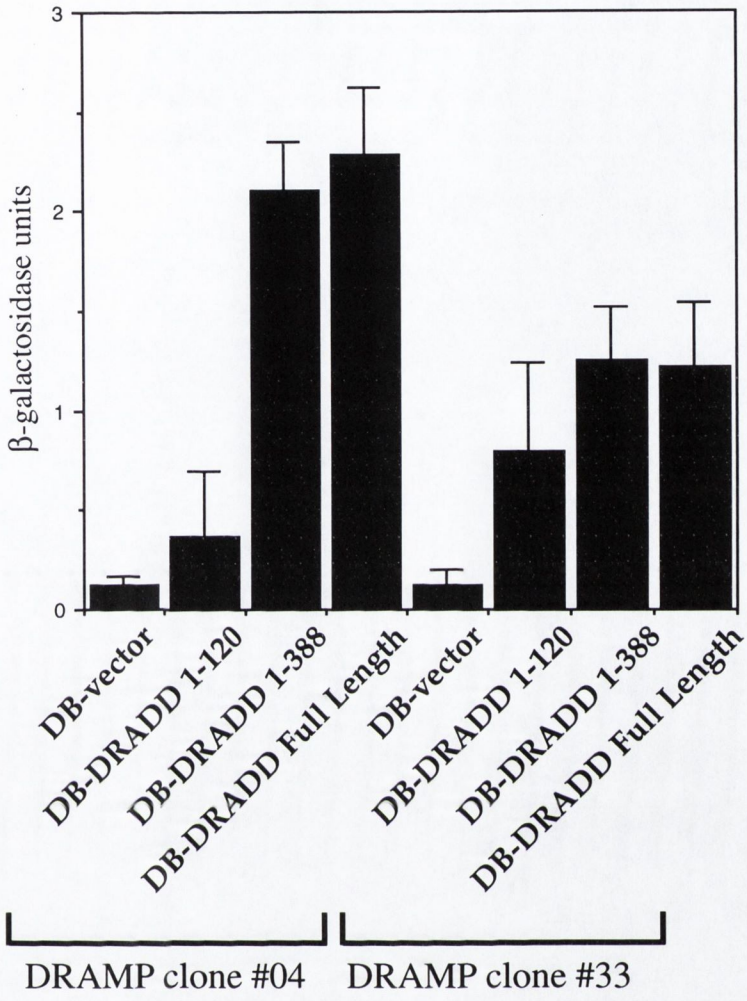

Figure 49

Assessment of the DRAMP binding motif within DRADD using the *LacZ* liquid protein-protein interaction assay.

Yeast co-transformants expressing the indicated DB-DRADD deletion mutants plus either AD-DRAMP clone #04 or #33 wer e lysed as described in Chapter II and subjected to the *LacZ* liquid assay. Error bars denote the standard error of the mean of three individual replicate samples. This experiment was conducted in collaboration with Helen Egan.

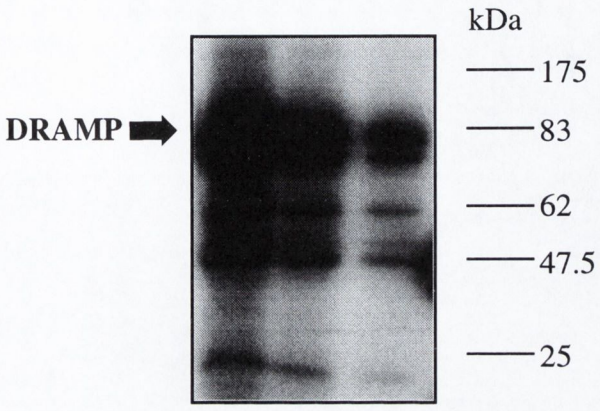

Figure 50

Autorad illustrating the molecular weight of *in vitro* transcribed and translated (ITT) DRAMP protein.

The pcDNA3 DRAMP plasmid was used as a source of template for ITT reactions as described in the materials and methods chapter. 2, 1 and 0.5 µl samples were subjected to 10% SDS-PAGE, followed by detection by enhanced fluorography. The full length DRAMP protein is indicated by an arrow. The smaller molecular weight bands represent internal translation initiation products.

5.3. Preliminary analysis of a further DRADD^{FL}-interacting library clone

Since the two-hybrid screening procedure yielded several other candidate clones that were represented by multiple copies, we conducted a preliminary analysis of a second group of clones. Of the original groups that were allocated on the basis of Alu-1 digestion patterns, two of these groupings contained three overlapping candidate clones. One of these (Group D) was chosen for further analysis. To discriminate whether the protein encoded by these clones was a genuine DRADD interactor—or whether it autonomously autoactivated the reporter systems—the plasmid isolation procedure that was described above was used to segregate the AD library clones #37 and #40 from contaminating DB bait plasmids. Each of the prey AD clones was then transformed, either alongside the pAS2-1 DB plasmid or with DB-DRADD^{FL} that was used in the initial screening procedure. Interestingly, whereas co-transformants expressing the unfused Gal-4 DB moiety alongside clones #37 or #40 failed to grow on histidine-deficient media, yeast harbouring either clone in combination with full length DRADD readily survived this selection procedure, indicative of a positive interaction with DRADD. In addition, when subjected to the *LacZ* reporter assay, histidine prototroph yeast colonies harboring either clone in combination with DRADD readily asssumed a blue colony colour, indicative of a genuine positive protein-protein interaction (Figure 51). Thus, the protein encoded by these clones genuinely interacted with DRADD.

To further characterize this DRADD-binding protein, clone#40 was sequenced, using the pACT-2-specific screening primer previously described, with the original PCR product obtained at the insert screening stage as template. Interestingly, BLASTX interrogation (Figure 52A) revealed that this clone was identical to a molecule called HPIP (Haematopoietic PBX-Interacting Protein; Accession number AF221521) that had recently been reported within the context of a two-hybrid screen using the homeodomain protein PBX1 as bait (Abramovich *et al.*, 2000). Analysis of the amino acid sequence retrieved from the published protein sequence revealed that our clone was a C-terminal

Key:

	AD Hybrid	DB Hybrid
1	Vector	DRADD F.L.
2	Clone # 40	Vector
3	Clone # 40	DRADD F.L.
4	Clone # 37	Vector
5	Clone # 37	DRADD F.L.
6	DRADD F.L.	Caspase-9 CARD

Figure 51

Two-hybrid LacZ colony lift assay illustrating interaction between library clones #37 and #40 in yeast.

Yeast transformants expressing library clones #37 and #40 in combination with the indicated DB fusions were streaked on histidine-deficient media. Five days later, *HIS3*-positive colonies growin on selective dropout media were subjected to the colony lift assay as described in Chapter II. A positive protein-protein interaction due to transactivation of the *LacZ* reporter gene is indicated by a blue colony colour. The DRADD/Caspase-9^{CARD} interaction is included as a positive control.

A

```
>ref|NP_065385.1|
Hematopoietic PBX-interacting protein [Homo sapiens]
gb|AAG02026.1|AF221521_1 (AF221521)
Hematopoietic PBX-interacting protein [Homo sapiens]

Length = 731
Score =  121 bits (301), Expect = 6e-28
Identities = 51/52 (98%), Positives = 51/52 (98%)
Frame = +1

Query:  4   KLQGLENWGQDPGVSANASKAWHQKSHFQNSREWSGKEKWWDGXRDRKAEHW 159
           KLQGLENWGQDPGVSANASKAWHQKSHFQNSREWSGKEKWWDG RDRKAEHW
Sbjct:  439 KLQGLENWGQDPGVSANASKAWHQKSHFQNSREWSGKEKWWDGQRDRKAEHW 490
```

B

```
MASCPDSDNSWVLAGSESLPVETLGPASRMDPESERALQAPHSPSKTDGK  50
ELAGTMDGEGTLFQTESPQSGSILTEETEVKGTLEGDVCGVEPPGPGDTV  100
VQGDLQETTVVTGLGPDTQDLEGQSPPQSLPSTPKAAWIREEGRCSSSDD  150
DTDVDMEGLRRRRGREAGPPQPMVPLAVENQAGGEGAGGELGISLNMCLL  200
GALVLLGLGVLLFSGGLSESETGPMEEVERQVLPDPEVLEAVGDRQDGLR  250
EQLQAPVPPDSVPSLQNMGLLLDKLAKENQDIRLLQAQLQAQKEELQSLM  300
HQPKGLEEENAQLRGALQQGEAFQRALESELQQLRARLQGLEADCVRGPD  350
GVCLSGDRGPQGDKAIREQGPREQEPELSFLKQKEQLEAEAQALRQELER  400
QRRLLGSVQQDLERSLQDASRGDPAHAGLAELGHRLAQKLQGLENWGQDP  450
GVSANASKAWHQKSHFQNSREWSGKEKWWDGQRDRKAEHWKHKKEESGRE  500
RKKNWGGQEDREPAGRWKEGRPRVEESGSKKEGKRQGPKEPPRKSGSFHS  550
SGEKQKQPRWREGTKDSHDPLPSWAELLRPKYRAPQGCSGVDECPRQEGL  600
TFFGTELAPVRQQELASLLRTYLARLPWAGQLTKELPLSPAFFGEDGIFR  650
HDRLRFRDFVDALEDSLEEVAVQQTGDDDEVDDFEDFIFSHFFGDKALKK  700
RSGKKDKHSQSPRAAGPREGHSHSHHHHHRG                      731
```

C

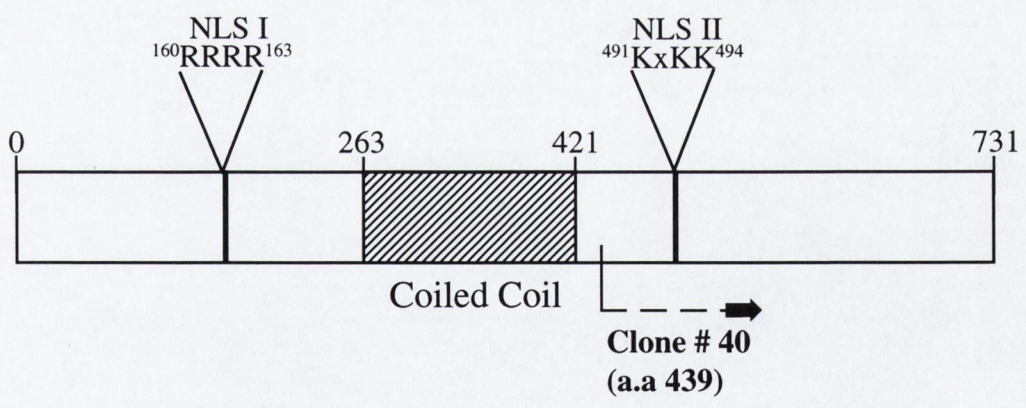

Figure 52

The identity of the protein encoded by clone #40.

A, Results of a BLASTX database search using the nucleotide sequence of clone #40 as a probe. An alignment of the Query (Clone#40) and Subject (HPIP protein) is shown and indicates the strart position of clone #40 as amino acid 439 of full length HPIP.

B, The amino acid sequence of full length HPIP protein (Accession No. AF221521).

C, Schematic diagram illustrating the structure/features of HPIP protein. The putative coiled-coil region and NLSs are indicated. Numbers denote amino acid positions.

fragment of the 731 amino acid protein (Figure 52B). Interestingly, the PSORT II software revealed the presence of a coiled coil motif within the centre of the molecule, flanked by two putative NLSs. A schematic diagram incorporating these observations is illustrated in Figure 52C.

BLASTP database searches based on the full length protein encoded by HPIP/Clone #40 revealed a similarity to the human homologue of yeast Cell Cycle Progression 8 protein (Accession No. AF011794, 28% identity over amino acids 586-694 of HPIP) and Trichohyalin (Accession No. L09190, 23% identity over a.a. 219-540 of HPIP). In addition, this analysis revealed that HPIP was similar to proteins that were found to resemble DRAMP, including NuMA, Myosin heavy chain and Plectin. This was likely due to the mutual possession of coiled coil motifs in all of these molecules. The significance of the DRADD/HPIP interaction will be the subject of future studies.

5.4. DISCUSSION

5.4.1. Summary

In this study we used a yeast two-hybrid-based protein-protein interaction screen to identify novel DRADD interaction partners, one of which we have termed DRAMP (**DR**ADD-**A**ssociated **M**yosin-like **P**rotein). We screened approximately $6x10^6$ clones, or twice the complexity of the Jurkat cDNA library. From this, we obtained a total of 22 clones encoding overlapping portions of a sequence that was identical to a molecule previously identified by several groups, as Heart Muscle Protein (GenBank Accession No. D21094) and Mitofilin (GenBank Accession No. AF148646), respectively (Icho *et al.*, 1994; Odgren *et al.*, 1996; Gieffers *et al.*, 1997). A second DRADD-interactor, HPIP (Abramovich *et al.*, 2000), represented by three library clones, was also identified.

In addition, the screening procedure yielded two copies of several other protein species, some of which were predicted as distinct groups at the Alu-1 digestion stage (Tables 15 and 21). However, the presence of two copies of many other clones was only subsequently revealed by DNA sequencing/database interrogation These were not anticipated by Alu-1 banding patterns alone (Table 18). Further work will be required to establish whether these uncharacterized proteins actually constitute genuine DRADD-interactors.

In preliminary analysis we have shown that DRAMP and HPIP interact with DRADD, since two individual clones of both of these proteins activated the two-hybrid system reporter genes (Figures 47 and 51). Moreover, further analysis using DRADD two-hybrid deletion mutants revealed that DRAMP interacts with the N-terminus of DRADD (Figure 49).

5.4.2. The DRADD/DRAMP interaction

Interestingly, inspection of the DRAMP amino acid sequence revealed the presence of a motif within the C-terminus of the molecule that weakly resembled the CARD motif present in the N-termini of caspases and their associated adaptor molecules (Hoffman *et al.*, 1997). Our analysis of the amino acid sequence of DRAMP library clones suggests that this region coincides with the minimal DRADD-binding motif (Table 20 and Figure 45). Clearly, deletional analysis will be required to establish the precise interaction surfaces on both of these molecules. Given their apparent common interaction motif within DRADD, it will be interesting to evaluate whether caspase-9/DRAMP binding to DRADD are mutually compatible.

5.4.3. Sequence analysis of DRAMP

In the absence of experiments to establish whether DRAMP plays a role as a modulator of the pro-apoptotic activity of DRADD, we have characterized the molecule by analysis of its amino acid sequence. In agreement with the observations of others, inspection of the full-length DRAMP sequence revealed the presence of a region within the centre of the molecule characterized by the presence of multiple alpha helices (Icho *et al.*, 1994). Further analysis of this helical-rich region using the PSORT II algorithm predicted a coiled-coil motif within the centre of the molecule (Figure 45B). This motif is typified by heptad amino acid repeats comprising a hydrophobic core of two amino acids and a helical backbone defined by five hydrophilic amino acids (Lupas, 1996). Moreover, this portion of the molecule was found to resemble several coiled-coil-containing proteins, including the nuclear proteins NuMA and TPR, and the myosin family of molecular motor proteins, as judged by analysis using the BLAST algorithm.

5.4.4. What is the role of DRAMP?

Given the similarity of DRAMP to several species of coiled-coil proteins, what speculative functional inference can we make? Interestingly, this motif has been found to play a role as an oligomerization surface in several species of coiled-coil molecule, including transcription factors, molecular motors/levers and cytoskeletal components (Lupas, 1996). On this basis, it is tempting to envisage a scenario whereby the formation of DRAMP aggregates via the coiled coil region enhances or enables DRADD to activate caspase-9 in an oligomerization-dependent manner. DRAMP may thus constitute an oligomerization platform for DRADD.

On the basis of sequence similarity and the possession of a common coiled coil motif, DRAMP may play a structural role, like NuMa (Lydersen and Pettijohn, 1980), perhaps as a nuclear tether to maintain DRADD within a particular subcellular locality. Alternatively, given the similarity of DRAMP to myosin or kinesin-like molecular motors, it is possible that DRAMP may act as a DRADD translocase to mediate movement of DRADD from one defined subcellular locality to another (Block,1996; Spudich, 1994), perhaps in response to specific pro-apoptotic stimuli. In this regard, a hallmark feature of the molecular motors is an ATPase capacity. This is a prerequisite for the ability of the kinesins to physically move along microtubules while engaging in organelle transport (Cross, 1997), or for the actin-binding myosins to facilitate muscle contraction (Block, 1996).

5.4.5. Is DRAMP a motor protein?

In an attempt to speculatively predict whether DRAMP fulfils this ATPase requirement, the amino acid sequence of the molecule was inspected for the presence of conserved nucleotide binding motifs (Walker *et al.*, 1982). In agreement with one report this analysis revealed an N-terminal motif that somewhat resembles Walker's A and B nucleotide binding boxes (Walker, 1982; Icho *et al.*, 1994)) (Figure 53). However, a closer inspection of the candidate peptide sequences revealed that several of the key amino acid determinants of

A

Walker's 'A' consensus

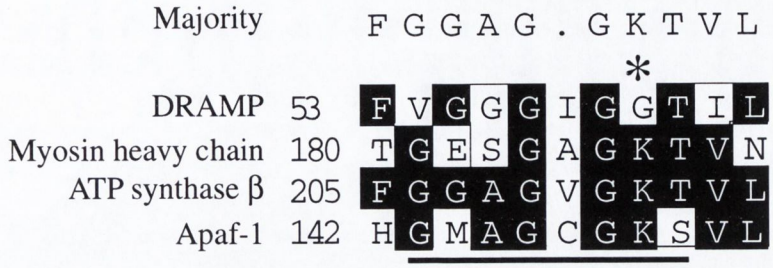

B

Walker's 'B' consensus

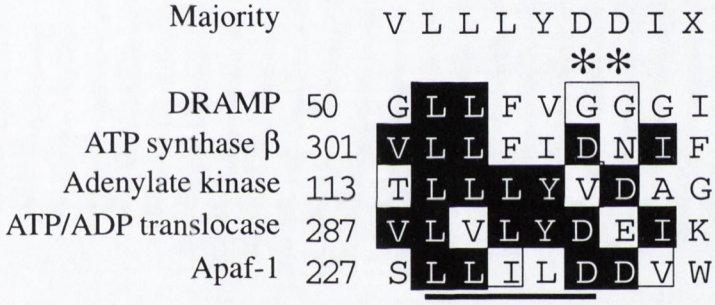

Figure 53

Alignment of DRAMP with human proteins containing Walker's A and B nucleotide binding consensus sequences.

A, Walker's A Box. Alignment of the A-box-like motif within DRAMP with the A box motifs of known nucleotide binding proteins (Human Myosin heavy chain, Accession No. P13535; Human ATP synthase β, Accession No. AAA51809; Human Apaf-1, Accession No. AF013263). The minimal A box consensus sequence is underlined. The invariant Lysine (K) residue, missing in the DRAMP sequence is denoted by an asterisk.

B, Walker's B Box. Alignment of the B-box-like motif within DRAMP with the B box motifs of known nucleotide binding proteins (Human ATP synthase β, Accession No. AAA51809; Human Adenylate kinase, Accession No. KIHUA; Human ATP/ADP translocase, Accession No. AAA51736; Human Apaf-1, Accession No. AF013263) The minimal B box consensus sequence is underlined. The absence of a conserved aspartate (D) residue in one or other of the two positions marked is denoted by an asterisk.

both Walkers A and B boxes are missing in DRAMP (Figure 53). This concurs with the observations of Odgren and colleagues (Odgren *et al.*, 1996). Specifically, these include the absence of an invariant lysine (K) residue within the Walker's A consensus and the lack of a conserved aspartate residue in either of two possible positions as indicated, within the Walker's B consensus (Walker, 1982) (Figure 53). It is thought that the conserved aspartate residue in either of the indicated positions within the P-loop plays an important role in magnesium binding (Walker *et al.*, 1982). On this basis, it therefore seems unlikely that DRAMP possesses an ATPase capacity. However, this observational premise must be subject to experimentation. Moreover, it will be interesting to determine whether DRAMP expression has any effect on the subcellular localization of DRADD in both healthy and dying cells.

5.4.6. What is the subcellular localization of DRAMP?

In an attempt to predict the subcellular localization of DRAMP based on the amino acid sequence of the molecule, we subjected the full-length sequence to analysis using the PSORT and PSORT II algorythms (Nakai and Horton, 1999). Interestingly, in addition to identifying the putative NLS, these programs predicted that DRAMP possesses a putative post-mitochondrial import cleavage site, suggesting that the molecule may be subject to mitochondrial import and subsequent proteolytic maturation (Schatz, 1996). In agreement with this prediction, two groups have reported that Mitofilin, a molecule identical to DRAMP sequence sublocalizes to mitochondria (Odgren *et al.*, 1996; Gieffers *et al.*, 1997). Moreover, one of these studies demonstrated that radiolabeled Mitofilin can be imported into purified yeast mitochondria and report a downshift in molecular weight of Mitofilin upon mitochondrial import (Gieffers *et al.*, 1997). This suggests the proteolytic removal of the signal peptide from the molecule upon mitochondrial import (Gieffers *et al.*, 1997; Schatz, 1996). In agreement with our identification of two putative transmembrane regions within DRAMP/Mitofilin, this group speculate that the molecule may be tethered within the inner mitochondrial membrane, with the C-terminus projecting into the intermembrane space (Gieffers *et al.*, 1997).

Our data suggest that DRADD is a nuclear-sublocalized molecule that does not appear to translocate to another cellular compartment in response to a variety of death stimuli. One speculative hypothesis that reconciles the apparent contradiction in the subcellular localization of these interacting partners would envisage that DRAMP itself translocates from the mitochondrial intermembrane space in response to specific pro-apoptotic stimuli. Indeed, many reports provide compelling evidence for a key role of mitochondrial escapees as regulators of cell death. For example, the translocation of cytochrome c from the mitochondrial intermembrane space to the cytosol signals the assembly of the Apaf-1/Caspase-9 apoptosome (Liu *et al.*, 1996; Adrain and Martin, 2001; Green, 2000). Moreover, the nuclease AIF has been demonstrated to translocate from mitochondria into the nucleus upon mitochondrial damage (Susin *et al.*, 1999). Additionally, the IAP-neutralizing molecule SMAC/DIABLO undergoes release from mitochondria upon triggering of the death program (Du *et al.*, 2000; Verhagen *et al.*, 2000).

Intriguingly within this context, inspection of the DRAMP amino acid sequence revealed the presence of a putative bipartite nuclear localization signal (NLS), suggesting that DRAMP may be subject to nuclear import. Moreover, in support of this, Mitofilin was identified by Odgren and colleagues within the context of an antibody generated in mice immunized with total nuclear matrix proteins (Odgren *et al.*, 1996). This suggests that a fraction of the total pool of DRAMP may reside within the nucleus. It well established that molecules possessing transmembrane motifs can be found tethered to a variety of organelle membranes. For example, studies concerning the subcellular localization of death antagonist Bcl-2 revealed that this protein decorates endoplamic reticulum and nuclear membranes, in addition to the mitochondrial membrane (Hockenbery *et al.*, 1990; Krajewski *et al.*, 1993). Further studies will therefore evaluate the subcellular localization of DRAMP in healthy cells and determine whether this protein is subject to translocation/nuclear import upon induction of the death program.

5.4.7. DRAMP and LC-8: parallels?

It is interesting to note a recent report concerning the interaction between LC8—a component of the dynein motor complex—and the BH-3-only death agonist, Bim (Pukalakath *et al.*, 1999). In healthy cells, Bim remains associated the dynein motor complex, as judged by sucrose gradient co-sedimentation analysis (Pukalakath *et al.*, 1999). However, upon induction of apoptosis by a range of stimuli, including cytokine withdrawal, DNA damage and cytopathic drugs, Bim and LC8 together dissociate from the multimolecular motor complex in a Z-VAD-insensitive manner and can be found in association with Bcl-2 under these conditions (Pukalakath *et al.*, 1999). Thus, the ability of a motor-like protein to modulate apoptosis is not without precedent.

5.4.8. Conclusion

Our premise for conducting the DRADD two-hybrid screen was to obtain a death domain-containing protein that may help to place DRADD within a defined cell death context. However, analysis of approximately 1/4 of the total clones from this screen failed to identify any putative DD molecules. The success of the screening procedure was nonetheless validated by our retrieval of multiple copies of a DRADD-interactor, DRAMP. One explanation for the inability of this screen to detect DD molecules may relate to the relative lack of abundance of these adaptors within the context of the Jurkat cDNA library used for screening. In this regard, it is interesting to note that the initial Bim 2-hybrid screen described above obtained no copies of LC-8 in initial screenings of bone marrow and brain cDNA libraries (Pukalakath *et al.*, 1999). However, subsequent screening of a HeLa cell library obtained a total of 52 clones of LC-8 (Pukalakath *et al.*, 1999). This clearly emphasizes the value of a multiple library-based screening approach in obtaining rare or cell-type-specific interactors. Thus, re-screening using a cDNA library derived from different target tissue may succeed in retrieving different DRADD-specific binding partners than were obtained from our single Jurkat cDNA library-based screen.

Another reason why this screen did not identify DD molecules may relate to inhibitory properties associated with the full-length DRADD molecule. DRADD, much like Apaf-1 cannot constitutively promote apoptosis upon overexpression. This may suggest that DRADD requires post-translational modification, such as a co-factor-induced conformational change, in order to realize its death-inducing properties. Thus, the folding of the full-length DRADD molecule may restrict access of the death domain to other death domain species. On the basis that our truncation-based approach resulted in a spontaneously active Apaf-1, we would have preferred to use the death-domain-only DB-DRADD$^{387-657}$ mutant for screening. Unfortunately, as discussed previously, this approach was prevented due to the propensity the DB-DRADD$^{387-657}$ mutant to autoactivate the two-hybrid reporter genes.

While ideally, our screening approach aspired to cloning molecules that interact with DRADD via a classical homophilic DD/DD interaction, our identification of DRAMP as a novel interaction partner will enable further molecular dissection of the role of DRADD in apoptotic signaling pathways.

CHAPTER VI:
General Discussion

6.1. Summary

This thesis focused on the molecular mechanisms by which caspase-9-binding partners Apaf-1 and DRADD contribute to the regulation of apoptosis. We have demonstrated that Apaf-1, the proximal death adaptor molecule in the cytochrome *c*/mitochondrial pathway, regulates apoptosis primarily through a caspase-aggregating mechanism. Using a variety of protein-protein interaction assays, we have shown that Apaf-1 directly forms oligomers, mediated by an evolutionarily conserved dimerization surface: the CED-4-homologous domain. Significantly, the WDR region appears to inhibit both caspase-9 recruitment to the Apaf-1 CARD and Apaf-1 oligomerization.

The data presented in Chapter IV reveal that another molecule, DRADD, can act as a caspase-9-binding death adaptor under certain circumstances. Our observations that DRADD is a CARD-bearing death domain adaptor protein that resides within the nuclear compartment, suggests that there may be Apaf-1-independent death-inducing mechanisms that activate caspase-9 via DRADD. Moreover, given the subcellular localization of DRADD, it is possible that pro-apoptotic stimuli that exert their effects within the nucleus may provoke assembly of a DRADD/caspase-9 complex analogous to the cytoplasmic apoptosome. Further studies will evaluate this hypothesis.

Our dissection of DRADD function has revealed several interesting parallels with the caspase-9 adaptor, Apaf-1. In particular, two-hybrid experiments suggest that DRADD and Apaf-1 share an ability to form oligomers and therefore may activate caspase-9 via an induced-proximity mechanism. Moreover, our observations also suggest that overexpressed full length Apaf-1 and DRADD do not constitutively promote apoptosis. Truncation of both of these caspase-9 adaptors generated constitutively active molecules, suggesting that some form of post-translational modification is required to unlock their pro-apoptotic activity. While we have yet to determine the specific stimulus or cofactor that acts as a death-inducing ligand for DRADD, much evidence suggests that cytochrome *c* binding to Apaf-1 may unlock the death-inducing properties of the latter.

Interestingly, experiments suggest that the tumour suppressor molecule Rb may act as a co-factor for DRADD-associated apoptosis, since co-expression of these molecules induces apoptosis. However, the specific cellular conditions under which this occurs remain to be elucidated. In addition, our observation that DRADD undergoes proteolytic cleavage during apoptosis may suggest another mechanism by which the molecule is regulated. While the functional consequence(s) of Bax-induced DRADD cleavage still remain obscure, there is a well established precedent for caspase-mediated activation of death effector function with Bid (Li *et al.*, 1998; Luo *et al.*, 1998; Gross *et al.*, 1999). In addition, caspases may play a role in modulating the activity and subcellular localization of nuclear death effector domain protein, DEDD (Stegh *et al.*, 1998).

Chapter V of this thesis described work aimed at obtaining DRADD-interacting molecules as a means of identifying other components of the putative DRADD/caspase-9 pathway. While this screen failed to find a binding partner for the DRADD death domain, it successfully retrieved multiple copies of a DRADD-interacting partner, DRAMP. Intriguingly, preliminary analysis of the DRAMP sequence suggests that the molecule resembles coiled-coil motif containing proteins, including the molecular motors myosin and kinesin. The premise that DRAMP modulates DRADD function by regulating its subcellular distribution will form an important basis for future work.

6.2. Concluding comments: Chapter III

In agreement with the observations on Apaf-1 oligomerization detailed in Chapter III (Adrain *et al.*, 1999), several other groups have reported that Apaf-1 can self-associate (Srinivasula *et al.*, 1998; Hu *et al.*, 1998b). In particular, the work of Hu and colleagues concurs with our observation that Apaf-1 self-association is mediated via the CED-4-homologous motif (Hu *et al.*, 1998b). In addition, this group also provided evidence that the WDR negatively regulates Apaf-1 oligomerization through the formation of an intramolecular fold within Apaf-1, between the CED-4 region and the WDR (Hu *et al.*, 1998b). These data suggest that disruption of the CED-4/WDR interaction thus frees up the oligomerization surface, enabling Apaf-1 dimerization and caspase-9 recruitment/activation. This was subsequently confirmed by the same group who showed that an Apaf-1 mutant incapable of the WDR/CED-4 fold spontaneously promoted caspase-9 activation (Hu *et al.*, 1999).

In summary, recent developments suggests the following scenario whereby Apaf-1 promotes caspase-9 activation (see Figure 54). In healthy cells, Apaf-1 exists as a monomer and cannot bind dATP (Saleh *et al.*, 1999). A two-step process modulates the assembly of a multimolecular Apaf-1 oligomeric complex. Following efflux from mitochondria, cytochrome *c* interaction with the Apaf-1 WDR promotes dATP binding. This induces a conformational change in the molecule, exposing the CED-4-homologous region and enabling the formation of Apaf-1 oligomers (Jiang *et al.*, 2000; Benedict *et al.*, 2000). It appears that procaspase-9 and cytochrome *c* synergistically promote dATP binding and Apaf-1 oligomerization (Jiang *et al.*, 2000).

Studies from several groups employing gel filtration techniques as a means of analyzing the Apaf-1/caspase-9 apoptosome suggest that the complex is relatively stable (Cain *et al.*, 1999; Zou *et al.*, 1999; Saleh *et al.*, 1999; Cain *et al.*, 2000). In cells induced to undergo apoptosis, Apaf-1 rapidly shifts in molecular weight from a ~ 130 kDa monomer to a ~700 kDa multimeric complex, minimally containing Apaf-1/caspase-9 and cytochrome *c*. Because experimental evidence indicates that

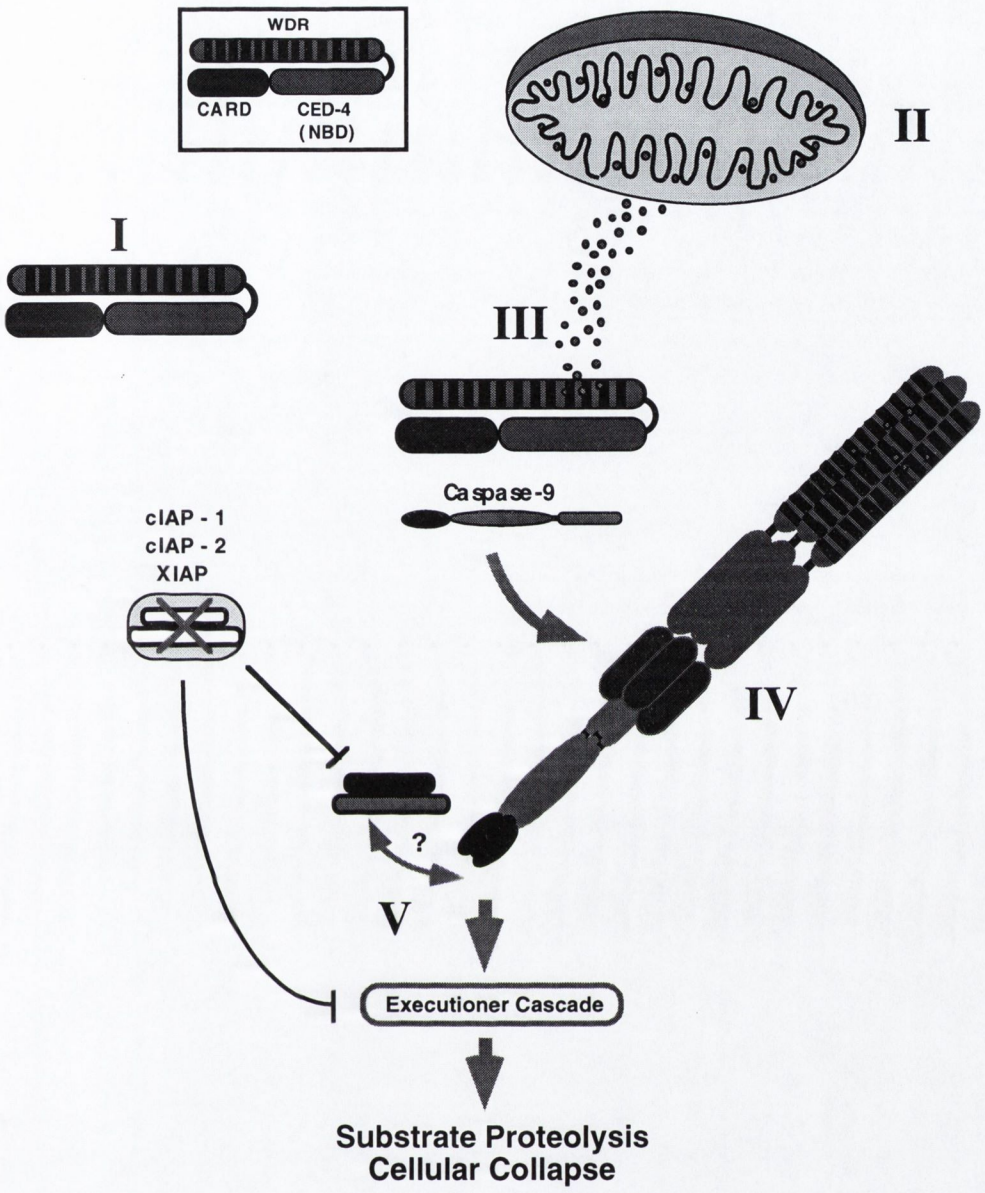

Figure 54

Schematic diagram illustrating assembly of the Apaf-1 apoptosome

In the absence of cytosolic cytochrome *c*, Apaf-1 exists in a monomeric form (**I**). The ability of the molecule to oligomerize/recruit caspase-9 is repressed by the WDR region binding to and occluding the CED-4 oligomerization surface. In cells triggered to undergo apoptosis, diverse upstream signaling events provoke cytochrome *c* release (**II**). Within the cytoplasm, cytochrome *c* binds to the C-terminal WDR region of Apaf-1 (**III**). This induces a conformational change in Apaf-1, exposing the CED-4 region. As a result, caspase-9 becomes recruited and Apaf-1 forms an oligomeric complex, mediated by dimerization of adjacent CED-4-homologous domains of Apaf-1 (**IV**). Active caspase-9 then cleaves downstream caspases-3 and -7, initiating a proteolytic cascade (**V**). During apoptosis, active caspase-9 may get released from the apoptosome or may remain associated with Apaf-1.

the apoptosome complex contains a 1:1 stoichiometric ratio of Apaf-1: caspase-9, this would suggest a complex composed of three copies of each of these subunits (Zou *et al.*, 1999). In addition, several groups have demonstrated the formation of a 1400 kDa apoptosome complex (Cain *et al.*, 1999; Zou *et al.*, 1999; Saleh *et al.*, 1999; Cain *et al.*, 2000). However, only the 700 kDa apoptosome has been found to possess proteolytic activity, suggesting that this is the biologically active complex (Cain *et al.*, 2000).

Intriguingly, a variety of evidence suggests that the multimolecular apoptosome may not be simply a scaffold for caspase-9 activation. Rather, gel filtration analysis of the apoptosome suggests that almost all caspase processing activity resides in the fractions containing the Apaf-1/caspase-9 apoptosome complexes, rather than in eluted fractions containing free caspase-9 (Cain *et al.*, 2000; Rodriguez and Lazebnik, 1999). Moreover, it has been reported that Apaf-1-complexed mature caspase-9 possesses more than 1000 times the activity of its uncomplexed active counterpart. These data suggest that the apoptosome constitutes a *bona fide* biologically active multimolecular proteolytic complex somewhat akin to the proteasome, with Apaf-1/caspase-9 complexes acting as an active holoenzyme.

In addition to characterization of the Apaf-1 apoptosome, the specific hierarchy of proteolytic signaling events distal to caspase-9 activation in the Apaf-1 pathway has also been revealed (Slee *et al.*, 1999b). Downstream of apoptosome formation, caspases-3 and -7 become activated by caspase-9-catalyzed proteolytic cleavage. In turn, active caspase-3 cleaves caspases-2 and -6, and active caspase-6 can then activate long prodomain caspases -8 and -10. Work undertaken in the laboratory has begun to characterize the specific role of caspases activated via the Apaf-1/caspase-9 pathway in modulating substrate cleavage during apoptosis (Slee, Adrain and Martin, 2001).

6.3. Concluding remarks: Chapter IV

A variety of evidence (reviewed in Chapter I) suggests a role for nuclear proteins as regulators of apoptosis. Indeed, several of the transcriptional targets of the p53 tumour suppressor have been identified as death agonistic relatives of the Bcl-2 family (Miyashita *et al.*, 1995; Oda *et al.*, 2000). However, as previously discussed (Chapter IV), current evidence suggests that the caspase-activating properties of these molecules arise from their ability to engage the Apaf-1/caspase-9 apoptosome pathway within the cytoplasm.

In contrast, our identification of DRADD as a nuclear-localized death domain adaptor molecule that recruits caspase-9 and promotes caspase-9-dependent apoptosis, suggests that there may be additional mechanisms by which pro-apoptotic signaling mechanisms are engaged from within the nuclear compartment. In support of this, caspase-9, a key modulator of nuclear damage and anti-cancer drug-induced cell death (Kuida *et al.*, 1998; Hakem *et al.*, 1998) has been demonstrated to reside within the nucleus (Ritter *et al.*, 2000). Preliminary experiments suggest that cells undergoing DNA damage-associated apoptosis fail to significantly relocalize GFP-DRADD. It is therefore tempting to speculate that DRADD/caspase-9 may constitute a novel death-inducing apoptosome that actually assembles within the nucleus (Figure 55).

If DRADD constitutes one of the components of a putative nuclear apoptosome (Figure 55), what factors are likely to influence the assembly of such a structure? Two-hybrid experiments suggested that like Apaf-1, DRADD is capable of forming oligomers, suggesting that DRADD could activate caspase-9 via an induced proximity mechanism. Apaf-1 and DRADD cannot constitutively self-associate however, and in the case of Apaf-1, oligomerization is regulated by binding of the co-factor, cytochrome *c* (Adrain *et al.*, 1999). Similar to Apaf-1, DRADD oligomerization was readily detectable in yeast within the context of truncated versions of the molecule. Clearly, further experiments will be necessary to determine whether post-translational modification or the binding of a molecular

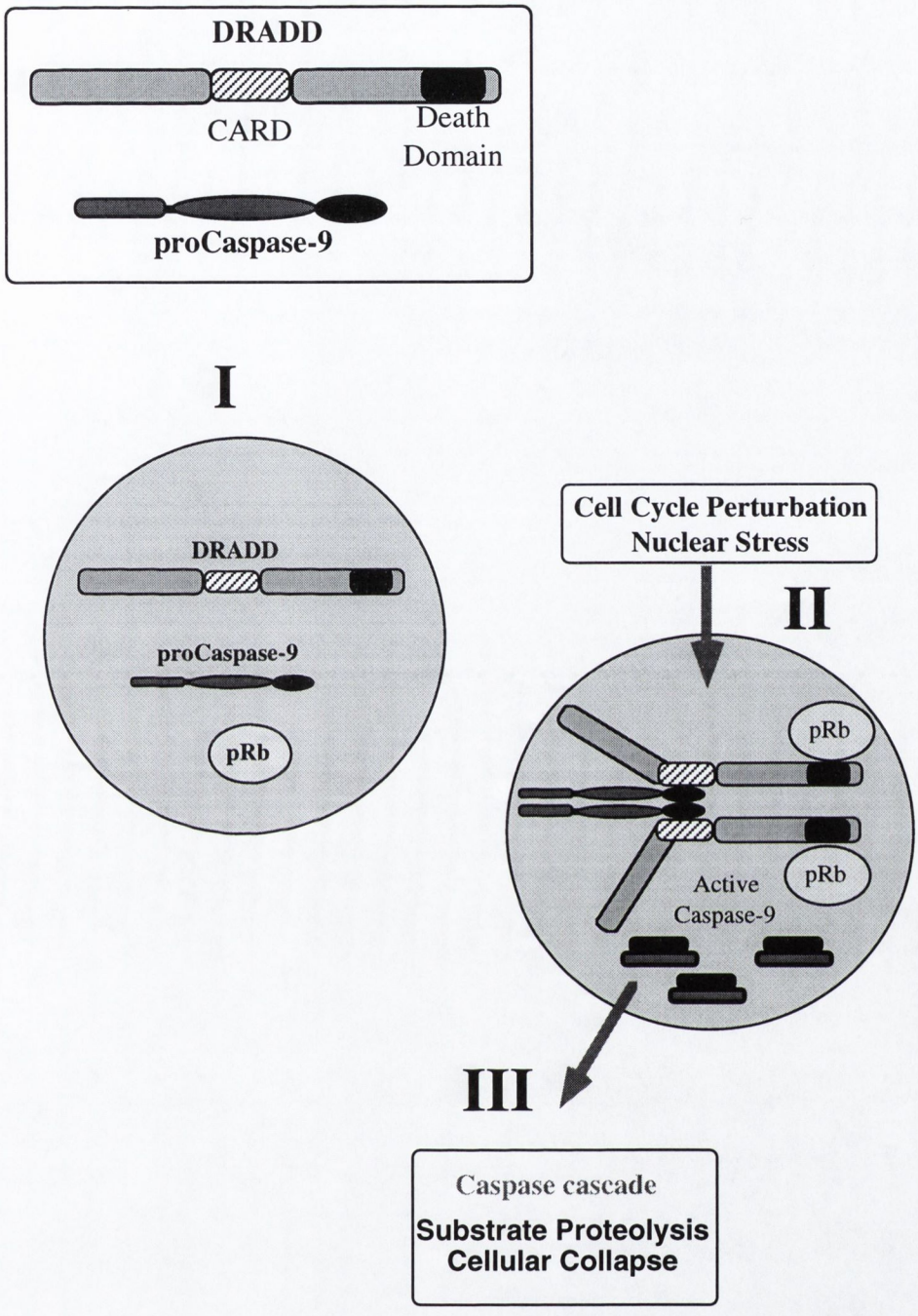

Figure 55

Schematic diagram illustrating a hypothetical "Nuclear Apoptosome" complex composed of DRADD and Caspase-9, regulated by the Retinoblastoma protein, pRb.

(**I**) In the nuclei of healthy cells, in the absence of a death stimulus, DRADD cannot spontaneously form oligomers or activate caspase-9 molecules. However, in cells that have sustained cytotoxic levels of nuclear damage, or where normal regulation of the cell cycle is impaired, some form of post-translational modification of DRADD provokes the formation of DRADD oligomers (**II**). This process may be positively regulated by pRb binding to the DRADD C-terminus. As a result, induced proximity of Caspase-9 within the DRADD apoptosome complex leads to activation of Caspase-9 within the nucleus (**II**). Finally, the death signal originating within the nucleus may become amplified via a caspase cascade within the cytoplasm, leading to cellular collapse and apoptosis (**III**).

co-factor is required to promote the formation of nuclear oligomers of DRADD, capable of modulating caspase-9 activation (Figure 55). However, the preliminary data presented within Chapter IV suggests that pRb and DRADD not only interact, but can also provoke apoptosis when co-expressed. It is thus tempting to speculate that in some situations, pRb may act as a co-factor for DRADD-induced apoptosis (Figure 55). Ongoing studies using an antibody to endogenous DRADD and nuclear cell extracts will thus investigate whether DRADD undergoes multimerization in response to specific pro-apoptotic signaling events.

Continuing upon the theme of factors that regulate cell death from within the nucleus, there is evidence to suggest a role for the Promyelocytic Leukaemia Protein (PML) in the regulation of nuclear apoptosis and cell cycle progression (Hess and Korsmeyer, 1998; Matera, 1999). Interestingly, whereas in healthy cells this protein sublocalizes to nuclear matrix regions termed PML organizational domains (PODS), the sublocalization of the molecule becomes disrupted in cells expressing viral oncogenes (Borden *et al.*, 1997) and in cells derived from Acute Promyelocytic leukaemia (AP) patients (Dyck *et al.*, 1994; Weis *et al.*, 1994). These data suggest that the particular sublocalization of PML may be important in terms of regulating its function.

While the role of PML is as yet obscure, a variety of functions have tentatively been attributed to the molecule. For instance, PODs are known to be centres of transcription, containing a high density of mRNA transcripts and in agreement with this, a recent study suggests that PML may act as a transcriptional co-activator of p53 (Guo *et al.*, 2000). In addition, other studies suggest that PML may have growth suppressing, anti-tumourigenic functions, since viral transduction-mediated expression of PML actually leads to an accumulation of G1-arrested cells (Le *et al.*, 1998). Moreover, in these cells, pRb was found to be predominantly hypophosphorylated, a status which Durfee and colleagues reported was conducive to DRADD/pRb binding (Durfee *et al.*, 1994; Le *et al.*, 1998). In addition, two recent studies suggest that PML and Daxx may collaborate to regulate apoptosis (Torii *et al.*, 1999; Zhong *et al.*, 2000). Moreover, a further

study reported that cells subjected to nuclear damaging stimuli including ionizing irradiation and cisplatin, upregulated PML levels, possibly through a mechanism involving post-translational stabilization of the latter. Finally, targeted deletion of the PML gene highlights an involvement of the molecule in several apoptotic signaling pathways, including Fas and ionizing radiation (Wang *et al.*, 1998).

Intriguingly, several studies have reported that pRb and PML actually colocalize within nuclear bodies (Labbaye *et al.*, 1999; Ferbeyre *et al.*, 2000). Moreover, these proteins can be co-immunoprecipitated, suggesting that they might interact within the nuclear compartment (Labbaye *et al.*, 1999; Ferbeyre *et al.*, 2000). Since we have demonstrated that DRADD interacts with Rb, future studies will evaluate whether the association between PML and Rb can regulate the formation of DRADD apoptosomes within the nuclear matrix.

6.4. Concluding remarks: Chapter V

Using a two-hybrid screening approach, we have identified DRAMP as a DRADD-binding partner. Preliminary analysis of the DRAMP amino acid sequence suggests that the molecule possess a coiled coil motif and shares some similarity with the molecular motor myosin.

We have established that DRADD resides within the nucleus and does not appear to inducibly relocate in response to a variety of pro-apoptotic stimuli. It is therefore interesting to note a report regarding the cloning of Mitofilin, a protein that is identical to DRAMP (Odgren *et al.*, 1996). This protein was identified using a reverse genetic approach. From a pool of antibodies generated against total nuclear matrix proteins, one antibody reacted strongly with a protein that decorates mitochondrial membranes: mitofilin (Odgren *et al.*, 1996). Thus, on the basis of these data, it is plausible that DRAMP is a mitochondrial protein that is also present to some extent within the nuclear matrix.

Because we have identified a putative NLS within DRAMP, one speculative hypothesis based on the nuclear apoptosome model detailed above (Section 6.3; Figure 55) may be that pro-apoptotic stimuli that provoke the release of apoptogenic factors such as cytochrome *c* and SMAC/Diablo from mitochondria could also provoke the translocation of DRAMP (Figure 56), possibly to the nuclear compartment. Future work will thus examine the subcellular localization of DRAMP in healthy and apoptotic cells to investigate the possibility that DRAMP may act as a death ligand for DRADD within the nuclear compartment.

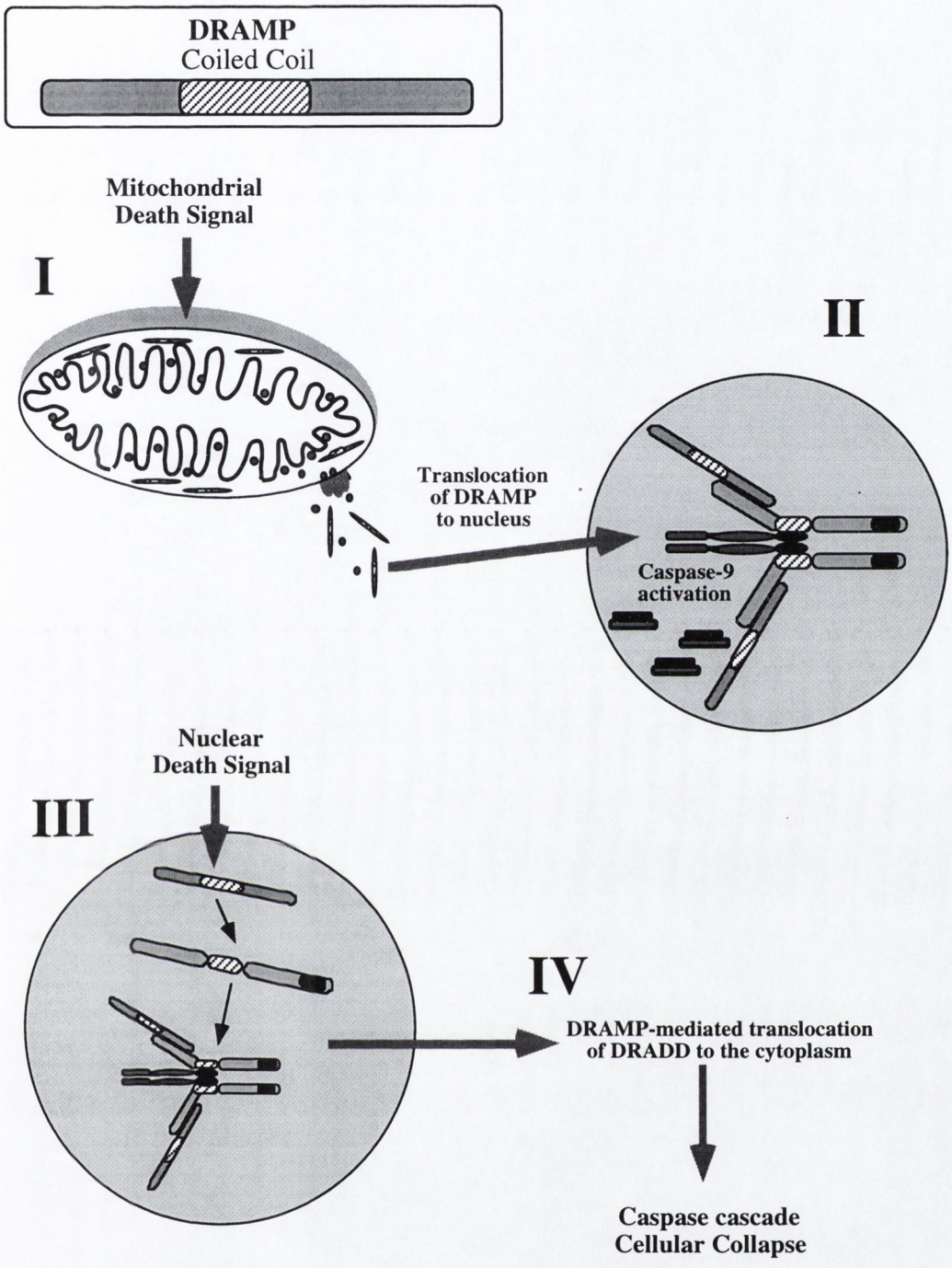

Figure 56

Models illustrating the hypothetical role of DRAMP as a regulator of the pro-apoptotic activity of DRADD.

If DRAMP is a mitochondrial protein, model (**I**) envisages a scenario whereby a pro-apoptotic stimulus provokes its translocation from mitochondria into the nuclear compartment, where DRAMP may act as a co-factor that promotes the assembly of the DRADD/Caspase-9 nuclear apoptosome (**II**). Alternatively, assuming that a fraction of the cellular pool of DRAMP actually resides within the nuclear matrix, stimuli that provoke nuclear damage may engage a DRADD apoptosome that utilizes DRAMP as a nuclear tether or oligomerization platform (**III**). A further scenario (**IV**) may involve the DRAMP-mediated transport of DRADD into the cytoplasm as a means of disseminating the pro-apoptotic signal throughout the cell.

APPENDIX

Table 22

Table illustrating plasmids that were generated by the author for work undertaken in Chapter III

Plasmid name	Vector	Insertion sites (5′-3′)	Forward primer sequence (5′-3′)	Reverse primer sequence (5′-3′)
pBluescript. Apaf-1 ΔCED-3	pBluescript	BamH-1/ BamH-1	#59	#61
pcDNA3. Apaf-1 ΔWD40	pcDNA3	BamH-1/ Xho-1	#22	#60
pcDNA3. Apaf-1 CED-4	pcDNA3	BamH-1/ BamH-1	#59	#15
pcDNA3. Apaf-1 CED-4/Linker	pcDNA3	BamH-1/ Xho-1	#59	#60
GST-Apaf-1 1-601	pGEX4TK-2	BamH-1/ BamH-1	#22	#16
AD-Apaf-1 CED-4/Linker	pACT-2	Sma-1/ BamH-1	#14	#16
AD-Apaf-1 Linker	pACT-2	Sma-1/ BamH-1	#56	#16
DB-Apaf-1 CED-3	pAS2-1	Sma-1/ BamH-1	#13	#17
DB-Apaf-1 CED-4	pAS2-1	Sma-1/ BamH-1	#14	#15
DB-Apaf-1 CED-4/Linker	pAS2-1	Sma-1/ BamH-1	#14	#16
DB-Apaf-1 Linker	pAS2-1	Sma-1/ BamH-1	#56	#16
pGBT-8 DBApaf-1 CED-4	pAS2-1	Sma-1/ Sal-1	Subcloned from pAS2-1 DB Apaf-1 CED-4	

Table 23

Table illustrating plasmids that were generated by the author for work undertaken in Chapters IV and V

Plasmid name	Vector	Insertion sites	Forward Primer	Reverse Primer
DB-DRADD F.L.	pAS2-1	Subcloned from the AD-DRADD F.L. library clone using Sma-1/Xho-1 and inserted into Sal-1/Sma-1 sites within the pAS2-1 vector		
DB-DRADD 1-120	pAS2-1	Sma-1/ BamH-1	#80	# 84
DB-DRADD 1-388	pAS2-1	Sma-1/ BamH-1	#80	#81
DB-DRADD 387-657	pAS2-1	Sma-1/ BamH-1	#82	#83
AD-DRADD 1-120	pACT-2	Sma-1/ BamH-1	#80_	#84
AD-DRADD 1-388	pACT-2	Sma-1/ BamH-1	#80	#81
AD-DRADD 387-657	pACT-2	Sma-1/ BamH-1	#82	#83
pcDNA3. DRADD 289-657	pcDNA3	BamH-1/ Xho-1	#91	#52
GFP-DRADD F.L.	pEGFPC3	Xho-1/ BamH-1	#144	#145
GFP-DRADD 1-388	pEGFPC3	Xho-1/ BamH-1	#144	#81
GFP-DRADD 289-657	pEGFPC3	Xho-1/ BamH-1	#146	#145
GFP-DRADD 387-657	pEGFPC3	Xho-1/ BamH-1	#177	#145
GFP-DRADD 441-657	pEGFPC3	Xho-1/ BamH-1	#178	#145

Table 24

Table illustrating the oligonucleotide primers that were used to generate some of the plasmids used for work undertaken in the thesis

Primer No.	Name	Sequence (5′-3′)	Forward or reverse
#13	Apaf-1 MetF	AGACCCGGGAATGGATGCAAAAGCT	F
#14	Apaf-1 Pro92F	AGACCCGGGACCTGTTGTCTCTTCT	F
#15	Apaf-1 Leu 412R	CCGGGTACCGGATCCTCAAAGAGACTTATTTAC	R
#16	Apaf-1 Arg 601R	AATGGTACCGGATCCTCAGCGGACAACTAAGCG	R
#17	Apaf-1 Leu86R	TATGGTACCGGATCCTCAGAGAAGGGCAGCAAG	R
#22	Apaf-1 Met F Gex	GACGGATCCATGGATGCAAAAGCT	F
#52	DRADD STOPR	CTGGCTCGAGCTAACTATTTGTCTCATT	R
#56	Apaf-1 Leu413F	ATACCCGGGGTTATTCTGTGATCGG	F
#59	Apaf-1 Pro92FII	GACGGATCCGCCATGCCTGTTGTCTCTTCT	F
#60	Apaf-1 Arg 601RII	TACGCTCGAGTTAGCGGACAACTAAGCG	R
#61	Apaf-1 StopR	CGCGGATCCTTATTCTAAAGTCTGTAA	R
#80	DRADD MetF	TTACCCGGGGATGTCTCCGACGCCG	F
#81	DRADD Trp388R	CGGGATCCCTACCAGTTTTCTTC AGT	R
#82	DRADD Asn387F	ATACCCGGGGAACTGGAACTCGTGG	F
#83	DRADD Ser 657R	CGGGATCCCTAACTATTTGTCTCATT	R
# 84	DRADD Val 120R	GCGGATCCCTAAACATTTTTTTCGAC	R
#91	DRADD Leu 289F	AAGGATCCGCATGTTGAAAACAGGA	F
#144	DRADD MetF EGFP	ATACTCGAGATG TCT CCG ACG CCG	F
#145	DRADD EGFP R	AATGAGACAAATAGTGGGATCCGCG	R
#146	DRADD Leu 289 EGFP	ATACTCGAGTTGAAAACAGGAGGA	F
#177	DRADD EGFPASN387 F	ATACTCGAGAACTGGAACTCGTGG	F
#178	DRADD EGFP Leu 441F	AGTCTCGAGCTTTGGAATCTTTGC	F
#156	pACT-2 SCREENF	TTCGATGATGAAGATACCCC	F
#157	pACR-2 SCREENR	GAACTTGCGGGGTTTTTCAG	R

Table 25

Table identifying the origin of some of the plasmids used for work undertaken in this thesis.

Plasmid name	Made by/supplied by
pcDNA3 DRADD F.L.	Dr Mary Harte
pcDNA3 FLAG DRADD F.L.	Dr Mary Harte
pcDNA3 DRADD 1-388	Dr Mary Harte
pcDNA3 DRADD 387-657	Dr Mary Harte
pcDNA3 DRADD 356-657	Dr Mary Harte
pcDNA3 DRAMP F.L.	Dr Helen Egan
pcDNA3 Caspase-9	Dr Helen Egan
pcDNA3 Caspase-9 C->A mutant	Dr Helen Egan
pcDNA3 Caspase-3 C->A mutant	Dr Helen Egan
pcDNA3 Caspase-8	Laboratory of Dr Vishva Dixit
pET21b Caspase-2	Laboratory of Dr Emad Alnemri
pGEX4TK-2 Caspase-9^{CARD} (a.a. 1-130)	Dr Mary Harte
pcDNA3.1 His C Fas IC	Dr Helen Egan
pcDNA3.1 His C TNFR IC	Dr Helen Egan
pcDNA3.1 His C DR-4 IC	Dr Helen Egan
pcDNA3.1 His C DR-5 IC	Dr Helen Egan
pcDNA3 DR-4 F.L.	Laboratory of Dr Henning Walczak
pcDNA3 DR-5 F.L.	Laboratory of Dr Henning Walczak
pcDNA3 FADD	Laboratory of Dr Vishva Dixit
pRK RIP	Laboratory of Dr David Goeddel
pRK TRADD	Laboratory of Dr David Goeddel
pcDNA3 crmA	Laboratory of Dr Vishva Dixit
pEBS Bcl-X	Laboratory of Dr Vishva Dixit
pcDNA3 Bax	Laboratory of Dr Doug Green
pRC cmv p53	Laboratory of Dr Moshe Oren
pCMV Rb	Laboratory of Dr Jean Wang
pcDNA3 Apaf-1 F.L.	Laboratory of Dr Xiaodong Wong
pGEX4TK-2 Apaf-1 1-412	Dr Mary Harte
pACT-2 Apaf-1 ΔCED-3	Dr Mary Harte
pACT-2 Apaf-1 ΔWD40	Dr Mary Harte
pACT-2 Apaf-1 CED-3	Dr Mary Harte
pACT-2 Apaf-1 CED-4	Dr Mary Harte

REFERENCES

REFERENCES

Abbas AK (1996). Die and Let Live: Eliminating Dangerous Lymphocytes *Cell* **84**, 655-657.

Abramovich C, Shen WF, Pineault N, Imren S, Montpetit B, Largman C, Humphries RK (2000). Functional cloning and characterization of a novel nonhomeodomain protein that inhibits the binding of PBX1-HOX complexes to DNA. *J Biol Chem.* **275**, 26172-7.

Adrain C and Martin SJ (2001). The mitochondrial apoptosome: a killer unleashed by the cytochrome seas. *Trends Biochem Sci.* Accepted.

Adrain C, Harte MT, Egan, H, Carlin WJ, Slee EA, Martin SJ (2001). DRADD, a nuclear-localized death domain protein, interacts with caspase-9 and Rb to promote apoptosis. Submitted.

Adrain C, Slee EA, Harte MT, Martin SJ (1999). Regulation of apoptotic protease activating factor-1 oligomerization and Apoptosis by the WD-40 repeat region. *J Biol Chem.* **274**, 20855-60.

Agami R, Blandino G, Oren M, Shaul Y (1999). Interaction of c-Abl and p73alpha and their collaboration to induce apoptosis. *Nature* **399**, 809-13.

Alnemri ES, Livingston DJ, Nicholson DW, Salvesen G, Thornberry NA, Wong WW,Yuan J (1996). Human ICE/CED-3 protease nomenclature. *Cell* **87**, 171.

Ashkenazi A, Dixit VM. (1998). Death receptors: signaling and modulation. *Science* **281**, 1305-8.

Attardi LD, Reczek EE, Cosmas C, Demicco EG, McCurrach ME, Lowe SW, Jacks T. (2000). PERP, an apoptosis-associated target of p53, is a novel member of the PMP-22/gas3 family. *Genes Dev.* **14**, 704-18.

Bakhshi A, Jensen JP, Goldman P, Wright JJ, McBride OW, Epstein AL, Korsmeyer SJ (1985). Cloning the chromosomal breakpoint of t(14;18) human lymphomas: clustering around JH on chromosome 14 and near a transcriptional unit on 18. *Cell* **41**, 899-906.

Barde YA (1989). Trophic factors and neuronal survival. *Neuron* **2**, 1525-34.

Bauer MK, Wesselborg S, Schulze-Osthoff K (1997). The Caenorhabditis elegans death protein Ced-4 contains a motif with similarity to the mammalian 'death effector domain'. *FEBS Lett.* **402**, 256-8.

Benedict MA, Hu Y, Inohara N, Nunez G (2000). Expression and functional analysis of Apaf-1 isoforms. Extra Wd-40 repeat is required for cytochrome c binding and regulated activation of procaspase-9. *J Biol Chem.* **275**, 8461-8.

Bergeron L, Perez GI, Macdonald G, Shi L, Sun Y, Jurisicova A, Varmuza S, Latham KE, Flaws JA, Salter JC, Hara H, Moskowitz MA, Li E, Greenberg A, Tilly JL, Yuan J (1998). Defects in regulation of apoptosis in caspase-2 deficient mice. *Genes Dev.* **12**, 1304-14.

Beyaert R, Kidd VJ, Cornelis S, Van de Craen M, Denecker G, Lahti JM, Gururajan R, Vandenabeele P, Fiers W (1997). Cleavage of PITSLRE kinases by ICE/CASP-1 and CPP32/CASP-3 during apoptosis induced by tumor necrosis factor. *J Biol Chem.* **272**, 11694-7.

Bissonnette RP, Echeverri F, Mahboubi A, Green DR (1992). Apoptotic cell death induced by c-myc is inhibited by bcl-2. *Nature* **359**, 552-4.

Block SM (1996). Fifty ways to love your lever: myosin motors. *Cell* **87**, 151-7.

Boldin MP, Goncharov TM, Goltsev YV, Wallach D (1996). Involvement of MACH, a novel MORT1/FADD-interacting protease, in Fas/APO-1- and TNF receptor-induced cell death. *Cell* **85**, 803-15.

Boldin MP, Varfolomeev EE, Pancer Z, Mett IL, Camonis JH, Wallach D (1995). A novel protein that interacts with the death domain of Fas/APO1 contains a sequence motif related to the death domain. *J Biol Chem.* **270**, 7795-8.

Borden KL, CampbellDwyer EJ, Salvato MS (1997). The promyelocytic leukemia protein PML has a pro-apoptotic activity mediated through its RING domain. *FEBS Lett.* **418**, 30-4.

Bossy-Wetzel E, Newmeyer DD, Green DR (1998). Mitochondrial cytochrome c release in apoptosis occurs upstream of DEVD-specific caspase activation and independently of mitochondrial transmembrane depolarization. *EMBO J.* **17**, 37-49.

Buckley CD, Pilling D, Henriquez NV, Parsonage G, Threlfall K, Scheel-Toellner D, Simmons DL, Akbar AN, Lord JM, Salmon M (1999). RGD peptides induce apoptosis by direct caspase-3 activation. *Nature* **397**, 534-9.

Bump NJ, Hackett M, Hugunin M, Seshagiri S, Brady K, Chen P, Ferenz C, Franklin S, Ghayur T, Li P, Licari P, Mankovich J, Shi L, Greenberg AH, Miller LK, Wong WW (1995). Inhibition of ICE family proteases by baculovirus antiapoptotic protein p35. *Science* **269**, 1885-8.

Caelles C, Helmberg A, Karin M (1994). p53-dependent apoptosis in the absence of transcriptional activation of p53-target genes. *Nature* **370**, 220-3.

Cain K, Bratton SB, Langlais C, Walker G, Brown DG, Sun XM, Cohen GM (2000). Apaf-1 oligomerizes into biologically active approximately 700-kDa and inactive approximately 1.4-MDa apoptosome complexes. *J Biol Chem.* **275**, 6067-70.

Cain K, Brown DG, Langlais C, Cohen GM (1999). Caspase activation involves the formation of the aposome, a large (approximately 700 kDa) caspase activating complex. *J Biol Chem.* **274**, 22686-92.

Caspari T (2000). How to activate p53. *Curr Biol.* **10**, R315-7.

Cecconi F, Alvarez-Bolado G, Meyer BI, Roth KA, Gruss P (1998). Apaf1 (CED-4 homolog) regulates programmed cell death in mammalian development. *Cell* **94**, 727-37.

Chaudhary D, O'Rourke K, Chinnaiyan AM, Dixit VM (1998). The death inhibitory molecules CED-9 and CED-4L use a common mechanism to inhibit the CED-3 death protease. *J Biol Chem.* **273**, 17708-12.

Chehab NH, Malikzay A, Appel M, Halazonetis TD (2000). Chk2/hCds1 functions as a DNA damage checkpoint in G(1) by stabilizing p53. *Genes Dev.* **14**, 278-88.

Cheng Y, Deshmukh M, D'Costa A, Demaro JA, Gidday JM, Shah A, Sun Y, Jacquin MF, Johnson EM, Holtzman DM (1998). Caspase inhibitor affords neuroprotection with delayed administration in a rat model of neonatal hypoxic-ischemic brain injury. *J Clin Invest.* **101**, 1992-9.

Chinnaiyan AM, Chaudhary D, O'Rourke K, Koonin EV, Dixit VM (1997a). Role of CED-4 in the activation of CED-3. *Nature* **388**, 728-9.

Chinnaiyan AM, O'Rourke K, Lane BR, Dixit VM (1997b). Interaction of CED-4 with CED-3 and CED-9: a molecular framework for cell death. *Science* **275**, 1122-6.

Chinnaiyan AM, O'Rourke K, Yu GL, Lyons RH, Garg M, Duan DR, Xing L, Gentz R, Ni J, Dixit VM (1996a). Signal transduction by DR3, a death domain-containing receptor related to TNFR-1 and CD95. *Science* **274**, 990-2.

Chinnaiyan AM, Tepper CG, Seldin MF, O'Rourke K, Kischkel FC, Hellbardt S, Krammer PH, Peter ME, Dixit VM (1996b). FADD/MORT1 is a common mediator of CD95 (Fas/APO-1) and tumor necrosis factor receptor-induced apoptosis. *J Biol Chem.* **271**, 4961-5.

Choisy-Rossi C, Yonish-Rouach E (1998). Apoptosis and the cell cycle: the p53 connection. *Cell Death Differ.* **5**, 129-31.

Clem RJ, Fechheimer M, Miller LK (1991). Prevention of apoptosis by a baculovirus gene during infection of insect cells. *Science* **254**, 1388-90.

Cohen PL, Eisenberg RA (1991). Lpr and gld: single gene models of systemic autoimmunity and lymphoproliferative disease. *Ann Rev Immunol.* **9**, 243-69.

Colussi PA, Harvey NL, Kumar S (1998). Prodomain-dependent nuclear localization of the caspase-2 (Nedd2) precursor. A novel function for a caspase prodomain. *J Biol Chem.* **273**, 24535-42.

Conradt B, Horvitz HR (1998). The C. elegans protein EGL-1 is required for programmed cell death and interacts with the Bcl-2-like protein CED-9. *Cell* **93**, 519-29.

Cotter TG, Martin SJ (1996). Techniques in Apoptosis. A user's guide. Portland Press, London.

Cross RA (1997). Reversing the kinesin ratchet—a diverting tail. *Nature* **389**, 15-6.

Datta SR, Katsov A, Hu L, Petros A, Fesik SW, Yaffe MB, Greenberg ME (2000). 14-3-3 proteins and survival kinases cooperate to inactivate BAD by BH3 domain phosphorylation. *Mol Cell.* **6**, 41-51.

Datta SR, Dudek H, Tao X, Masters S, Fu H, Gotoh Y, Greenberg ME (1997). Akt phosphorylation of BAD couples survival signals to the cell-intrinsic death machinery. *Cell* **91**, 231-41.

De Maria R, Zeuner A, Eramo A, Domenichelli C, Bonci D, Grignani F, Srinivasula SM, Alnemri ES, Testa U, Peschle C (1999). Negative regulation of erythropoiesis by caspase-mediated cleavage of GATA-1. *Nature* **401**, 489-93.

del Peso L, Gonzalez VM, Inohara N, Ellis RE, Nunez G (2000). Disruption of the CED-9.CED-4 complex by EGL-1 is a critical step for programmed cell death in Caenorhabditis elegans. *J Biol Chem.* **275**, 27205-11.

del Peso L, Gonzalez VM, Nunez G (1998). Caenorhabditis elegans EGL-1 disrupts the interaction of CED-9 with CED-4 and promotes CED-3 activation. *J Biol Chem.* **273**, 33495-500.

Deveraux QL, Roy N, Stennicke HR, Van Arsdale T, Zhou Q, Srinivasula SM, Alnemri ES, Salvesen GS, Reed JC (1998). IAPs block apoptotic events induced by caspase-8 and cytochrome c by direct inhibition of distinct caspases. *EMBO J.* **17**, 2215-23.

Du C, Fang M, Li Y, Li L, Wang X (2000). Smac, a mitochondrial protein that promotes cytochrome c-dependent caspase activation by eliminating IAP inhibition. *Cell* **102**, 33-42.

Duan H, Dixit VM (1997). RAIDD is a new 'death' adaptor molecule. *Nature* **385**, 86-9.

Duan H, Orth K, Chinnaiyan AM, Poirier GG, Froelich CJ, He WW, Dixit VM (1996). ICE-LAP6, a novel member of the ICE/Ced-3 gene family, is activated by the cytotoxic T cell protease granzyme B. *J Biol Chem.* **271**, 16720-4.

Dumaz N, Meek DW (1999). Serine15 phosphorylation stimulates p53 transactivation but does not directly influence interaction with HDM2. *EMBO J.* **18**, 7002-10.

Durfee T, Mancini MA, Jones D, Elledge SJ, Lee WH (1994). The amino-terminal region of the retinoblastoma gene product binds a novel nuclear matrix protein that co-localizes to centers for RNA processing. *J Cell Biol.* **127**, 609-22.

Dyck JA, Maul GG, Miller WH Jr, Chen JD, Kakizuka A, Evans RM (1994). A novel macromolecular structure is a target of the promyelocyte-retinoic acid receptor oncoprotein. *Cell* **76**, 333-43.

Ellis HM, Horvitz HR (1986). Genetic control of programmed cell death in the nematode C. elegans. *Cell* **44**, 817-29.

Ellis J, Jones D (1998). Structure and function of proteins controlling strain-specific pathogen resistance in plants. *Curr Opin Plant Biol.* **1**, 288-93.

Enari M, Sakahira H, Yokoyama H, Okawa K, Iwamatsu A, Nagata S (1998). A caspase-activated DNase that degrades DNA during apoptosis, and its inhibitor ICAD. *Nature* **391**, 43-50.

Enari M, Hug H, Nagata S (1995). Involvement of an ICE-like protease in Fas-mediated apoptosis. *Nature* **375**, 78-81.

Eskes R, Desagher S, Antonsson B, Martinou JC (2000). Bid induces the oligomerization and insertion of Bax into the outer mitochondrial membrane. *Mol Cell Biol.* **20**, 929-35.

Evan GI, Wyllie AH, Gilbert CS, Littlewood TD, Land H, Brooks M, Waters CM, Penn LZ, Hancock DC (1992). Induction of apoptosis in fibroblasts by c-myc protein. *Cell* **69**, 119-28.

Fadok VA, Bratton DL, Rose DM, Pearson A, Ezekewitz RA, Henson PM (2000). A receptor for phosphatidylserine-specific clearance of apoptotic cells. *Nature* **405**, 85-90.

Fadok VA, Savill JS, Haslett C, Bratton DL, Doherty DE, Campbell PA, Henson PM (1992). Different populations of macrophages use either the vitronectin receptor or the phosphatidylserine receptor to recognize and remove apoptotic cells. *J Immunol.* **149**, 4029-35.

Ferbeyre G, de Stanchina E, Querido E, Baptiste N, Prives C, Lowe SW (2000). PML is induced by oncogenic ras and promotes premature senescence. *Genes Dev.* **14**, 2015-27.

Fields S, Song O (1989). A novel genetic system to detect protein-protein interactions. *Nature* **340**, 245-6.

Friedlander RM, Gagliardini V, Hara H, Fink KB, Li W, MacDonald G, Fishman MC, Greenberg AH, Moskowitz MA, Yuan J (1997). Expression of a dominant negative mutant of interleukin-1 beta converting enzyme in transgenic mice prevents neuronal cell death induced by trophic factor withdrawal and ischemic brain injury. *J Exp Med* **185**, 933-40.

Fritsche M, Haessler C, Brandner G (1993). Induction of nuclear accumulation of the tumor-suppressor protein p53 by DNA-damaging agents. *Oncogene* **8**, 307-18.

Fulda S, Scaffidi C, Susin SA, Krammer PH, Kroemer G, Peter ME, Debatin KM (1998). Activation of mitochondria and release of mitochondrial apoptogenic factors by betulinic acid. *J Biol Chem.* **273**, 33942-8.

Gajkowska B, Motyl T, Olszewska-Badarczuk H, Gniadecki R, Koronkiewicz M (2000). Structural association of bax with nuclear matrix and cytomatrix revealed by embedment-free immunogold electron microscopy. *Cell Biol Int.* **24**, 649-56.

Gervais FG, Xu D, Robertson GS, Vaillancourt JP, Zhu Y, Huang J, LeBlanc A, Smith D, Rigby M, Shearman MS Clarke EE, Zheng H, Van Der Ploeg LH, Ruffolo SC, Thornberry NA, Xanthoudakis S, Zamboni RJ, Roy S, Nicholson DW (1999). Involvement of caspases in proteolytic cleavage of Alzheimer's amyloid-beta precursor protein and amyloidogenic A beta peptide formation. *Cell* **97**, 395-406.

Gieffers C, Korioth F, Heimann P, Ungermann C, Frey J (1997). Mitofilin is a transmembrane protein of the inner mitochondrial membrane expressed as two isoforms. *Exp Cell Res.* **232**, 395-9.

Goldstein JC, Waterhouse NJ, Juin P, Evan GI, Green DR (2000). The coordinate release of cytochrome c during apoptosis is rapid, complete and kinetically invariant. *Nat Cell Biol.* **2**, 156-62.

Gong JG, Costanzo A, Yang HQ, Melino G, Kaelin WG Jr, Levrero M, Wang JY (1999). The tyrosine kinase c-Abl regulates p73 in apoptotic response to cisplatin-induced DNA damage. *Nature* **399**, 806-9.

Green DR (20000. Apoptotic pathways: paper wraps stone blunts scissors. *Cell* **102**, 1-4.

Gross A, Yin XM, Wang K, Wei MC, Jockel J, Milliman C, Erdjument-Bromage H, Tempst P, Korsmeyer SJ (1999). Caspase cleaved BID targets mitochondria and is required for cytochrome c release, while BCL-XL prevents this release but not tumor necrosis factor-R1/Fas death. *J Biol Chem* **274**, 1156-63.

GS, Bredesen DE, Rosenthal RE, Fiskum G, Reed JC (1999). Release of caspase-9 from mitochondria during neuronal apoptosis and cerebral ischemia. *Proc Natl Acad Sci U S A.* **96**, 5752-7.

Guo A, Salomoni P, Luo J, Shih A, Zhong S, Gu W, Paolo Pandolfi P (2000). The function of PML in p53-dependent apoptosis. *Nat Cell Biol.* **2**, 730-736.

Hahne M, Rimoldi D, Schroter M, Romero P, Schreier M, French LE, Schneider P,Bornand T, Fontana A, Lienard D, Cerottini J, Tschopp J (1996). Melanoma cell expression of Fas(Apo-1/CD95) ligand: implications for tumor immune escape. *Science.* **274**, 1363-6

Hakem R, Hakem A, Duncan GS, Henderson JT, Woo M, Soengas MS, Elia A, de la Pompa JL, Kagi D, Khoo W, Potter J, Yoshida R, Kaufman SA, Lowe SW, Penninger JM, Mak TW (1998). Differential requirement for caspase 9 in apoptotic pathways in vivo. *Cell* **94**, 339-52.

Hamon Y, Broccardo C, Chambenoit O, Luciani MF, Toti F, Chaslin S, Freyssinet JM, Devaux PF, McNeish J, Marguet D, Chimini G (2000). ABC1 promotes engulfment of apoptotic cells and transbilayer redistribution of phosphatidylserine. *Nat Cell Biol.* **2**, 399-406.

Haupt Y, Maya R, Kazaz A, Oren M (1997). Mdm2 promotes the rapid degradation of p53. *Nature* **387**, 296-9.

Haupt Y, Rowan S, Shaulian E, Vousden KH, Oren M (1995). Induction of apoptosis in HeLa cells by trans-activation-deficient p53. *Genes Dev.* **9**, 2170-83.

Hengartner MO (1997). Cell Death. *C.elegans II.* Cold spring harbour laboratory press, Chapter **15**, 383-415.

Hengartner MO, Horvitz HR (1994). C. elegans cell survival gene ced-9 encodes a functional homolog of the mammalian proto-oncogene bcl-2. *Cell* **76**, 665-76.

Hengartner MO, Ellis RE, Horvitz HR (1992). Caenorhabditis elegans gene ced-9 protects cells from programmed cell death. *Nature* **356**, 494-9.

Hensey CE, Hong F, Durfee T, Qian YW, Lee EY, Lee WH (1994). Identification of discrete structural domains in the retinoblastoma protein. Amino terminal domain is required for its oligomerization. *J Biol Chem.* **269**, 1380-7.

Hess JL, Korsmeyer SJ (1998). Life, death and nuclear spots. *Nat Genet.* **20**, 220-2.

Heusel JW, Wesselschmidt RL, Shresta S, Russell JH, Ley TJ (1994). Cytotoxic lymphocytes require granzyme B for the rapid induction of DNA fragmentation and apoptosis in allogeneic target cells. *Cell* **76**, 977-87.

Hockenbery D, Nunez G, Milliman C, Schreiber RD, Korsmeyer SJ (1990). Bcl-2 is an inner mitochondrial membrane protein that blocks programmed cell death. *Nature* **348**, 334-6.

Hofmann K, Bucher P, Tschopp J (1997). The CARD domain: a new apoptotic signalling motif. *Trends Biochem Sci.* **22**, 155-6.

Hogg A, Bia B, Onadim Z, Cowell JK (1993). Molecular mechanisms of oncogenic mutations in tumors from patients with bilateral and unilateral retinoblastoma. *Proc Natl Acad Sci U S A.* **90**, 7351-5.

Honarpour N, Du C, Richardson JA, Hammer RE, Wang X, Herz J. Adult Apaf-1-deficient mice exhibit male infertility (2000). *Dev Biol.* **218**, 248-58.

Hsieh JK, Chan FS, O'Connor DJ, Mittnacht S, Zhong S, Lu X (1999). RB regulates the stability and the apoptotic function of p53 via MDM2. *Mol Cell* **3**. 181-93.

Hu Y, Benedict MA, Ding L, Nunez G (1999). Role of cytochrome c and dATP/ATP hydrolysis in Apaf-1-mediated caspase-9 activation and apoptosis. *EMBO J.* **18**, 3586-95.

Hu Y, Benedict MA, Wu D, Inohara N, Nunez G (1998a). Bcl-XL interacts with Apaf-1 and inhibits Apaf-1-dependent caspase-9 activation. *Proc Natl Acad Sci U S A.* **95**, 4386-91.

Hu Y, Ding L, Spencer DM, Nunez G (1998b). WD-40 repeat region regulates Apaf-1 self-association and procaspase-9 activation. *J Biol Chem.* **273**, 33489-94.

Huang DC, O'Reilly LA, Strasser A, Cory S (1997). The anti-apoptosis function of Bcl-2 can be genetically separated from its inhibitory effect on cell cycle entry. *EMBO J.* **16**, 4628-38.

Humphries P, Kenna P, Farrar GJ (1992). On the molecular genetics of retinitis pigmentosa. *Science* **256**, 804-8.

Icho T, Ikeda T, Matsumoto Y, Hanaoka F, Kaji K, Tsuchida N (1994). A novel human gene that is preferentially transcribed in heart muscle. *Gene* **144**, 301-6.

Inohara N, Gourley TS, Carrio R, Muniz M, Merino J, Garcia I, Koseki T, Hu Y, Chen S, Nunez G (1998). Diva, a Bcl-2 homologue that binds directly to Apaf-1 and induces BH3-independent cell death. *J Biol Chem.* **273**, 32479-86.

Inoue H, Nojima H, Okayama H (1990). High efficiency transformation of Escherichia coli with plasmids. *Gene* **96**, 23-8.

Irmler M, Hofmann K, Vaux D, Tschopp J (1997). Direct physical interaction between the Caenorhabditis elegans 'death proteins' CED-3 and CED-4. *FEBS Lett.* **406**, 189-90.

Ishizaki Y, Jacobson MD, Raff MC (1998). A role for caspases in lens fiber differentiation. *J Cell Biol.* **140**, 153-8.

James C, Gschmeissner S, Fraser A, Evan GI (1997). CED-4 induces chromatin condensation in Schizosaccharomyces pombe and is inhibited by direct physical association with CED-9. *Curr Biol.* **7**, 246-52.

Jacobson MD, Weil M, Raff MC (1997). Programmed cell death in animal development. *Cell* **88**, 347-54.

Jenne DE, Masson D, Zimmer M, Haefliger JA, Li WH, Tschopp J (1989). Isolation and complete structure of the lymphocyte serine protease granzyme G, a novel member of the granzyme multigene family in murine cytolytic T lymphocytes. Evolutionary origin of lymphocyte proteases. *Biochemistry* **28**, 7953-61.

Jiang X, Wang X (2000). Cytochrome c promotes caspase-9 activation by inducing nucleotide binding to apaf-1. *J Biol Chem.* **275**, 31199-203.

Juin P, Hueber AO, Littlewood T, Evan G (1999). c-Myc-induced sensitization to apoptosis is mediated through cytochrome c release. *Genes Dev.* **13**, 1367-81.

Jurgensmeier JM, Xie Z, Deveraux Q, Ellerby L, Bredesen D, Reed JC (1998). Bax directly induces release of cytochrome c from isolated mitochondria. *Proc Natl Acad Sci U S A.* **95**, 4997-5002.

Kelekar A, Thompson CB (1998). Bcl-2-family proteins: the role of the BH3 domain in apoptosis. *Trends Cell Biol.* **8**, 324-30.

Kerr JF, Wyllie AH, Currie AR (1972). Apoptosis: a basic biological phenomenon with wide-ranging implications in tissue kinetics. *Br J Cancer* **26**, 239-57.

Khosravi R, Maya R, Gottlieb T, Oren M, Shiloh Y, Shkedy D (1999). Rapid ATM dependent phosphorylation of MDM2 precedes p53 accumulation in response to DNA damage. *Proc Natl Acad Sci U S A.* **96**, 14973-7.

Kitson J, Raven T, Jiang YP, Goeddel DV, Giles KM, Pun KT, Grinham CJ, Brown R, Farrow SN (1996). A death-domain-containing receptor that mediates apoptosis. *Nature.* **384**, 372-5.

Kluck RM, Bossy-Wetzel E, Green DR, Newmeyer DD (1997). The release of cytochrome c from mitochondria: a primary site for Bcl-2 regulation of apoptosis. *Science* **275**, 1132-6.

Komatsu K, Miyashita T, Hang H, Hopkins KM, Zheng W, Cuddeback S, Yamada M, Lieberman HB, Wang HG (2000). Human homologue of S. pombe Rad9 interacts with BCL-2/BCL-xL and promotes apoptosis. *Nat Cell Biol.* **2**, 1-6.

Krajewski S, Krajewska M, Ellerby LM, Welsh K, Xie Z, Deveraux QL, Salvesen GS, Bredesen DE, Rosenthal RE, Fiskum G, Reed JC (1999). Release of caspase-9 from mitochondria during neuronal apoptosis and cerebral ischemia. *Proc Natl Acad Sci U S A.* **96**, 5752-7.

Krajewski S, Tanaka S, Takayama S, Schibler MJ, Fenton W, Reed JC (1993). Investigation of the subcellular distribution of the bcl-2 oncoprotein: residence in the nuclear envelope, endoplasmic reticulum, and outer mitochondrial membranes. *Cancer Res.* **53**, 4701-14.

Kudla G, Montessuit S, Eskes R, Berrier C, Martinou JC, Ghazi A, Antonsson B (2000). The destabilization of lipid membranes induced by the C terminal fragment of caspase 8-cleaved bid is inhibited by the N terminal fragment. *J Biol Chem.* **275**, 22713-8.

Kuida K, Haydar TF, Kuan CY, Gu Y, Taya C, Karasuyama H, Su MS, Rakic P, Flavell RA (1998). Reduced apoptosis and cytochrome c-mediated caspase activation in mice lacking caspase 9. *Cell* **94**, 325-37.

Kuida K, Lippke JA, Ku G, Harding MW, Livingston DJ, Su MS, Flavell RA (1995). Altered cytokine export and apoptosis in mice deficient in interleukin-1 beta converting enzyme. *Science* **267**, 2000-3.

Kuida K, Zheng TS, Na S, Kuan C, Yang D, Karasuyama H, Rakic P, Flavell RA (1996). Decreased apoptosis in the brain and premature lethality in CPP32 deficient mice. *Nature* **384**, 368-72.

Kumar S, Tomooka Y, Noda M (1992). Identification of a set of genes with developmentally down-regulated expression in the mouse brain. Biochem *Biophys Res Commun.* **185**, 1155-61.

Labbaye C, Valtieri M, Grignani F, Puglisi R, Luchetti L, Masella B, Alcalay M, Testa U, Peschle C (1999). Expression and role of PML gene in normal adult hematopoiesis: functional interaction between PML and Rb proteins in erythropoiesis. *Oncogene* **18**, 3529-40.

Lazebnik YA, Kaufmann SH, Desnoyers S, Poirier GG, Earnshaw WC (1994). Cleavage of poly(ADP-ribose) polymerase by a proteinase with properties like ICE. *Nature* **371**, 346-7.

Le XF, Vallian S, Mu ZM, Hung MC, Chang KS (1998). Recombinant PML adenovirus suppresses growth and tumorigenicity of human breast cancer cells by inducing G1 cell cycle arrest and apoptosis. *Oncogene* **16**, 1839-49.

Lennon SV, Martin SJ, Cotter TG (1991). Dose-dependent induction of apoptosis in human tumour cell lines by widely diverging stimuli. *Cell Prolif.* **24**, 203-14.

Li H, Zhu H, Xu CJ, Yuan J (1998). Cleavage of BID by caspase 8 mediates the mitochondrial damage in the Fas pathway of apoptosis. *Cell* **94**, 491-501.

Li P, Nijhawan D, Budihardjo I, Srinivasula SM, Ahmad M, Alnemri ES, Wang X (1997). Cytochrome c and dATP-dependent formation of Apaf-1/caspase-9 complex initiates an apoptotic protease cascade. *Cell* **91**, 479-89.

Lin Y, Ma W, Benchimol S (2000). Pidd, a new death-domain-containing protein, is induced by p53 and promotes apoptosis. *Nat Genet.* **26**, 122-7.

Liu X, Kim CN, Yang J, Jemmerson R, Wang X (1996). Induction of apoptotic program in cell-free extracts: requirement for dATP and cytochrome c. *Cell* **86**, 147-57.

Lu X, Lane DP (1993). Differential induction of transcriptionally active p53 following UV or ionizing radiation: defects in chromosome instability syndromes? *Cell* **75**, 765-78.

Luo X, Budihardjo I, Zou H, Slaughter C, Wang X (1998). Bid, a Bcl2 interacting protein, mediates cytochrome c release from mitochondria in response to activation of cell surface death receptors. *Cell* **94**, 481-90.

Lupas A (1996). Coiled coils: new structures and new functions. *Trends Biochem Sci.* **21**, 375-82.

Lydersen BK, Pettijohn DE (1980). Human-specific nuclear protein that associates with the polar region of the mitotic apparatus: distribution in a human/hamster hybrid cell. *Cell* **22**, 489-99.

Marguet D, Luciani MF, Moynault A, Williamson P, Chimini G (1999). Engulfment of apoptotic cells involves the redistribution of membrane phosphatidylserine on phagocyte and prey. *Nat Cell Biol.* **1**, 454-6.

Macleod KF, Hu Y, Jacks T. Loss of Rb activates both p53-dependent and independent cell death pathways in the developing mouse nervous system. *EMBO J.* **15**, 6178-88.

Mancini M, Nicholson DW, Roy S, Thornberry NA, Peterson EP, Casciola-Rosen LA, Rosen A (1998). The caspase-3 precursor has a cytosolic and mitochondrial distribution: implications for apoptotic signaling. *J Cell Biol.* **140**, 1485-95.

Martin SJ, Amarante-Mendes GP, Shi L, Chuang TH, Casiano CA, O'Brien GA, Fitzgerald P, Tan EM, Bokoch GM, Greenberg AH, Green DR (1996a). The cytotoxic cell protease granzyme B initiates apoptosis in a cell-free system by proteolytic processing and activation of the ICE/CED-3 family protease, CPP32, via a novel two-step mechanism. *EMBO J.* **15**, 2407-16.

Martin SJ, Finucane DM, Amarante-Mendes GP, O'Brien GA, Green DR (1996b). Phosphatidylserine externalization during CD95 induced apoptosis of cells and cytoplasts requires ICE/CED-3 protease activity. *J Biol Chem.* **271**, 28753-6.

Martin SJ, Green DR (1995a). Apoptosis and cancer: the failure of controls on cell death and cell survival. *Crit Rev Oncol Hematol.* **18**, 137-53.

Martin SJ, Green DR (1995b). Protease activation during apoptosis: death by a thousand cuts? *Cell* **82**, 349-52.

Martin SJ, Reutelingsperger CP, McGahon AJ, Rader JA, van Schie RC, LaFace DM, Green DR (1995c). Early redistribution of plasma membrane phosphatidylserine is a general feature of apoptosis regardless of the initiating stimulus: inhibition by overexpression of Bcl-2 and Abl. *J Exp Med.* **182**, 1545-56.

Martin SJ, Newmeyer DD, Mathias S, Farschon DM, Wang HG, Reed JC, Kolesnick RN, Green DR (1995d). Cell-free reconstitution of Fas-, UV radiation- and ceramide-induced apoptosis. *EMBO J.* **14**, 5191-200.

Martin SJ (1993). Protein or RNA synthesis inhibition induces apoptosis of mature human CD4+ T cell blasts. *Immunol Lett.* **35**, 125-34.

Martin SJ, Bonham AM, Cotter TG (1990). The involvement of RNA and protein synthesis in programmed cell death (apoptosis) in human leukaemia HL-60 cells. *Biochem Soc Trans.* **18**, 634-6.

Marzo I, Brenner C, Kroemer G (1998). The central role of the mitochondrial megachannel in apoptosis: evidence obtained with intact cells, isolated mitochondria, and purified protein complexes. *Biomed Pharmacother.* **52**, 248-51.

Masumoto J, Taniguchi S, Ayukawa K, Sarvotham H, Kishino T, Niikawa N, Hidaka E, Katsuyama T, Higuchi T, Sagara J (1999). ASC, a novel 22-kDa protein, aggregates during apoptosis of human promyelocytic leukemia HL-60 cells. *J Biol Chem.* **274**, 33835-8.

Matera AG (1999). Nuclear bodies: multifaceted subdomains of the interchromatin space. *Trends Cell Biol.* **9**, 302-9.

Mathews FS (1985). The structure, function and evolution of cytochromes. *Prog Biophys Mol Biol.* **45**, 1-56.

Matsuoka S, Huang M, Elledge SJ (1998). Linkage of ATM to cell cycle regulation by the Chk2 protein kinase. *Science.* **282**, 1893-7.

Miyashita T, Reed JC (1995). Tumor suppressor p53 is a direct transcriptional activator of the human bax gene. *Cell* **80**, 293-9.

Medema JP, de Jong J, van Hall T, Melief CJ, Offringa R (1999). Immune escape of tumors in vivo by expression of cellular FLICE-inhibitory protein. *J Exp Med.* **190**, 1033-8.

Medema JP, Scaffidi C, Kischkel FC, Shevchenko A, Mann M, Krammer PH, Peter ME (1997). FLICE is activated by association with the CD95 death-inducing signaling complex (DISC). *EMBO J.* **16**, 2794-804.

Meinl E, Fickenscher H, Thome M, Tschopp J, Fleckenstein B (1998). Anti-apoptotic strategies of lymphotropic viruses. *Immunol Today* **19**, 474-9.

Metzstein MM, Stanfield GM, Horvitz HR (1998). Genetics of programmed cell death in C. ele*gans:* past, present and future. *Trends Genet* **14**, 410-6.

Minn AJ, Kettlun CS, Liang H, Kelekar A, Vander Heiden MG, Chang BS, Fesik SW, Fill M, Thompson CB (1999). Bcl-xL regulates apoptosis by heterodimerization-dependent and –independent mechanisms. *EMBO J.* **18**, 632-43.

Minn AJ, Velez P, Schendel SL, Liang H, Muchmore SW, Fesik SW, Fill M, Thompson CB (1997). Bcl-x(L) forms an ion channel in synthetic lipid membranes. *Nature* **385**, 353-7.

Mittl PR, Di Marco S, Krebs JF, Bai X, Karanewsky DS, Priestle JP, Tomaselli KJ, Grutter MG (1997). Structure of recombinant human CPP32 in complex with the tetrapeptide acetyl-Asp-Val-Ala-Asp fluoromethyl ketone. *J Biol Chem.* **272**, 6539-47.

Miura M, Zhu H, Rotello R, Hartwieg EA, Yuan J (1993). Induction of apoptosis in fibroblasts by IL-1 beta-converting enzyme, a mammalian homolog of the C. elegans cell death gene ced-3. *Cell* **75**, 653-60.

Miyashita T, Reed JC (1995). Tumor suppressor p53 is a direct transcriptional activator of the human bax gene. *Cell* **80**, 293-9.

Moriishi K, Huang DC, Cory S, Adams JM (1999). Bcl-2 family members do not inhibit apoptosis by binding the caspase activator Apaf-1. *Proc Natl Acad Sci U S A.* **96**, 9683-8.

Muchmore SW, Sattler M, Liang H, Meadows RP, Harlan JE, Yoon HS, Nettesheim D, Chang BS, Thompson CB, Wong SL, Ng SL, Fesik SW (1996). X-ray and NMR structure of human Bcl-xL, an inhibitor of programmed cell death. *Nature* **381**, 335-41.

Mukae N, Enari M, Sakahira H, Fukuda Y, Inazawa J, Toh H, Nagata S (1998). Molecular cloning and characterization of human caspase-activated DNase. *Proc Natl Acad Sci U S A.* **95**, 9123-8.

Muzio M, Chinnaiyan AM, Kischkel FC, O'Rourke K, Shevchenko A, Ni J, Scaffidi C, Bretz JD, Zhang M, Gentz R, Mann M, Krammer PH, Peter ME, Dixit VM (1996). FLICE, a novel FADD-homologous ICE/CED-3-like protease, is recruited to the CD95(Fas/APO-1) death-inducing signaling complex. *Cell* **85**, 817-27.

Nataraj A, Pathak S, Hopwood V, McDonnel T, Ananthaswamy H (1994) Bcl-2 oncogene blocks differentiation and extends viability but does not immortalize normal human keratinocytes. *Int. J. Oncology* **4**, 1211-1218.

Nagata S (1997). Apoptosis by death factor. *Cell* **88**, 355-65.

Nagata S, Suda T (1995). Fas and Fas ligand: lpr and gld mutations. *Immunol Today* **16**, 39-43.

Nakagawa T, Zhu H, Morishima N, Li E, Xu J, Yankner BA, Yuan J (2000). Caspase-12 mediates endoplasmic-reticulum-specific apoptosis and cytotoxicity by amyloid-beta. *Nature* **403**, 98-103.

Nakai K, Horton P (1999). PSORT: a program for detecting sorting signals in proteins and predicting their subcellular localization. *Trends Biochem Sci.* **24**, 34-6.

Neer EJ, Schmidt CJ, Nambudripad R, Smith TF (1994). The ancient regulatory protein family of WD-repeat proteins. *Nature* **371**, 297-300.

Newmeyer DD, Bossy-Wetzel E, Kluck RM, Wolf BB, Beere HM, Green DR (2000). Bcl-xL does not inhibit the function of Apaf-1. *Cell Death Differ.* **7**, 402-7.

Newmeyer DD, Farschon DM, Reed JC (1994). Cell-free apoptosis in Xenopus egg extracts: inhibition by Bcl-2 and requirement for an organelle fraction enriched in mitochondria. *Cell* **79**, 353-64.

Newton K, Harris AW, Bath ML, Smith KGC, Strasser A (1998). A dominant interfering mutant of FADD/MORT1 enhances deletion of autoreactive thymocytes and inhibits proliferation of mature T lymphocytes. *EMBO J.* **17**, 706-18.

Nicholson DW (1999). Caspase structure, proteolytic substrates, and function during apoptotic cell death. *Cell Death Differ.* **6**, 1028-42.

Nicholson DW, Ali A, Thornberry NA, Vaillancourt JP, Ding CK, Gallant M, Gareau Y, Griffin PR, Labelle M, Lazebnik YA, Munday NA, Raju SM, Smulson ME, Yamin TT, Yu VL, Miller DK (1995). Identification and inhibition of the ICE/CED-3 protease necessary for mammalian apoptosis. *Nature* **376**, 37-43.

Oda E, Ohki R, Murasawa H, Nemoto J, Shibue T, Yamashita T, Tokino T, Taniguchi T, Tanaka N (2000). Noxa, a BH3-only member of the Bcl-2 family and candidate mediator of p53-induced apoptosis. *Science* **288**, 1053-8.

Odgren PR, Toukatly G, Bangs PL, Gilmore R, Fey EG (1996). Molecular characterization of mitofilin (HMP), a mitochondria-associated protein with predicted coiled coil and intermembrane space targeting domains. *J Cell Sci.* **109**, 2253-64.

Ona VO, Li M, Vonsattel JP, Andrews LJ, Khan SQ, Chung WM, Frey AS, Menon AS, Li XJ, Stieg PE, Yuan J, Penney JB, Young AB, Cha JH, Friedlander RM (1999). Inhibition of caspase-1 slows disease progression in a mouse model of Huntington's disease. *Nature* **399**, 263-7.

Pan G, Bauer JH, Haridas V, Wang S, Liu D, Yu G, Vincenz C, Aggarwal BB, Ni J, Dixit VM (1998a). Identification and functional characterization of DR6, a novel death domain-containing TNF receptor. *FEBS Lett.* **431**, 351-6.

Pan G, O'Rourke K, Dixit VM (1998b). Caspase-9, Bcl-XL, and Apaf-1 form a ternary complex. *J Biol Chem.* **273**, 5841-5.

Pan G, Ni J, Wei YF, Yu G, Gentz R, Dixit VM (1997a). An antagonist decoy receptor and a death domain-containing receptor for TRAIL. *Science* **277**, 815-8.

Pan G, O'Rourke K, Chinnaiyan AM, Gentz R, Ebner R, Ni J, Dixit VM (1997b). The receptor for the cytotoxic ligand TRAIL. *Science* **276**, 111-3.

Pitti RM, Marsters SA, Lawrence DA, Roy M, Kischkel FC, Dowd P, Huang A, Donahue CJ, Sherwood SW, Baldwin DT, Godowski PJ, Wood WI, Gurney

AL, Hillan KJ, Cohen RL, Goddard AD, Botstein D, Ashkenazi A (1998). Genomic amplification of a decoy receptor for Fas ligand in lung and colon cancer. *Nature* **396**, 699-703.

Poe M, Blake JT, Boulton DA, Gammon M, Sigal NH, Wu JK, Zweerink HJ (1991). Human cytotoxic lymphocyte granzyme B. Its purification from granules and the characterization of substrate and inhibitor specificity. *J Biol Chem.* **266**, 98-103.

Polyak K, Xia Y, Zweier JL, Kinzler KW, Vogelstein B (1997). A model for p53-induced apoptosis. *Nature* **389**, 300-5.

Puthalakath H, Huang DC, O'Reilly LA, King SM, Strasser A (1999). The proapoptotic activity of the Bcl-2 family member Bim is regulated by interaction with the dynein motor complex. *Mol Cell.* **3**, 287-96.

Qin XQ, Livingston DM, Kaelin WG Jr, Adams PD (1994). Deregulated transcription factor E2F-1 expression leads to S-phase entry and p53-mediated apoptosis. *Proc Natl Acad Sci U S A.* **91**, 10918-22.

Ray CA, Black RA, Kronheim SR, Greenstreet TA, Sleath PR, Salvesen GS, Pickup DJ (1992). Viral inhibition of inflammation: cowpox virus encodes an inhibitor of the interleukin-1 beta converting enzyme. *Cell* **69**, 597-604.

Ritter PM, Marti A, Blanc C, Baltzer A, Krajewski S, Reed JC, Jaggi R (2000). Nuclear localization of procaspase-9 and processing by a caspase-3-like activity n mammary epithelial cells. *Eur J Cell Biol.* **79**, 358-64.

Rodriguez J, Lazebnik Y (1999). Caspase-9 and APAF-1 form an active holoenzyme. *Genes Dev.* **13**, 3179-84.

Roy N, Deveraux QL, Takahashi R, Salvesen GS, Reed JC (1997). The c-IAP-1 and c-IAP-2 proteins are direct inhibitors of specific caspases. *EMBO J.* **16**, 6914-25.

Rustgi AK, Dyson N, Bernards R (1991). Amino-terminal domains of c-myc and N myc proteins mediate binding to the retinoblastoma gene product. *Nature* **352**, 541-4.

Sahara S, Aoto M, Eguchi Y, Imamoto N, Yoneda Y, Tsujimoto Y (1999). Acinus is a caspase-3-activated protein required for apoptotic chromatin condensation. *Nature* **401**, 168-73.

Saito M, Korsmeyer SJ, Schlesinger PH (2000). BAX-dependent transport of cytochrome c reconstituted in pure liposomes. *Nat Cell Biol.* **2**, 553-5.

Sakaguchi K, Herrera JE, Saito S, Miki T, Bustin M, Vassilev A, Anderson CW, Appella E (1998). DNA damage activates p53 through a phosphorylation-acetylation cascade. *Genes Dev.* **12**, 2831-41.

Sakahira H, Enari M, Nagata S (1998). Cleavage of CAD inhibitor in CAD activation and DNA degradation during apoptosis. *Nature* **391**, 96-9.

Saleh A, Srinivasula SM, Acharya S, Fishel R, Alnemri ES (1999). Cytochrome c and dATP-mediated oligomerization of Apaf-1 is a prerequisite for procaspase-9 activation. *J Biol Chem.* **274**, 17941-5.

Salvesen GS, Dixit VM (1999). Caspase activation: the induced-proximity model. *Proc Natl Acad Sci U S A.* **96**, 10964-7.

Scaffidi C, Schmitz I, Krammer PH, Peter ME (1999). The role of c-FLIP in modulation of CD95-induced apoptosis. *J Biol Chem.* **274**, 1541-8.

Scaffidi C, Fulda S, Srinivasan A, Friesen C, Li F, Tomaselli KJ, Debatin KM, Krammer PH, Peter ME (1998). Two CD95 (APO-1/Fas) signaling pathways. *EMBO J.* **17**, 1675-87.

Schendel SL, Azimov R, Pawlowski K, Godzik A, Kagan BL, Reed JC (1999). Ion channel activity of the BH3 only Bcl-2 family member, BID. *J Biol Chem.* **274**, 21932-6.

Schendel SL, Montal M, Reed JC (1998). Bcl-2 family proteins as ion-channels. *Cell Death Differ.* **5**, 372-80.

Seshagiri S, Chang WT, Miller LK (1997a). Mutational analysis of Caenorhabditis elegans CED-4. *FEBS Lett.* **428**, 71-4.

Seshagiri S, Miller LK (1997b). Caenorhabditis elegans CED-4 stimulates CED-3 processing and CED-3-induced apoptosis. *Curr Biol.* **7**, 455-60.

Shaham S, Horvitz HR (1996). Developing Caenorhabditis elegans neurons may contain both cell-death protective and killer activities. *Genes Dev.* **10**, 578-91.

Schatz G (1996) The protein import system of mitochondria. *J Biol Chem.* **271**, 31763-6.

Shieh SY, Ahn J, Tamai K, Taya Y, Prives C (2000). The human homologs of checkpoint kinases Chk1 and Cds1 (Chk2) phosphorylate p53 at multiple DNA damage-inducible sites. *Genes Dev.* **14**, 289-300.

Shieh SY, Taya Y, Prives C (1999). DNA damage-inducible phosphorylation of p53 at N-terminal sites including a novel site, Ser20, requires tetramerization. *EMBO J.* **18**, 1815-23.

Shieh SY, Ikeda M, Taya Y, Prives C (1997). DNA damage-induced phosphorylation of p53 alleviates inhibition by MDM2. *Cell* **91**, 325-34.

Shresta S, Heusel JW, Macivor DM, Wesselschmidt RL, Russell JH, Ley TJ (1995). Granzyme B plays a critical role in cytotoxic lymphocyte-induced apoptosis. *Immunol Rev.* **146**, 211-21.

Siliciano JD, Canman CE, Taya Y, Sakaguchi K, Appella E, Kastan MB (1997). DNA damage induces phosphorylation of the amino terminus of p53. *Genes Dev.* **11**, 3471-81.

Slee EA, Adrain C, Martin SJ (1999a). Serial killers: ordering caspase activation events in apoptosis. *Cell Death Differ.* **6**, 1067-74.

Slee EA, Harte MT, Kluck RM, Wolf BB, Casiano CA, Newmeyer DD, Wang HG, Reed JC, Nicholson DW, Alnemri ES, Green DR, Martin SJ (1999b). Ordering the cytochrome c-initiated caspase cascade: hierarchical activation of caspases-2, -3, -6, -7, -8, and -10 in a caspase-9-dependent manner. *J Cell Biol.* **144**, 281-92.

Slee EA, Adrain C, Martin SJ (2001). Executioner caspases-3, -6 and -7 perform distinct, non-redundant, roles during the demolition phase of apoptosis. *J Biol Chem.* **276** 7320-26.

Soengas MS, Alarcon RM, Yoshida H, Giaccia AJ, Hakem R, Mak TW, Lowe S W (1999). Apaf-1 and caspase-9 in p53-dependent apoptosis and tumor inhibition. *Science* **284**, 156-9.

Song Q, Kuang Y, Dixit VM, Vincenz C (1999). Boo, a novel negative regulator of cell death, interacts with Apaf-1. *EMBO J.* **18**, 167-78.

Spector MS, Desnoyers S, Hoeppner DJ, Hengartner MO (1997). Interaction between the C. elegans cell-death regulators CED-9 and CED-4. *Nature* **385**, 653-6.

Spencer DM, Belshaw PJ, Chen L, Ho SN, Randazzo F, Crabtree GR, Schreiber SL (1996). Functional analysis of Fas signaling in vivo using synthetic inducers of dimerization. *Curr Biol.* **6**, 839-47.

Spudich JA (1994). How molecular motors work. *Nature* **372**, 515-8.

Srinivasula SM, Ahmad M, Fernandes-Alnemri T, Alnemri ES (1998). Autoactivation of procaspase-9 by Apaf-1-mediated oligomerization. *Mol Cell* **1**, 949-57.

Srinivasula SM, Fernandes-Alnemri T, Zangrilli J, Robertson N, Armstrong RC,Wang L, Trapani JA, Tomaselli KJ, Litwack G, Alnemri ES (1996). The Ced-3/interleukin 1beta converting enzyme-like homolog Mch6 and the lamin-cleaving enzyme Mch2alpha are substrates for the apoptotic mediator CPP32. *J Biol Chem.* **271**, 27099-106.

Stegh AH, Schickling O, Ehret A, Scaffidi C, Peterhansel C, Hofmann TG, Grummt I, Krammer PH, Peter ME (1998). DEDD, a novel death effector domain containing protein, targeted to the nucleolus. *EMBO J.* **17**, 5974-86.

Suda T, Takahashi T, Golstein P, Nagata S (1993). Molecular cloning and expression of the Fas ligand, a novel member of the tumor necrosis factor family. *Cell* **75**, 1169-78.

Sulston JE, Horvitz HR (1977). Post-embryonic cell lineages of the nematode, Caenorhabditis elegans. *Dev Biol.* **56**, 110-56.

Susin SA, Lorenzo HK, Zamzami N, Marzo I, Snow BE, Brothers GM, Mangion J, Jacotot E, Costantini P, Loeffler M, Larochette N, Goodlett DR, Aebersold R, Siderovski DP, Penninger JM, Kroemer G (1999). Molecular characterization of mitochondrial apoptosis-inducing factor. *Nature* **397**, 441-6.

Susin SA, Zamzami N, Kroemer G (1998). Mitochondria as regulators of apoptosis: doubt no more. *Biochim Biophys Acta.* **1366**, 151-65.

Takahashi R, Deveraux Q, Tamm I, Welsh K, Assa-Munt N, Salvesen GS, Reed JC (1998). A single BIR domain of XIAP sufficient for inhibiting caspases. *J Biol Chem.* **273**, 7787-90.

Tanaka M, Suda T, Takahashi T, Nagata S (1995). Expression of the functional soluble form of human fas ligand in activated lymphocytes. *EMBO J.* **14**, 1129-35.

Thome M, Schneider P, Hofmann K, Fickenscher H, Meinl E, Neipel F, Mattmann C, Burns K, Bodmer JL, Schroter M, Scaffidi C, Krammer PH, Peter ME, Tschopp J (1997). Viral FLICE-inhibitory proteins (FLIPs) prevent apoptosis induced by death receptors. *Nature* **386**, 517-21.

Thornberry NA, Rano TA, Peterson EP, Rasper DM, Timkey T, Garcia-Calvo M,Houtzager VM, Nordstrom PA, Roy S, Vaillancourt JP, Chapman KT, Nicholson DW (1997). A combinatorial approach defines specificities of members of the caspase family and granzyme B. Functional relationships established for key mediators of apoptosis. *J Biol Chem.* **272**, 17907-11.

Thornberry NA, Bull HG, Calaycay JR, Chapman KT, Howard AD, Kostura MJ, Miller DK, Molineaux SM, Weidner JR, Aunins J, Elliston KO, Ayala JM, Casano FJ, Chin J, Ding GJF, Egger LA, Gaffney EP, Limjuco G, Palyha OC, Raju SM, Rolando AM, Salley, JP, Yamin, TT, Lee TD, Shiveley JE, MacCross M, Mumford RA, Schmidt JA, Tocci MJ (1992). A novel heterodimeric cysteine protease is required for interleukin-1 beta processing in monocytes. *Nature* **356**, 768-74.

Tibbetts RS, Brumbaugh KM, Williams JM, Sarkaria JN, Cliby WA, Shieh SY, Taya Y, Prives C, Abraham RT (1999). A role for ATR in the DNA damage-induced phosphorylation of p53. *Genes Dev.* **13**, 152-7.

Torii S, Egan DA, Evans RA, Reed JC (1999). Human Daxx regulates Fas-induced apoptosis from nuclear PML oncogenic domains (PODs). *EMBO J.* **18**, 6037-49.

Trauth BC, Klas C, Peters AM, Matzku S, Moller P, Falk W, Debatin KM, Krammer PH (1989). Monoclonal antibody-mediated tumor regression by induction of apoptosis. *Science* **245**, 301-5.

Trent C, Wood WB, Horvitz HR (1988). A novel dominant transformer allele of the sex-determining gene her-1 of Caenorhabditis elegans. *Genetics* **120**, 145-57.

Tsujimoto Y, Cossman J, Jaffe E, Croce CM (1985). Involvement of the bcl-2 gene in human follicular lymphoma. *Science* **228**, 1440-3.

Unger T, Juven-Gershon T, Moallem E, Berger M, Vogt Sionov R, Lozano G, Oren M, Haupt Y (1999). Critical role for Ser20 of human p53 in the negative regulation of p53 by Mdm2. *EMBO J.* **18**, 1805-14.

Van Antwerp DJ, Martin SJ, Kafri T, Green DR, Verma IM (1996). Suppression of TNF-alpha-induced apoptosis by NF-kappaB. *Science.* **274**, 787-9.

van der Biezen EA, Jones JD (1998). The NB-ARC domain: a novel signalling motif shared by plant resistance gene products and regulators of cell death in animals. *Curr Biol.* **8**, R226-7.

van der Voorn L, Ploegh HL (1992). The WD-40 repeat. *FEBS Lett.* **307**, 131-4.

Vander Heiden MG, Thompson CB (1999). Bcl-2 proteins: regulators of apoptosis or of mitochondrial homeostasis? *Nat Cell Biol.* **1**, E209-16.

Vander Heiden MG, Chandel NS, Williamson EK, Schumacker PT, Thompson CB (1997). Bcl-xL regulates the membrane potential and volume homeostasis of mitochondria. *Cell* **91**, 627-37.

Varfolomeev EE, Schuchmann M, Luria V, Chiannilkulchai N, Beckmann JS, Mett IL, Rebrikov D, Brodianski VM, Kemper OC, Kollet O, Lapidot T, Soffer D, Sobe T, Avraham KB, Goncharov T, Holtmann H, Lonai P, Wallach D (1998). Targeted disruption of the mouse Caspase 8 gene ablates cell death induction by the TNF receptors, Fas/Apo1, and DR3 and is lethal prenatally. *Immunity* **9**, 267-76.

Vaux DL, Cory S, Adams JM (1988). Bcl-2 gene promotes haemopoietic cell survival and cooperates with c-myc to immortalize pre-B cells. *Nature* **335**, 440-2.

Verhagen AM, Ekert PG, Pakusch M, Silke J, Connolly LM, Reid GE, Moritz RL, Simpson RJ, Vaux DL (2000). Identification of DIABLO, a mammalian protein that promotes apoptosis by binding to and antagonizing IAP proteins. *Cell* **102**, 43-53.

Walczak H, Degli-Esposti MA, Johnson RS, Smolak PJ, Waugh JY, Boiani N, Timour MS, Gerhart MJ, Schooley KA, Smith CA, Goodwin RG, Rauch CT (1997). TRAIL-R2: a novel apoptosis-mediating receptor for TRAIL. *EMBO J.* **16**, 5386-97.

Walker JE, Saraste M, Runswick MJ, Gay NJ (1982). Distantly related sequences in the alpha- and beta subunits of ATP synthase, myosin, kinases and other ATP-requiring enzymes and a common nucleotide binding fold. *EMBO J.* **1**, 945-51.

Walker NP, Talanian RV, Brady KD, Dang LC, Bump NJ, Ferenz CR, Franklin S, Ghayur T, Hackett MC, Hammill LD, Herzog L, Hugunin M, Houy W, Mankovich JA, McGuiness L, Orlewicz E, Paskind M, Pratt CA, Reis P, Summani A, Terranova M, Welch JP, Xiong L, Möller A, Tracey DE, Kamen R, Wong WW (1994). Crystal structure of the cysteine protease interleukin-1 beta-converting enzyme: a (p20/p10)2 homodimer. *Cell* **78**, 343-52.

Wang J, Zheng L, Lobito A, Chan FK, Dale J, Sneller M, Yao X, Puck JM, Straus SE, Lenardo MJ (1999). Inherited human Caspase 10 mutations underlie defective lymphocyte and dendritic cell apoptosis in autoimmune lymphoproliferative syndrome type II. *Cell* **98**, 47-58.

Wang K, Yin XM, Chao DT, Milliman CL, Korsmeyer SJ (1996). BID: a novel BH3 domain-only death agonist. *Genes Dev.* **10**, 2859-69.

Wang S, Miura M, Jung YK, Zhu H, Li E, Yuan J (1998). Murine caspase-11, an ICE-interacting protease, is essential for the activation of ICE. *Cell* **92**, 501-9.

Wang ZG, Ruggero D, Ronchetti S, Zhong S, Gaboli M, Rivi R, Pandolfi PP (1998). PML is essential for multiple apoptotic pathways. *Nat Genet.* **20**, 266-72.

Wang ZH, Ding MX, Chew-Cheng SB, Yun JP, Chew EC (1999). Bcl-2 and Bax proteins are nuclear matrix associated proteins. *Anticancer Res.* **19**, 5445-9.

Wei MC, Lindsten T, Mootha VK, Weiler S, Gross A, Ashiya M, Thompson CB, Korsmeyer SJ (2000). tBID, a membrane-targeted death ligand, oligomerizes BAK to release cytochrome c. *Genes Dev.* **14**, 2060-71.

Weil M, Raff MC, Braga VM (1999). Caspase activation in the terminal differentiation of human epidermal keratinocytes. *Curr Biol.* **9**, 361-4.

Weil M, Jacobson MD, Coles HS, Davies TJ, Gardner RL, Raff KD, Raff MC (1996). Constitutive expression of the machinery for programmed cell death. *J Cell Biol.* **133**, 1053-9.

Weinberg RA (1995). The retinoblastoma protein and cell cycle control. *Cell* **81**, 323-30.

Weis K, Rambaud S, Lavau C, Jansen J, Carvalho T, Carmo-Fonseca M, Lamond A, Dejean A (1994). Retinoic acid regulates aberrant nuclear localization of PML-RAR alpha in acute promyelocytic leukemia cells. *Cell* **76**, 345-56.

Wiley SR, Schooley K, Smolak PJ, Din WS, Huang CP, Nicholl JK, Sutherland GR, Smith TD, Rauch C, Smith CA (1995). Identification and characterization of a new member of the TNF family that induces apoptosis. *Immunity* **3**, 673-82.

Wolter KG, Hsu YT, Smith CL, Nechushtan A, Xi XG, Youle RJ (1997). Movement of Bax from the cytosol to mitochondria during apoptosis. *J Cell Biol.* **139**, 1281-92.

Woo M, Hakem R, Soengas MS, Duncan GS, Shahinian A, Kagi D, Hakem A, McCurrach M, Khoo W, Kaufman SA, Senaldi G, Howard T, Lowe SW, Mak TW (1998). Essential contribution of caspase 3/CPP32 to apoptosis and its associated nuclear changes. *Genes Dev.* **12**, 806-19.

Wu D, Wallen HD, Inohara N, Nunez G (1997a). Interaction and regulation of the Caenorhabditis elegans death protease CED-3 by CED-4 and CED-9. *J Biol Chem.* **272**, 21449-54.

Wu D, Wallen HD, Nunez G (1997b). Interaction and regulation of subcellular localization of CED-4 by CED-9. *Science* **275**, 1126-9.

Wu GS, Burns TF, Zhan Y, Alnemri ES, El-Deiry WS (1999). Molecular cloning and functional analysis of the mouse homologue of the KILLER/DR5 tumor necrosis factor-related apoptosis-inducing ligand (TRAIL) death receptor. *Cancer Res.* **59**, 2770-5.

Wu YC, Horvitz HR (1998). The C. elegans cell corpse engulfment gene ced-7 encodes a protein similar to ABC transporters. *Cell* **93**, 951-60.

Xiao ZX, Chen J, Levine AJ, Modjtahedi N, Xing J, Sellers WR, Livingston DM (1995). Interaction between the retinoblastoma protein and the oncoprotein MDM2. *Nature* **375**, 694-8.

Xue D, Horvitz HR (1995). Inhibition of the Caenorhabditis elegans cell-death protease CED-3 by a CED-3 cleavage site in baculovirus p35 protein. *Nature* **377**, 248-51.

Yang E, Zha J, Jockel J, Boise LH, Thompson CB, Korsmeyer SJ (1995). Bad, a heterodimeric partner for Bcl-XL and Bcl-2, displaces Bax and promotes cell death. *Cell* **80**, 285-91.

Yang J, Liu X, Bhalla K, Kim CN, Ibrado AM, Cai J, Peng TI, Jones DP, Wang X (1997). Prevention of apoptosis by Bcl-2: release of cytochrome c from mitochondria blocked. *Science* **275**, 1129-32.

Yang X, Chang HY, Baltimore D (1998a). Essential role of CED-4 oligomerization in CED-3 activation and apoptosis. *Science* **281**, 1355-7.

Yang X, Chang HY, Baltimore D (1998b). Autoproteolytic activation of pro-caspases by oligomerization. *Mol Cell* **1** ,319-25.

Yang Y, Fang S, Jensen JP, Weissman AM, Ashwell JD (2000). Ubiquitin protein ligase activity of IAPs and their degradation in proteasomes in response to apoptotic stimuli. *Science* **288**, 874-7.

Yankner BA (1996). Mechanisms of neuronal degeneration in Alzheimer's disease. *Neuron* **16**, 921-32.

Yin XM, Wang K, Gross A, Zhao Y, Zinkel S, Klocke B, Roth KA, Korsmeyer SJ (1999). Bid-deficient mice are resistant to Fas-induced hepatocellular apoptosis. *Nature* **400**, 886-91.

Yonehara S, Ishii A, Yonehara M (1989). A cell-killing monoclonal antibody (anti-Fas) to a cell surface antigen co-downregulated with the receptor of tumor necrosis factor. *J Exp Med.* **169**, 1747-56.

Yoshida H, Kong YY, Yoshida R, Elia AJ, Hakem A, Hakem R, Penninger JM, Mak TW (1998). Apaf1 is required for mitochondrial pathways of apoptosis and brain development. *Cell* **94**, 739-50.

Young JL, Sukhova GK, Foster D, Kisiel W, Libby P, Schonbeck U (2000). The serpin proteinase inhibitor 9 is an endogenous inhibitor of interleukin 1beta-converting enzyme (caspase-1) activity in human vascular smooth muscle cells. *J Exp Med.* **191**, 1535-44.

Yuan J, Yankner BA (2000). Apoptosis in the nervous system. *Nature* **407**, 802-9.

Yuan J, Shaham S, Ledoux S, Ellis HM, Horvitz HR (1993). The C. elegans cell death gene ced-3 encodes a protein similar to mammalian interleukin-1 beta-converting enzyme. *Cell* **75**, 641-52.

Yuan J, Horvitz HR (1992). The Caenorhabditis elegans cell death gene ced-4 encodes a novel protein and is expressed during the period of extensive programmed cell death. *Development* **116**, 309-20.

Yuan J, Horvitz HR (1990). The Caenorhabditis elegans genes ced-3 and ced-4 act cell autonomously to cause programmed cell death. *Dev Biol.* **138**, 33-41.

Yuan ZM, Shioya H, Ishiko T, Sun X, Gu J, Huang YY, Lu H, Kharbanda S, Weichselbaum R, Kufe D (1999). p73 is regulated by tyrosine kinase c-Abl in the apoptotic response to DNA damage. *Nature* **399**, 814-7.

Zamzami N, Marchetti P, Castedo M, Hirsch T, Susin SA, Masse B, Kroemer G (1996). Inhibitors of permeability transition interfere with the disruption of the mitochondrial transmembrane potential during apoptosis. *FEBS Lett.* **384**, 53-7.

Zhao R, Gish K, Murphy M, Yin Y, Notterman D, Hoffman WH, Tom E, Mack DH, Levine AJ (2000). Analysis of p53-regulated gene expression patterns using oligonucleotide arrays. *Genes Dev.* **14**, 981-93.

Zheng TS, Hunot S, Kuida K, Flavell RA (1999). Caspase knockouts: matters of life and death. *Cell Death Differ* **6**, 1043-53.

Zhivotovsky B, Samali A, Gahm A, Orrenius S (1999). Caspases: their intracellular localization and translocation during apoptosis. *Cell Death Differ.* **6**, 644-51.

Zhivotovsky B, Orrenius S, Brustugun OT, Doskeland SO (1998). Injected cytochrome c induces apoptosis. *Nature* **391**, 449-50.

Zhong S, Salomoni P, Ronchetti S, Guo A, Ruggero D, Pandolfi PP. (2000) Promyelocytic leukemia protein (PML) and Daxx participate in a novel nuclear pathway for apoptosis. *J Exp Med.* **191**, 631-40.

Zhou Q, Snipas S, Orth K, Muzio M, Dixit VM, Salvesen GS (1997). Target protease specificity of the viral serpin CrmA. Analysis of five caspases. *J Biol Chem.* **272**, 7797-800.

Zou H, Li Y, Liu X, Wang X (1999). An APAF-1.cytochrome c multimeric complex is a functional apoptosome that activates procaspase-9. *J Biol Chem* **274**, 11549-56.

Zou H, Henzel WJ, Liu X, Lutschg A, Wang X (1997). Apaf-1, a human protein homologous to C. elegans CED-4, participates in cytochrome c-dependent activation of caspase-3. *Cell* **90**, 405-13.